CHARACTERISATION OF DISPERSION IN THE SPRAY REGIME OF SIEVE PLATE OPERATION

by

Manuel Alves da Silva Jerónimo

May, 1976

A thesis submitted for the degree of Doctor of Philosophy of the University of London and for the Diploma of Imperial College.

Department of Chemical Engineering
and Chemical Technology,
Imperial College
London, SW 7

ABSTRACT

A critical re-examination was conducted of the assumptions made by Fane and Sawistowski in their formulation of the free trajectory model of the spray regime. Independent determination of the parameters necessary for the model confirmed the validity of the projection velocity correlation used by these authors for sieve plates with small holes.

Simplifications in the model made it possible to deduce the functional form of the dispersion density and surface area profiles and present it in a form which required only the knowledge of a total number of five parameters, for complete description of the hydrodynamic state of a plate operating in the spray regime.

A general definition for systems classification was proposed based on sign of the time derivative of surface tension. It is equivalent to the different definitions used previously which were specific to the particular mass-transfer operation under consideration.

Effect of gas and liquid flow rates, hole diameter, fractional free area, mass transfer and of the use of a splash baffle on the behaviour of a small plate were also studied. In addition, a tentative prediction of dispersion density parameters is presented. Explanation of these effects was conducted with the help of a physical model of the phenomena occurring in the proximity of the hole.

A common basis for comparison of the froth-spray transition measurements was established. It was found that transition for strongly negative systems occurs with a gas velocity 25% smaller than that necessary for the other systems.

A meus Pais

ACKNOWLEDGEMENTS

The author wishes to offer his thanks and deep appreciation to Professor H. Sawistowski for his interest and precious advice during the course of this work.

I would also like to acknowledge the "Universidade do Porto" for a very generous leave of absence and the "Instituto de Alta Cultura" for the award of a scholarship covering the entire period of study.

Valuable assistance from the technical staff of the Department is gratefully acknowledged, in particular from the electronic workshop.

My thanks are also due to all my portuguese colleagues in the College for their pleasant and helpful companionship and especially to Dr. José Romão de Sousa for many stimulating discussions and also to Miss Maria Eduarda Nunes, Miss Maria José Pinto Dias, Mrs. Maria do Céu Pereira and Mr. José Luis Pereira for their invaluable assistance - especially during my stay in hospital.

Finally, I wish to thank all my family, especially my wife Maria José, for their understanding and support during this long period of study.

TABLE OF CONTENTS

Chapter One

Introduction

Sieve plate columns represent a type of equipment which is widely used for mass transfer operations. During the last decades they have replaced bubble cup plates as standard contactors since they are less expensive and have a lower pressure drop. In addition, continued research on sieve plates has removed the prejudice which surrounded their stability of operation.

The use of high gas or vapour velocities leads to the operation of the sieve plate in the spray regime. Under these conditions the behaviour of the column is different than in the froth regime in that the gas-liquid dispersion consists primarily of liquid drops providing the major contribution to the interfacial area for mass transfer.

The importance of the study of the spray regime has best been summarised in the A.J.V. Underwood Memorial Lecture delivered by F.J. Zuiderweg to the I. Chem. E. and S.C.I. in London on 3 May 1973: "Contrary to the earlier belief, the flow on bubble trays rarely shows vapour bubbles in a layer of liquid. Such a bubbling pattern is only obtained at high liquid level and with low vapour rates. For the inverse case, a regime in which atomised liquid is suspended by the vapour dominates". It follows that a significant amount of earlier work may have been misinterpreted due to failure in recognising the change in type of dispersion and in the mechanism of production of interfacial area. Only recently has the spray regime been studied in detail.

There has been some controversy surrounding the formation of dispersion in the spray regime. Some authors consider the dispersion

to be equivalent to a fluidised bed of droplets, whilst others claim that it comprises discrete droplets allowing well defined trajectories in the inter-plate space.

The most comprehensive contribution to the study of the spray behaviour and the efficiency of mass transfer in this regime was presented by Fane and Sawistowski.[1] They postulated that the atomised liquid had well defined trajectories and this was later substantiated by Lindsey's photographic study.[2] A free trajectory model was formulated on this assumption according to which drops were projected upwards with a certain initial projection velocity from near the plate and followed trajectories given by the solution of the equation of motion of the particle.

Experimental dispersion density profiles (liquid volumetric fraction in dispersion versus height above plate floor) have been successfully fitted by this model and subsequently used to predict plate efficiencies remarkably well.[1,3]

Nevertheless, limitations in the usefulness of the model exist by the need for prior knowledge of parameters concerning the initial projection velocity and the drop size distribution. The initial projection velocity was assumed to be known from correlation of existing experimental data based on the heights reached by projected drops. The drop size distribution was calculated by "fitting" experimental dispersion density profiles at <u>actual</u> conditions.

The purpose of the present work is to subject the assumptions made by Fane and Sawistowski to critical re-examination concentrating in particular on the parameters of the free trajectory model. This work will be conducted in two stages:

In the first stage, an analysis will be performed of the free trajectory model and of the dispersion density profiles, in particular

examining the importance of the various assumptions and their criticality.

The aim of the second stage will be to obtain independent information on the parameters of the model.

In addition, an attempt will be made to establish a common basis for comparison of the froth-spray transition measurements and to investigate the effect of presence of mass transfer on plate behaviour.

Chapter Two

LITERATURE SURVEY

2.1 Hydrodynamics of Sieve Plates

2.1.1 Regimes of Plate Operation

The structure of the two phase dispersion on the plate, and hence the magnitude of the interfacial area, mass transfer coefficient and time of phase contact for mass transfer, are determined by hydrodynamic conditions. Several regimes, characterised by different flow patterns can be observed and the factors affecting the formation of interfacial area and mass transfer act differently in each regime. It is, therefore, necessary to describe the fluid mechanics and mass transfer characteristics of each regime and to be able to predict transitions between them. However, the transition between various regimes is seldom very sharp and, depending on the type of system considered, not all regimes may always be present. On the other side, frequently several regimes coexist at different places on a large plate.

The occurrence of a particular regime depends strongly on gas velocity and is also influenced by the nature of the physical system. Thus, the various systems are best described by following the variations in the mean dispersion density (volumetric liquid fraction) of the gas-liquid dispersion on the plate with the superficial velocity of the gas (Figure 2.1). Surface-tension positive systems will be considered first. These are systems, for which surface tension increases with contact time between phases as a result of the mass and/or heat transfer taking place.*

---

*This generalizes the definition introduced by Zuiderweg and Harmens[4] for the case of two-component distillation systems.

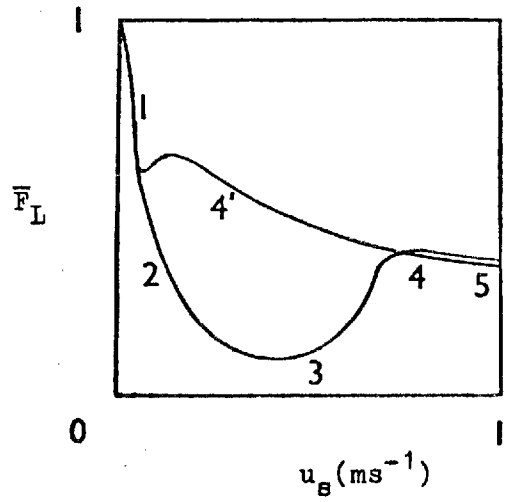

Fig.2.1.-Change of dispersion density with gas velocity on a sieve plate.

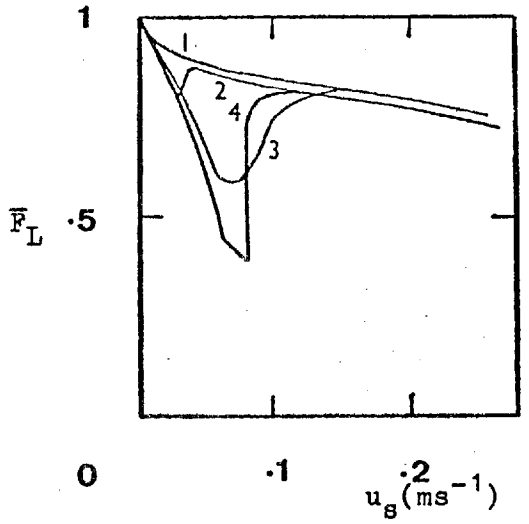

Fig.2.2.-Effect of surfactants on transition from the free bubbling regime to the froth regime. 1.Distilled water. 2.Impure distilled water. 3.Tap water. 4.Soap solution.

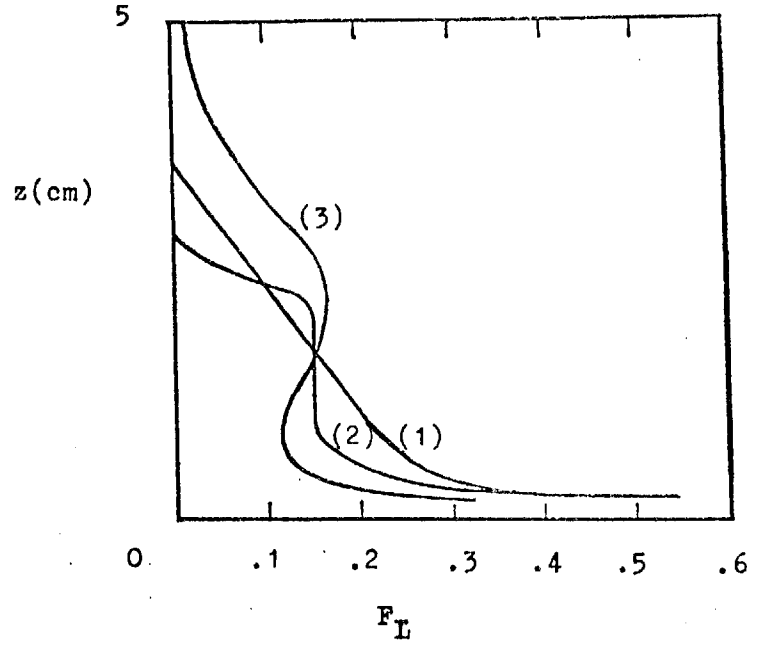

Fig.2.3.-Dispersion density profiles for cellular foam (1), froth (2) and spray (3) regimes of plate operation.

Initially, at a low gas velocity free bubbling (1) exists, for which with increasing gas rate (at constant liquid rate) the dispersion density falls monotonically. The dispersion consists of clouds of bubbles of narrow size range (formation size bubbles). The limit of this regime is reached, when the rate of arrival of bubbles at the surface becomes greater than their rate of coalescence. The regime changes then to cellular foam (2) and the bubbles deform into polyhedra. The dispersion density continues decreasing and can be as low as 8%. On increasing the gas rate, the liquid films thicken, the foam becomes mobile (3), and gradually breaks down with an increase in the dispersion density. Finally it degenerates into froth (4) characterised by a local maximum in the variation of dispersion density with gas rate. In this regime there is a vigorous liquid circulation and the dispersion density is greater than in the foam regime. The dispersion is extremely agitated and the surface is mobile. Further increase in gas velocity leads to phase inversion and hence to the formation of the spray regime (5).

With negative systems in which bubble coalescence is too fast to allow for foam formation there is direct transition from free bubbling (1) to froth (4') and then to spray (5).

It was observed[5] that for very pure liquids in the absence of mass transfer, even the free-bubbling regime can be almost absent - Figure 2.2.

The free bubbling and cellular foam regimes, although of considerable academic interest and with several important applications, are of little practical importance in sieve plate operation.

2.1.2 Dispersion density profiles and regimes of plate operation

Up to now only mean dispersion densities have been considered. Even some recent publications[6] characterize the dispersions by an overall froth density, but this does not mean that the dispersions are homogeneous. On the contrary, it has been shown by MacMillan,[7] Bernard and Sargent,[8] Fane and Sawistowski[1] and more recently by Fell *et al.*[9] that the dispersion density is also a function of the height above the plate floor. The representation of this function is called the dispersion density profile. Further, Fane and Sawistowski[1] have shown that the shape of this profile is characteristic of the regime of operation of the plate (Figure 2.3). They found that in the cellular foam regime the profile has almost a constant slope, in the froth regime there is a zone of constant density and in the spray regime there is a local maximum of the dispersion density profile at a certain height above the plate floor. The shape of the last profile will be deduced later by a simplified model of the spray regime.

2.1.3 Multiplicity of steady state hydrodynamic regime of sieve plate operation and hysteresis effects

The simplified picture presented so far is not always applicable. In fact, some instability phenomena can occur in the operation of sieve plates and some additional hydrodynamic regimes can be identified. For instance, the existence of two steady states, corresponding to two different regimes of hydrodynamic operation on sieve plates, for the same gas and liquid rates of flow, have been observed.[10-14] This is one special case of a more general phenomenon exhibited by dissipative systems. In general, if there is a sub-space of the space of the values of the variables of operation for which a multiplicity of states exists, a step change on

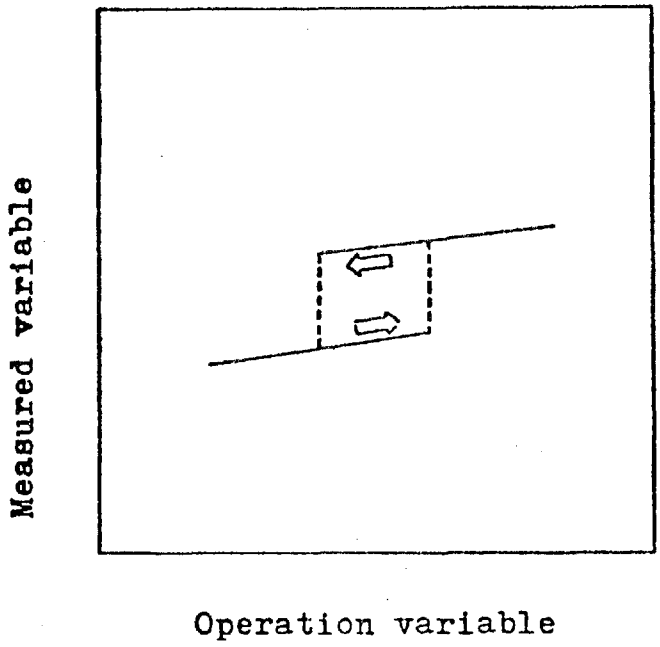

Fig.2.4.-Hysteresis-gap and step changes in measured variable.

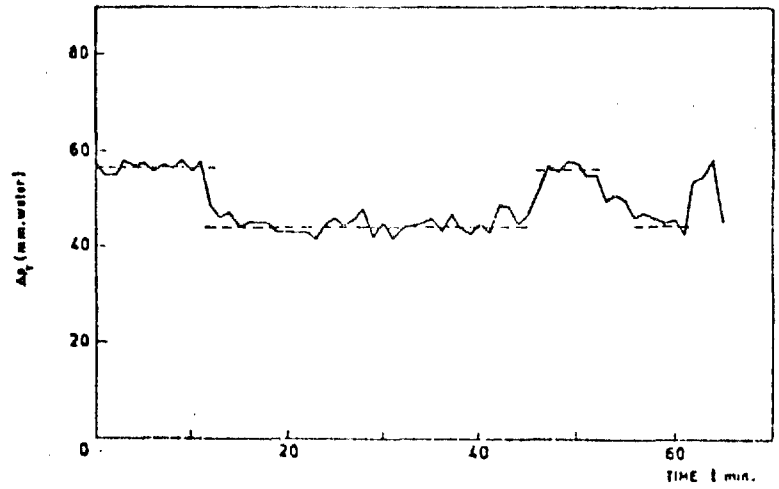

Fig.2.5.-Variation of pressure drop across the froth with time for a metastable state.[14]

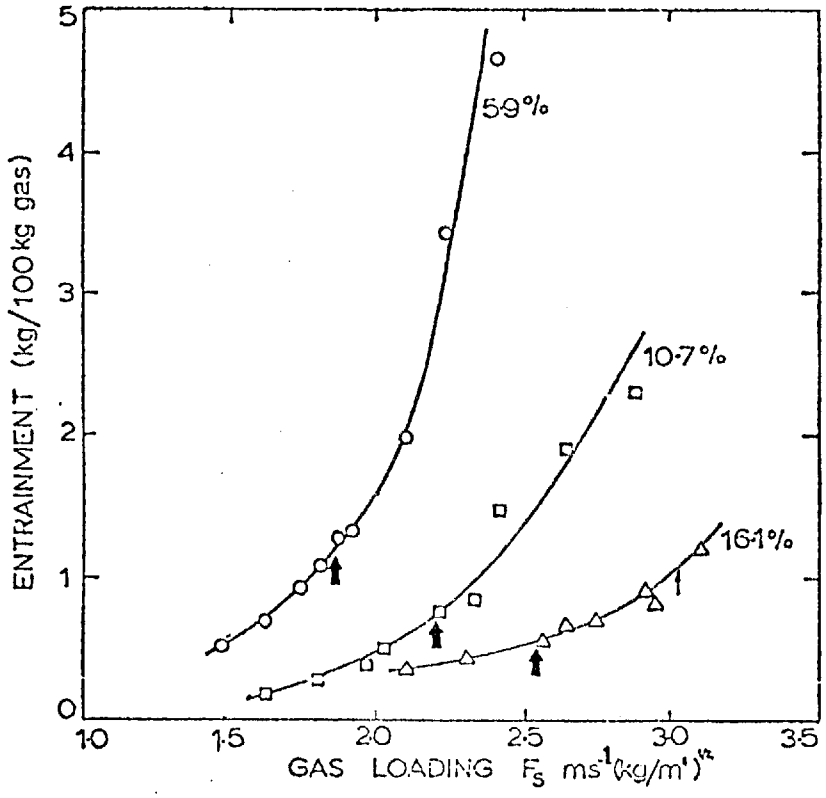

Fig.2.6.-Effect of phase inversion on entrainment. Points of phase inversion are heavily arrowed. $L=15 m^3 h^{-1} m^{-1}$.15

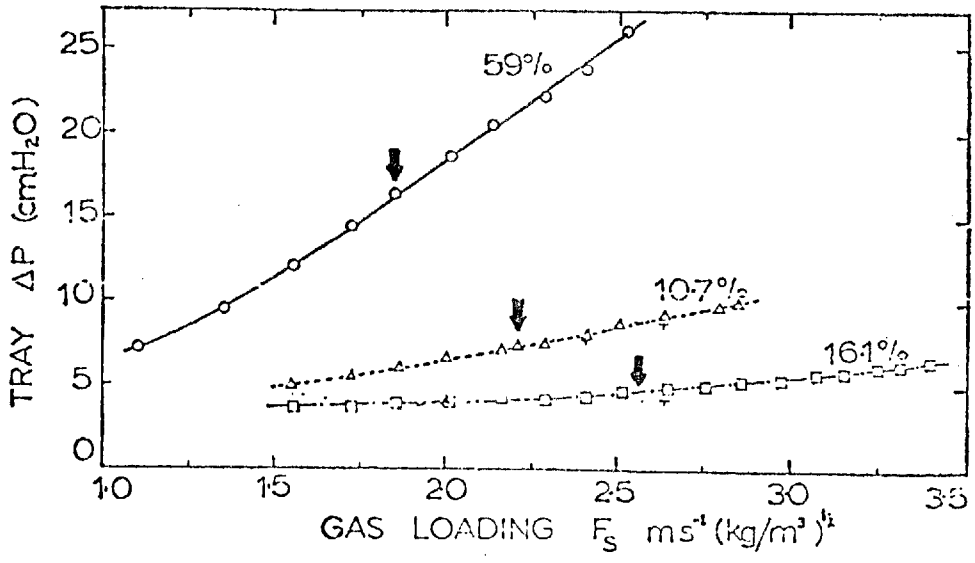

Fig.2.7.-Effect of phase inversion on pressure drop. Points of phase inversion are heavily arrowed. $L=15 m^3 h^{-1} m^{-1}$.15

several observable variables can be detected and a hysteresis gap be defined (Figure 2.4). Within this sub-space, the actual state is metastable and depends on the path followed to reach it. Sometimes spontaneous transitions exist from one state to the other in either direction as the result of any casual disturbance (Figure 2.5) and if the observable variables are time average values, they can seem to be continuous functions of the operation variables[15] (Figures 2.6 and 2.7). In this case, also the hysteresis effect is not well detected.

Sometimes the metastable states are oscillatory with well defined period and wave length. This is the case of overstability, since the restoring forces, opposed to a slight displacement are so strong as to overshoot the corresponding position on the other side of equilibrium. Three different types of regimes of overstability have been found (Figure 2.8), although not all of them have yet been detected on sieve plates. They are in increasing order of wave length and height of froth:

Type I - full wave oscillating regime

Type II - half wave oscillating regime

Type III - circulating oscillating regime

Type I oscillation is characterized by a nodal circle in the cases of circular columns without downcomers or by two parallel axes oriented in the directions of the transverse flux of liquid at the distances of 1/4 and 3/4 of the travel length. The wave length for this type of oscillations is the diameter of the plate.

Type II oscillation is characterized by a nodal axis, oriented in the direction of the transverse flux of liquid if one exists. The wave length for this type of oscillations is two times the diameter of the plate.

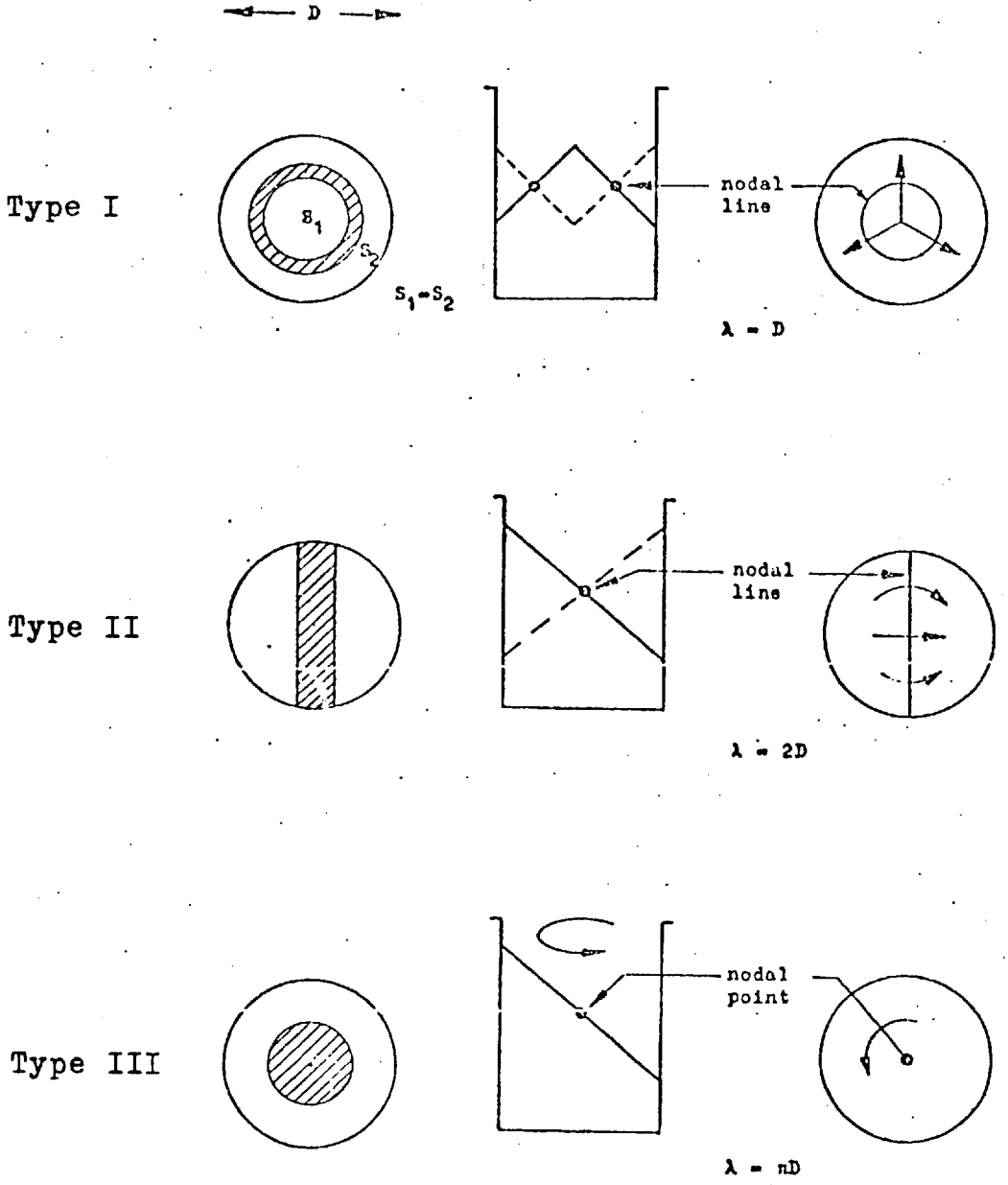

Fig.2.8.-Possible types of macroscopic periodic oscillations of the liquid on a sieve plate. The last one has not yet been observed.

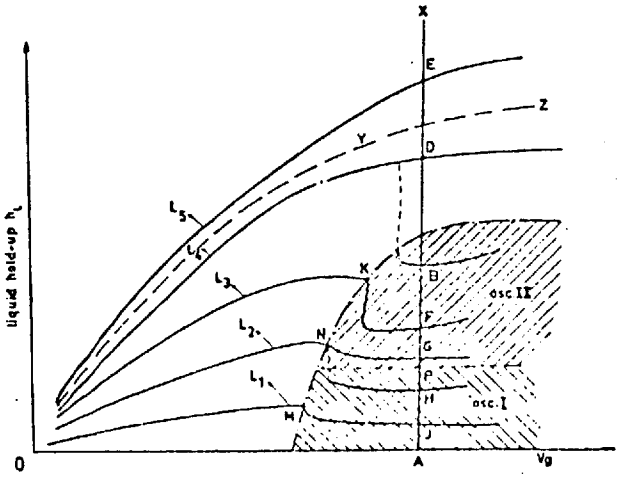

Fig.2.9.-Hold-up of liquid vs. gas flow rate at several liquid flow rates.[14]

Type III oscillation has only a nodal point. The wave length for this type of oscillations is π times the diameter of plate. Its occurrence on sieve plates has not yet been observed experimentally but it is to be expected to exist for very high hold-ups on sieve plates without downcomers working in similar hydrodynamic conditions to those found in Thomas steel converters, where this type of oscillation can happen.[16]

The occurrence of oscillations substantially increases weeping and entrainment, produces a wider variation in bubble diameters and generally lowers plate efficiency.

Sometimes cases of step changes in observable variables have been associated with phase inversion (see, e.g., the work of Shakhov[10] and others as discussed by Pinczewski & Fell).[17] However, these step changes occur more generally and seem not to be necessarily connected with phase inversion (Figure 2.9). They are the result of a reaction of the system to a situation that is no longer stable and in which a build-up of a metastable condition has already taken place. For instance, on sieve plates an increase in liquid hold-up may lead to oscillations in order to increase weeping or entrainment and thus reduce the hold-up to a more acceptable value.

In the cases presented by Shakhov[10] the froth regime can extend sufficiently far into the metastable state that after transition to spray regime the entrainment can be nearly total (Figure 2.10a-c).

In general, it can be said that the hydrodynamic behaviour of a sieve plate can be very complicated and very much dependent on geometric factors, such as for instance the existence of a splash baffle. Even the change in diameter can be very important, as can be seen from Figure 2.11a and 2.11b in which its effect is presented on stability limits and hysteresis gap.

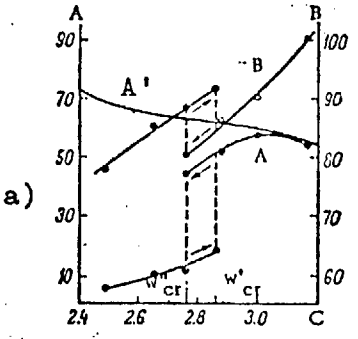

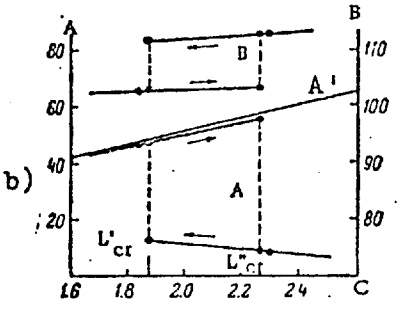

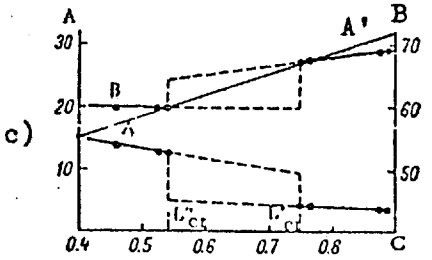

Fig.2.10.-Effect of air velocity and liquid flow rate on entrainment and pressure drop.
A. Entrainment (kg/100kg),
B. Pressure drop (mm water),
C. Air velocity (ms^{-1}) in a), and water flow rate ($m^3\ h^{-1}$) in b) and c),
A'. Line of total entrainment.

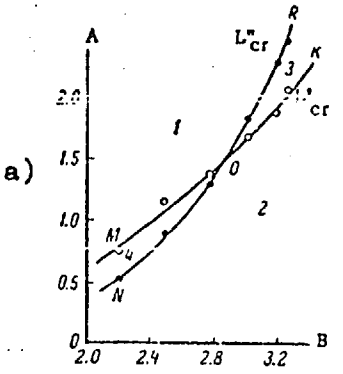

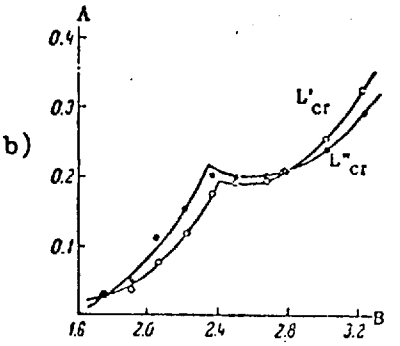

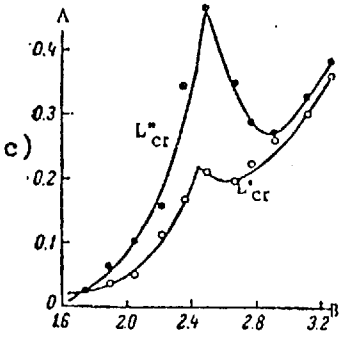

Fig.2.11.-Stability limits of the froth and spray regimes.
A. Critical liquid flow rate,
B. Air velocity.

a) D_c=600mm, water
b) D_c=142mm, water
c) D_c=142mm, aqueous glycerol solution.

L'_{cr} critical liquid rate for the transition froth-spray.

L''_{cr} critical liquid rate for the transition spray-froth.

When an aqueous solution of glycerol (viscosity about 6 times the viscosity of water and lower surface tension) was used, under otherwise constant conditions (Figure 2.11c), the spray regime remained much more stable and the instability region vanishes completely. At the same time, the transition from froth to spray was almost the same, so that the hysteresis gap was considerably increased (Figures 2.11b & 2.11c).

Note: Similar phenomena are also present in liquid-liquid systems. The occurrence of hysteresis phenomena associated with the existence of two different steady states have been described by Luhning and Sawistowski[28] in the case of liquid-liquid extraction.

In the case of equilibrated phases and moderate values of interfacial area it can be expected that dispersed phases of volume fraction about 0.6 can be stable since a potential barrier for inversion has to be attained. The volume fraction of dispersed phase can be made considerably higher than 0.6 by the presence of a solute in equilibrium decreasing interfacial tension. Low values of interfacial tension increase stability by allowing deformation to occur and hence producing a closer packed assembly of dispersed phase. The presence of mass transfer helps to create an "activated state" decreasing the potential barrier necessary for inversion, i.e., acting as a catalyst for phase inversion. This case can be considered very similar to the hysteresis phenomenon described on sieve plates by assuming the analogy between "too high hold-up of liquid" and "too high volume fraction of dispersed phase".

Prediction of occurrence of oscillations

A theoretical model presented by Hinze,[19] is considered consisting of a gas-agitated liquid layer on a horizontal sieve plate. The flow is assumed two-dimensional, and some simplifying assumptions are made. It is found that neutral and amplified oscillations can only occur in distinct regions of the wavelength range. The neutral stability was found to exist for wave lengths

$$N_1 = 2\left(1 - \frac{2(C_O A_f)^2}{(1 - \overline{F}_L)}\right)$$

and

$$N_2 = 2$$

with growth occurring for wave numbers $N_1 < N < N_2$, where:

A_f is the fractional free area of the sieve plate (-),

C_O is the orifice coefficient (-),

$\overline{F}_L$ is the mean liquid fraction by volume (-),

N is the wave number = $2\pi h_d/\lambda$ (-),

h_d is the mean dispersion height (m), and

λ is the wave length (m).

The encountered wave lengths are primarily determined by geometry. The hydrodynamic similarity, for the case of no cross flow of liquid is obtained with equal Froude numbers, as can be found by generalizing the results of Hinze for geometrically similar situations.[20]

Recently, Biddulph and Stephens,[11] reported that using as a basis the comprehensive theory of Hinze with some modifications, they were able to

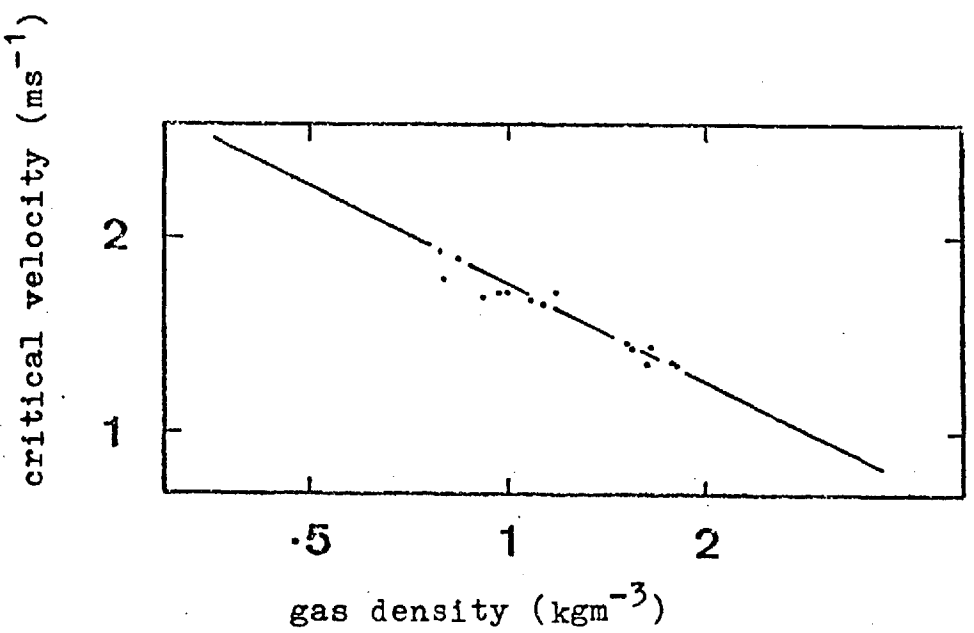

Fig.2.12.-Dependence of critical velocity for full wave oscillation on gas density.

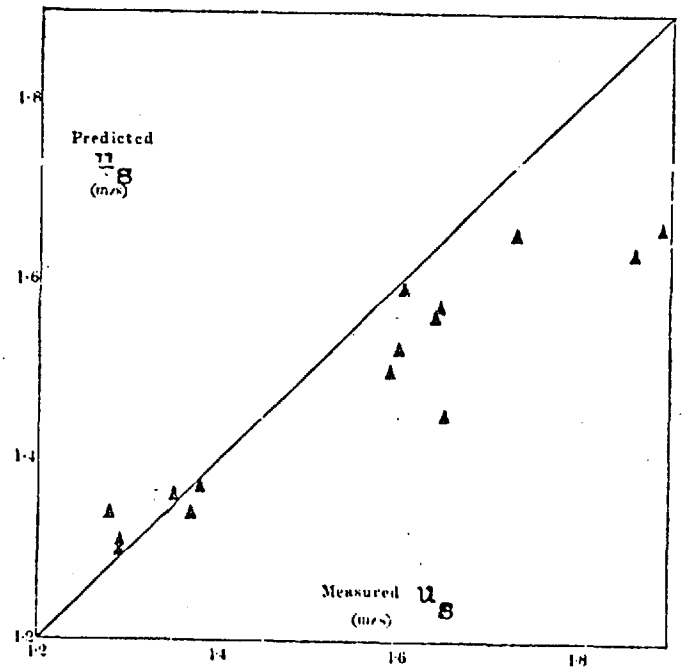

Fig.2.13.-Measured critical velocities for full wave oscillation compared with predicted values.[12]

develop a dimensionless number which should have critical values corresponding to full wave and half wave oscillations. The group is defined as

$$B_S = \frac{u_S \varepsilon h_d \rho_G}{g D^3 \rho_L \bar{F}_L}$$

where:

B_S is a dimensionless group,

D is the column diameter (m),

$\bar{F}_L$ is the mean liquid fraction (-),

g is the gravitational acceleration ($m\,s^{-2}$),

h_d is the mean dispersion height (m),

u_S is the superficial gas velocity ($m\,s^{-1}$)

ε is the eddy kinematic viscosity ($m^2\,s^{-1}$),

ρ_G, ρ_L are respectively gas and liquid density ($kg\,m^{-3}$).

For the system air-water it was found that when $B_S = 0.5 \times 10^{-5}$ full-wave oscillation is initiated and continues until, with increasing vapour rate, $B_S = 2.5 \times 10^{-5}$. At this condition half wave oscillation sets in.

However, if the Froude number is to be important, the product $u_S\sqrt{\rho_G}$ should appear, as is usually the case for two-phase phenomena, instead of the product $u_S\rho_G$ contained in the definition of B_S. In fact, when Biddulph's results from a later paper[12] are plotted on log-log paper (Figure 2.12) it is found that the transition velocity is inversely proportional to $\sqrt{\rho_G}$ and not to ρ_G. The validity of the criterion is therefore doubtful (Figure 2.13) and it needs re-examination.

Prevention of oscillations

When the hold-up on a plate builds up above a certain value and the system goes into the metastable state, periodic oscillations can appear due to the condition of overstability. If this happens, oscillations can be eliminated by reducing the restoring forces (responsible for the overstability). Biddulph *et al.*[12] managed to cut out full wave oscillations completely by a very effective and simple device based on the above mentioned principle. Single vertical expanded metal baffles installed along the nodal lines introduced a large damping effect on the horizontal component of froth velocity and that is usually large enough to suppress oscillations (by dissipation of energy of the restoring forces). A solid baffle is not desirable since this merely provides another wall for reflection of waves, with the likelihood of initiation of oscillations on both sides of the baffle.

2.1.4 Modelling

2.1.4.1 Regimes of continuous liquid phase

(i) Modelling based on the calculus of variations

Azbel,[21] Kim[22] and Takahashi[23] have shown theoretically that in the case of a one-dimensional model, the gas void fraction on a perforated plate is a function of the Froude number (based on the clear liquid height) and of the clear liquid height. They based their considerations on assuming spherical bubbles (Azbel), elliptical bubbles (Kim) or spherical-cap bubbles (Takahashi). On making the assumptions that:

(1) the energy of the dispersion consists of the sum of potential energy, kinetic energy and surface energy;

(2) the gas-liquid dispersion is stable for minimum of total energy;

(3) the liquid hold-up is a constant;

(4) the gas void fraction is unity at the top of the froth layer,

the following equations were obtained:

$$\varepsilon(z) = \sqrt{\frac{b\ Fr}{4\{(\sqrt{b\ Fr} + \frac{b\ Fr}{4} + 1) - \frac{z}{H_L}\}}}, \qquad (1)$$

where:

b = 1 according to Azbel,

$b = \frac{86}{5}$ according to Takahashi and

Fr = Froude number = $\frac{u_S^2}{gH_L}$,

g = gravitational acceleration (m s^{-2}),

H_L = hold-up (m),

u_S = superficial gas velocity (m s^{-1}),

z = height above plate (m),

ε = gas void fraction (-).

Taking $z = h_d$ (height of the dispersion) and $\varepsilon = 1$, equation (1) becomes:

$$h_d = H_L(1 + \sqrt{b\ Fr}), \tag{2}$$

and then the mean dispersion density, $\overline{F}_L$, and the mean gas void fraction, $\overline{\varepsilon}$, are respectively:

$$\overline{F}_L = \frac{1}{1 + \sqrt{b\ Fr}}, \tag{3}$$

$$\overline{\varepsilon} = \frac{\sqrt{b\ Fr}}{1 + \sqrt{b\ Fr}}. \tag{4}$$

Dividing equation (4) by equation (3) results in

$$\frac{\overline{\varepsilon}}{\overline{F}_L} = \sqrt{b\ Fr}. \tag{5}$$

Kim obtained:

$$\overline{F}_L = \frac{1}{1 + \sqrt[3]{\frac{\rho_\ell^2}{2\rho_m^2}}\ Fr} \tag{6}$$

and:

$$\frac{\overline{\varepsilon}}{\overline{F}_L} = \sqrt[3]{\frac{\rho_\ell^2}{2\rho_m^2}}\ Fr, \tag{7}$$

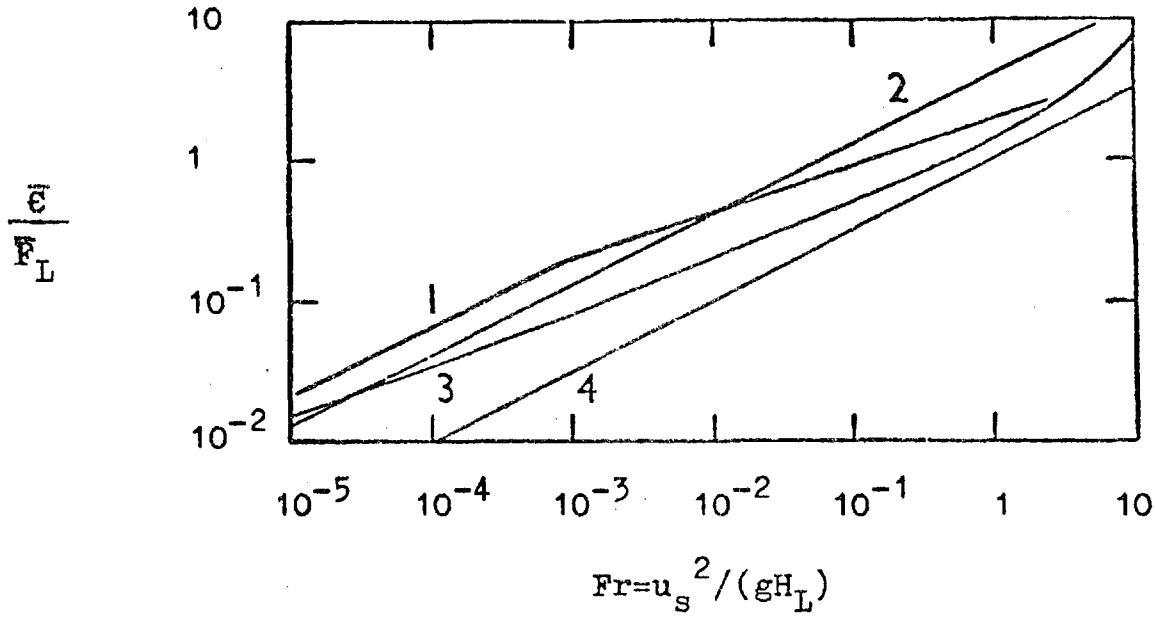

Fig.2.14.-Fractional gas-liquid ratio versus Froude number.

1 Experimental curve,
2,3,4 Theoretical correlations, respectively of Takahashi, Kim and Azbel.

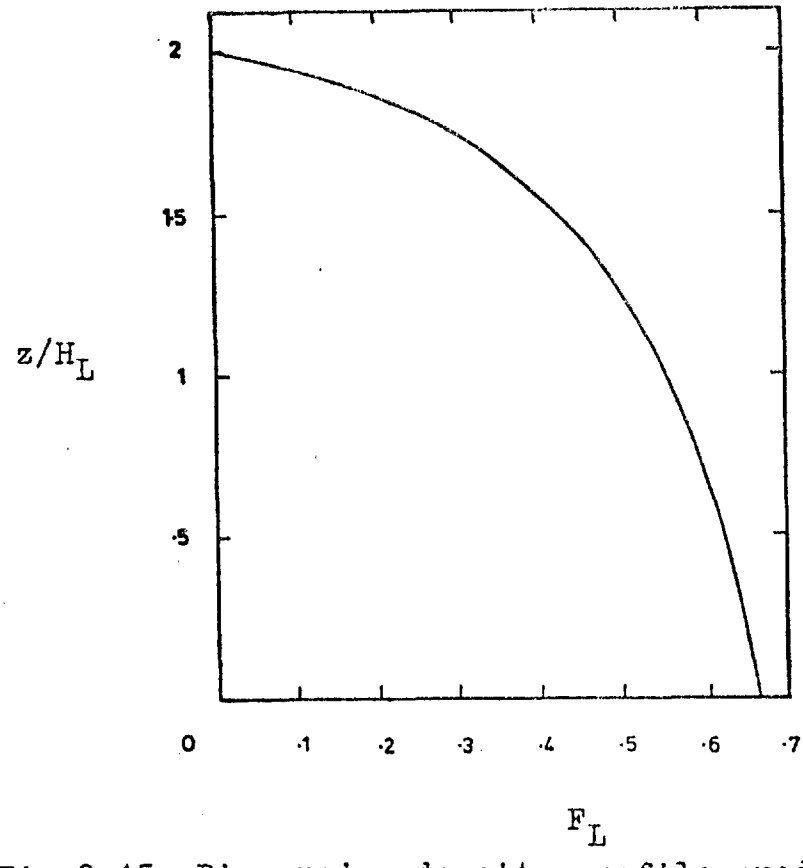

Fig.2.15.-Dispersion density profile predict by equation (1).

where:

$$\rho_m = \rho_\ell \left(1 + \frac{Fr}{6} + \sqrt[3]{\frac{Fr/2 + Fr^2/6 + Fr^3/108 + \sqrt{Fr^2/4 + Fr^3/54}}{2}} + \right.$$

$$\left. + \sqrt[3]{\frac{Fr/2 + Fr^2/6 + Fr^3/108 - \sqrt{Fr^2/4 + Fr^3/54}}{2}} \right)^{-1} , \qquad (8)$$

and:

$$\rho_\ell = \text{liquid density (Kg m}^{-3}\text{)}.$$

In Figure 2.14 these results can be compared with the "best" correlation of experimental results,[24] obtained for the air-water system:

$$\frac{\bar{\varepsilon}}{\bar{F}_L} = \sqrt{42.25\ Fr} \qquad \text{for } 10^{-5} < Fr \leq 8.5 \times 10^{-4} \qquad (9)$$

and:

$$\frac{\bar{\varepsilon}}{\bar{F}_L} = \sqrt[3]{8\ Fr} \qquad \text{for } 8.5 \times 10^{-4} < Fr < 1. \qquad (10)$$

The assumptions of Takahashi, Kim and Azbel that under steady-state conditions such a system of minimum energy will be formed on the plate is physically not substantiated. Furthermore, the type of dispersion density profile deduced by equation (1) (Figure 2.15) is not found experimentally, although it may be approximated by the experimental profiles found in the froth regime. Kolář[25,26] assumed that the dispersion is approximately homogeneous in any horizontal plane, i.e. in a quasi-stationary state the properties of the dispersion are only a function of the vertical distance from the plate. The starting point of his theoretical analysis was the

condition of minimum energy dissipation. This led him to a relation between the distance above the plate and the gas void fraction of the dispersion. With the aid of balances of forces and momentum this relation was transformed into a dependence of the pressure drop on the distance above the plate. The correlations arrived at were:

$$\frac{z}{H_L} = [\varepsilon_o/(1-\varepsilon_o)]\{(\varepsilon-\varepsilon_o)/\varepsilon\varepsilon_o + \ln[(1-\varepsilon_o)\varepsilon/(1-\varepsilon)\varepsilon_o]\} \tag{11}$$

and

$$\frac{z}{H_L} = \left[\frac{\varepsilon_o}{1-\varepsilon_o}\right]\left[(p_o-p)(1-\varepsilon_o)/(p_o-p_H)\varepsilon_o + \ln\frac{p_o-p_H}{p-p_H}\right] \tag{12}$$

where

$$\varepsilon = \varepsilon_o \text{ and } p = p_o \text{ for } z = 0$$

and:

$$\varepsilon = 1 \text{ and } p = p_H \text{ for } z = H$$

are the boundary conditions used by the author, and

H = height of the system given by the distance between the plates (m),

H_L = hold-up (m),

p = pressure ($N\ m^{-2}$),

z = height above plate (m),

ε = gas void fraction.

Experimentally Červenka and Kolář[27] found that

$$\varepsilon_o = 0.824 \exp\left(-3.6\, H_L^{1/2} u_S^{-1/4}\right) \qquad (13)$$

and almost 90% of the ε_o values are said to differ from the computed values by less than 10%. The value of ε corresponding to the experimental heights of dispersion was supposed to be a constant value close to unity. The optimum value for closest fit of the experimental data was 0.975. The visually observed height of the dispersion thus represents the distance from the plate where the gas void fraction reaches 0.975. Almost 90% of the experimental values of the height of the dispersion differ from the computed values by less than 15%.

The one-dimensional model of the structure of the gas-liquid dispersion due to Kolář[26] had been tested by Čermák and Rosenbaum[28] using a method based on electrical conductivity. A very good agreement of the experimental data with those given by equation (11) under the cellular foam regime and on transition to the adjoining regimes was found. The fact that in some experiments, particularly those with moving froth and in the so-called oscillatory regime, good agreement between experimental and fitted data was not achieved over the whole range of heights of dispersion, led them to introduce another parameter into equation (11), which thus became

$$\frac{z}{H_L} = \left(\frac{\varepsilon_o}{1-\varepsilon_o}\right)\left[\frac{\varepsilon-\varepsilon_o}{\varepsilon\varepsilon_o} + \ln\left(\frac{(1-\varepsilon_o)\varepsilon}{(1-\varepsilon)\varepsilon_o}\right)\right] + \kappa\,. \qquad (14)$$

Physically this approach may be interpreted as a boundary below which the simplifying assumptions of Kolář's model are not met (such as the effect of the presence of plate). This approach provided a better fit in the above-mentioned cases for a narrower range of z (the upper part of the dispersion).

The average value of κ for the moving froth regime is $0.28 \frac{h_d}{H_L}$ and for the oscillatory regime it is $0.35 \frac{h_d}{H_L}$.

Examples of density profiles deduced by equation (11) are presented in Figure 2.16. The shapes of these profiles are similar to the experimental ones in the froth and foam regime neglecting, of course, the contribution of the pool of liquid near the plate floor. This equation has been recently applied by Steiner *et al.*[61] to dispersion profiles measured by a γ-ray absorption technique. Good agreement between experiment and theory is found for cellular foams. For froths reasonable agreement is reported above the pool of liquid.

(ii) Modelling of the free bubbling regime

Ho *et al.*[6] proposed a correlation for the relation of the void fraction, $\bar{\varepsilon}$, on velocity, u_S, in the free bubbling regime. This correlation is:

$$u_S = 0.36 \frac{\bar{\varepsilon}(1 - \bar{\varepsilon})\{\gamma g(\rho_\ell - \rho_g)\}^{1/4}}{\rho_\ell^{1/2}} \qquad (15)$$

where:

g = gravitational acceleration (9.81 m s^{-2}),

u_S = superficial gas velocity (m s^{-1}),

ρ_ℓ = liquid density (Kg m^{-3}),

ρ_g = gas density (kg m^{-3}), and

γ = surface tension (N m^{-1}).

This relation is not a function of the liquid hold-up, H_L.

A more fundamental approach to the modelling of the free bubbling regime has to be based on the mechanism of bubble formation and on the

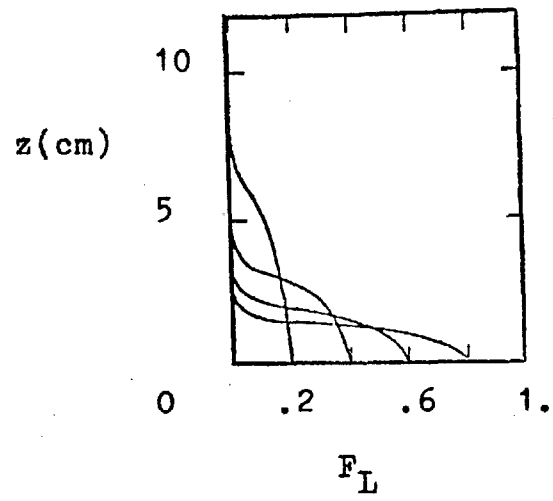

Fig.2.16.-Dispersion density profiles predicted by equation (11).

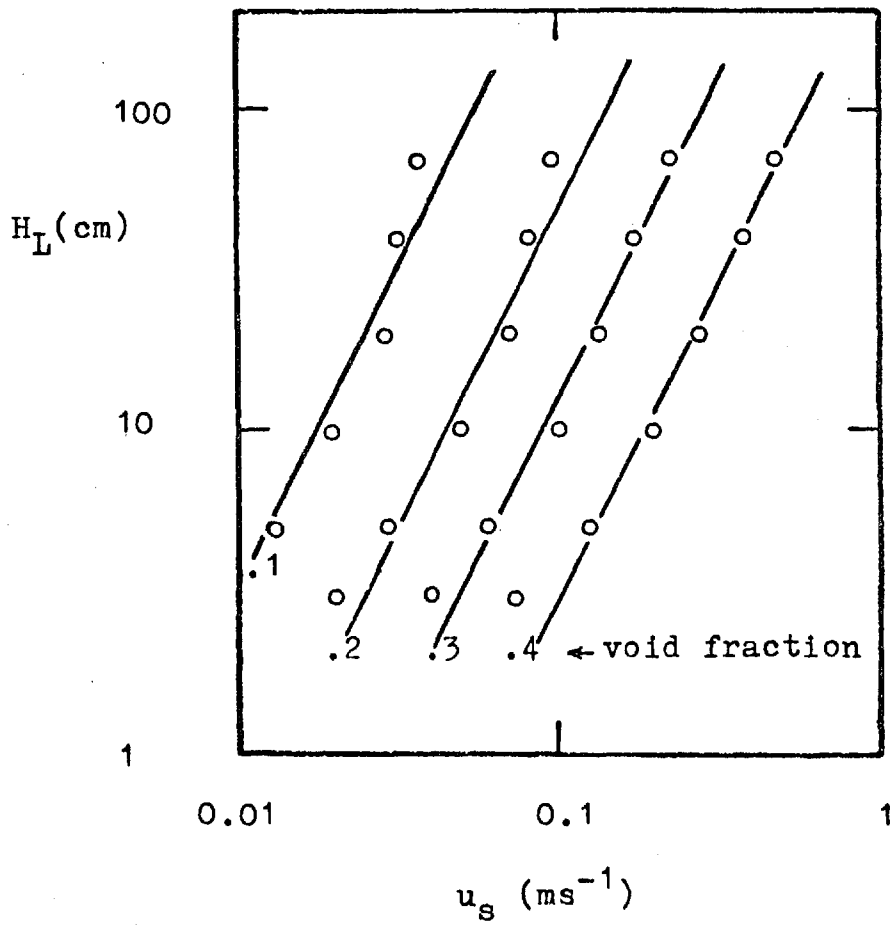

Fig.2.17.- Variation of hold-up, H_L, with superficial gas velocity, u_s, and void fraction, as parameter.

velocity of swarms of bubbles. Some promising results have been obtained in this field.[29-33] However, this regime is not usually encountered in the operation of sieve plates.

(iii) Modelling of the cellular foam regime

For the cellular foam regime the model of Ho *et al.*[6,34] has been developed based on equating the upward flow of liquid due to the upward flow of gas with the downward flow of liquid in the plateau borders of the cellular foam. The derived relation is:

$$u_S = 1.71 \times 10^{-3} \left(\frac{d}{\kappa}\right)^2 \frac{\rho_L g}{\mu_L} \bar{\varepsilon}^2 (1 - \bar{\varepsilon}) \qquad (16)$$

where:

d = volume average diameter of bubbles (m),

κ = constant,

μ_L = viscosity of liquid (Ns m^{-2}),

and the other symbols have the previously defined meaning.

Ho and Prince[34] found for κ the value 0.81, but Hartland and Barber[35] reworking equation (16) and assuming that:

(i) the only liquid carried upwards is in the films,

(ii) any flow due to transport of the borders upwards can be neglected,

showed that κ is always greater than one.

In fact κ is defined by:

$$\kappa = 1 + \varepsilon_f/\varepsilon_b \ , \qquad (17)$$

where:

ε_f = liquid hold-up fraction in the films,

ε_b = liquid hold-up fraction in the borders.

Values of κ were calculated from equation (16) using the data of Ho and Prince,[34] Calderbank and Moo-Young[36] and Rennie and Smith.[37] As expected all were greater than one and the mean value was 1.39.

The approach to bubble formation proposed by Kumar *et al.*[32,33] can be used to predict the diameter of the bubbles.

(iv) Modelling of the froth regime

For the froth regime there exists no satisfactory model. However the equation of Davidson *et al.*[38] for slug flow:

$$u_S = \frac{\bar{\varepsilon}}{1 - 1.2\,\bar{\varepsilon}}\ 0.35\ \sqrt{gD} \qquad (18)$$

can be used[6] on the condition that the diameter of the column is taken for D if it is not greater than 0.1 m - the limit-size for stability of slugs[39] (Ellis *et al.*[39] have also verified that the voidage is independent of the diameter of the column for columns larger than 0.1 m). For larger columns it seems to be better to take D = 0.1 m.

According to eqn. (18) the relation between u_S and $\bar{\varepsilon}$ is not a function of H_L. This is contrary to the previous models of Azbel,[21] Kim[22] and Takahashi[23] which predict a dependence on Froude number $(\frac{u_S^2}{gH_L})$ and hence on H_L. Actually Figure 2.17, which was drawn from the experimental results of Takahashi,[24] indicates that for H_L between 5 and 40 cm the dependence of ε on H_L is as predicted by the Froude number dependence.

For higher values of H_L, it becomes more dependent on H_L and probably also on geometric factors.

4.1.4.2. Modelling of the spray regime

(i) Formation of drops

Two models have been proposed of the nature of spray above a sieve plate: the fluidization model[6,40,41] and the free trajectory model[1] due to Fane and Sawistowski. In the fluidization model it is assumed that a fluidized gas-liquid bed starts forming above a certain local gas velocity. This is accompanied by a considerable increase in the residence time of drops in the dispersion and hence a significant shift of liquid hold-up from the froth to the spray. In the free-trajectory model it is assumed that the drops are formed at the holes and possess a normal trajectory of an object moving through a gaseous medium with a certain initial projection velocity. There is experimental evidence[3] to substantiate the free trajectory model, so that attention will only be focused on aspects relevant to this model.

The modelling of the spray regime has consequently to be based on the mechanism of drop formation and momentum transfer between gas and liquid to project the drops upwards. Subsequently the equation of motion of drops can be applied and solved.

(ii) Mechanisms for drop formation

Several mechanisms for drop formation have been observed. Newitt *et al.*,[42] as well as Gleim *et al.*[43] have studied drops produced by bursting of single bubbles which rise to the surface of a liquid. After some drainage, the liquid film ruptures in many places simultaneously. The holes in the film grow quickly until the liquid film is no longer

continuous. The remaining liquid of the film coalesces into several droplets with diameters between 10 and 100 μm. By another mechanism bubbles also cause the formation of much larger drops. When the thin liquid forming the upper half of the bubble disintegrates, the remaining crater is filled in with liquid by a wavelike motion of the surface of the liquid surrounding the crater. The motion of the undulations produces a vertical rise of a filament of liquid from the centre of the crater. The filament breaks up by Rayleigh's[44] instability. The diameters of these drops can vary from 100 to 3000 μm or even more.

Another mechanism was observed by Teller,[45] at velocities high enough to permit a continuous passage of vapour without individual bubble formation. Under these conditions the principal forces are the surface tension and the inertia forces of gas, so that the drops formed by this mechanism are expected to have the size given by:

$$d_p \propto \frac{\gamma}{\rho_G u_G^2} \tag{19}$$

To compute the projection velocity of these drops the expression

$$u_p \propto \frac{(u_G^2 \gamma_G)^{3/2}}{\rho_L (g\gamma)^{1/2}} \tag{20}$$

was proposed by Jerónimo and Sawistowki.[46] However these are not the only drops formed in the spray regime. Fane, Lindsey and Sawistowski[3] observed large drops formed from break-up of ligaments by unstable long waves. These drops have a diameter proportional to the diameter of the ligament from which they result and their projection velocity is equal to the velocity of the ligament at the moment of break-up. The investigation was conducted by still and ciné photography. According to photographic evidence from single-hole experiments, the mechanism of drop

formation takes the form of a cyclic process consisting of bubble growth at the hole, rupture of bubble top accompanied by the formation of fine drops, break-up of the resulting cylindrical liquid sheet into almost vertical ligaments and the break-up of the ligaments into relatively large drops. Within the range of hole velocities and liquid submergencies employed no evidence was found of continuous jetting. At the transition point, the hole was jetting for 70% of the time and bubbling through the remaining 30%.[47] (Azbel[48] theoretically predicts the impossibility of a continuous jet under the conditions usually used in practice, but continuous jetting was described by Prince *et al.*[31] on the evidence of their two-dimensional experiments and the same was assumed by Nielsen[49] in his model of drop formation). On multi-orifice plates the cyclic nature of the process was observed to be retained but, on account of bubble interaction and smaller fluctuation in chamber pressure below the plate, the frequency of bubble formation was increased. Since, in addition, the cyclic processes occurring at different holes were shifted in phase, the individual stages of drop formation were less pronounced. No evidence has been found for the existence of a fluidized bed of liquid drops. On the contrary well defined trajectories of drops have been recorded.

Nielsen[49] proposed a model to predict the projection velocity based on the momentum exchange between gas and liquid, prior to sheet break-up. The distance before break-up was known from photographic observation so that an effective friction factor could be determined to give good agreement between theory and experiment. For the system air-water this friction factor was found to be equal to 10, a value considered unrealistic by Pinczewski and Fell.[50] In fact, for similar conditions Levich[51] suggested a value of 10^{-2}. According to Pinczewski and Fell, Nielsen *et al.*[49] have failed to account for a major portion of the total momentum transfer by

making no allowance for momentum transfer after sheet rupture. Pinczewski and Fell introduced therefore a new parameter - the duration of the vapour rush. It is suggested by Jerónimo and Sawistowski[46] that this model can explain the upper envelope of projection velocities of drops in the spray regime.

Another mechanism of disintegration of drops was described by Lane[52] on the basis of the Weber number. Eisenklam[53] found for the critical Weber number a value of 14 in the case of inviscid fluids and 20 for highly viscous cases. In spray regime this mechanism is believed to occur (and if so) only near the plate floor where gas velocity is highest.

A complete description of the phenomenon of drop formation is not, as yet, possible because of the complexity of the process and because the interaction between the pool of liquid on the plate floor and the adjacent jets issuing from surrounding orifices is not fully understood. However for a single jet Chawla's[54] study seems to be an approach worth following.

(iii) Dimensional analysis approach to phenomena of drop formation

Formation of drops in the spray regime by the break-up of cylindrical jets is a very simplified picture of actual conditions. In fact, drops can be and are formed by the action of a gas stream on a mass of liquid of any arbitrary shape. A general investigation of this phenomenon can be conducted by applying dimensional analysis concepts to the Navier-Stokes equation.

The Navier-Stokes equation can be written as

$$\rho \frac{d\underline{v}}{dt} = - \text{grad } p + \mu \Delta \underline{v} + \underline{f} \qquad (21)$$

Assume some disturbance on the interface. Gas velocity over the crest of a protuberance increases due to the resulting decrease in cross section, so by the Bernoulli equation, the gas pressure there becomes less than the average pressure, while at the base of the protuberance the pressure is higher than its average value. Therefore, the protuberance which has been formed somehow on the liquid surface tends to increase. The higher the relative velocity between the gas and the liquid, the more pronounced is this effect. An increase in the size of the protuberance on the liquid surface results in detachment of drops from the surface.

To analyse the order of magnitude of the different terms of the Navier-Stokes equation, $\underline{a}$ and $\underline{T}$ have been chosen as the characteristic dimension and the period of this motion, respectively. This gives:

1st term: $$O[\rho \frac{d\underline{v}}{dt}] = \rho \frac{v}{T} = \rho \frac{a}{T^2} \tag{22}$$

2nd term: $$O[\text{grad } p] = \frac{p_\gamma + p_G}{a}, \tag{23}$$

with $$\frac{p_\gamma}{a} \sim \frac{\gamma}{a^2} \tag{24}$$

and $$\frac{p_G}{a} \sim \frac{\rho_G u_G^2}{a} \tag{25}$$

3rd term: $$O[\mu \Delta \underline{v}] = \mu \frac{v}{a^2} = \frac{\mu}{aT} \tag{26}$$

4th term: $$O[\underline{f}] = \begin{pmatrix} 0 \\ \rho g \end{pmatrix}, \quad \text{usually negligible}$$

$$\text{as } a << \frac{\rho_G u_G^2}{\rho g} \tag{27}$$

For the second term there are two limiting cases:

(a) $p_\gamma >> p_G$ and (b) $p_\gamma << p_G$. Hence

A - Aerodynamic effect negligible

In this case $p_\gamma >> p_G$.

A1 - Low viscosity liquid

For such a case $\frac{\rho a}{T^2} \sim \frac{\gamma}{a^2}$, so that $T \sim \sqrt{\frac{a^3\rho}{\gamma}}$ (28)

For the viscous effect to be considered negligible it is necessary that

$$\frac{\mu}{aT} << \frac{\gamma}{a^2} \quad \text{which with (28) gives}$$

$$\frac{\mu}{\sqrt{\rho a \gamma}} << 1 \tag{29}$$

This condition is applicable to water when

$$a >> 10^{-6} \text{ cm} \tag{30}$$

A2 - High viscosity liquid

If inequality (29) is reversed, the inertia term can be neglected and

$$\frac{\mu}{aT} \sim \frac{\gamma}{a^2} \quad \text{or} \quad T \sim \frac{\mu a}{\gamma} \tag{31}$$

B - Aerodynamic effect important

For this case $p_G >> p_\gamma$

B1 - Low viscosity liquid

$$\frac{\rho a}{T^2} \sim \frac{\rho_G u_G^2}{a} \quad \text{or} \quad T \sim \frac{a}{u_G}\sqrt{\frac{\rho}{\rho_G}} \tag{32}$$

Hence

$$\frac{\mu}{aT} << \frac{\rho_G u_G^2}{a} \quad \text{which with (32) gives}$$

$$\frac{\mu}{a u_G \sqrt{\rho \rho_G}} << 1 \tag{33}$$

For air-water $au_G >> 0.3\ cm^2\ s^{-1}$ and, as u_G has to be high enough for $p_G >> p_\gamma$, water can almost always be considered as a low viscosity liquid.

B2 - High viscosity liquid

As with case A2, the inertia term can be neglected so that

$$\frac{\mu}{aT} \sim \frac{\rho_G u_G^2}{a} \quad \text{or} \quad T \sim \frac{\mu}{\rho_G u_G^2} \tag{34}$$

C - Comparison with results obtained for cylindrical jets

A) For cylindrical jets,[55] when $p_\gamma >> p_G$,

$$\frac{L}{D} = 12[We^{1/2} + 3\frac{We}{Re}] \tag{35}$$

with: L = length to break-up,

D = 2a

$$We = \frac{\rho D \bar{u}^2}{\gamma}$$

$$Re = \frac{\rho D \bar{u}}{\mu}$$

For constant velocity the time for break-up is:

$$t_b = \frac{L}{\bar{u}} \text{ so that}$$

$$t_b = 24a\left[\left(\frac{2\rho a}{\gamma}\right)^{1/2} + \frac{3\mu}{\gamma}\right] \tag{36}$$

Comparing this with (28) and (31) the proportionality constants become $24\sqrt{2}$ and 72 respectively if $\underline{a}$ is taken as the radius of the jet and $\underline{T}$ as the time for jet break-up. The diameter of the drops is related to the radius of the jet by

$$d_p = 3.8a \tag{37}$$

B) In the case of cylindrical jets when aerodynamic effect is important and liquid viscosity is low it is necessary to differentiate between the cases of long and short waves. The times necessary for atomization of the entire mass of the jet and for break-up of the jet into large drops are of same order of magnitude[125] and given by (32). However, while the diameter of the drops resulting from short waves is independent of a:

$$d_p \simeq \frac{\gamma}{\rho_G u_G^2} \tag{38}$$

the diameter of the drops formed from long waves is given by (37).

For the case B2 it seems that the time for total break-up of the jet is given by (34) with the numerical coefficient equal to five.[125]

A1 and B 1 are the most important cases in the spray regime. As an immediate and important conclusion one can expect that the size of large drops will not be affected by surface tension, but by the geometry of plate. Conversely, the size of small drops will not be affected by geometry but by surface tension. In fact, in case B1, equation (38), represents equilibrium between surface tension forces and forces acting in the liquid as a result of depression caused by the velocity increase over the crests and flow separation (Figure 2.18).

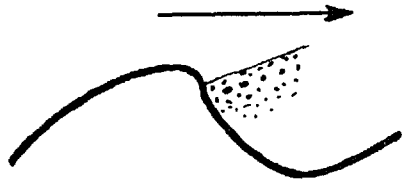

Fig.2.18.- Flow separation producing atomization.

(iv) Movement of drops

Once the drops are formed with a certain initial velocity they will move according to Newton's law. The drag force acting on them is difficult to predict accurately, since it is a function of relative velocity of drops and the surrounding gas, of the acceleration, size and shape of the drop, of the physical properties of the two phases, and of spatial concentration of drops. Additionally a drag reduction effect is experienced by drops which find themselves in the wake of a preceding drop and a drag increase is induced by adsorption of insoluble tensio-active agents. The last two effects will however not be considered here.

From the above considerations dimensional analysis gives

$$c_D = \phi(Re, Su, Ac, \frac{\rho_o}{\rho_i}, \frac{\mu_o}{\mu_i}, \varepsilon) \qquad (39)$$

where:

$$C_D = \frac{\text{Drag}}{\text{frontal area.} \dfrac{\rho_o v_R^2}{2}} \tag{40}$$

$$Re = \frac{dv_R\rho_o}{\mu_o}, \qquad Su = \frac{\gamma d\rho_o}{\mu_o^2}, \qquad Ac = \frac{d}{v^2}\frac{dv}{dt}$$

The effect of acceleration can be very considerable with bubbles but it is believed to be very small with drops in gases, since ρ_i/ρ_o is very large. The effect of the group μ_o/μ_i can also be neglected. Then

$$C_D = \phi(Re, Su, \varepsilon) \tag{41}$$

A solution is known for the case of $\varepsilon = 1$[56,57] and the effect of ε is afterwards taken into consideration.[58] Good reviews on the motion of drops and bubbles are available.[59,60]

(v) Free-trajectory model of the spray regime

Fane and Sawistowski[1] derived the free-trajectory model assuming that a continuously replenished shallow pool of liquid, present on the plate floor, was atomized at a constant rate by high-velocity gas passing through the holes. It was also assumed that there exists a certain distribution of drop sizes, each of them associated with a specific projection velocity and that there was no coalescence or break-up of drops in flight. The equation of motion of drops can be solved and the dispersion density profile determined. This model will be discussed in greater detail in Chapter 4.

2.1.5 The froth-spray transition on sieve plates

2.1.5.1 Definition

The froth-spray transition on sieve plates is, in most cases, not sharp and a definition is therefore required for correlation purposes. Taking into account the use of the plate, such a definition is best considered from the point of view of effectiveness of mass transfer. Thus the transition point corresponds to a condition in which the contribution to the total interfacial area presented by the surface of liquid drops is greater than the simultaneous contribution provided by the surface of gas bubbles.[62] A criterion formulated in such a way is important since plate performance in the froth regime seems to be independent of surface tension,[63-65] but it is supposed to be inversely proportional to surface tension in the spray regime.[1,63,66] The latter effect is mainly the result of the influence of surface tension on the formation of interfacial area.

2.1.5.2 Methods of determination of transition

The pattern of the liquid dispersion density profile is characteristic of the regime of operation of the plate. In the foam regime the liquid fraction decreases steadily with increase in height above the plate floor; in the froth regime there is a region of almost constant liquid fraction; in the spray regime there is a maximum in the profile at a certain height. Thus transition could be defined as the velocity at which maximum in the profile begins to develop. This definition, however, is not very practical.

The criterion of definition of transition as stated initially suffers from the serious disadvantage of difficulty of determination. Methods

have therefore been employed for measurement of parameters, which are associated with the transition and are easily determined experimentally. Two types of parameters can be considered:

(i) parameters which rely on measurement of overall values for the whole plate;

(ii) parameters based on measurement of local values at an individual hole.

Type (i) methods include measurement of entrainment, optical transmittivity of dispersion, pressure drop and analysis of sound. Measurements of frequency of liquid bridging, RMS velocity and pressure drop resulting from pulsation are examples of type (ii) methods.

(i) Methods relying on measurement of overall values

(i.1) Entrainment

The use of entrainment as a criterion for transition was first suggested by Shakhov *et al.*[10] and subsequently also used by Banerjee *et al.*[67,68] and Pinczewski *et al.*[15] Entrainment can be measured by an impingement process on a plate and collection of the liquid or by mass balance of a non-volatile compound added to the liquid flowing down the column. When entrainment is plotted versus gas velocity on log-log paper a change in slope occurs at transition.

(i.2) Optical transmittivity of dispersion

If a light source and a photocell are placed in a plane above the froth, the transition from froth to spray will be accompanied by a decrease in light transmittivity due to scattering of light by drops crossing the light beam. Porter and Wong[40] used this method by adding liquid to a

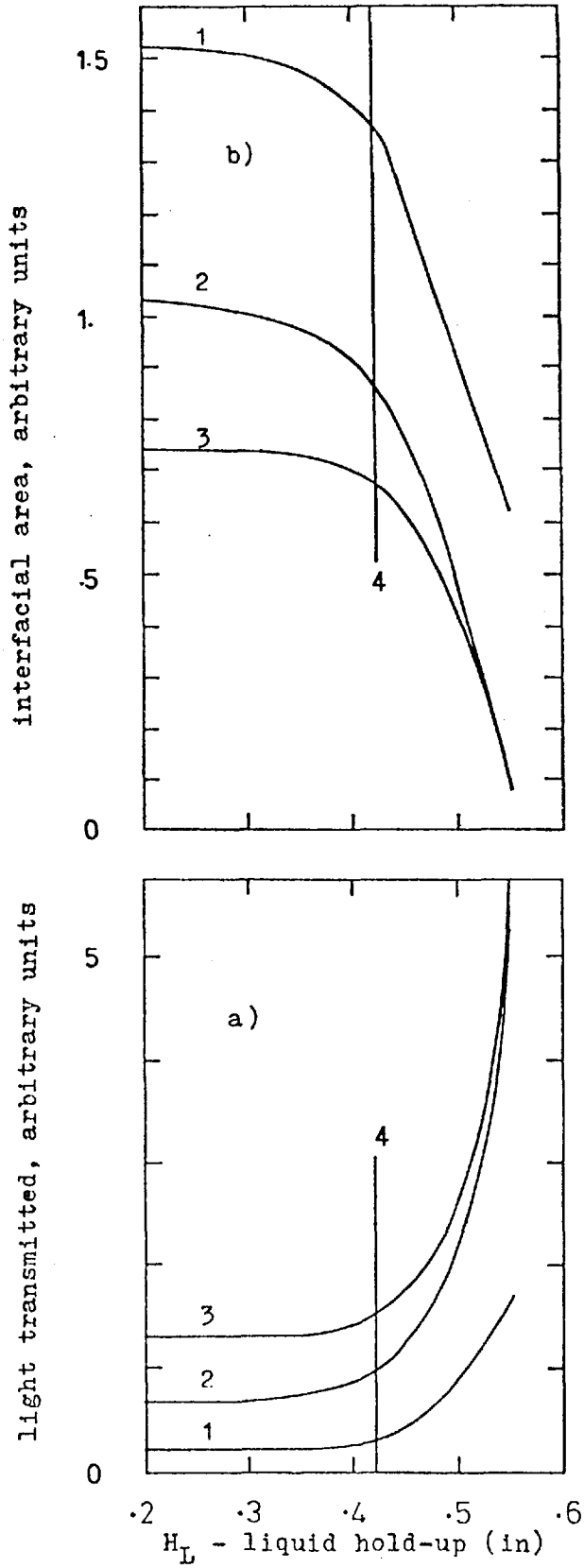

Fig. 2.19.- Variation of optical transmittivity and area of drops with head of liquid on plate at constant hole velocity. 1.-7.5cm; 2.-9cm; 3.-10cm above plate; 4.-Transition taken by Porter and Wong.

static plate (zero liquid flow). Typical results are shown in Figure 2.19(a). The spray-froth transition was taken as the point of increase in the amount of light received by the photocell. If the results are recalculated in terms of the surface area of the drops, Figure 2.19(b) is obtained. From this figure it can be seen that the transition point chosen by the authors corresponds to a condition where the surface area of drops is already very large and this, according to the criterion adopted for definition of transition, corresponds to a point well within the spray regime.

(i.3) Pressure drop

If the pressure drop is plotted versus gas velocity in log-log paper, a change in slope occurs at transition. This method can nevertheless be improved. A study of the residual pressure drop, that is of the difference between the total pressure drop and the sum of the dry pressure drop and the liquid head was conducted by Payne and Prince.[47] The point of transition was taken to correspond to the maximum of the residual pressure drop. Simultaneous measurements of optical transmittivity indicate that the residual pressure drop criterion predicts phase transition at a higher hold-up and thus lower gas velocity than proposed by Porter and Wong.

From ciné observations of a single hole it was found that at the transition, as defined by the maximum in residual pressure drop, the hole was jetting for 70% of the time and bubbling through the remaining 30% (Figure 2.20), that is, just midway through the range of transition depths. This is another indication of the arbitrariness of the point of inversion.

(i.4) Analysis of sound

The pattern of noise generated during the flow of gas through the holes submerged in the liquid changes radically at transition. A microphone can detect the sound generated by the gas and the signal analysed on an oscilloscope (or simply amplified and listened to). The wave patterns produced on the oscilloscope screen at low gas velocities are smooth and have long wave lengths. As the gas velocity through the holes increases, an irregularity in the wave length, as well as in the amplitude, is marked in the transition region of gas velocity. At higher gas velocities, the pattern again attains a uniform amplitude. The results of transition obtained by this method[67-69] agree with those obtained using the residual pressure drop.[47] These results agree also with the maximum in Sauter mean diameter of drops projected above plate and with a change in slope of entrainment results.[67-69]

(ii) Methods relying on local measurement

(ii.1) Liquid bridging at the holes

On inserting an electrical conductivity probe from below the plate into the hole and using a conducting liquid, no current will flow when the tip of the probe is surrounded by gas. Bubbling conditions will therefore result in periodic bridging of the hole with the bridging frequency dropping to zero at steady jetting. This technique was employed by Pinczewski and Fell.[9] It is seen that above a certain gas velocity the bridging frequency started to decrease rapidly, passed through a small local maximum and then decreased again but rather slowly. The authors consider that the point of phase transition corresponds to the appearance of the local maximum. However, these results show that the resistance

probe technique gives a transition which corresponds to the depth at which jetting first falls below 100%, i.e., when the system has just entered the transition region to the froth regime. However if the point where bridging frequency starts to decrease rapidly is taken as the criterion for transition, the result is coincident with that given by the residual pressure drop method.

(ii.2) RMS velocity at the hole

The gas flow through the hole fluctuates when there is liquid on the plate because pulsations of the liquid around the orifice periodically restrict the flow. The pressure drop resulting from a fluctuating gas flow is higher than that from a steady flow.[70] Thus, the orifice pressure drop during bubbling and jetting will be higher than the dry plate pressure drop. Velocity fluctuations within the orifice were measured[47] by inserting there a miniature hot wire anemometer probe. Results showed that the RMS velocity reached a maximum at the transition given by the maximum in residual pressure drop.

(ii.3) Pressure drop at the hole due to pulsation

By the above mentioned results, it was expected that the increase in orifice pressure drop resulting from flow pulsations would be greater at the transition. Actually, at low depths of liquid, the measured pressure drop was almost equal to the dry pressure drop (pressure drop when no liquid was on the plate). When the difference between the actual pressure drop in the presence of liquid and the dry pressure drop is plotted versus liquid depth a maximum appears at the transition as given by methods (i.3) and (ii.2).

2.1.5.3 Comparison of results obtained by the different methods

The methods of entrainment, residual pressure drop, sound analysis, RMS velocity at the holes and pulsation pressure drop give approximately the same result for the froth-spray transition. Hence, they will be considered here as "equivalent" methods. The method of liquid bridging at the holes, as applied by Pinczewski and Fell[9] locates the transition when, according to the other criteria, the system is still in the spray regime. However, if the point where the bridging frequency first begins to fall rapidly (for increasing gas velocity at fixed head of liquid) is taken as the transition point then the result is equivalent to that given by the other above mentioned methods. Although the method of optical transmittivity gives a systematic deviation in the direction towards initial criterion of Pinczewski and Fell, the results obtained are not too far apart from those given by the "equivalent" methods.

The transition obtained by the "equivalent" methods occurs necessarily near the transition, as defined previously on the basis of mass transfer considerations, since the optical transmission method gives a transition for the system just in the spray regime according to the other "equivalent" methods.

It has already been mentioned that the results of Pinczewski for transition correspond to spray conditions, as given by the other methods. Under those conditions the maximum in dispersion density profile is already visible.[15] Hence, a criterion of transition based on the appearance of a local maximum in density profile should also give results close to those of the "equivalent" methods.

Conclusion: If the criterion of transition for the light transmission technique is changed so that transition is located at a point somewhere midway of the sudden increase in transmittivity and if the criterion of frequency of bridging is changed as above mentioned, all transition results will be very similar and will comply approximately with the adopted definition based on the availability of interfacial area for mass transfer.

2.1.5.4 Transition induced by instability of plate operation

Sometimes the transition froth-spray on sieve-plates is very sharp.[10-12] This happens when the regime, which exists before transition takes place, becomes unstable and a critical condition is attained with an exponential growth of the instability. As a result of oscillations in the height of the froth, local points of low depth can occur periodically, inducing there the momentaneous appearance of the spray regime. If the resulting increase in entrainment together with the increase of weeping at other points of bigger depth are large enough to reduce the depth to a value consistent with the existence of the spray regime, then the transition occurs sharply with step changes in entrainment and pressure drop. Otherwise states of stationary oscillation remain. This mechanism is much more complicated than that of the normal inversion and one can deduce the paramount importance of the influence of plate geometry and of stability of flow rates on it. This can explain the obscurity existing around these cases.

2.1.5.5 Transition froth-spray and hydrodynamics of hole operation

The operation of a submerged hole was studied by Muller and Prince.[31] They found that the operation of a hole can be divided into six different regimes. Three are bubbling regimes - the deformed bubble, the perfect bubble and imperfect bubble regimes. The first two correspond to the froth and free bubbling regimes respectively whereas the third one represents a special case of plate behaviour in which bubbles are larger than the liquid depth. The jetting regime was divided into steady jetting and pulsating jetting and these two correspond to the spray regime on sieve plates. A sixth regime is also identified as the regime of meniscus flow and has no counter part in the practical range of operation of a sieve plate.

2.1.5.6 Transition correlations

Various attempts were made to correlate the froth-spray transition. Most of the presented correlations are difficult to employ as they relate the hold-up to the velocity at transition. Thus, they do not allow for an independent determination of the transition point. This applies to the correlations of Porter and Wong,[40] and of Ho *et al.*,[6] both based on fluidized bed considerations, and the graphical correlation of Payne and Prince[47] based on dimensional analysis. However, Jerónimo and Sawistoswki[71] were able to correlate the data of Pinczewski and Fell[9] in terms of hole velocity at transition alone, by utilizing the approach of Kutateladze and Styrikovich.[72] After some rearrangements, Kutateladze equation can be presented in the form:

$$We_t^O = 0.429\ Bo^{1/3} A_f^{-2} \tag{42}$$

Introducing an empirical correction factor, F_c, for crossflow of liquid, the final equation is:

$$We_t = 0.429\ Bo^{1/3} (A_f F_c)^{-2} \tag{43}$$

where We_t is the value of the Weber number at transition, defined by $u_t^2 \rho_G d/\gamma$ and Bo is the Bond number given by $gd^2\Delta\rho/\gamma$. The correction factor is

$$F_c = 1 + 0.000104 L_v^{-0.59} A_f^{-1.79} \tag{44}$$

However, most of the fundamental work on transition was conducted in the absence of mass transfer and its validity under mass transfer conditions has not yet been established.

2.2 Mass Transfer on Plate

2.2.1 General concepts

From the practical point of view, the performance of a given plate can be calculated by comparison with an ideal concept - the ideal stage - by a "black box" relation, that is, ignoring completely what happens on the plate. Theoretically the performance of the plate can be predicted by macroscopic analysis of processes taking place inside the "black box". In the first case the so-called Murphree,[73] Hausen[74] or Standart[75] plate efficiencies are used. In the second case a local efficiency is defined and a relation established between this concept and the mass transfer parameters for different cases of hydrodynamic behaviour of the liquid and gas on plate. Finally the relation between local and plate efficiencies can be obtained for known hydrodynamic conditions.

The column efficiency, that is, the relation between the number of theoretical plates and the actual number of plates can also be obtained. A correction for the effect of entrainment on efficiency[76] can also be considered when necessary. The flux of information can, therefore, be sketched by the diagram:

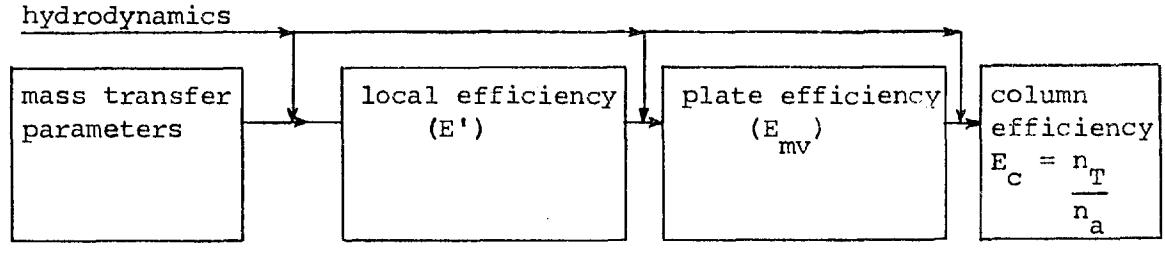

Several models exist for prediction of plate efficiency from mass transfer parameters.

2.2.2 Interaction of mass transfer and hydrodynamics

The process of mass transfer introduces some changes in the hydrodynamics behaviour and consequently affects the mass transfer rate. These changes appear for two different reasons:

(a) Flow velocity across the interface which changes velocity, temperature and concentration profiles.

(b) Heterogeneous mass transfer rates across the interface can produce Marangoni effects[77] - movements of interface which promote changes in interfacial area and introduce or suppress surface renewal phenomena.

At small mass transfer rates the bulk flow is important only in calculating the fluxes of the different species across the interface and changes in profiles are negligible. For higher mass-transfer rates, corrections have to be considered because of the dependence of the velocity, temperature and concentration profiles on the flow velocity through the interface. This effect can be quantified,[78] assuming the validity of one mass transfer theory. However, distillation, absorption and desorption are generally regarded as cases of small mass fluxes, that is flow velocity through the interface is too small to cause appreciable changes in profiles.

At the interface, a condition of balance of forces acting in each phase must be fulfilled. In the absence of mass and heat transfer, these forces include pressure and viscosity terms, and if curvature or deformation of the interface is considerable, also surface tension terms. In the presence of mass (or heat) transfer, another term has to be introduced: the gradient of interfacial tension at the interface induced by the transfer. This gradient of interfacial tension produces interfacial movements from which changes in drag coefficient,[79] interfacial area,[79]

and mass and heat transfer coefficients[80] result. Zuiderweg and Harmens[4] observed for the first time the influence of surface tension gradients on mass transfer in distillation and in absorption. They distinguished three types of systems with respect to the changes in surface tension developing in the reflux flow. The systems were denoted as negative, positive and neutral according to the sign of the "increase" of the surface tension of the reflux flow. It became an accepted fact that in plate-column distillation surface-tension positive systems exhibit higher plate efficiencies than either neutral or negative systems. This was explained in terms of higher interfacial area in the case of positive mixtures resulting from its stabilization by the Marangoni effect. However, the work of Zuiderweg and Harmens was done in the foam regime and applies to columns operating in the foam regime only and as such their findings cannot be used in the spray regime. In the latter regime the effects of gradients of surface tension on the deformation of interfacial area are in fact reversed, as explained by Bainbridge and Sawistowski[66] considering the "necking" stage in the drop formation just prior to its detachment. Fane and Sawistowski[81] confirmed that at higher gas velocities, efficiencies of negative systems could be higher than those of positive systems, for similar values of all the important physical properties. The validity of the "necking" model was also confirmed by Boyles and Ponter[82] in a photographic study of drops formed as a result of a disturbance upon the surface of a negative liquid system. Recently Burkholder and Berg[83] studied the instability and break-up of laminar liquid jets in gaseous surroundings in systems with mass transfer. They found that mass transfer (of a surface tension lowering solute) into the jet is destabilizing and promotes break-up while mass transfer out of the jet is stabilizing (produces longer jets). Surface adsorption, as

reported, may counteract strongly the stabilizing or destabilizing effects of mass transfer although it has a negligible effect on jet stability in the absence of mass transfer.

However, surface tension gradients not only influence the magnitude of the interfacial area but also change the intensity of surface renewal, as was pointed out by Danckwerts, Smith and Sawistowski.[84] More recently, the surface renewal effects were studied by Ellis and Biddulph[85] and by Moens.[86-88] The first systematic experimental study of the surface tension-driven instabilities seems to have been conducted by Block.[89] The first mathematical analysis (for a gas-liquid system) was due to Pearson,[90] whereas Sternling and Scriven[91] considered the case of two liquid phases. Several generalizations of the analysis have been published recently.[92-105]

Chapter Three

EXPERIMENTAL

3.1 Equipment for Absorption and Desorption

Two existing sieve plate columns[2] operating in series made it possible to conduct the operation in closed circuit. This resulted in some advantages concerning the control of flowrates and temperatures and gave results for absorption and desorption at the same time and conditions (such as the state of purity of solutions). The equipment for absorption and desorption is shown in Figure 3.1 and is described in detail by Lindsey.[2] Small modifications included the installation of four storage vessels (QVF, reference V250-12); a temperature control system, consisting of a laboratory contact thermometer, a relay Sunvic type HVR and an on-off magnetic valve from Magnetic Devices Ltd., code No.5ON205 NL1/1 acting on cooled glycol solution fed from a refrigeration unity and the blower B3, Secomak model No.74, 0.65 kW with characteristic curve shown in Figure 3.2.

The columns employed were rectangular in cross-section, 0.11 m by 0.19 m. One column contained two plates 0.53 m apart, the upper plate being the test plate used for dispersion density and specific interfacial area determinations. The other column contained three plates. Each plate had 148 holes, 3 mm in diameter, placed 9.5 mm equilateral triangular pitch. The hole area formed 10% of the active plate area, or 7% of the superficial area of the column. The weir heights were 19 mm and the length of liquid travel 70 mm (Figure 3.3). The liquid-sampling points were placed as shown in Figure 3.1. The sampling was conducted via small coolers through which refrigerated glycol solution was circulated. The gas-sampling points were placed on the walls of the

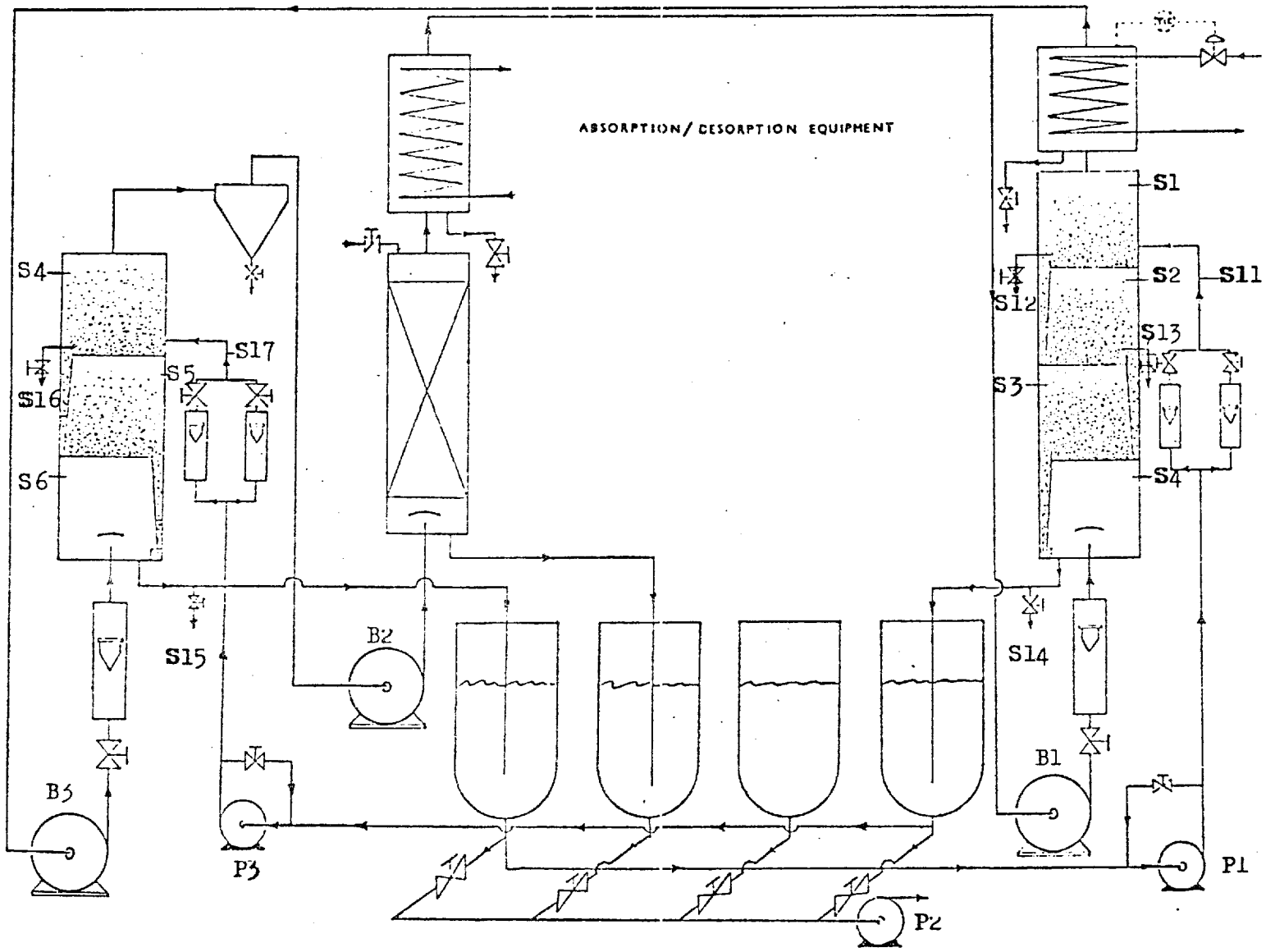

Fig. 3.1.- Line diagram of absorption / desorption equipment.

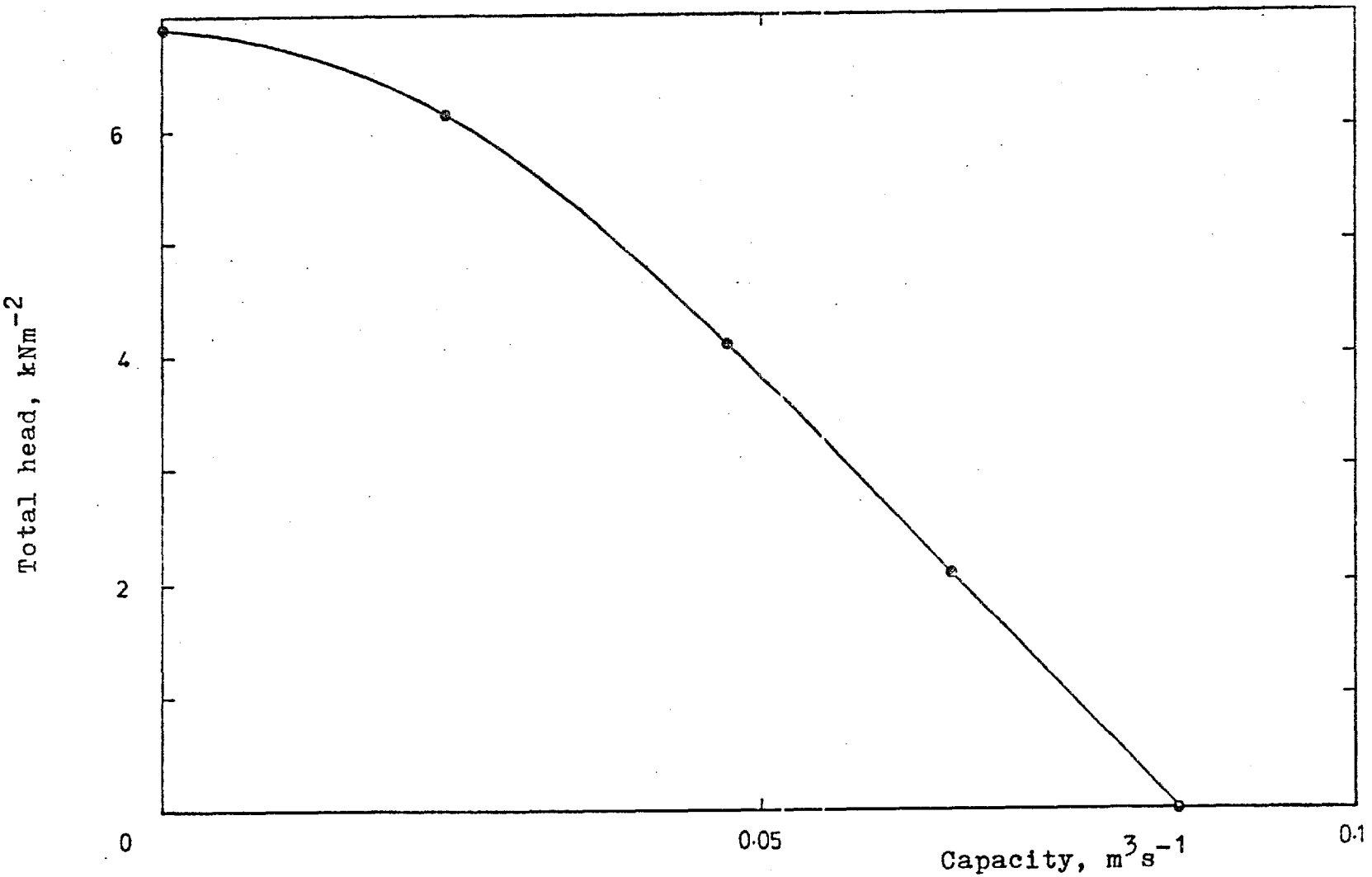

Fig. 3.2.- Characteristic curve of "Secomak" blower mod. no 74.

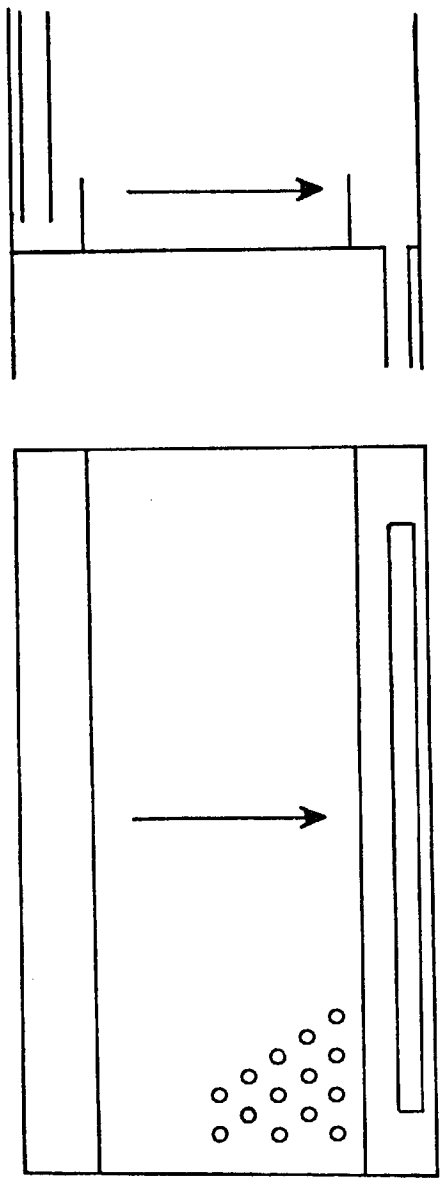

SCALE 1/2

Fig. 3.3.- Diagram of plate lay-out.

columns, near the upper part of the plates. Pieces of 13 mm o.d. copper pipe were used protected from impingement of liquid droplets.

The study of the spray regime is the primary aim of this work. This regime is more easily achieved for low weir heights if the gas flow is high and the liquid flow rate is small. It is also preferable to work at room temperature and atmospheric pressure as this makes the design and handling of the equipment much easier. In order to minimise errors in efficiency determinations it is also advisable to have similar gradients of operating and equilibrium lines. This coupled with the requirement of small liquid/gas ratios indicates the use of a system of fairly low slope of the equilibrium line. The system air-diluted aqueous methanol solution meets these requirements. The equilibrium line for very dilute solutions at room temperature is approximately given by

$$y = 0.24x$$

where $\underline{y}$ is the mole fraction of methanol in gas phase and $\underline{x}$ is the mole fraction of methanol in liquid phase. Thus for approximately parallel operation and equilibrium lines liquid rate (molar) will have to be about 1/4 of gas rate (molar). Other advantages of the system air-dilute aqueous methanol include the possibility of achievement of large surface tension gradients with small changes of physical properties other than surface tension; ease of analysis of liquid compositions with existing equipment, small cost and safe manipulation. The toxicity of the vapours was of little concern, since diluted solutions were used, there was no deliberate exhaust of vapours and sufficient renewal of laboratory air was provided.

3.2 Gamma-ray Absorption

3.2.1 Principles

The measurement of dispersion density by gamma ray absorption provides information on vertical distribution of liquid and on total hold-up by integration of the liquid distribution over the height above the plate.

The intensity of a mono-energetic beam of gamma radiation transmitted through a homogeneous medium is given by:

$$\ln \frac{I_o}{I} = \mu \rho \ell \qquad (1)$$

where μ is the mass-absorption coefficient, dependent on the radiation energy and on absorbing medium, ρ is the density of the absorbing medium and ℓ is the path-length, I_o is the incident intensity of radiation and I is the intensity of radiation after absorption.

3.2.2 Description

The source of γ-radiation used was a 0.8 millicurie Caesium 137 slug giving a mono-energetic beam of radiation ($\lambda \simeq 10^{-12}$ cm). Half-life is about 30 years and γ-energy is 0.67 Mev. The radioactive source and the radiation counter tube were collimated so that the plate area 'seen' by the rays had a percentage free area similar to the whole plate.

The absorption coefficients for water and methanol calculated from the data of Davidson and Evans[106] for a photon of energy 0.68 Mev is 8.5×10^{-3} m^2 kg^{-1}. One method of checking if the collimating system is good enough consists of comparing the actual path length with the theoretical value. Bad collimation tends to give smaller effective path

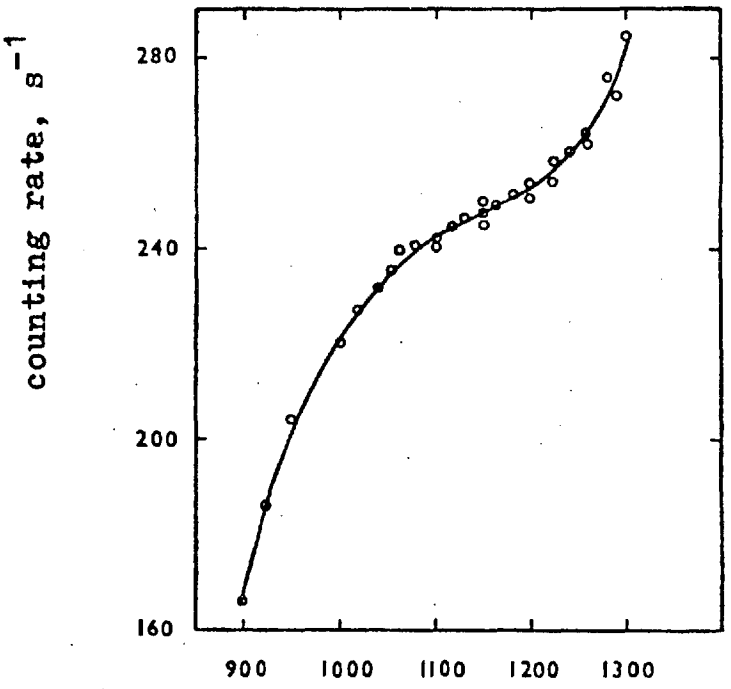

Fig. 3.4.- Effect of E.H.T. applied potential on counting rate.

Table 3.1

COUNTING EQUIPMENT SETTINGS

E.H.T.	1150 V
Head amplifier time constant	0.02 μs
Main amplifier:	
gain	65.5 dB
differentiating time c.	1 μs
integration time c.	1 μs
Discriminator:	
level	0.16 V
dead time	10 μs

length and hence decreased sensitivity. In this case the actual path length is about 0.19 m and its effective value 0.193 m. It can then be concluded that the sensitivity of the method for measuring small density changes is about the maximum attainable.

The counting equipment used was described in detail by Fane.[107]

3.2.3 Calibration of the gamma ray system

The first stage of calibration consisted of finding optimum settings of each module. The voltage to be applied to the photomultiplier was selected from the plateau obtained when the counting-rate was plotted versus electric potential, as shown in Figure 3.4. The final settings of the other modules were carried out with an oscilloscope and are given in Table 3.1.

Corrections for dead time from equation

$$\frac{I_{cor.}}{I} = \frac{1}{1 - I\ t_d}$$

where t_d is the dead time, were negligible.

Since the absorption coefficients for water and for methanol were the same, the calibration curve was independent of the composition of the liquid mixture, according to equation (3.1). The constant value of $\mu\ell$ was determined by filling the column with water and with methanol. The result was 1.6418×10^{-3} m^3 kg^{-1} and no differences were detected with change in position above plate floor so that the equation for determination of the liquid fraction, F_L, was:

$$F_L = \frac{609.1}{\rho_\ell} \ln (I_O/I) \qquad (2)$$

where ρ_ℓ is the liquid density (kg m^{-3}).

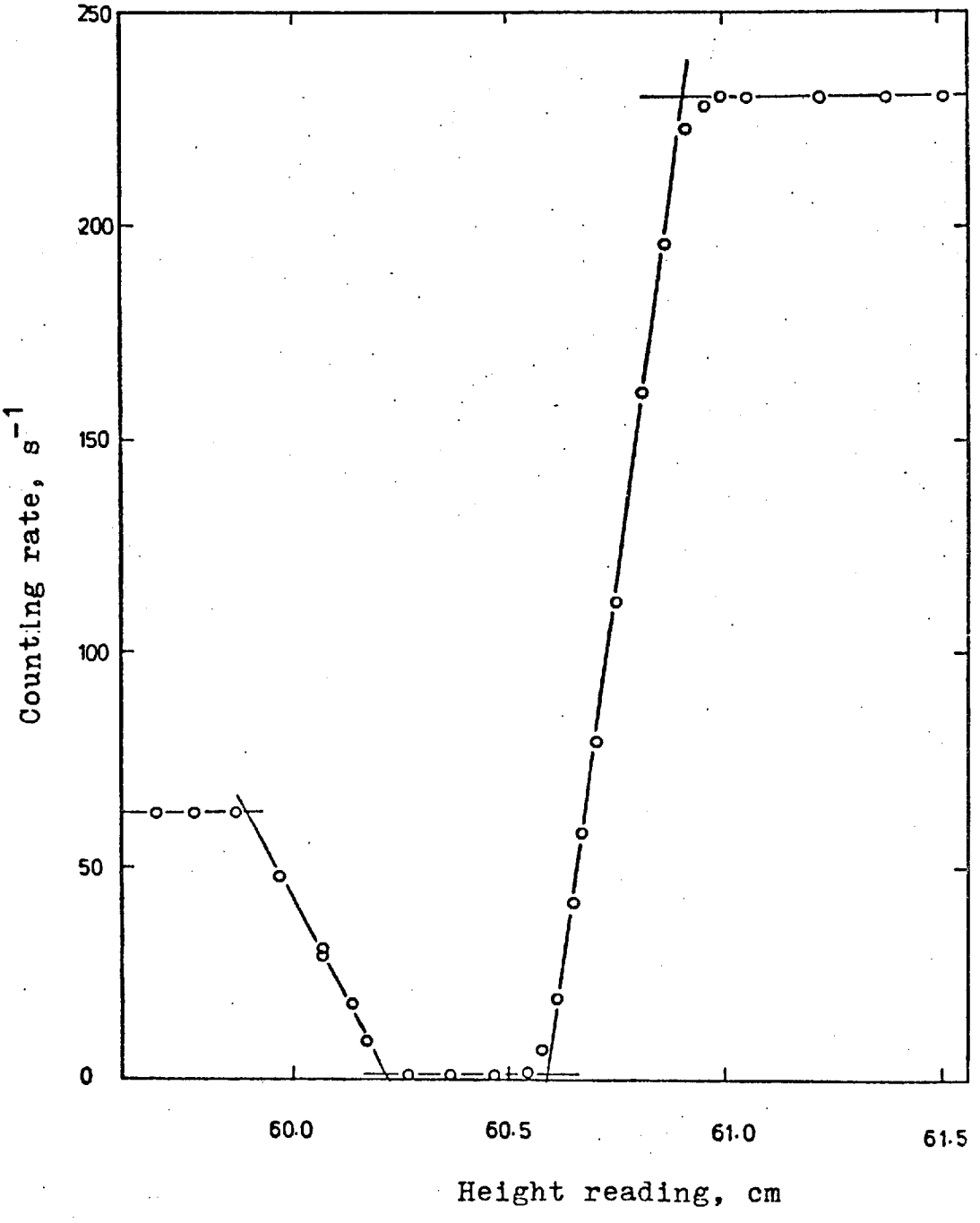

Fig. 3.5.- Actual counting rate near the plate floor.

3.2.4 Correction for plate absorption

When the height above plate floor at which measurement is to be made is very low, corrections have to be introduced for absorption by the plate.

The gamma-ray beam is 3.2 mm wide, so that corrections are made for readings below 1.6 mm above the plate floor. Figure 3.5 represents the effect of plate absorption for levels close to the plate floor. Accordingly, the plate floor level is at an arbitrary reading of $z = 60.69$ cm (fixed by positioning of the scale), and when the reading is 60.53 cm the beam goes completely through the plate. For levels between these two readings only a fraction of the beam crosses the dispersion and under these circumstances, both intensity and height must be corrected.

The corrected level of the beam is the mean level of the part which crosses the dispersion

$$z_{cor} = z + \frac{(60.85 - z)}{2} \tag{3}$$

The correct value of I_0 is a fraction of the value of I_0 expected in the absence of the plate and is given by:

$$(I_0)_{cor} = \frac{z - 60.53}{0.32} I_0 \tag{4}$$

3.2.5 Estimation of the error in dispersion density

Since the intensity of radiation is a Poisson distribution, the standard deviation is equal to its square root so that for 10^4 counts, the precision is 1%. Using 100 seconds to record the number of counts, the measured values were almost always above 2×10^4, so that the precision of each determination of I under these conditions is expected to be better than 0.7%.

To estimate the error in F_L the following method was used:

If a calculated variable, R, is a function of the experimental variables, u_j

$$R = F(u_j), \quad j = 1,2,\ldots,n, \tag{5}$$

then the variance of R, $(\Delta R)^2$ is

$$(\Delta R)^2 = \sum_{j=1}^{n} \left(\frac{\partial F}{\partial u_j}\right)^2 (\Delta u_j)^2 \tag{6}$$

where Δu_j is the standard deviation of u_j.

$$\text{As} \quad F_L = \frac{609.1}{\rho_\ell} \ln \left(\frac{I_o}{I}\right) \tag{7}$$

neglecting error in $\frac{609.1}{\rho_\ell}$ and as

$$\Delta I = \sqrt{I} \qquad \text{(Poisson distribution)} \tag{8}$$

and

$$\Delta I_o = \frac{\sqrt{I_o}}{\sqrt{n}} \ ,$$

where n is the number of times I_O is measured (usually above 4), then:

$$\Delta F_L = \frac{609.1}{\rho_\ell} \left(\frac{1}{nI_O} + \frac{1}{I}\right)^{1/2} . \tag{9}$$

Consider two cases:

(a) Suppose that $I \sim I_O$ ($F_L \to 0$)

$$\Delta F_L = \frac{609.1}{\rho_\ell I_O^{1/2}} \left(\frac{n+1}{n}\right)^{1/2} \tag{10}$$

Take $I_O = 24300$ (typical value), then $\Delta F_L = 0.0055$ if $n = 1$

$\Delta F_L = 0.0039$ if $n = \infty$.

(b) Suppose that $I = 20600$ ($F_L \simeq 0.1$)

then $\Delta F_L = 0.0058$ if $n = 1$

$\Delta F_L = 0.0043$ if $n = \infty$.

Conclusion: The expected standard deviation of experimental points of the liquid profile is around 0.005 for any experimental conditions.

3.3 Light Probe

3.3.1 Principles

If the following conditions apply:

1. There is a transparent continuous phase;
2. There are random particle locations;
3. The size of particles is greater than 0.10 mm (that is, the minimum value of $\alpha = \frac{\pi d}{\lambda}$ is 450);
4. The particles are subject to random orientation in the light beam;
5. The particles have no concave surfaces;
6. The light source emits an incoherent parallel light beam;
7. The light detector receives only parallel light.

then $$a = -\frac{4}{\ell} \ln f \qquad (11)$$

where: a is the interfacial area per unit of volume of dispersion, m^{-1},

ℓ is the optical path length, m,

f is the fraction of light transmitted through the dispersion.

The maximum recommended value of ℓ is[108]

$$\ell_{max} = \frac{9.18}{a} \qquad (12)$$

However the applicability of the method assumes that the dispersed phase is randomly dispersed. This is not always the case and if the velocity of the particles is a function of their diameter (and/or position), a considerable difference exists between the spatial interfacial area and that of the generated dispersion. Nevertheless, in several processes

with dispersed particles, the characteristic velocity of the particles of the dispersed phase is a function of the dimension (and/or position) of the considered particles. If that function is known, or if it can be obtained by modelling, the use of the light transmission technique can easily be extended to these cases.

Suppose a sieve plate is operating in the spray regime. The volume fraction of drops of liquid at level i is then (assuming drops are spherical):

$$F_{L_i} = \frac{\pi}{6} \sum_j \frac{n_j d_j^3}{v_{ji}} \tag{13}$$

and the interfacial area per unit volume of dispersion, as given by the light transmission technique, is:

$$a_i = \pi \sum_j \frac{n_j d_j^2}{v_{ji}} \tag{14}$$

where: n_j is the number of drops with diameter d_j and v_{ji} is the velocity of drops of size d_j at level i.

The Sauter mean diameter at level i is:

$$\bar{d}_i = \frac{6F_{L_i}}{a_i} \tag{15}$$

If the drops were assumed to be randomly dispersed, the volume fraction of the liquid, the interfacial area per unit volume of dispersion and the Sauter mean diameter would be independent of the height above plate, that is, constant everywhere. Furthermore, the measured Sauter mean diameter at generation level could only be identical with the Sauter mean diameter of the population of generated drops if the projection velocity of drops

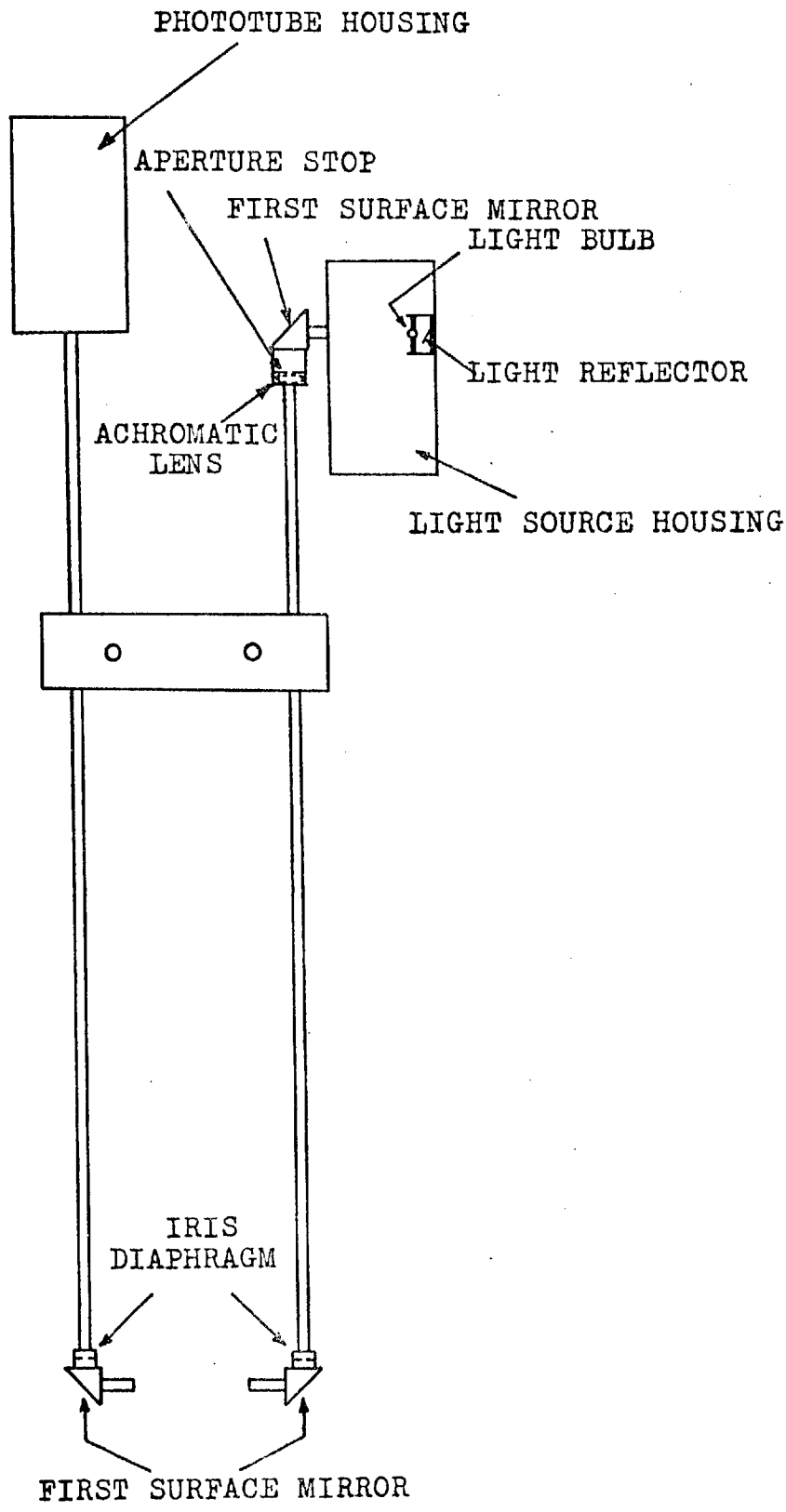

Fig. 3.6.- The experimental light probe

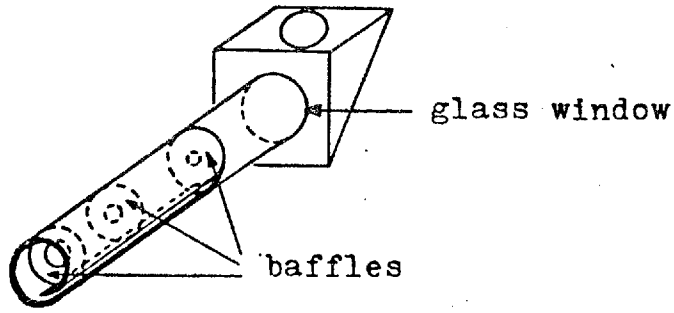

Fig. 3.7.- Detail of one of the horizontal portions of tubing adjacent to the optical gap.

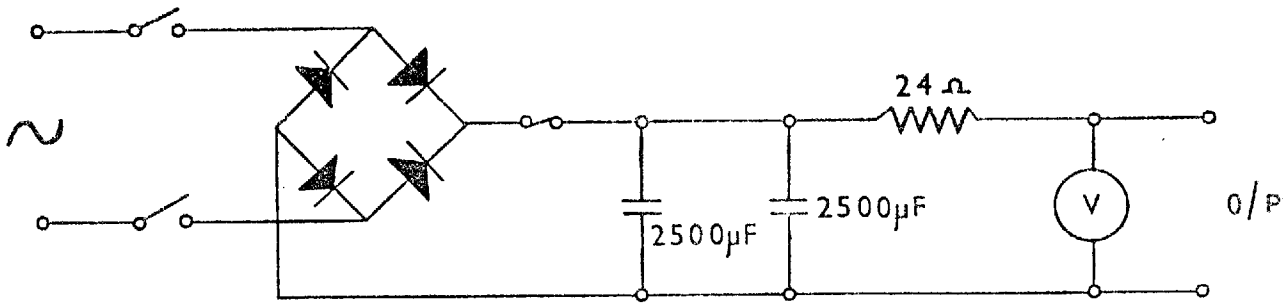

Fig. 3.8.- Power supply.

were independent of their diameter, as can be seen by inspection of equations (3.13) to (3.15).

3.3.2 Description

The light probe, represented in Figure 3.6, consists of two parallel brass tubings 13 mm O.D., 15 cm apart and 75 cm long. The aluminium bars which fix the spacing between the tubes are fixed to a hydraulic lifting system in order to move simultaneously the light prove and the gamma ray absorption assembly. The light source housing is fixed to the top of one tube, whereas the top of the other tube carries the photo-multiplier tube housing. At the bottom of both brass tubes are two first surface mirrors and two horizontal sections of tubing adjacent to the optical gap; they are threaded so that different tube lengths can be inserted to change the optical length. They can be removed when necessary to clean the glass windows placed at the extremity of the horizontal tubes next to the mirrors. These windows were proved to be necessary to prevent changes in pressure on plate from being transmitted to the tubing with the result of drops becoming entrained and wetting the mirrors, thus invalidating subsequent readings. In order to avoid sporadic projection of drops onto the windows, several baffles were mounted inside the horizontal tubes (see Figure 3.7). The collected drops were discharged through the longitudinal slit in the bottom of the tubing. In addition the shape of the end section of the tube was changed as indicated in Figure 3.7 to avoid direct entrance of drops through the slit. The baffles were fixed with "Araldite".

The light source housing was made of aluminium sheet. It contained a support for a high pressure mercury vapour lamp ("Wotam", ref. HBO 50W/3). This lamp was chosen because it provides an almost point light source of high brightness and stability.

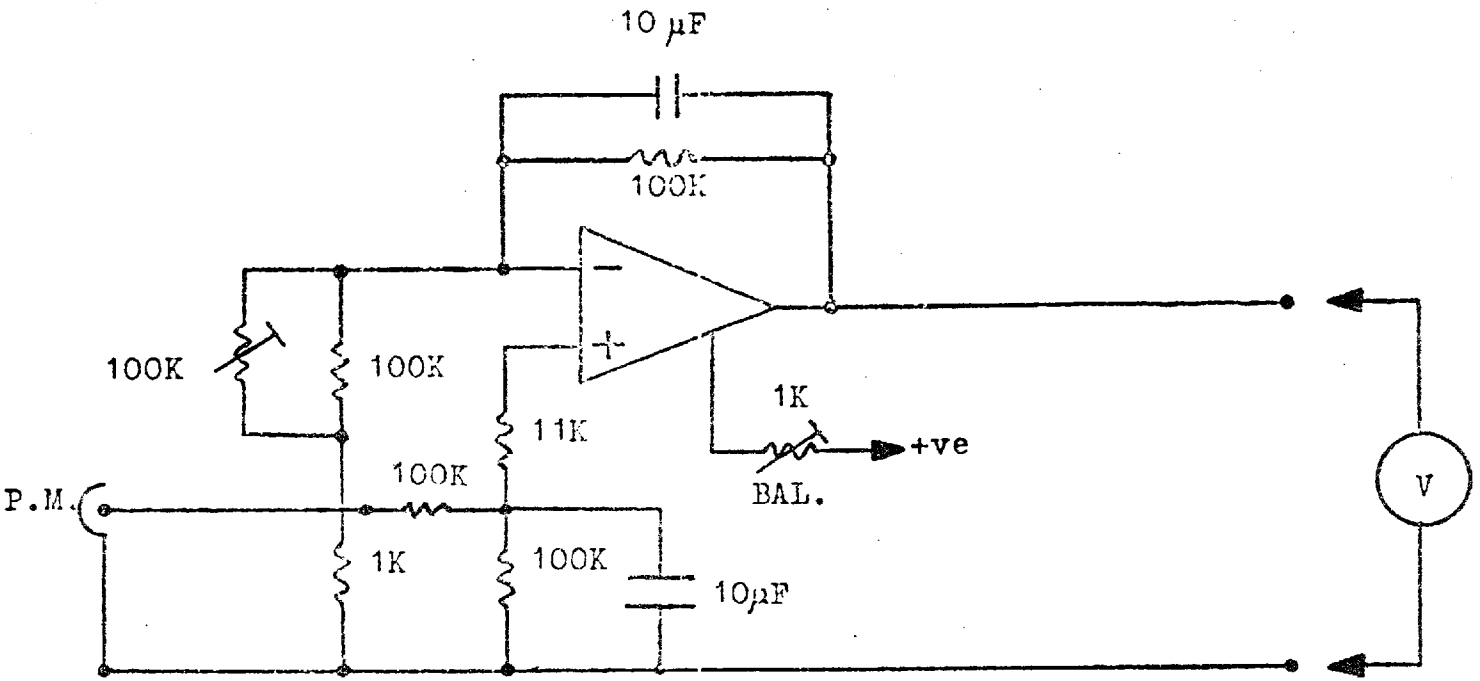

Fig. 3.9.- Photomultiplier amplifier

The beam of light passes horizontally through a hole in the housing. After reflection on a first surface mirror it traverses an achromatic lens (focal distance 15 cm), goes down one vertical tube, is reflected again, passes the optical test path, is reflected again, travels vertically upwards through the other tube and is received by the phototube (EMI photomultiplier tube ref. 9698B).

The lamp is fed by stabilized direct current from a power supply built in the Department (Figure 3.8).

The phototube housing is cylindrical in shape, 10 cm in diameter and 16 cm high, attached by means of a flange to the top of one of the vertical tubes. This is fed by an EHT power unit (A.E.R.E. type 1359A) which allows a continuous change in potential from ±0.2 kV to ±5 kV. Usually about -700 V were used.

The current generated by the phototube was amplified and measured, using a photomultiplier amplifier, built in the Department (see Figure 3.9). It is provided with two knobs, one for adjustment of zero when no light reaches the tube and the other to adjust the reading at full scale when all the light is received by the photocell. This way the fraction of light transmitted through the dispersion could be read directly.

The calibration of the photomultiplier amplifier and meter was performed at the electronic workshop.

To increase precision of reading and to allow continuous reading and registration the signal was taken from the terminals of the meter, divided and fed to a Hitachi-Perkin-Elmer model 159 flatbed recorder, as indicated in Figure 3.10. As shown in Figure 3.11, perfect linearity was obtained.

First surface mirrors and optical black paint were used to help to ensure that the phototube received only parallel light. The lamp had no

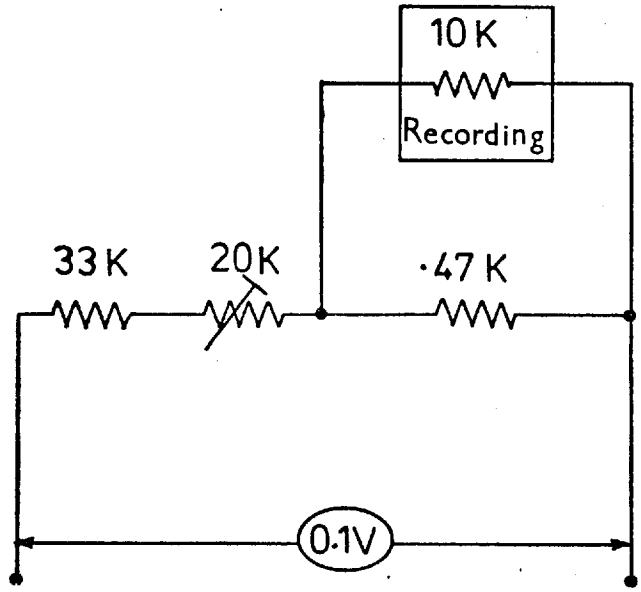

Fig. 3.10.- Attenuation of signal to feed to the recorder.

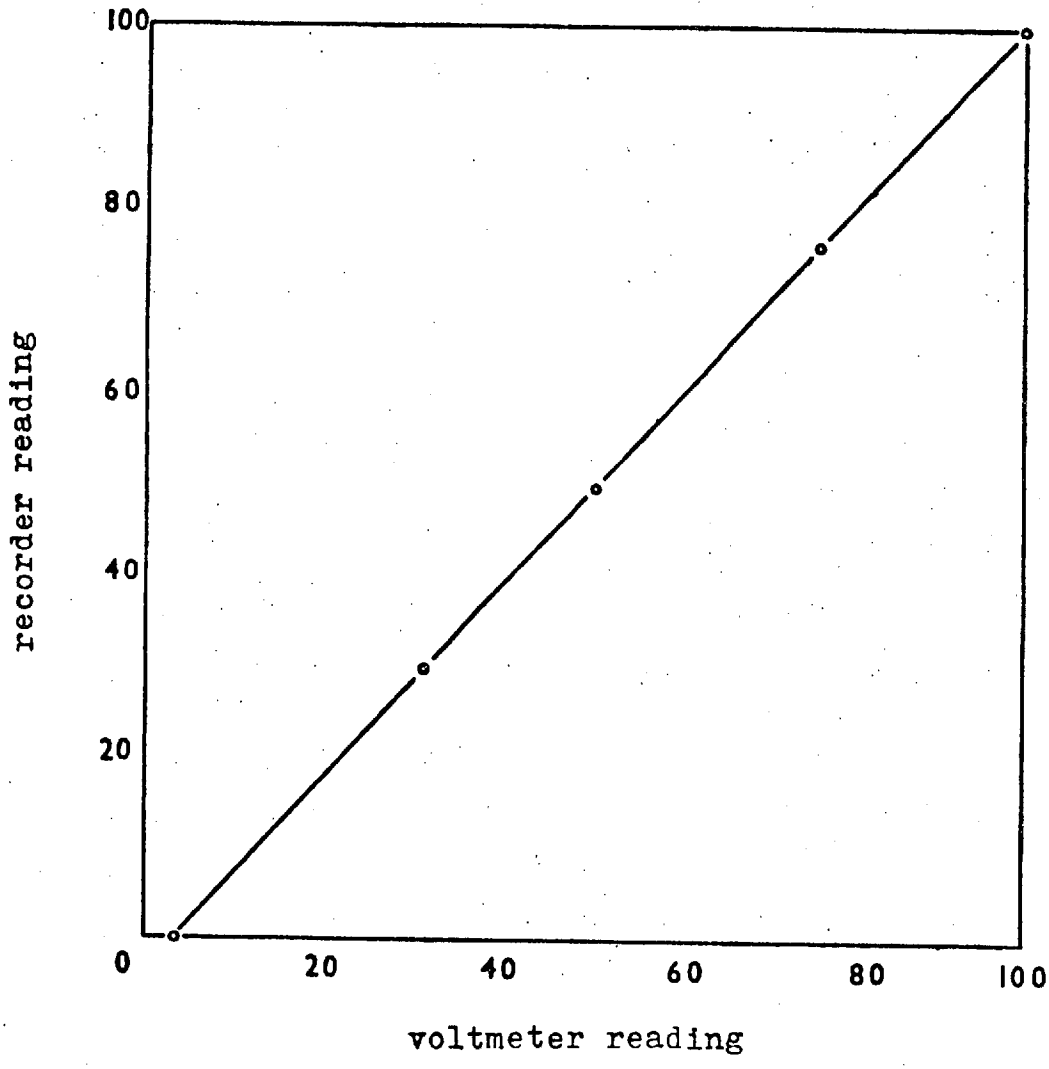

Fig. 3.11.- Relation between recorder and voltmeter readings.

starting electrode so that ignition was done with the help of a H.F. Tester, Model T.2., connected to a H.T. Unit type 1, both from Edwards High Vacuum Ltd.

3.3.3 Estimation of error in specific area

Possible sources of error include reading errors, adjustment errors and errors arising from non-parallel light received by the photomultiplier tube.

(i) Reading errors

If the readings errors are assumed to be constant, say 1% of full scale, then the relative error in area is given by:

$$\frac{\Delta a}{a} = \frac{1}{\ln f} \frac{\Delta f}{f} \qquad (16)$$

and is represented as function of f in Figure 3.12.

(ii) Adjustment errors

Adjustment errors resulted from the fact that the light intensity usually decreased with time. Periodic checks were made by lifting the probe up to a fixed high level where the interfacial area was small and the reading known from previous measurements. The adjustment for the other extremum - total absorption of light - was proved not to be necessary. If the reading f_o corresponds to a = O, the errors in $\underline{a}$ are a function of f_o. To give an indication of these errors, they are presented in Table 3.2.

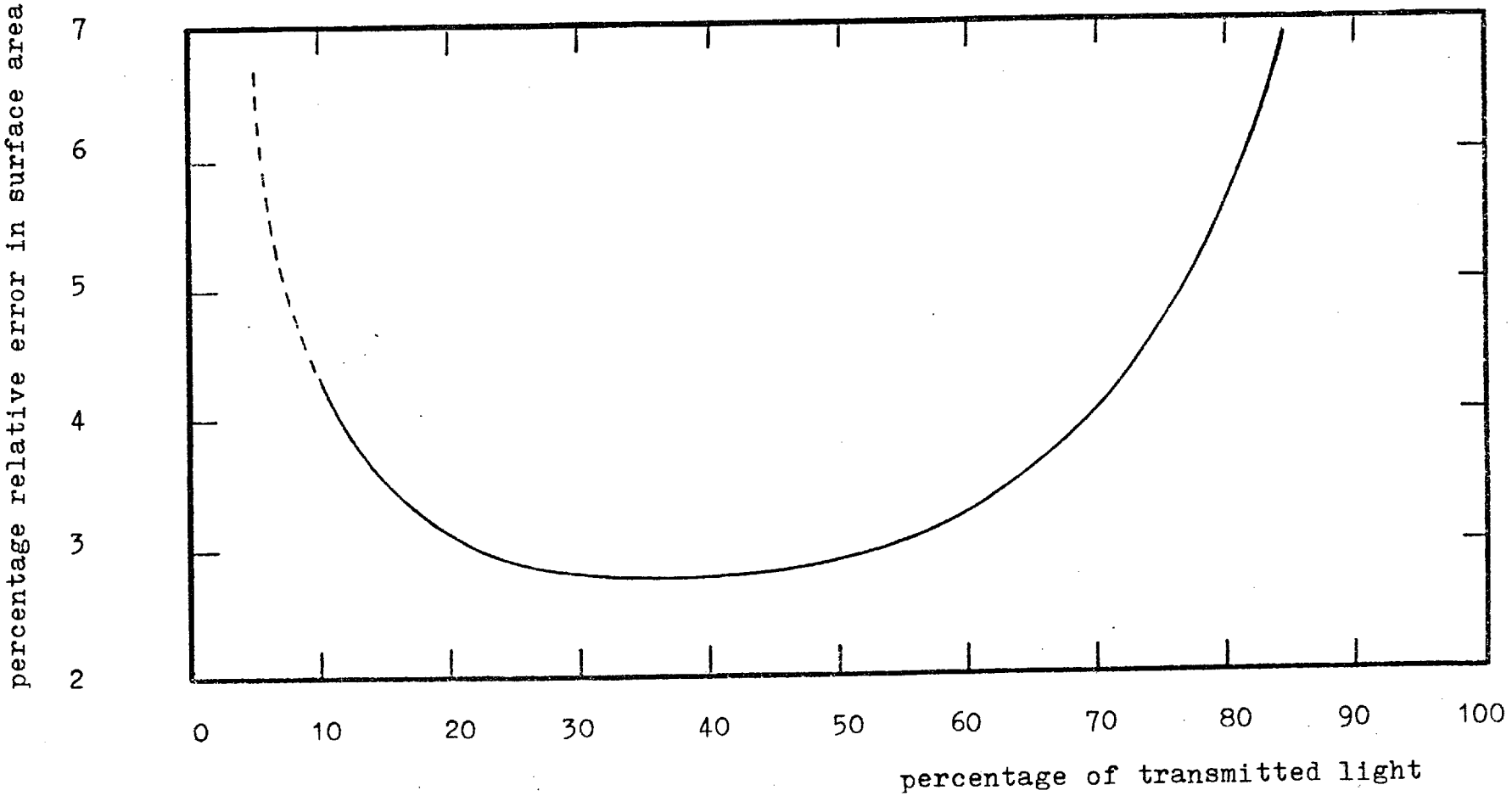

Fig. 3.12.- Error in surface area due to reading error of 1% of full scale.

Table 3.2

Error in surface area due to error in initial adjustment in reading

values of f_o	error in a (cm^{-1})
1	0
.99 or 1.01	0.014
.98 or 1.02	0.029
.97 or 1.03	0.043
.96 or 1.04	0.058
.95 or 1.05	0.072
.90 or 1.11	0.149
.85 or 1.18	0.230
.80 or 1.25	0.315

(iii) Error from the non-parallel light

The last condition, referred to as necessary for the application of equation (3.11), was that all light received by the detector had to be parallel. However, there is always some light which is not parallel and is received at a small angle. To estimate the error involved thereby an assumption is made that the drops are spherical. Incident light which is perpendicular to the surface of the sphere will not be deviated. However light whose angle of incidence is different from zero will be deviated and the degree of deviation will increase with the angle of incidence. A circle can thus be defined on the sphere surface such that the light incident within it will be received by the detector and the light incident outside it will not be received. If the incident radiation is parallel and uniform, the relative error in detected area is given by the transverse

area of the referred circle to the transverse area of the sphere. If this is small (say $\leq 5^{o}$) the angular deviation of a ray is (see Figure 3.13):

$$\Delta = 2(j - j/\eta), \tag{17}$$

where j is the incidence angle, in degrees, and η is the refractive index of the dispersed medium.

The transmitted light will be proportional to the surface area

$$\pi(r\ j\ \frac{\pi}{180})^2 ,$$

where r is the radius of the sphere.

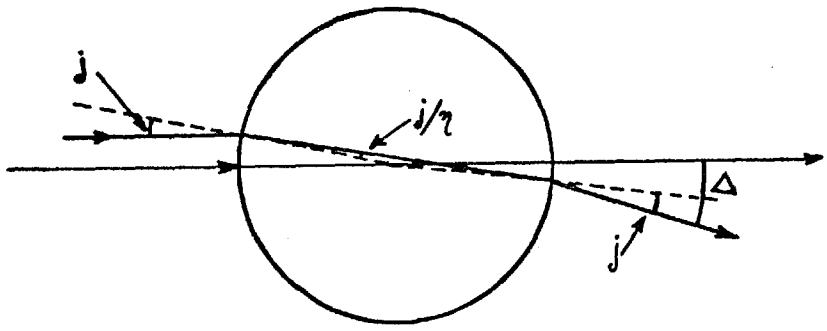

Fig. 3.13.- Deviation of a ray by a transparent sphere.

The relative error is then

$$\frac{\pi(r\ j\ \frac{\pi}{180})^2}{\pi r^2} = (\frac{\pi}{180}\ j)^2$$

Eliminating j by equation (3.17)

$$\text{relative error} = (\frac{\pi}{180}\ \frac{\eta\Delta}{2(\eta - 1)})^2 \tag{18}$$

For water $\eta = 1.33$ so that

$$\text{relative error} = 0.00124\Delta^2$$

or

$$\text{\% relative error} = 0.124\Delta^2 \ , \tag{19}$$

that is if the phototube receiving angle is less than 1°, associated relative error in area is 0.12%.

3.4 Chromatograph

The chromatographic unit employed was Perkin Elmer model 452 with hot-wire detector. The separation column was a stainless-steel tube, 2 m long and 6 mm diameter packed with Porapak Q (stable up to 250°C). The output from the chromatograph was quantified by an electronic integrator (Perkin Elmer model D2) and the result printed by a Kienzle digital printer. The record of the peaks was provided by a Hitachi-Perkin-Elmer model 159 flatbed recorder.

The experimental conditions were:

oven temperature	:	130°C
injection block temp.	:	2
range	:	8
detector supply	:	6
carrier gas	:	H_2 15 psi
chart speed	:	low

Under these conditions the molar ratio methanol/water in the liquid samples (1 µl) was given by

$$X = 0.6955 \frac{\text{meth. reading}}{\text{water reading}}$$

The analysis of gas samples was difficult since a large amount of air was injected and changes in base line occur making the reproducibility rather poor. The composition of the gas samples for the same conditions was given by:

$$\text{moles of water} = \frac{\text{water reading}}{13.850 \times 10^9}$$

$$\text{moles of methanol} = \frac{\text{methanol reading}}{19.915 \times 10^9}$$

$$\text{moles of air} = \frac{\text{methanol reading}}{17.009 \times 10^9}$$

3.5 Rotameters

Rotameters were used for the measurement of gas and liquid rates. The calibration of the liquid rotameters was made by measurement of the amount of water collected over a measured interval of time. The calibration of gas rotameter was done by a standard meter.

Calibration results were correlated by a 2nd degree polynomial, giving the program the standard error and relative errors of the measured rates, and furnishing a Table to allow a direct reading of the rate. The correlation equation was used directly in the program for modelling the spray regime. Examples of those Tables are included in Appendix I.

The effect of physical properties was not important except for the smaller rotameter used for measurement of liquid rates. A graph was therefore prepared for the latter (Appendix I) in which a correction factor was represented as function of the property group $\frac{\sqrt{\rho}}{\mu}$ (ρ in g/cm^3 and μ in cP) and with the reading as a parameter. The actual volumetric flow rate is

$$Q_{actual} = Q_{table} \times \frac{\text{correction factor}}{\sqrt{\rho}}$$

Chapter Four

Results

4.1 The Free-Trajectory Model of Spray Regime

In the free-trajectory model it is assumed that a continuously replenished shallow pool of liquid present on the plate floor is atomized at a constant rate by the gas passing through the holes at high velocity. It is also assumed that there exists a distribution of drop sizes, that each drop size has associated with it a specific projection velocity and that the drops retain their identity during their life time in the spray, that is there is no coalescence or break-up in flight. Under these conditions the equation of motion of individual drops can be solved and mass transfer calculated.

4.1.1 Parameter requirements of the free-trajectory model

There is experimental evidence confirming the presence of clearly defined drop trajectories and the absence of fluidization effects,[2] lending strong support to the viability of the free-trajectory model. However, the utilization of the model requires prior knowledge of initial projection velocity of drops and their drag coefficients to solve the equation of motion, of spray characteristics and liquid hold-up to produce the dispersion density profile, and of mass transfer coefficients to predict plate efficiency.

The validity of the model has so far been only tested by curve fitting of the measured dispersion density profile and by prediction of plate efficiencies.

(a) Spray characteristics

On the basis of information contained in literature[1,45,109-111] it has been assumed that the throughput drop-size distribution at plate level was log normal. These characteristics have been obtained by curve fitting.

(b) Hold-up

The hold-up was obtained by integration of the measured dispersion density profiles.

(c) Drag coefficients

Drag coefficients were estimated on the basis of the work of Hughes and Gilliland.[56]

(d) Initial projection velocity

The data of Aiba and Yamada[110] have been correlated by Fane and Sawistowski[1] leading to the following relation:

$$v_p = 0.4(0.004/d_p)^{0.93} \qquad (1)$$

where v_p is the initial projection velocity and d_p is the diameter of drop. Although the data cover a comprehensive range of hole velocities, orifice submergences and liquid physical properties, nevertheless it was felt that it represents an oversimplification of the phenomenon.

(e) Mass transfer coefficients

The following correlations have been used:

$$Sh_G = 2.0 + 0.6\, Re_G^{1/2}\, Sc_G^{1/3}$$

$$K_L(t) = (D_E/\pi t)^{1/2}\{1 + 2\exp(-d_p^2/4D_E t)\} - 2D_E/d_p$$

respectively for the gas and the liquid phases.

4.1.2 Limitations of the free trajectory model and aim of this work

At present, the free trajectory model of the spray regime relies on equation (1) for the initial projection velocity and on the experimental determination of the dispersion density profile. It is felt that this equation represents an oversimplification of the phenomena of drop formation and is regarded as the least reliable step in the model. In the next section therefore, the sensitivity of the model to values of initial projection velocity will be analysed. For independent testing of equation (1) it is necessary to conduct experiments which will allow the determination of dispersion density profiles as well as of interfacial areas or velocity of drops.

On the other hand, it is convenient to be able to predict the performance in the spray regime without need of prior experimentation. This implies a need for the determination of the function F_L, the volumetric liquid fraction in the dispersion (the 'dispersion density')

$$F_L = f(z, \text{operating variables, physical properties, geometry}) \qquad (2)$$

In order to achieve this objective, first of all it is necessary to be able to characterize the dispersion density profile. This will be attempted by the free trajectory model, but sufficiently simplified so that the functional form of equation (2) can be obtained for fixed values of the operating variables, physical properties and geometry. For such a case this relation yields a family of curves corresponding to different parameters of the free trajectory model. These parameters can be obtained with reference to experimental results. Subsequently the effect of operating variables, physical properties and geometry on parameters

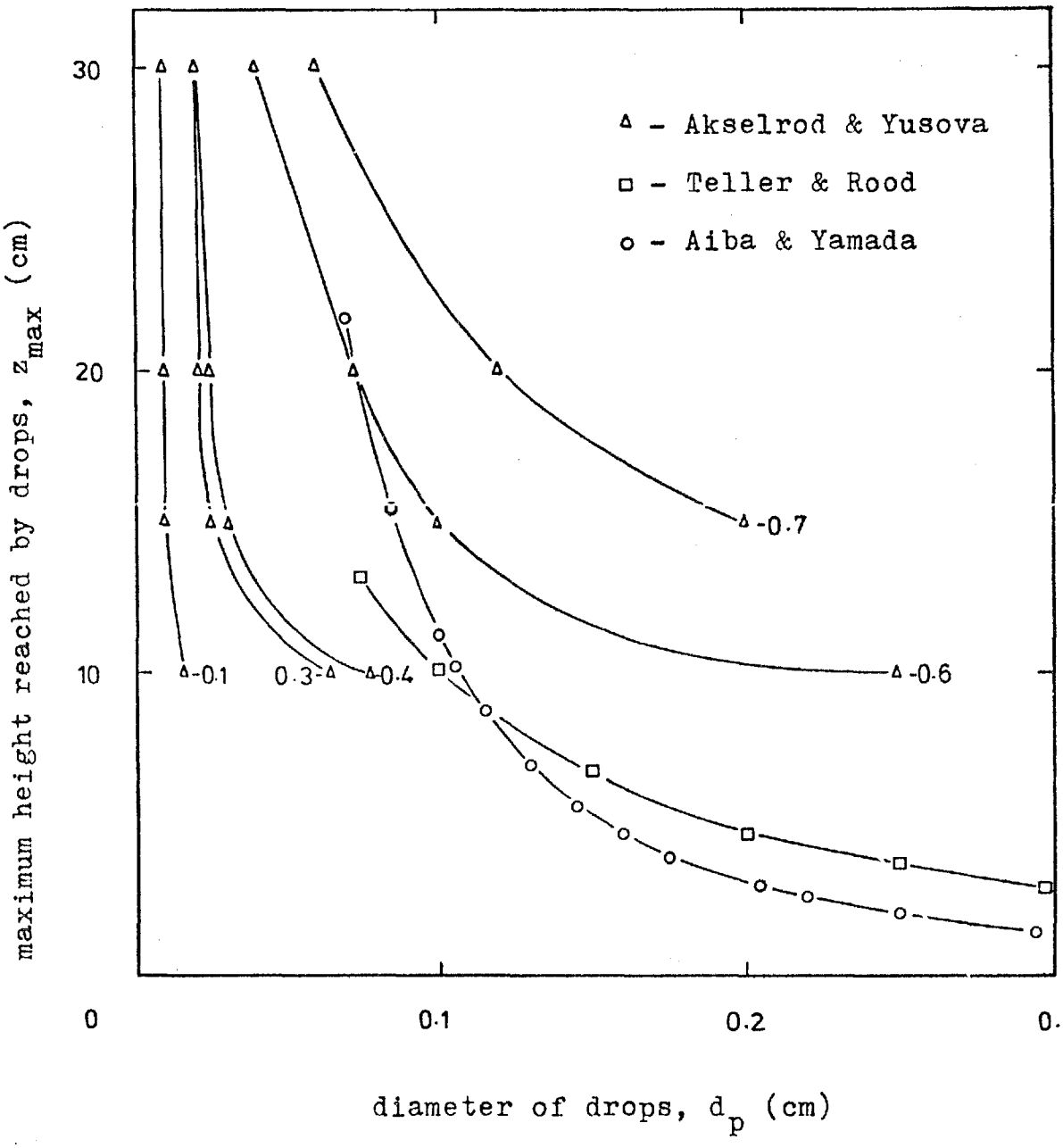

Fig. 4.1.- Maximum height reached by drops as a function of drop diameter (parameter: superficial gas velocity, ms^{-1}).

characterizing the dispersion will be determined. Finally, determination of interfacial areas as well as of dispersion density will be attempted to allow for confirmation of validity of equation (1) or its substitution by a more appropriate correlation.

4.1.3 Effect of initial projection velocity used in the model on predicted results

Fane and Sawistowski correlated Aiba and Yamada's data on projection velocity by the equation:

$$v_p = 0.4\ (0.004/d_p)^{0.93} \qquad (1)$$

Akselrod and Yusova,[112] however, obtained different results for the projection velocity of drops, as can be seen in Figure 4.1, where the maximum height reached by the drops is given instead of the projection velocity, since the former was the measured variable. There is in fact a large uncertainty in the prediction of the projection velocity. For instance, Akselrod and Yusova's data indicate a dependence of the projection velocity on the superficial velocity.

It is important to have an idea of the effect of the changes in projection velocity on the results of the model. It was verified that for drops of size above 1 mm (mean drop size seems to be in the range 1-2 mm) the error in the calculated maximum height on the assumption of no friction loss is less than 5% with superficial velocity as high as 1.5 ms^{-1}. If this is the case, then:

$$z_{max} = \frac{v_p^2}{2g} \qquad (3)$$

$$t_{life} = \frac{2v_p}{g} \tag{4}$$

where z_{max} is the maximum height reached by a drop, m

v_p is the projection velocity of the drop, ms^{-1},

g is the gravitational acceleration = 9.8 ms^{-2},

t_{life} is the life time of the drop, s.

Consequently

$$\frac{dz_{max}}{z_{max}} = 2\frac{dv_p}{v_p} \tag{5}$$

and

$$\frac{dt_{life}}{t_{life}} = \frac{dv_p}{v_p} \tag{6}$$

The following conclusions can thus be drawn:

1. Relative error in maximum height reached by a drop is two times the relative error in projection velocity.

2. Relative error in life time is equal to the relative error in projection velocity.

A general expression for the initial projection velocity of the form:

$$v_p = Ad_p^B \tag{7}$$

will be assumed. This equation is represented by a straight line in log-log coordinates. The effect of translation and rotation of the line will also be considered. After that the effect of a statistical distribution of initial velocities will be analysed.

(i) Change of velocity by a constant factor

The results obtained for v_p, as given by equation (1), are compared with those obtained when $v_2 = 1.2\ v_p$ and $v_3 = v_p/1.2$ in Table I. The dispersion density profile used was obtained in run 33. The calculated hold-up was always 2.122 mm.

Table I

Comparison of results using various initial projection velocities differing by a constant factor

proj. veloc. (m/s)	d_{gm} (mm)	stdv (mm)	d_{Sauter} (mm)	$N_p \times 10^{-6}$	N_{OG}	E_{MV}	Ent $\times 10^{6}$	$\frac{d\bar{d}}{dh}$
$v_p/1.2$	1.53	0.39	1.72	9.123	0.546	0.421	0.262	0.05
v_p	1.84	0.48	2.07	5.303	0.414	0.339	0.426	0.05
$1.2v_p$	2.21	0.59	2.50	3.043	0.312	0.268	1.38	0.05

The following conclusions can be drawn from the table. The increase in projection velocity by the factor 1.2 produced:

1. increase of d_{Sauter} by the factor 1.2
2. decrease of N_p by the factor 1.2^3
3. decrease of $\bar{a}(h)$ by the factor 1.2
4. increase of $\bar{d}(h)$ by the factor 1.2
5. decrease of N_{OG} by the factor $1.2^{1.54}$
6. increase of entrainment by a factor $1.2^{2.68 \text{ to } 6.44}$

(ii) Change of slope of projection velocity function for equal velocity of the drops with diameter d_{pm}

The results obtained when the velocity of the drops with diameter d_{pm} was maintained but the exponent of expression (1) was changed by a constant factor, are summarised in Table II.

Table II

Effect of change in exponent of expression (1), for a fixed velocity of drop with diameter d_{pm}

exponent	d_{gm} (mm)	stdv (mm)	d_{Sauter} (mm)	$N_p x10^{-6}$	N_{OG}	E_{MV}	$Entx10^6$	$\frac{dd_{Sauter}}{dh}$
0.775	1.71	0.62	2.10	5.696	0.430	0.350	0.917	0.06
0.93	1.84	0.48	2.07	5.303	0.414	0.339	0.426	0.05
1.126	1.91	0.38	2.18	5.117	0.400	0.330	0.400	0.04

The following conclusions can be drawn from Table II.

The increase of the exponent by the factor 1.2 produced:

1. A negligible change in d_{Sauter}
2. A decrease in N_{OG} by the factor $1.2^{0.2}$
3. A decrease in N_p by $1.2^{0.2}$ to 0.4
4. A decrease in slope of $\bar{d}(h)$ by the factor 1.2
5. A decrease in entrainment by a factor $1.2^{0.3}$ to 4.2

The most interesting result is the inverse relation between the functions $v_p(d_p)$ and $d_{Sauter}(h)$, which will be later deduced using a simplified model. The same result suggests an alternative way to obtain the function $v_p(d_p)$ by experimental determination of the $d_{Sauter}(h)$.

(iii) Effect of a statistical distribution of projection velocities on model results

An analysis of Pinczewski's data[113] for projection velocities suggests their statistical nature.[46] Hence the effect of a statistical distribution of projection velocities is simulated using the model.

To simulate the effect of a statistical distribution of velocities, a discrete approximation to a continuous distribution of initial velocities around the value given by expression (1) was obtained considering κ non-overlapping intervals of $1/\kappa$ probability. It was assumed that all the drops in a particular interval have the initial velocity corresponding to the medium point in the interval, which was calculated on the assumption of considering the distribution of initial velocities to be normal with standard deviation, δ, given by:[46]

$$\delta = 8.2 \times 10^{-5} \left(\frac{v_p}{d_p}\right)$$

The results are summarised in Table III.

Table III

No proj. veloc.	$N_p \times 10^{-6}$	N_{OG}	E_{MV}	Ent $\times 10^{6}$
1	5.303	0.414	0.339	0.426
5	5.322	0.415	0.340	0.767
10	5.321	0.415	0.340	1.16

The main conclusion of Table III is that the effect of the use of a statistical distribution of projection velocities is small on the results of mass transfer, but the entrainment is strongly affected. It seems

therefore that if the model is expected to give good results for entrainment it needs a larger degree of sophistication.

Unfortunately, Pinczewski's results on projection velocities of drops do not cover drops larger than one millimetre, and it is this size range which largely contributes to mass transfer, because mean drop diameters of generated drops are usually bigger than one millimetre and standard deviation of the distributions are usually small. This lack of experimental data makes the extrapolation of the results on projection velocities to drops larger than one millimetre questionable.

In order to improve the model, it is necessary to obtain experimental evidence on the diameter of drops at several levels above the plate floor as a function of the operating variables. An instrument that can be used for this purpose is being developed in the Department.[114] It will be able to evaluate the drops characteristics by digital computation without the presence of a photographic intermediary. The basis of the instrument is the projection of the drop images onto a photomatrix with the number of covered matrix elements providing a measure of drop sizes and shapes. This information is digitalized and suitable programmes will transform it into the required data.

However, this method is not yet operational, so that a simple light probe was developed for the measurement of interfacial areas at different levels above the plate floor.

A computer programme fed with the experimental data on density and interfacial area of the dispersion could provide the expression for projection velocity (of the type of expression (1)) and the parameters characterising the population of generated drops. This program is rather time consuming and it does not show directly the effect of the different parameters so that a simplification, although of lower precision, was attempted.

4.1.4 Simplification of the model

(i) Effect of drag

In order to simplify the model of Fane and Sawistowski for the spray regime, the effect of the drag force was first investigated. The model was applied in two ways to run 33.

a) Using the drag coefficients from the work of Hughes and Gilliland.

b) Assuming a drag coefficient equal to zero.

The profiles, based on these two assumptions, are shown in Figures 4.2 to 4.4 and are found to be very similar.

At the same time the maximum calculated heights attained by the drops when the drag force was included or neglected were compared. It was seen that, on neglecting drag, the maximum height attained by a drop was slightly smaller for drops larger than 0.57 mm and larger for drops smaller than this value. This effect is however small as can be seen from Figure 4.5.

The effect of drag on mass transfer to drops was also investigated. The total mass transfer was higher by 10% when drag was neglected. This was expected because the absence of drag tends to increase the velocity difference between gas and drop thus increasing the mass transfer rate. The effect is represented in Figure 4.6.

Conclusion: the effect of the drag force on dispersion density profiles and mass transfer rates can, in general, be considered small. It is of the same order of magnitude as the contribution to mass transfer of the liquid pool under fully developed spray conditions. However, they act in the opposite direction and hence the result will be unchanged when both the effect of the pool and the drag are neglected.

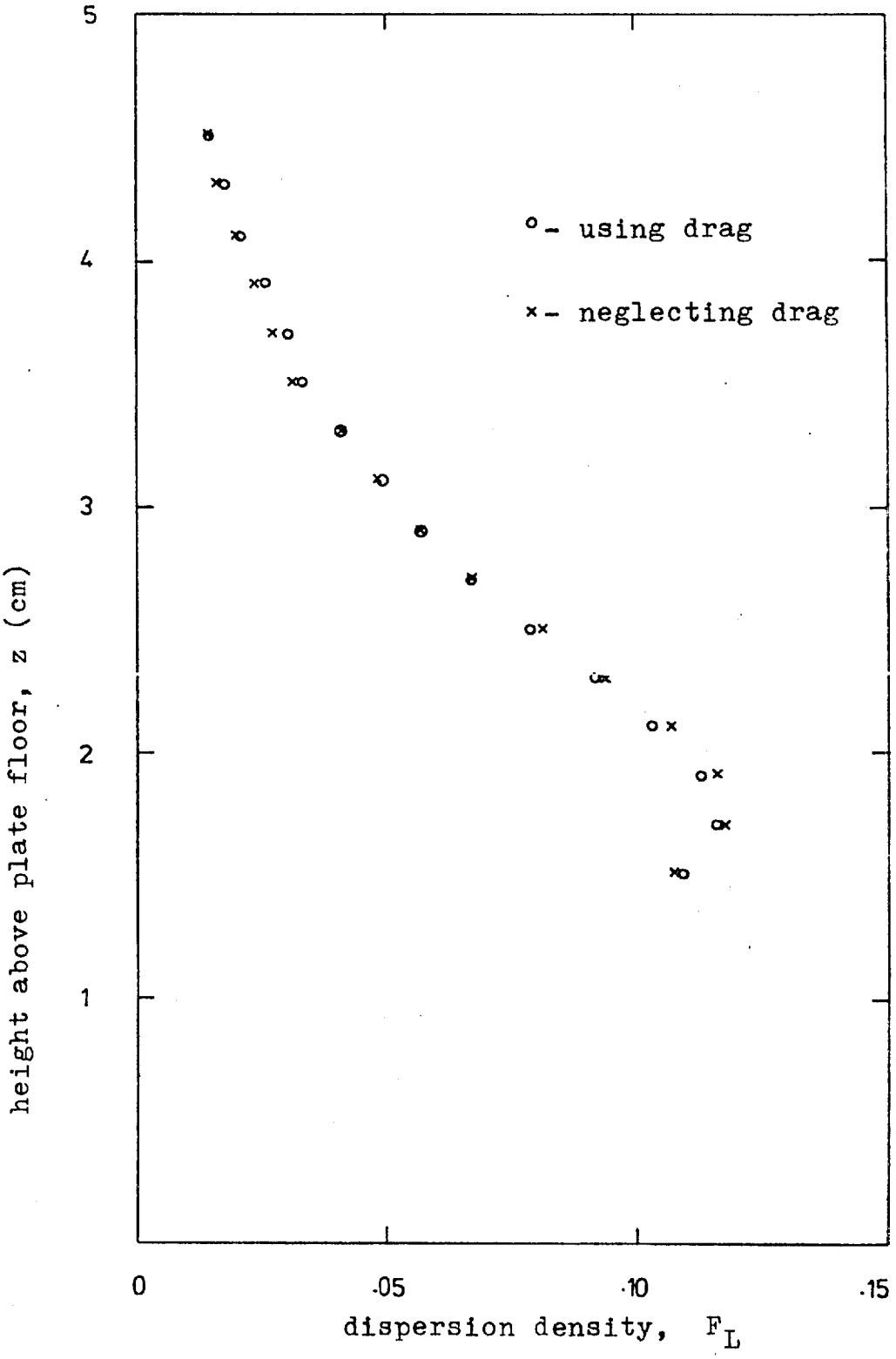

Fig.4.2.- Dispersion density profiles obtained from model for run 33 using or neglecting drag.

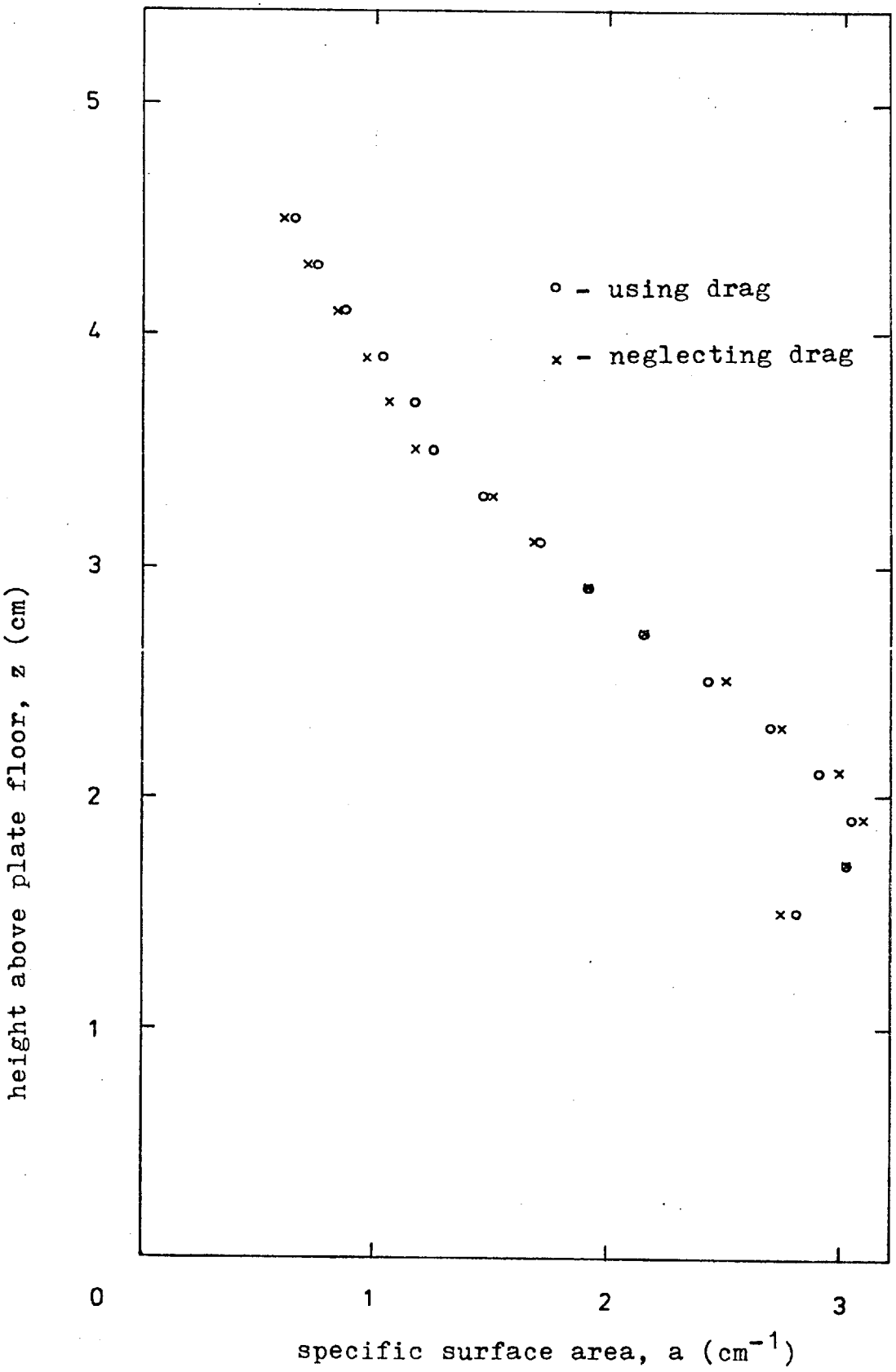

Fig.4.3.- Specific surface area profiles obtained from model for run 33 using or neglecting drag.

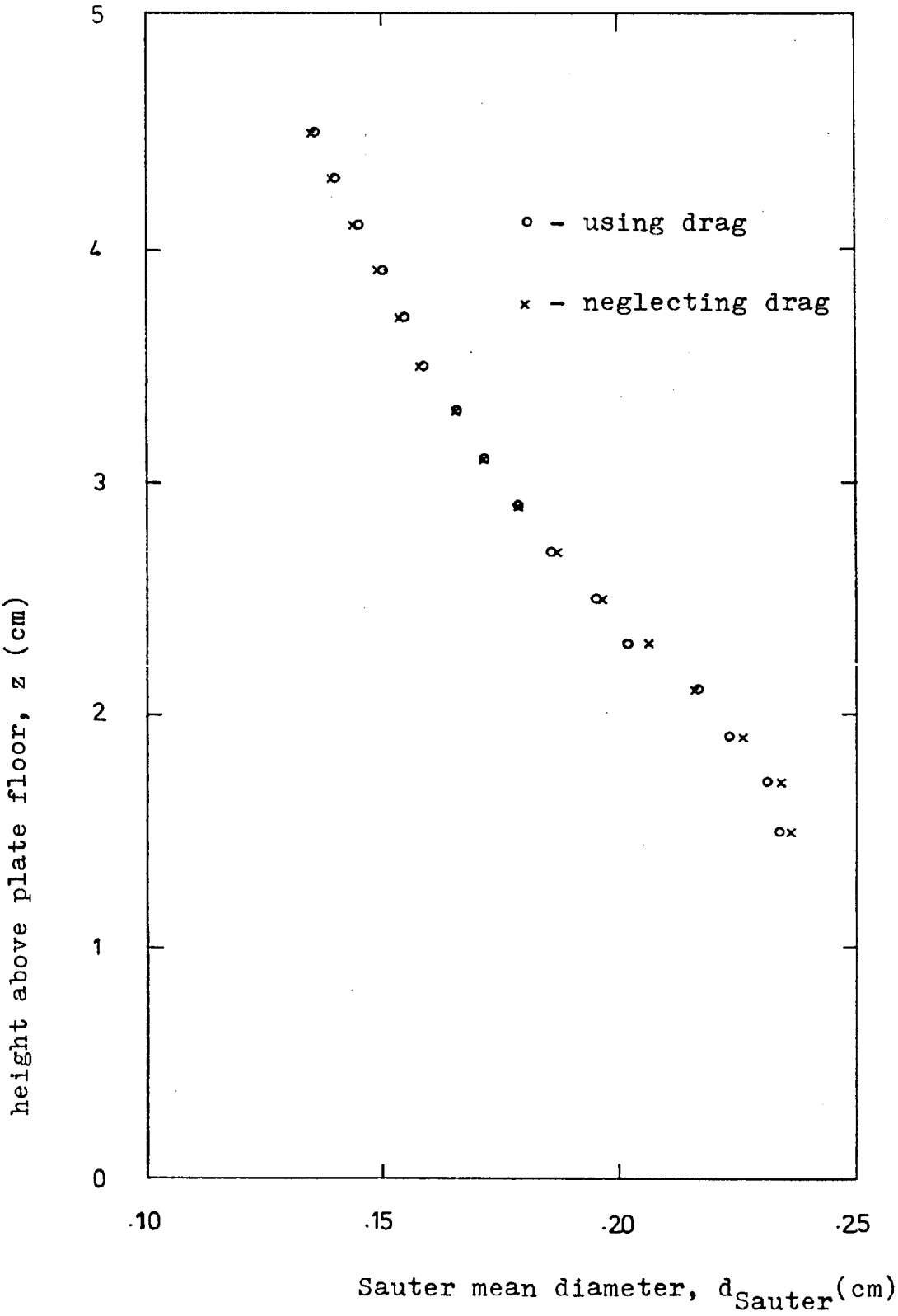

Fig.4.4.- Sauter mean diameter profiles obtained from model for run 33 using or neglecting drag.

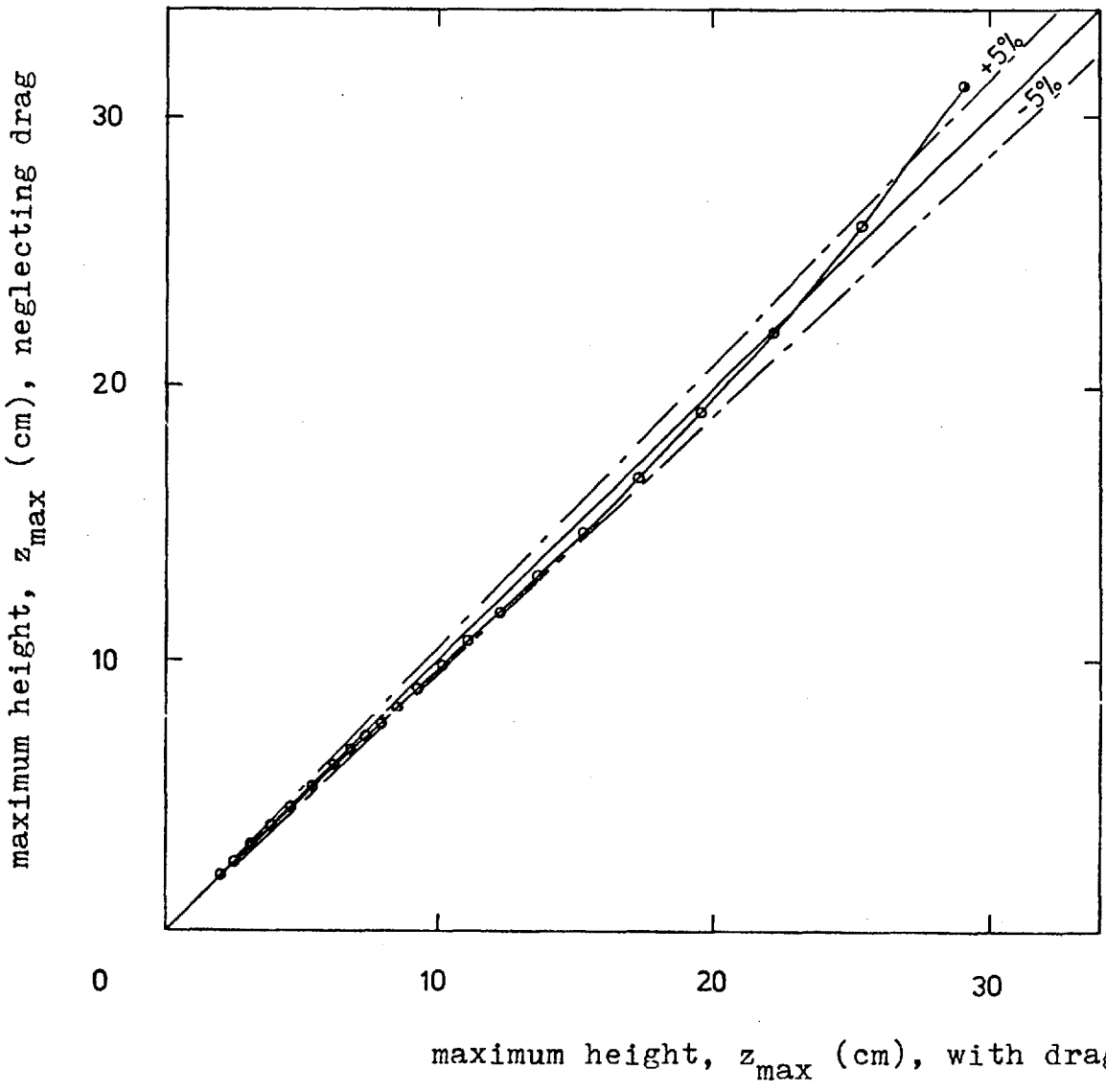

Fig.4.5.- Effect of neglecting drag on maximum height reached by drops.

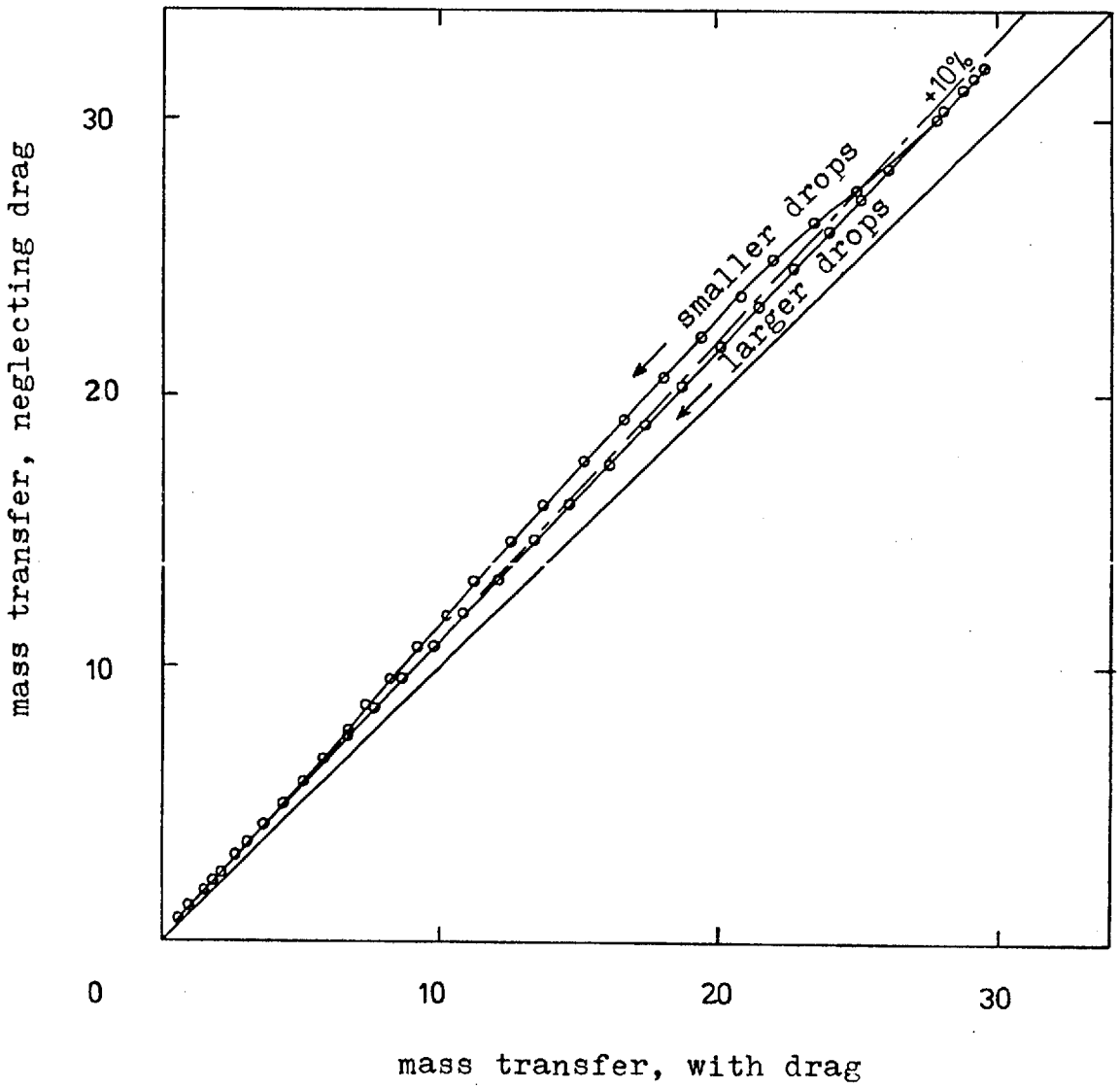

Fig.4.6.- Effect of neglecting drag on mass transfer.

(ii) Simplification introduced by zero-drag condition

If drag is neglected the computation of the trajectories of the drops is easy, reducing significantly the computation time.

The contribution of the drops to the dispersion density profile will now be discussed in detail. If V is the volumetric upward flow rate of drops of a given size range per unit of cross-sectional area of the column, then, by conservation:

$$V = v_p F^u_{Lp} = v F^u_L \qquad \text{for } 0 < z < z_{max}, \tag{8}$$

where:

v_p is the projection velocity of drops

v is the upwards velocity of drops at level z.

F^u_{Lp} is the volumetric liquid fraction at projection level, for drops in upward motion.

F^u_L is the volumetric liquid fraction at the level z, for drops in upward motion.

For not entrained drops, the volumetric liquid fraction, F_L is twice F^u_L, and

$$\frac{F_L}{F_{Lp}} = \frac{v_p}{v}$$

But

$$v = \sqrt{v_p^2 - 2gz} = \sqrt{2g(z_{max} - z)}$$

where h_{max} is the maximum height reached by the drops.

Thus:

$$\frac{F_L}{F_{Lp}} = \frac{1}{\sqrt{1 - z/z_{max}}}$$

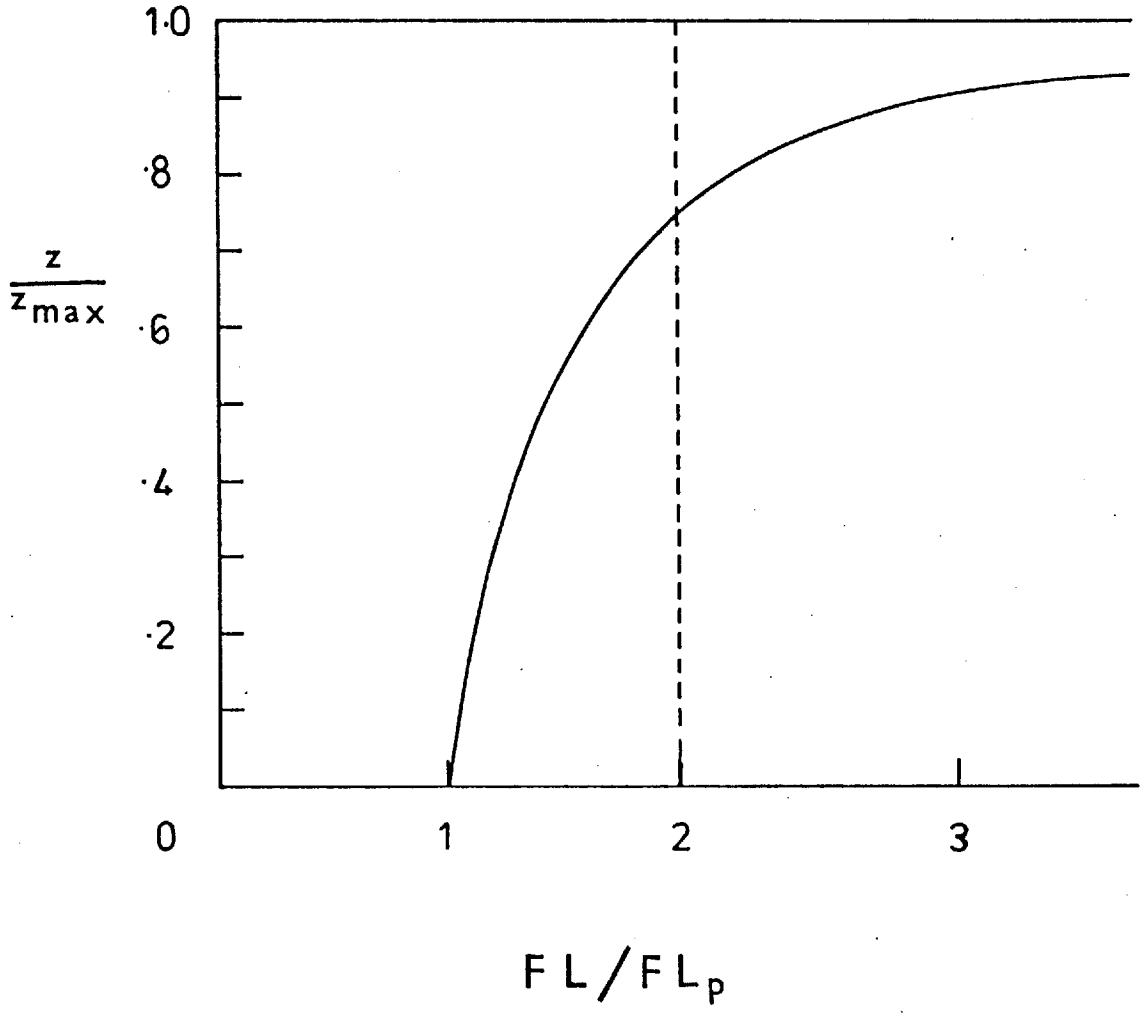

Fig.4.7.- Contribution of each drop to dispersion density profile (drag neglected).

Some computed values of expression (9) are presented in Table IV and used in Figure 4.7.

Table IV

z/z_{max}	0	0.1	0.2	0.3	0.4	0.5	0.6	0.7	0.8	0.9	0.92	1
F_L/F_{Lp}	1	1.05	1.12	1.20	1.29	1.41	1.58	1.82	2.24	3.16	3.53	∞

The following conclusions can be drawn from the table:

Contribution of each drop to the profile is mainly around the value $z = z_{max}$. This suggests a further possible simplification, if necessary - contributions to profiles coming only from drops at their maximum height.

The medium value of F_L/F_{Lp} will be given by

$$\left\langle \frac{F_L}{F_{Lp}} \right\rangle = \frac{1}{z_{max}} \int_0^{z_{max}} \left(\frac{F_L}{F_{Lp}}\right) dz$$

Using equation (9) and rearranging

$$\left\langle \frac{F_L}{F_{Lp}} \right\rangle = \int_0^1 \frac{1}{\sqrt{1 - z/z_{max}}} \, d(z/z_{max}) = 2$$

Hold-up of drops

Hold-up of drops of given size will be

$$2F_{Lp}\, z_{max} \qquad (10')$$

But as $$F_{Lp} = 2F^u_{Lp} = \frac{2n}{v_p} \frac{\pi d_p^3}{6} \qquad (10'')$$

where n is the number of drops of size d_p generated per unit time, the hold-up of drops of size d_p is then

$$\frac{4n}{v_p} \frac{\pi d_p^3}{6} \frac{v_p^2}{2g} = n. \frac{\pi d_p^3}{6} \frac{2v_p}{g} \tag{10}$$

This represents the volumetric flow rate of generated drops times their residence time on plate for the given size range. Then the total hold-up of drops is:

$$H_D = \int_0^{N_p} \frac{\pi d_p^3}{6} \frac{2v_p}{g} \, dN \tag{11}$$

where N is the cumulative number of generated drops.

Take $$v_p = A \, d_p^B \tag{7}$$

and $$dN = N_p \, f_\sigma(x) dx \tag{12}$$

where $$x = \ln \frac{d_p}{d_{gm}} \tag{13}$$

and $$f_\sigma(x) = \frac{1}{\sqrt{2\pi}\,\sigma} e^{-x^2/2\sigma^2} \tag{14}$$

Using equations (7), (12) and (13), the hold-up becomes:

$$H_D = \frac{A\pi d_{gm}^{(3+B)} N_p}{3g} \int_{-\infty}^{+\infty} e^{(3+B)x} f_\sigma(x) dx \tag{15}$$

However:

$$e^{(3+B)x} f_\sigma(x) dx = e^{\frac{[(3+B)\sigma]^2}{2}} f_\sigma(y) dy \tag{16}$$

where

$$y = x - (3 + B)\sigma^2 \tag{17}$$

Using equation (16) in equation (15):

$$H_D = \frac{A\pi d_{gm}^{(3+B)}}{3g} N_p e^{\frac{[(3+B)\sigma]^2}{2}} \tag{18}$$

since

$$\int_{-\infty}^{+\infty} f_\sigma(y)dy = 1. \tag{19}$$

Define

$$d_V = d_{gm} e^{\frac{(3+B)\sigma^2}{2}} \quad \text{and} \tag{20}$$

$$v_V = Ad_V^B \tag{21}$$

Then hold-up becomes

$$H_D = N_p \frac{\pi d_V^3}{6} \cdot \frac{2v_V}{g} \tag{22}$$

That is, d_V is the equivalent diameter of a mono-dispersed distribution giving the same hold-up with the same number of generated drops.

Total superficial area of dispersion

Similarly to equation (11), the total superficial area is:

$$A_D = \int_0^{N_p} \pi d_p^2 \frac{2v_p}{g} dN \tag{23}$$

$$= \frac{2A\pi d_{gm}^{(2+B)}}{g} N_p e^{\frac{[(2+B)\sigma]^2}{2}} \tag{24}$$

Again, by defining

$$d_A = d_{gm}\, e^{\frac{(2+B)\sigma^2}{2}} \tag{25}$$

and $$v_A = A\, d_A^{\,B} \tag{26}$$

it follows that

$$A_D = N_p \pi d_A^{\,2} \cdot \frac{2v_A}{g} \tag{27}$$

where d_A is the equivalent diameter of a monodispersed distribution giving the same total interfacial area with the same number of generated drops.

The Sauter mean diameter of the dispersion will be:

$$d^{Disp}_{Sauter} = \frac{6H_D}{A_D} = \frac{d_V^{\,3} v_V}{d_A^{\,2} v_A} \tag{28}$$

By (20), (21), (25) and (26):

$$d^{Disp}_{Sauter} = d_{gm}\, e^{(\frac{5}{2} + B)\sigma^2} = d^{Proj.\ drops}_{Sauter}\ e^{B\sigma^2} \tag{29}$$

(iii) A further simplification of the Fane and Sawistowski model for the spray regime

It will now be assumed that:

a) There is no drag effect

b) Contributions to liquid fraction and superficial area come only from drops at maximum level

c) Initial projection velocity of drops is a function of drop size

according to the general equation

$$v_p = A\, d_p^{B}\,, \tag{30}$$

where A is a positive constant and B has a negative constant value. This equation in the model of Fane and Sawistowski is:

$$v_p = 0.002355\, d_p^{-0.93} \quad (= 0.4\ (0.004/d_p)^{0.93}) \tag{31}$$

(iii.1) Relation between projection velocity function and profile of Sauter mean diameter of drops

If there exist experimental data on profiles of liquid fraction and specific area, the profile of Sauter mean diameter can be obtained. In this case the parameters A and B of equation (30) can be determined under the above mentioned assumptions in the following way:

The maximum height reached by a drop is

$$z = \frac{v_p^2}{2g} \tag{32}$$

and the size, d_p, of the drop whose maximum height is z is given by:

$$z = \frac{A^2}{2g}\, d_p^{2B} \tag{33}$$

This is the maximum size of drops existing at height z. Taking logarithms eq. (33) gives:

$$\log z = \log \frac{A^2}{2g} + 2B \log d_p \tag{34}$$

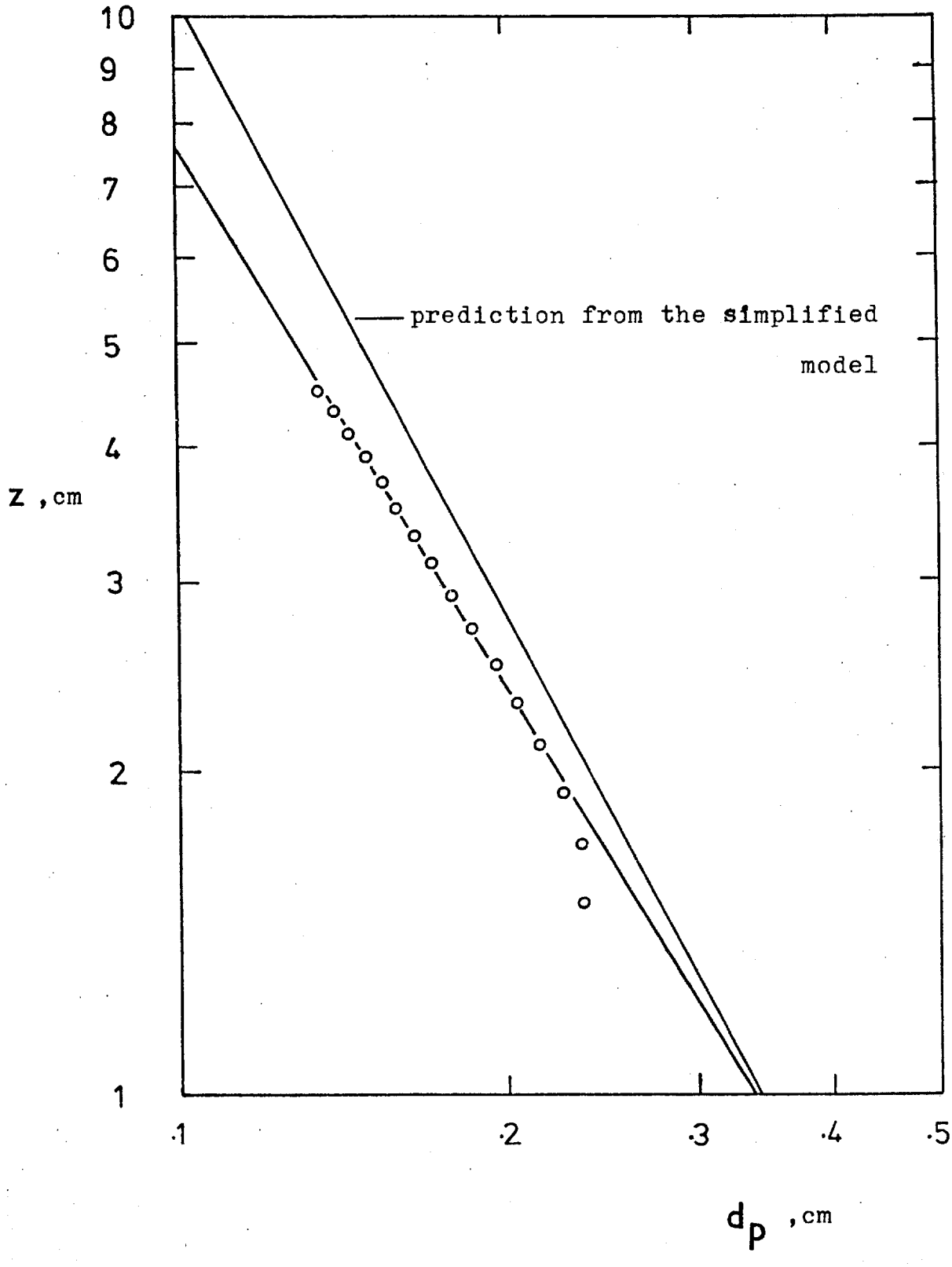

Fig.4.8.- Sauter mean diameter profile (in log-log paper) for run 33 and prediction from simplified model.

Equation (34) represents a straight line of slope 2B and intercept $\log \frac{A^2}{2g}$ on log-log paper.

To check the errors involved using these simplifications, the model results of run 33 were investigated. From Figure 4.8 it can be seen that the Sauter diameter is slightly lower than the maximum diameter and the difference is between 7 and 12%, being smaller for the most predominant sizes of drops. The expression for projection velocity arrived at was

$$v_p = 0.39\ (0.004/d_p)^{0.83} \qquad (35)$$

which is very similar to the one used in the model (eq. 31).

Conclusion: By a simple representation on log-log paper of experimental values of the Sauter mean diameter, obtained from experimental data of dispersion density and specific area profiles, it is possible to obtain a relation between projection velocity and drop diameter. Such a relation is very useful for modelling of the spray regime.

(iii.2) Relation between distribution of drops and profiles of dispersion density and specific area

It was shown that population of generated drops can be represented by log-normal distribution. Introducing the simplifying assumptions it is possible to deduce the type of spatial distribution of volume and surface area of drops given, respectively, by the profiles of dispersion density and area per unit volume of dispersion (subsequently referred to as specific surface area).

From equation (10'), the hold-up of a drop of size d_p is:

$$H_D = 2F_{Lp}\, z_{max} \qquad (36)$$

By equations (8) and (10")

$$F_{Lp} = 2 \frac{\pi d_p^3}{6Ad_p^B} \tag{37}$$

so that the hold-up becomes:

$$H_D = \frac{\pi d_p^3}{6} \cdot \frac{2Ad_p^B}{g} . \tag{38}$$

This is the product of volume and residence time.

Under the above mentioned simplifying assumptions,

$$F_L = - \frac{A\pi d_p^{(3+B)}}{3g} \frac{dN}{dz} \quad \text{(N decreases when z increases)} \tag{39}$$

and similarly,

$$a = - \frac{2A\pi d_p^{(2+B)}}{g} \frac{dN}{dz} \tag{40}$$

where:

F_L and a are the local values of the dispersion density and specific surface area, N is the cumulative number distribution function of projected drops, d_p is the diameter of the drops changing direction at the height z above the plate floor, (so, dN is the total number of drops changing direction at heights between z and z + dz).

Defining z_{gm} as the maximum height reached by drops with diameter d_{gm}, using equation (33) and since

$$d(\ln \frac{z}{z_{gm}}) = \frac{dz}{z} \tag{41}$$

equations (39) and (40) become, respectively:

$$F_L = -\frac{A\pi d_{gm}^{(3+B)}}{3g\, z_{gm}} \left(\frac{z}{z_{gm}}\right)^{\frac{3-B}{2B}} f_\sigma\left(\frac{1}{2B} \ln \frac{z}{z_{gm}}\right) \tag{42}$$

$$a = -\frac{2A\pi d_{gm}^{(2+B)}}{g z_{gm}} \left(\frac{z}{z_{gm}}\right)^{\frac{2-B}{2B}} f_\sigma\left(\frac{1}{2B} \ln \frac{z}{z_{gm}}\right) \tag{43}$$

where

$$f_\sigma(x) = \frac{1}{\sqrt{2\pi}\sigma}\, e^{-x^2/2\sigma^2} \tag{44}$$

is the normal distribution of x with mean zero and standard deviation σ.

However, as

$$x^n = e^{n \ln x} \tag{45}$$

and

$$e^{mx} f_\sigma(x) = e^{\frac{(m\sigma)^2}{2}} f_\sigma(x - m\sigma^2) \tag{46}$$

then:

$$F_L = -\frac{A\pi d_{gm}^{(3+B)} N_p}{3g\, z_{gm}}\, e^{\frac{[(3-B)\sigma]^2}{2}} f_\sigma\left(\frac{1}{2B} \ln \frac{z}{z_{gm} e^{2B(3-B)\sigma^2}}\right) \tag{47}$$

But as

$$f_\sigma(x) = \frac{1}{b}\, f_{|\sigma/b|}(x/b), \tag{48}$$

the final expression for F_L become:

$$F_L = -\frac{A\pi d_{gm}^{(3+B)} N_p}{6Bg\, z_{gm}} e^{\frac{[(3-B)\sigma]^2}{2}} f_{|2B\sigma|}\left(\ln \frac{z}{z_{gm} e^{2B(3-B)\sigma^2}}\right) \tag{49}$$

Similarly:

$$a = -\frac{A\pi d_{gm}^{(2+B)} N_p}{Bg\, z_{gm}} e^{\frac{[(2-B)\sigma]^2}{2}} f_{|2B\sigma|}\left(\frac{z}{z_{gm} e^{2B(2-B)\sigma^2}}\right) \tag{50}$$

Equations (49) and (50) show that both profiles are expressed by log-normal distribution functions of the height, with standard deviation $-2B\sigma$ and heights of maximum dispersion profile and specific surface area, respectively $z_{gm} e^{2B(3-B)\sigma^2}$ and $z_{gm} e^{2B(2-B)\sigma^2}$, where z_{gm} is the maximum height reached by the drop of geometric mean diameter, d_{gm}, and σ is the standard deviation of the log normal distribution of population of generated drops.

The total hold-up will be:

$$H_D = \int_0^\infty F_L\, dz = \int_{-\infty}^\infty F_L\, zd\left(\ln \frac{z}{z_{gm} e^{2B(3-B)\sigma^2}}\right) \tag{51}$$

which gives the previously obtained result

$$H_D = \frac{AN_p \pi d_{gm}^{(3+B)}}{3g} e^{\frac{(3+B)^2}{2}\sigma^2} \tag{52}$$

Define:

$$d_V = d_{gm} e^{\frac{(3+B)\sigma^2}{2}} \tag{53}$$

$$v_V = Ad_V^B$$

so that:

$$H_D = N_p \frac{\pi d_V^3}{6} \frac{2v_V}{g} \tag{55}$$

This shows that the hold-up of drops is equal to that given by the same number of drops of size D_V projected with the initial velocity of the drops of the same size.

Similarly, for the total interfacial area equation (27) is obtained.

However, under the simplifying assumptions being considered it seems more realistic to say that

$$F_L \alpha - d_p^3 \frac{dN}{dz}$$

and not to $-d_p^{(3+B)} \frac{dN}{dz}$ as was done before, because near the upper part of the trajectory the movement of the drops is independent of size (no drag) and only this portion of the trajectory is considered as contributing to the profiles. Under these conditions, the final expressions arrived at are:

$$F_L \alpha - \frac{N_p}{z_{gm}} \frac{\pi}{6} d_{gm}^3 e^{\frac{[(3-2B)\sigma]^2}{2}} f_{|2B\sigma|}\left(\ln \frac{z}{z_{gm} e^{2B(3-2B)\sigma^2}}\right) \tag{56}$$

$$a \propto -\frac{N_p}{z_{gm}} \pi d_{gm}^2 e^{\frac{[(2-2B)\sigma]^2}{2}} f_{|2B\sigma|}\left(\frac{z}{z_{gm} e^{2B(2-2B)\sigma^2}}\right) \qquad (57)$$

Equations (56) and (57) differ from equations (49) and (50) by the value of the height of the maximum of the profiles. However, this difference is in general small. The ratio of the values given by the two cases is always $e^{2B^2\sigma^2}$. If B is of the order of -0.93 and σ of the order of 0.2 ÷ 0.3, then the difference in the height of the maximum value of the profiles in the two cases is of the order of 7 to 17%. The standard deviation is the same for both cases.

4.1.5 Characterisation of dispersion density and specific area profiles

As previously indicated, the dispersion density profiles of drops, as well as their specific area profiles can be fitted by log-normal distribution functions. Three parameters are necessary to characterise each profile. For the sake of convenience the selected parameters are:

The geometric mean height, z^p_{gm},

the corresponding value of the profile, M, and the standard deviation, σ_p.

Let $x = \ln \frac{z}{z^p_{gm}}$ and

$\frac{dN}{dx}$ = measured value of profile,

where z is the height above plate.

Then the log-normal distribution is:

$$\frac{dN}{dx} = \frac{N_T}{\sigma_p \sqrt{2\pi}} e^{-\frac{x^2}{2\sigma_p^2}} = N_T f_{\sigma_p}(x) \qquad (58)$$

The maximum value of $\frac{dN}{dx}$ (at $z = z_{gm}^{p}$, that is at $x = 0$) is:

$$M = \frac{N_T}{\sigma_p \sqrt{2\pi}}$$

The methods available for estimation of parameters of the log-normal distribution are:

(i) the method of maximum likelihood,

(ii) the method of moments,

(iii) the method of quantiles, and

(iv) the graphical method.

An additional group of methods can be considered to exist covering all those methods which are hybrids of the other four types.

The best method is considered to be the method of maximum likelihood, but it is costly on computing time; the method of moments is not recommended; the method of quantiles is easily applied and the best results are obtained for geometric mean and variance when 27,73 and 7,93 quantiles are used respectively; the graphical method is also easily applied and provides simultaneously a test of log normality.

However, the present problem is more complex since part of the distribution is removed, because in the lower part of the dispersion, the contribution of the pool (and ligaments) is overlapping the contribution of drops.

The estimation of the parameters will therefore be performed by a least squares technique applied to the experimental values. The method is

as follows:

(i) Given the set of experimental points

(P_i^E, z_i), $(i = 1,...n)$,

(ii) Guess initial values of M, z_{gm}^p and σ_p,

(iii) Compute values of profile, P_i^C, corresponding to z_i,

$(i = 1,...n)$

(iv) Compute total square error:

$$F = \sum_{i=1}^{n} (P_i^C - P_i^E)^2$$

(v) Compute

$$\frac{\partial F}{\partial M}, \quad \frac{\partial F}{\partial z_{gm}^p} \text{ and } \frac{\partial F}{\partial \sigma_p}$$

(vi) Get M, z_{gm}^p and σ_p which minimize F (that is, values for which

$$\frac{\partial F}{\partial M} = \frac{\partial F}{\partial z_{gm}^p} = \frac{\partial F}{\partial \sigma_p} = 0).$$

The subroutine used for minimization is due to Powell.[115]

This process was successfully applied to the present experimental results and to those of Pinczewski *et al.*[116] as well as to those of Fane and Sawistowski.[1] Results are presented in appendix III.

4.1.6 Determination of parameters of model from measurement of dispersion density and specific superficial area profiles

The relevant hydrodynamic parameters necessary for the simplified model are the initial velocity of the drops, the characteristics of population of generated drops and liquid hold-up. Once these parameters are known, mass transfer can be calculated to predict plate efficiency. The hold-up of the drops can be calculated by integration of the computed dispersion density profile. Then:

$$[H_D]_{z_1}^{z_2} = \int_{z_1}^{z_2} \frac{dN}{dx}\, dz \,, \tag{60}$$

where

$$x = \ln \frac{z}{z_{gm}^{FL}} \tag{61}$$

But:

$$dz = z_{gm}^{FL}\, e^{x}\, dx$$

so that eq. (60) becomes:

$$[H_D]_{z_1}^{z_2} = \int_{x_1 = \ln \frac{z_1}{z_{gm}^{FL}}}^{x_2 = \ln \frac{z_2}{z_{gm}^{FL}}} \frac{dN}{dx}\, z_{gm}^{FL}\, e^{x}\, dx \tag{62}$$

Using the value of $\frac{dN}{dx}$ given by (58), equation (62) gives:

$$[H_D]_{z_1}^{z_2} = z_{gm}^{FL}\, \frac{N_T\, e^{\frac{\sigma_{FL}^2}{2}}}{\sigma_{FL}\sqrt{2\pi}} \int_{x_1}^{x_2} e^{-\left(\frac{x}{\sigma_{FL}\sqrt{2}} - \frac{\sigma_{FL}}{\sqrt{2}}\right)^2} dx \tag{63}$$

Let

$$\bar{x} = x - \sigma_{FL}^2$$

Then

$$[H_D]_{z_1}^{z_2} = z_{gm}^{FL}\, \frac{e^{\frac{\sigma_{FL}^2}{2}}\, N_T}{\sigma_{FL}\sqrt{2\pi}} \int_{\sigma_{FL}^2 + \ln \frac{z_1}{z_{gm}^{FL}}}^{\sigma_{FL}^2 + \ln \frac{z_2}{z_{gm}^{FL}}} e^{\frac{\bar{x}^2}{2\sigma_{FL}^2}}\, d\bar{x} \tag{64}$$

By integration:

$$[H_D]_{z_1}^{z_2} = z_{gm}^{FL} e^{\frac{\sigma_{FL}^2}{2}} \frac{N_T}{2} [1 + erf(- \frac{\sigma_{FL}}{\sqrt{2}} + \frac{1}{\sigma_{FL}\sqrt{2}} \ln \frac{z_2}{z_{gm}^{FL}}) -$$

$$- erf (- \frac{\sigma_{FL}}{\sqrt{2}} + \frac{1}{\sigma_{FL}\sqrt{2}} \ln \frac{z_1}{z_{gm}^{FL}})] \quad (65)$$

The total hold-up is:

$$H_D = \sqrt{2\pi}\, z_{gm}^{FL} M_{FL} \sigma_{FL} e^{\frac{\sigma_{FL}^2}{2}} \quad (66)$$

Similarly the total surface area of the dispersion is:

$$A_D = \sqrt{2\pi}\, z_{gm}^{a} M_a \sigma_a e^{\frac{\sigma_a^2}{2}} \quad (67)$$

However equations (18) and (27) hold:

$$H_D = N_p \frac{A\pi d_{gm}^{(3+B)}}{3g} e^{\frac{[(3+B)\sigma]^2}{2}} \quad (68)$$

$$A_D = N_p \frac{2A\pi d_{gm}^{(2+B)}}{g} e^{\frac{[(2+B)\sigma]^2}{2}} \quad (69)$$

and from equations (49) and (50)

$$\sigma_{FL} = \sigma_a = - 2B\sigma \quad (70),(71)$$

$$z_{gm}^{FL} = z_{gm} e^{2B(3-B)\sigma^2} \quad (72)$$

$$z_{gm}^{a} = z_{gm} e^{2B(2-B)\sigma^2} \quad (73)$$

where $z_{gm} = \frac{(Ad_{gm}^{B})^2}{2g}$ (74)

The total number of variables used in the hydrodynamic model is equal to 14:

H_D, z_{gm}^{FL}, M_{FL}, σ_{FL}, A_D, z_{gm}^{a}, M_a, σ_a, N_p, d_{gm}, z_{gm}, σ,A,B.

Number of independent relations = 9:

(equations (66) to (74)).

Number of independent variables = 5.

So, the information necessary for completing the hydrodynamic knowledge of the spray regime requires information on the value of any five of the above-mentioned variables. Consider three important cases:

(i) A and B are known

Fane and Sawistowski assumed that A and B were known. Under these circumstances from measurements of dispersion density profiles the other three necessary variables could have been obtained:

$$z_{gm}^{FL}, \quad M_{FL}, \quad \sigma_{FL}.$$

The parameters necessary for the model can be obtained as follows:

From eq. (49), (66) and (68)

$$-2B\sigma = \sigma_{FL} \tag{75}$$

$$z_{FL}^{M} = z_{gm} e^{2B(3-B)\sigma^2} \tag{76}$$

$$H_D = \sqrt{2\pi}\, z_{gm}^{FL} M_{FL} \sigma_{FL} e^{\frac{\sigma_{FL}^2}{2}} = N_p \frac{\pi d_{gm}^{3}}{6} \frac{2Ad_{gm}^{B}}{g} e^{\frac{[(3+B)\sigma]^2}{2}} \tag{77}$$

Then:

$$\sigma = -\frac{\sigma_{FL}}{2B} \tag{78}$$

$$d_{gm} = \left(\frac{\sqrt{2g\, z_{gm}^{FL}}}{A}\, e^{\frac{B-3}{4B}\sigma_{FL}^2}\right)^{1/B} \tag{79}$$

$$N_p = \frac{\sqrt{2\pi}\; z_{gm}^{FL}\, M_{FL}\, \sigma_{FL}\, e^{\sigma_{FL}^2/2}}{\frac{\pi d_{gm}^3}{6}\,\frac{2Ad_{gm}^B}{g}\, e^{\frac{[(3+B)\sigma]^2}{2}}} \tag{80}$$

The specific superficial area profile can thus be predicted. The parameters characterising this profile are given by:

$$z_{gm}^a = z_{gm}^{FL}\, e^{-\sigma_{FL}^2/2B} \tag{81}$$

$$M_a = 6\left(\frac{z_{gm}^{FL}}{z_{gm}^a}\right)\left(\frac{M_{FL}}{d_{gm}}\right) e^{-\frac{5+2B}{8B^2}\sigma_{FL}^2} \tag{82}$$

$$\sigma_a = \sigma_{FL}$$

The value of d_{gm} given by eq. (79), e.g. for run 33, was 7.5%, above the result from the "exact" model, that is slightly higher than the lower errors in Figure 4.8, as expected.

(ii) B is known

The value of 0.93 can be supposed to apply and in this case four variables need to be determined. These variables can be the same three previous ones and for example the total superficial area or superficial

area at a given level. For this purpose a pseudo-first-order fast reaction can be used. For this purpose dilute CO_2 can be absorbed in aqueous solutions of NaOH. However the introduction of ionic solutions changes the interfacial conditions and the results can be affected. Another method consists of the use of a light probe located at a given level, known to be above the height of maximum superficial area, or even obtaining a profile of specific area.

Given dispersion density profile and specific area at any height above that corresponding to the maximum of the profile the parameter A can be calculated as follows:

$$x_a = \ln \frac{z}{z_{gm}^a} \tag{84}$$

Elimination of z_{gm}^a using eq. (81) gives

$$x_a = x_{FL} + \frac{\sigma_{FL}^2}{2B} \tag{85}$$

where $$x_{FL} = \ln \frac{z}{z_{gm}^{FL}} \tag{86}$$

But $$a(z) = M_a e^{-\frac{x_a^2}{2\sigma_{FL}^2}} \tag{87}$$

Then $$M_a = a(z)\, e^{\frac{x_a^2}{2\sigma_{FL}^2}} \tag{88}$$

From eq. (66), (67) and (70)

$$\frac{H_D}{A_D} = \frac{z_{gm}^{FL} M_{FL}}{z_{gm}^a M_a} \tag{89}$$

From eq. (68), (69), (70) and (71)

$$\frac{H_D}{A_D} = \frac{d_{gm}}{6} e^{\frac{5+2B}{8B^2}\sigma^2_{FL}} \tag{90}$$

From eq. (89) and (90)

$$d_{gm} = 6 \frac{z^{FL}_{gm}}{z_{gm}{}^{a}} \frac{M_{FL}}{M_a} e^{-\frac{5+2B}{8B^2}\sigma^2_{FL}} \tag{91}$$

Since

$$\frac{z^{FL}_{gm}}{z_{gm}{}^{a}} = e^{\frac{\sigma^2_{FL}}{2B}} \tag{92}$$

eq. (91) becomes:

$$d_{gm} = 6 \frac{M_{FL}}{M_a} e^{\frac{2B-5}{8B^2}\sigma^2_{FL}} \tag{93}$$

From eq. (88):

$$d_{gm} = 6 \frac{M_{FL}}{a(z)} e^{(\frac{2B-5}{8B^2}\sigma^2_{FL} - \frac{x_a^2}{2\sigma^2_{FL}})} \tag{94}$$

Since

$$A = \sqrt{\frac{2g\, z^{FL}_{gm}}{d_{gm}{}^{B}}} e^{\frac{B-3}{4B}\sigma^2_{FL}} \tag{95}$$

Finally:

$$A = \sqrt{2g\, z_{gm}^{FL}}\, \left(\frac{a(z)}{6M_{FL}}\right)^{B} e^{-\frac{\sigma_{FL}^2}{8B} + \frac{Bx_a^2}{2\sigma_{FL}^2}} \tag{96}$$

If at any height the values a(z) and $F_L(z)$ are known, then

$$d_{Sauter}(z) = \frac{6F_L(z)}{a(z)} \tag{97}$$

As $d_{Sauter}(z)$ is approximately equal to the diameter of drops changing direction of motion there,

$$v_p = Ad_p^{B} = \sqrt{2gz} \tag{98}$$

or
$$A = \left(\frac{a(z)}{6F_L(z)}\right)^{B} \sqrt{2gz} \tag{99}$$

If the values of a and F_L are known at one value of z, and as B is assumed to be known, only two unknown parameters remain, which are d_{gm} and σ.

(iii) Neither of the parameters is known

In this case two variables other than z_{gm}^{FL}, M_{FL} and σ_{FL} need to be determined. Per example a specific superficial area profile can be obtained by a light probe and z_{gm}^{a} and M_a be determined. In this case, the parameter required for the initial projection velocity as well as the spray characteristics can be determined from:

$$\sigma = \frac{\ln(z_{gm}^{a}/z_{gm}^{FL})}{\sigma_{FL}} \tag{100}$$

$$B = -\frac{\sigma_{FL}}{2\sigma} \tag{101}$$

$$d_{gm} = 6\left(\frac{z_{gm}^{FL}}{z_{gm}^{a}}\right)\left(\frac{M_{FL}}{M_{a}}\right) e^{-\left(\frac{5}{2}+B\right)\sigma^2} \tag{102}$$

$$A = \frac{\sqrt{2g\, z_{gm}^{FL}}}{d_{gm}^{B}}\, e^{\frac{B-3}{4B}\sigma_{FL}^{2}} \tag{103}$$

4.2 Dispersion Density Profiles

4.2.1 Introduction

The factors affecting the dispersion density profiles, as well as those affecting specific surface area profiles and mass transfer performance are:

a) Flow rates of gas and liquid

b) Physical properties of gas and liquid

c) Geometry of plate and column

Attention has been concentrated on the most important factors in each group. As was referred to before, the upper parts of the dispersion density profiles are similar and can be adjusted by a log-normal distribution function which is characterised by three parameters. The parameters which are used to describe those distributions are the geometric mean height, x_2, standard deviation, x_3 and another parameter that has to be a measure of the total volume (in this case the total hold-up of drops) or for the sake of ease of practical determination, the maximum value of the dispersion density, x_1. The experimental dispersion density profiles are presented in appendix III. The curves shown were obtained by fitting of experimental points. As the importance of these studies is more applicable to the spray regime, almost all the results were obtained for this regime.

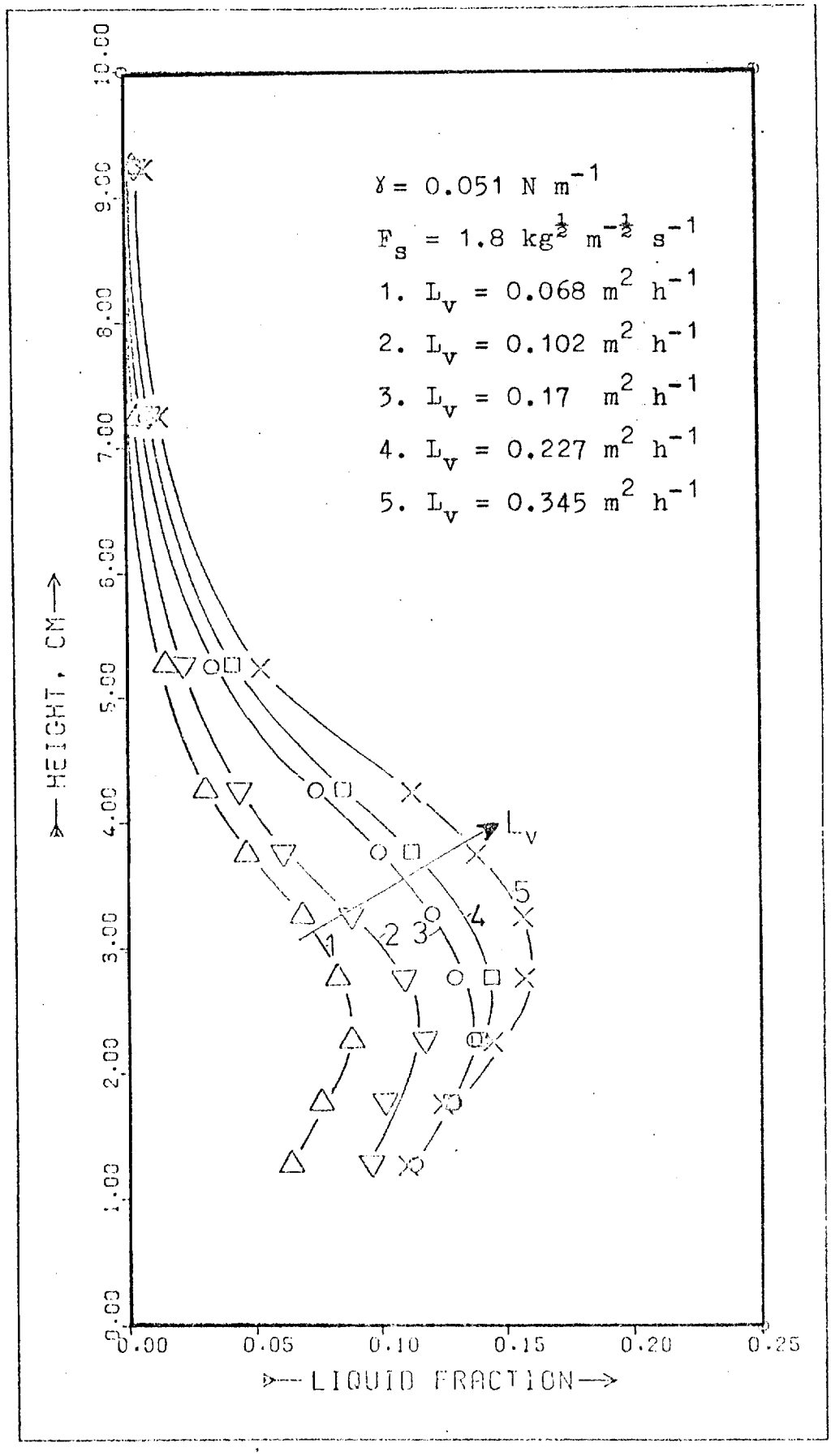

Fig. 4.9.- Effect of liquid cross-flow rate on dispersion density profiles (spray regime).

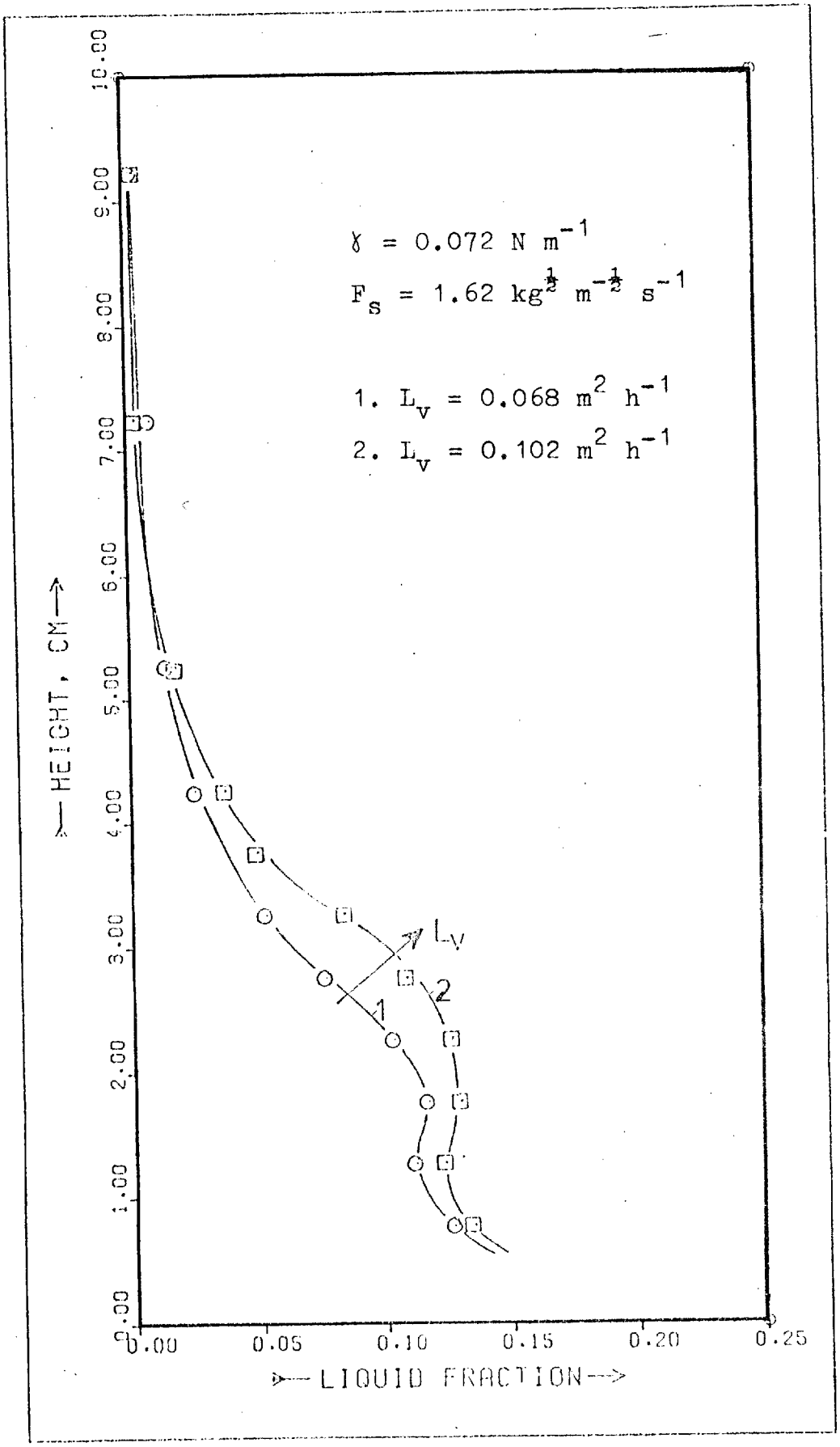

Fig. 4.10.- Effect of liquid cross-flow rate on dispersion density profiles (spray regime).

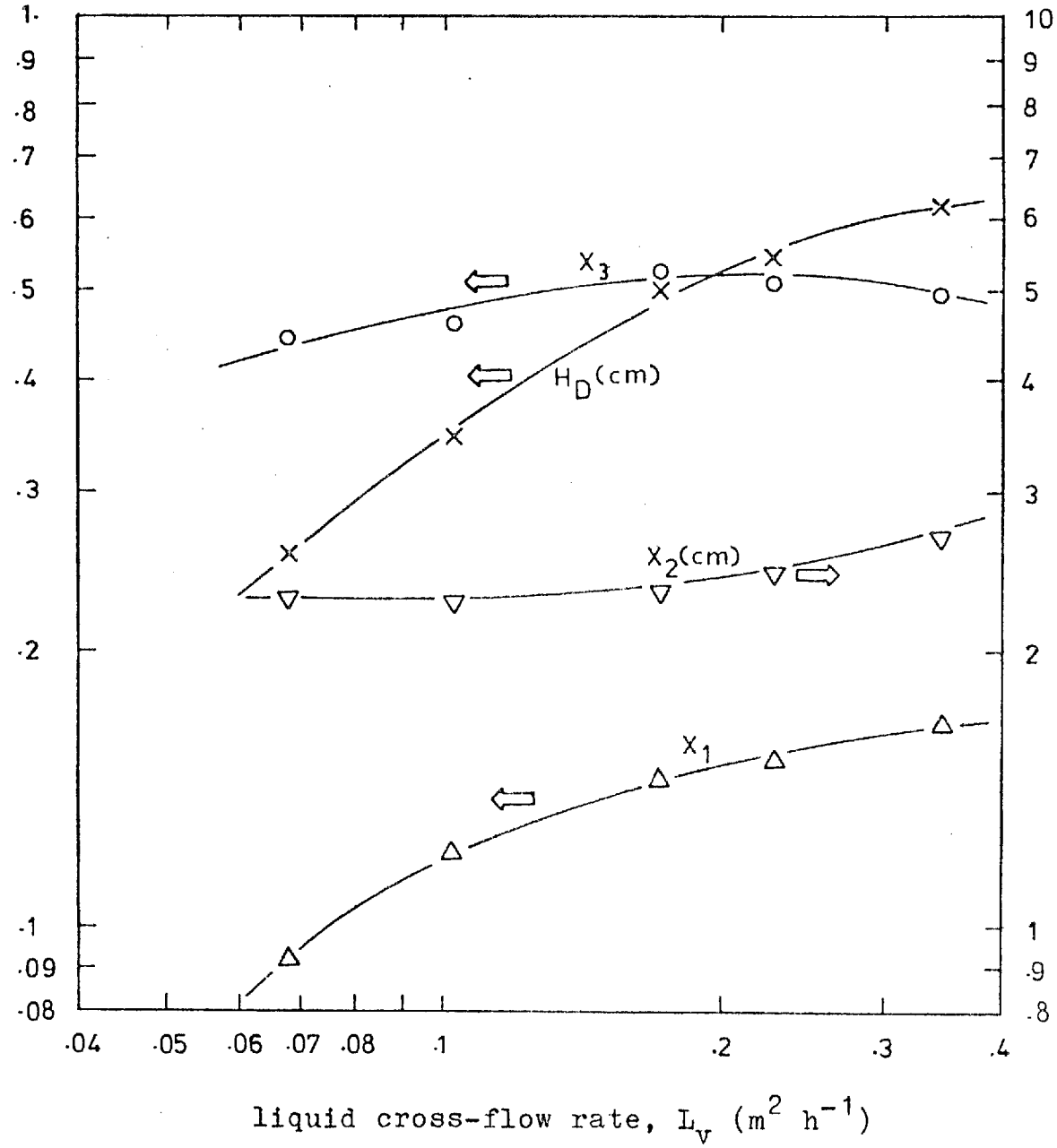

Fig. 4.11.- Effect of liquid cross-flow rate on dispersion density parameters and hold-up. F_s = 1.8 $kg^{\frac{1}{2}}\ m^{-\frac{1}{2}}\ s^{-1}$; γ = 0.051 N m^{-1}.

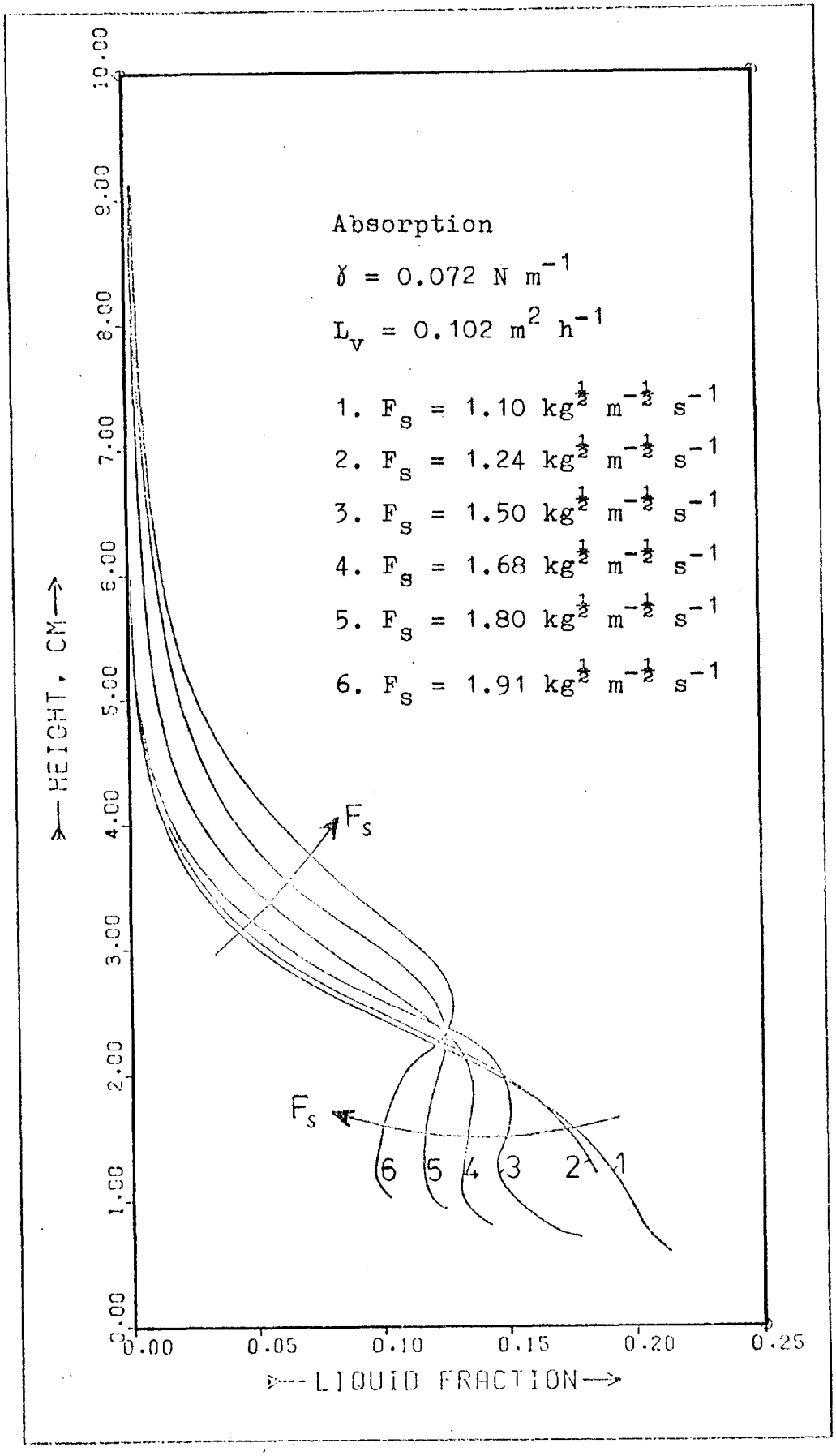

Fig. 4.12.- Effect of gas flow-rate on dispersion density profiles (froth/spray regimes, strongly negative system).

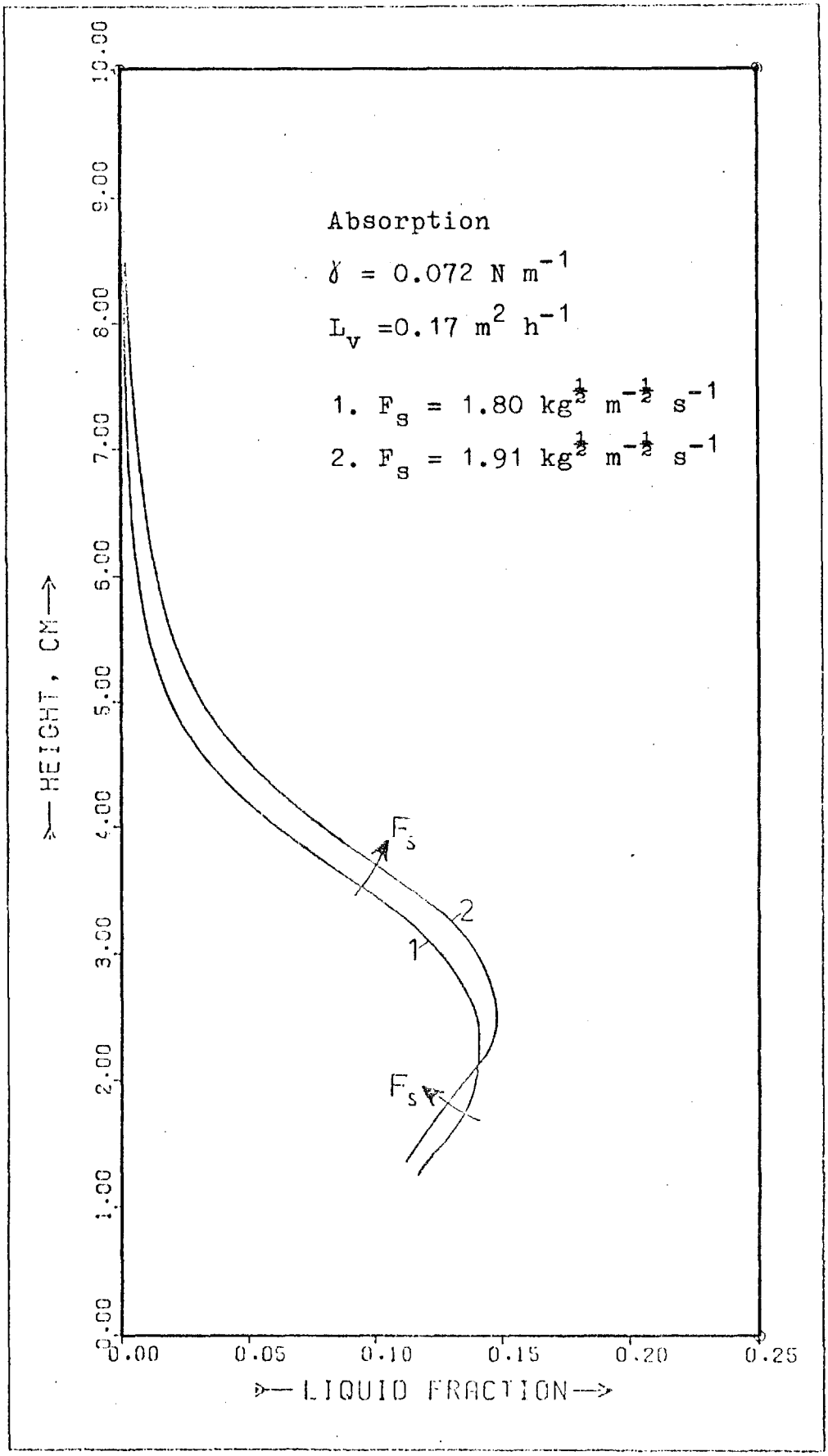

Fig. 4.13.- Effect of gas flow-rate on dispersion density profiles (spray regime, strongly negative system).

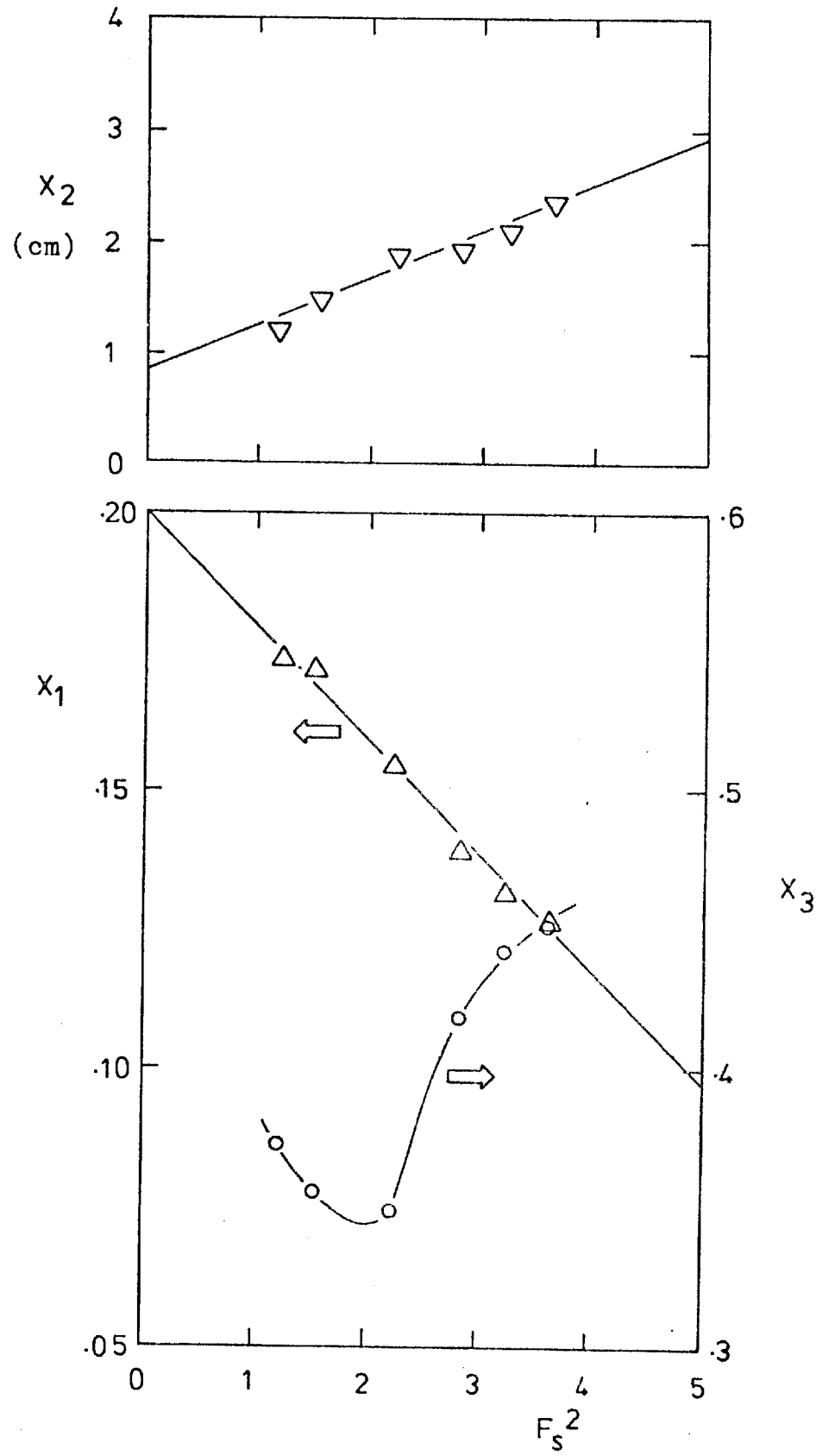

Fig. 4.14.- Effect of gas flow-rate on dispersion density parameters (froth-spray regimes, strongly negative system).

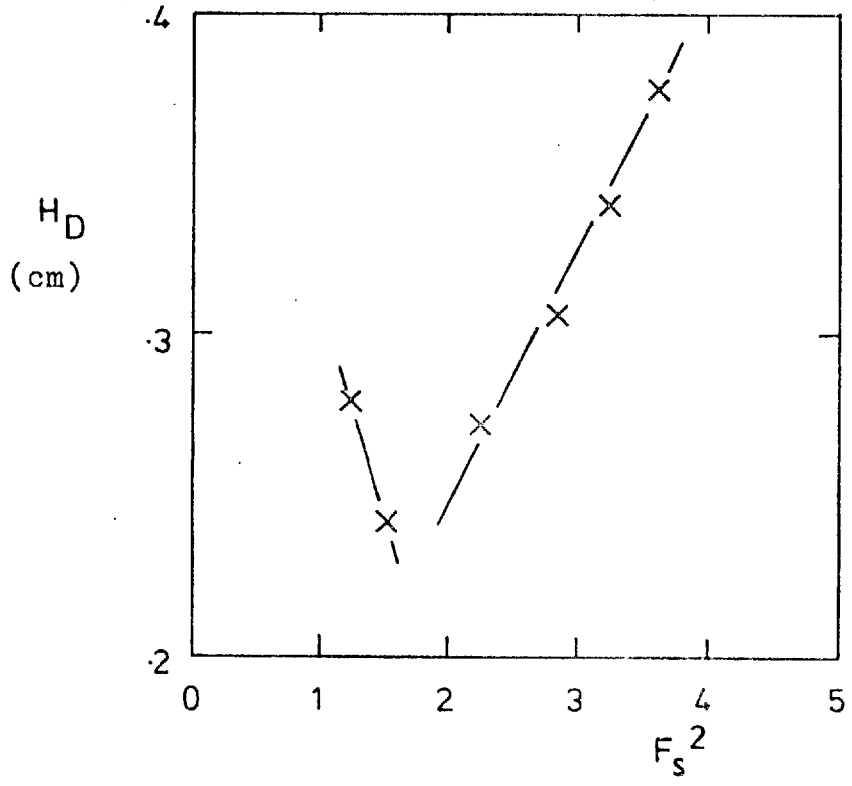

Fig. 4.15.- Effect of gas flow-rate drops hold-up (froth-spray regimes, strongly negative system).

4.2.2 Factors affecting the dispersion density profiles and the hold-ups

(i) Effect of liquid rate at constant gas rate

The effect of liquid rate on dispersion density profile is shown in Figures 4.9 and 4.10 which are representative of the encountered behaviour. The effect on parameters characterizing the dispersion density profile can be seen in Figure 4.11. The maximum value of the profile (x_1) and the corresponding height (x_2) increase with liquid rate in the spray regime. The increase in height (x_2) is very small. The standard deviation (x_3) remains approximately constant. The hold-up of drops increases substantially with liquid rate, although to a power smaller than one. The same findings can be reached using the data of Pinczewski and Fell at much higher values of liquid and gas rates.

(ii) Effect of gas rate at constant liquid rate

The effect of gas rate at constant liquid rate on dispersion density profile can be seen in Figures 4.12 and 4.13. The effect on parameters characterizing the dispersion density profile is shown in Figure 4.14. The maximum value of the dispersion density (x_1) decreases with gas rate either in the froth or in the spray regime. The height of maximum value of dispersion density profile increases continuously with increase in gas velocity either in the froth or in the spray regimes. The standard deviation of dispersion profile goes through a minimum with the increase in gas rate when the regime changes from froth to spray. The hold-up of drops also goes through a minimum, as can be seen in Figure 4.15.

(iii) Effect of gas rate at constant gas/liquid ratio

These results are shown in section (v).

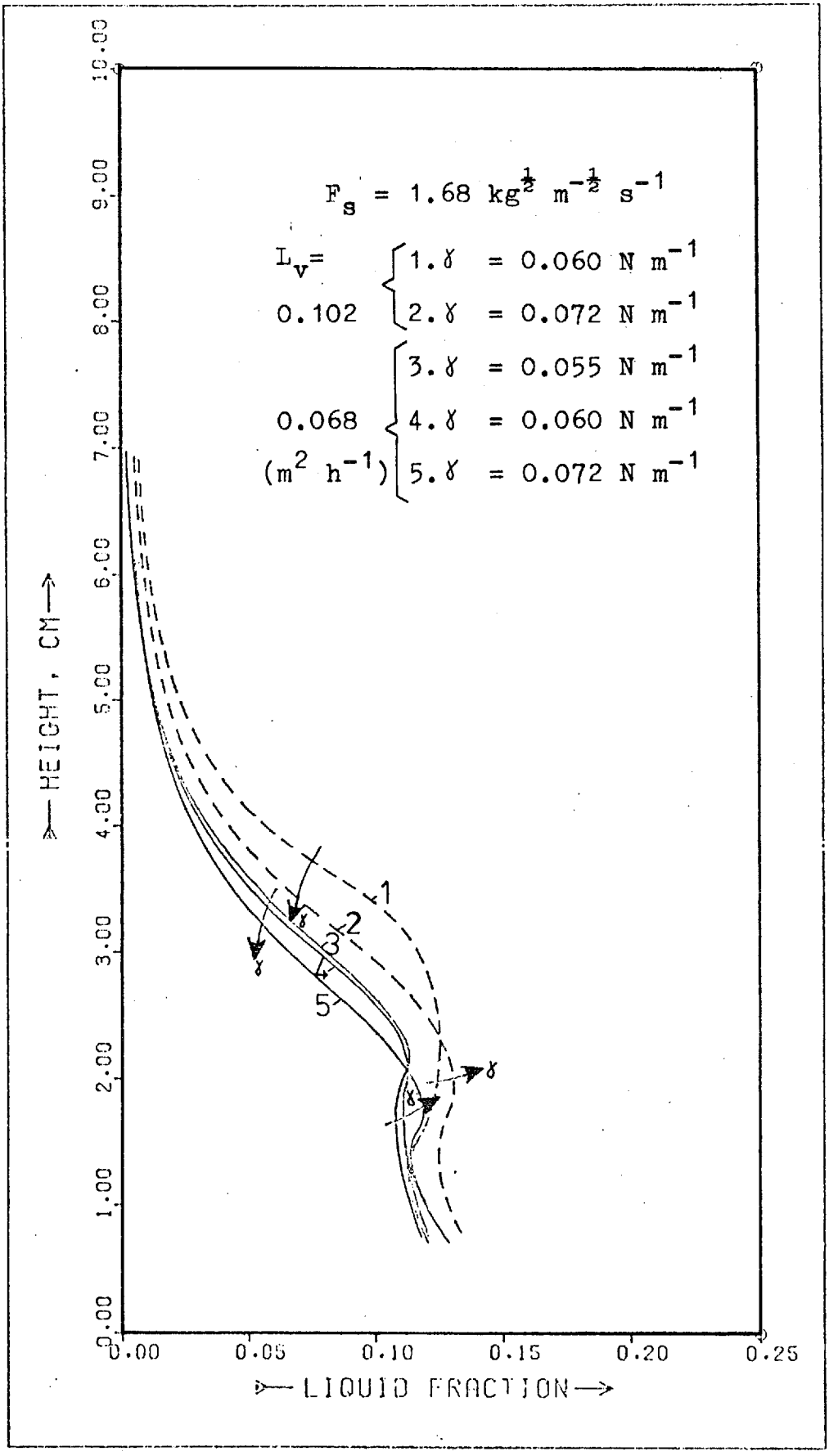

Fig. 4.16.- Effect of surface tension on dispersion density profiles (spray regime).

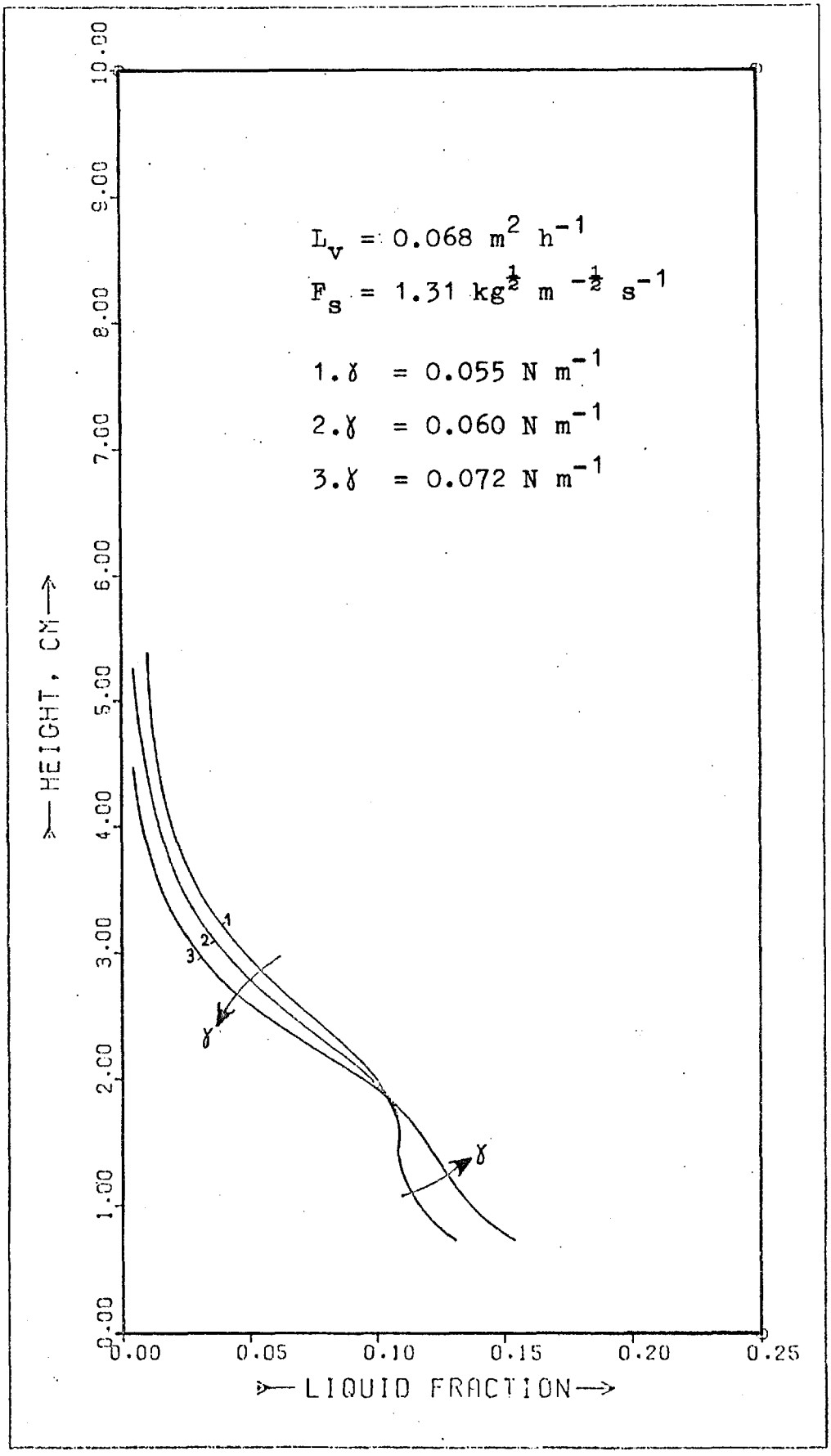

Fig. 4.17.- Effect of surface tension on dispersion density profiles (froth regime).

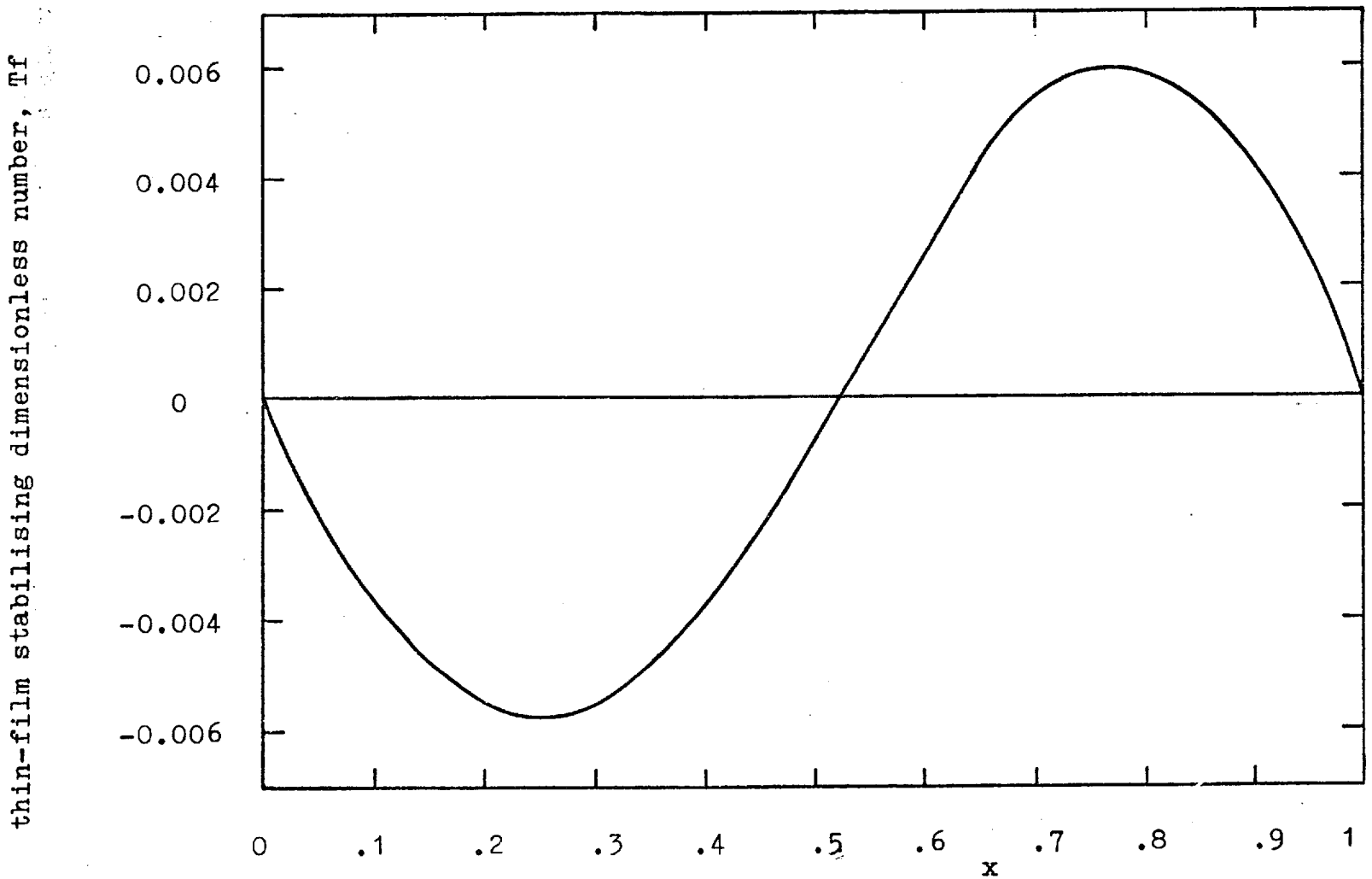

Fig. 4.18.- Variation of the thin-film stabilising number for system benzene-cyclohexane with mole fraction of benzene at total reflux.

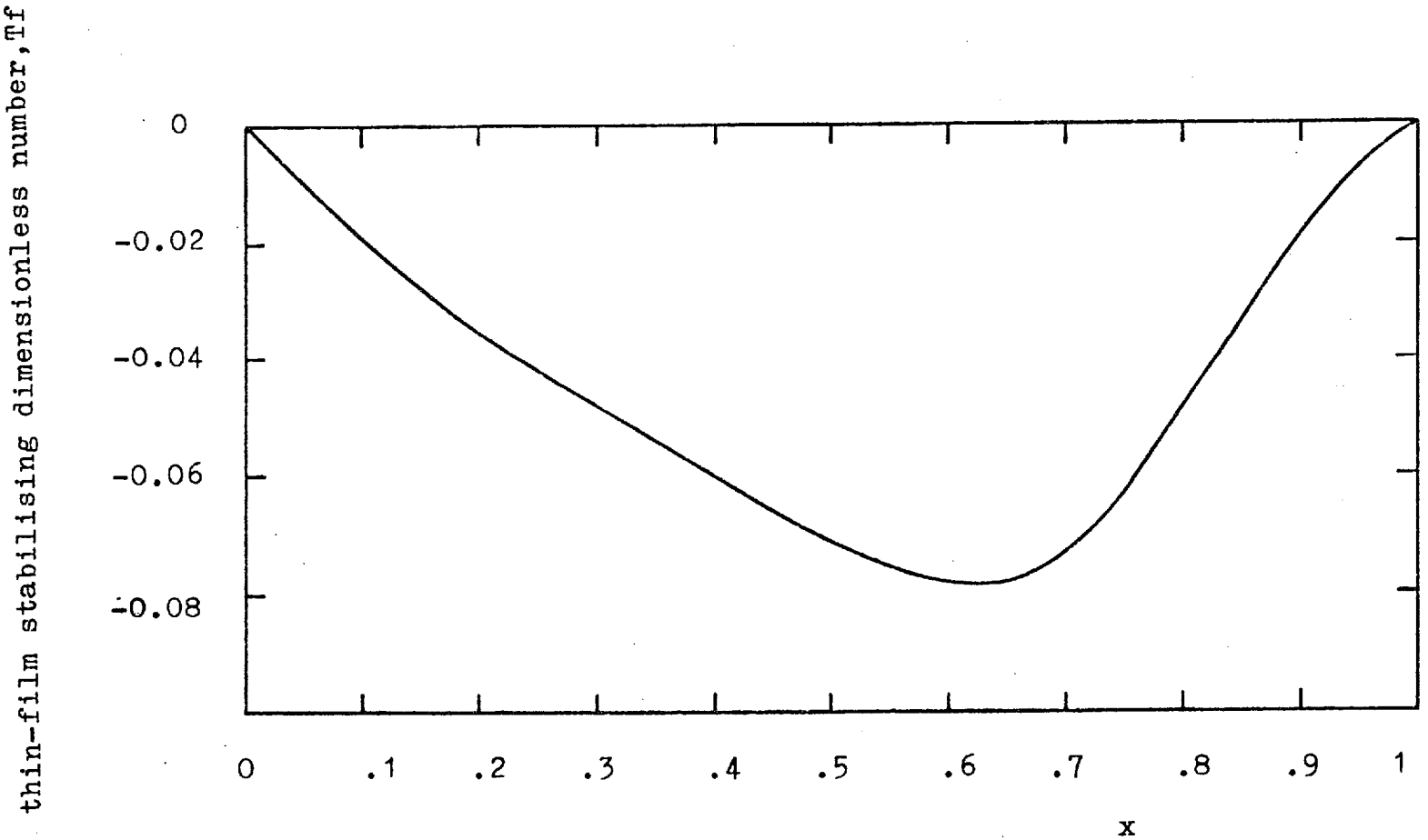

Fig. 4.19.- Variation of the thin-film stabilising number for negative system benzene-n-heptane, with mole fraction of benzene.

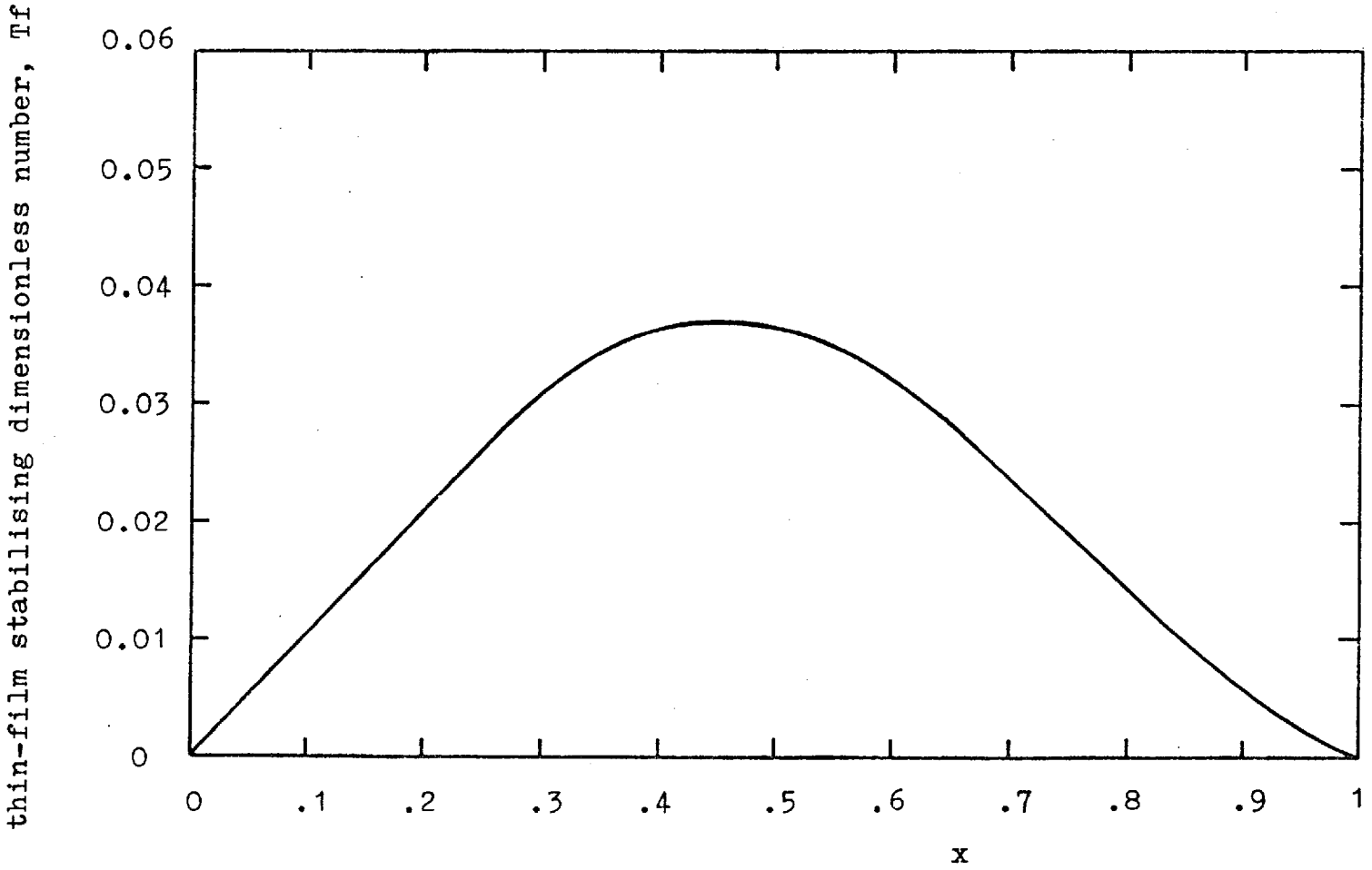

Fig. 4.20.- Variation of the thin-film stabilising number for positive system n-heptane-toluene with mole fraction of n-heptane.

(iv) Effect of surface tension

The effect of surface tension on dispersion density profiles can be seen in Figures 4.16 and 4.17. When the surface tension increased, at the same gas and liquid rate, the maximum value of the liquid fraction increased slightly, the corresponding height decreased and the standard deviation of the dispersion increased very slowly. The hold-up of drops decreased.

(v) Effect of mass transfer

Experimental results of the effect of mass transfer on dispersion density profile can be best correlated if a thin-film stabilising dimensionless number Tf is defined by

$$Tf = \frac{\gamma^* - \gamma_i}{\gamma_i} \qquad (104)$$

and if a classification of the systems is done as follows, according to the value of Tf:

strongly positive system	$Tf > 0.01$
weakly positive system	$0 < Tf < 0.01$
weakly negative system	$-0.01 < Tf < 0$
strongly negative system	$Tf < -0.01$.

γ_i is the surface tension corresponding to the liquid composition at interface and γ^* is the surface tension corresponding to the liquid composition in equilibrium with the bulk of gas phase (see Chapter 5).

The thin-film stabilising dimensionless numbers for the systems A: benzene-cyclohexane, B: benzene-n-heptane and C: n-heptane-toluene at total reflux were calculated and are presented as a function of liquid composition in Figures 4.18, 4.19 and 4.20, respectively.

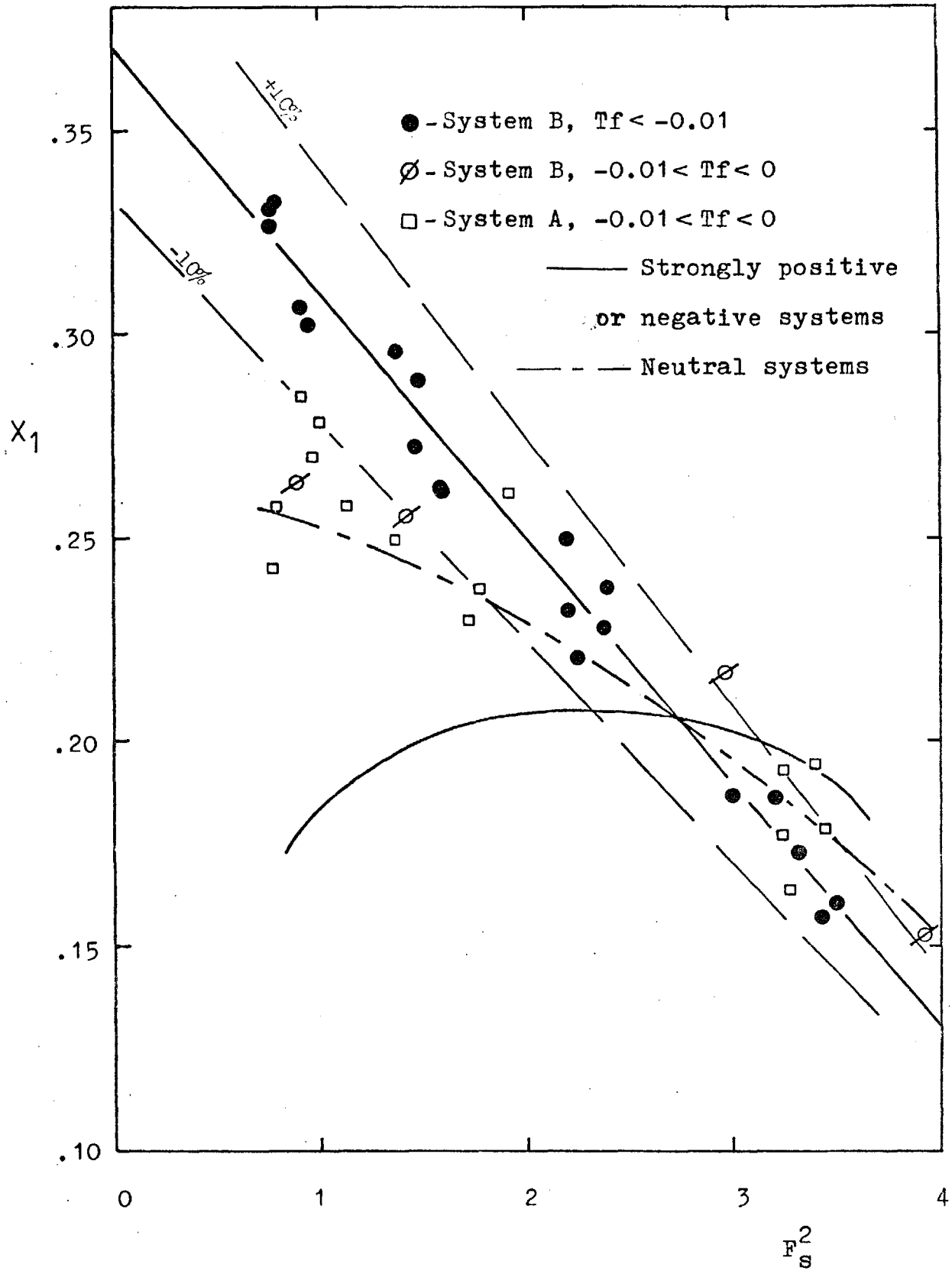

Fig. 4.21.- Variation of maximum value of dispersion density profile with F_s for negative systems.

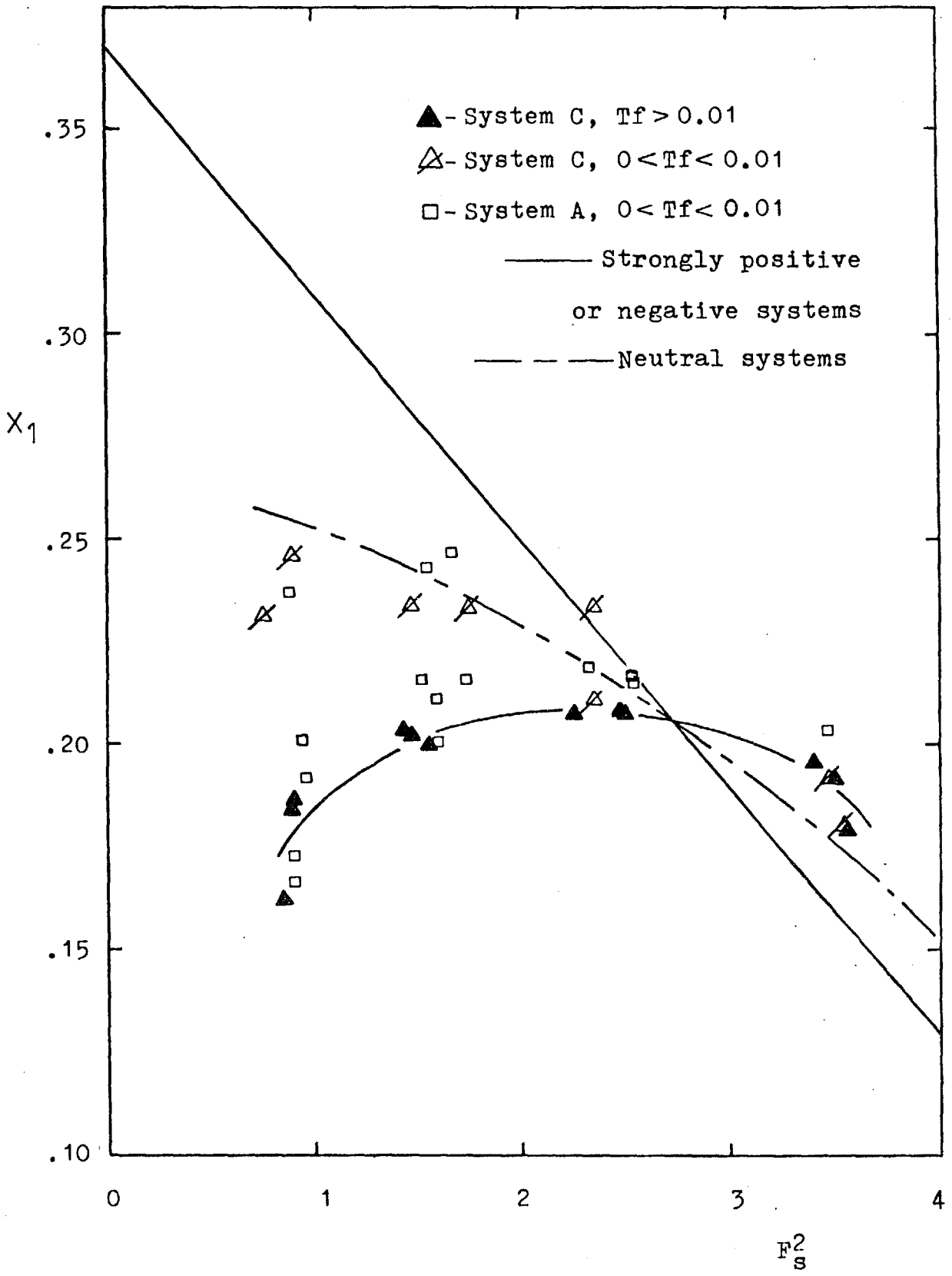

Fig. 4.22.- Variation of maximum value of dispersion density profile with F_s for positive systems.

(v.1) Maximum value of liquid fraction

In the spray regime, neglecting the contribution of the pool to the liquid dispersion profile, there exists a maximum in the dispersion profile somewhere above the plate floor. In the froth regime the profile is almost constant up to a certain height, and above it the liquid profile decreases. Above this height most of the liquid is in the form of droplets projected by the gas during bursting of bubbles. This part of the profile can be "fitted" as has been done for the spray regime and the value of the maximum of the profile (x_1) can be regarded as the medium value of the liquid fraction of the profile, since it is approximately constant for most of the liquid on the plate. Fane's results were fitted in this way and if the maximum value of the density is represented as a function of gas velocity, and if strongly positive systems are defined as those for which Tf > 0.010, then all the experimental points are located on the same line with a maximum at transition. For strongly negative systems, that is when -Tf > 0.010, all the experimental points are located on the same descending line, without any noticeable change at transition. For moderately positive or negative systems, the behaviour is intermediate and also a neutral line can be estimated.

The results for negative and positive systems are represented respectively in Figures 4.21 and 4.22.

For negative systems there is a linear relation between x_1 and F_s^2 given by

$$x_1^- = 0.37 - 0.06\ F_s^2 \qquad (105)$$

If Figures 4.21 and 4.22 are compared with Figure 2.1 one can confirm the overlapping of curves represented there.

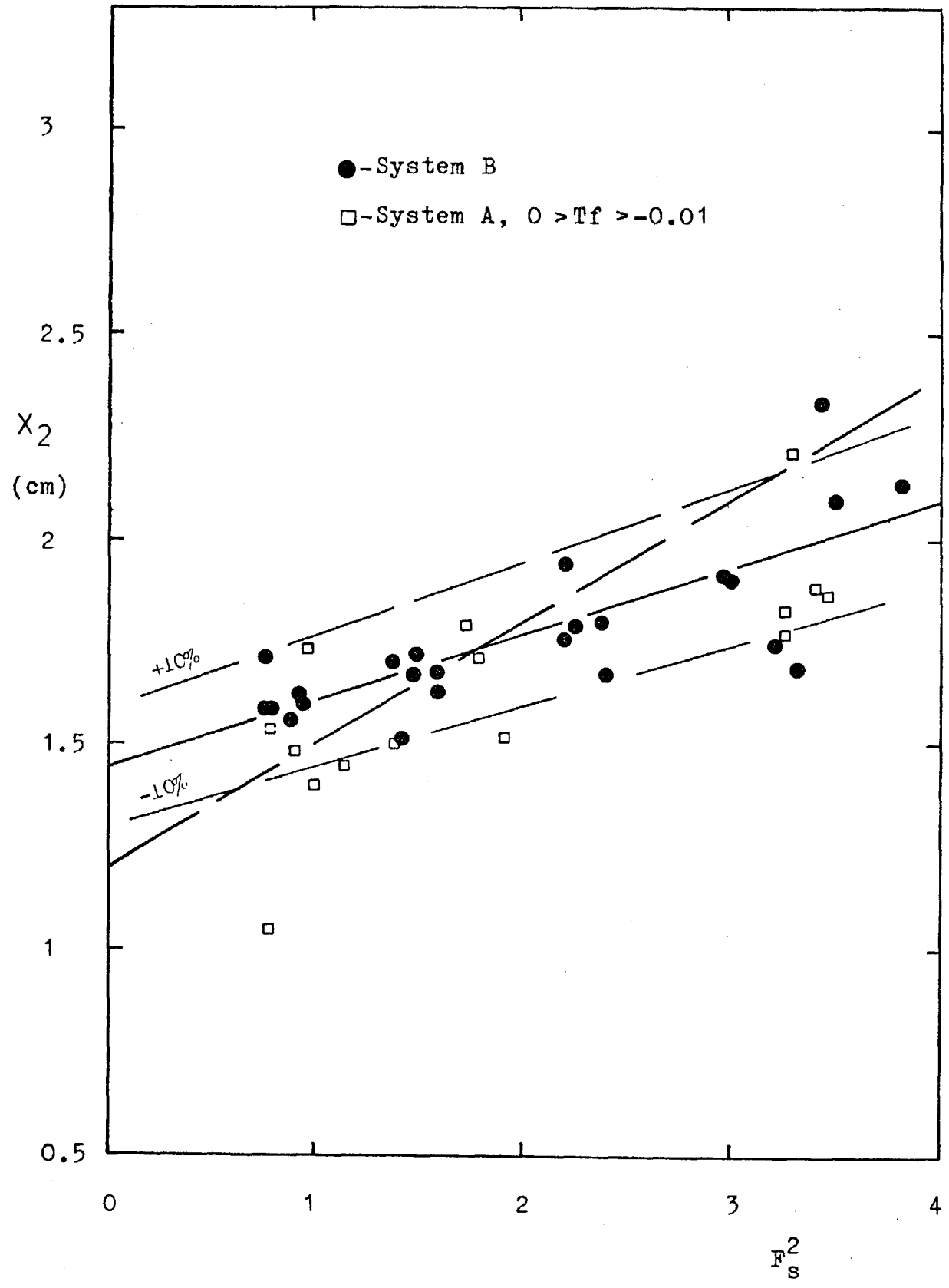

Fig. 4.23.- Variation of height of maximum density of liquid with F_s for negative systems.

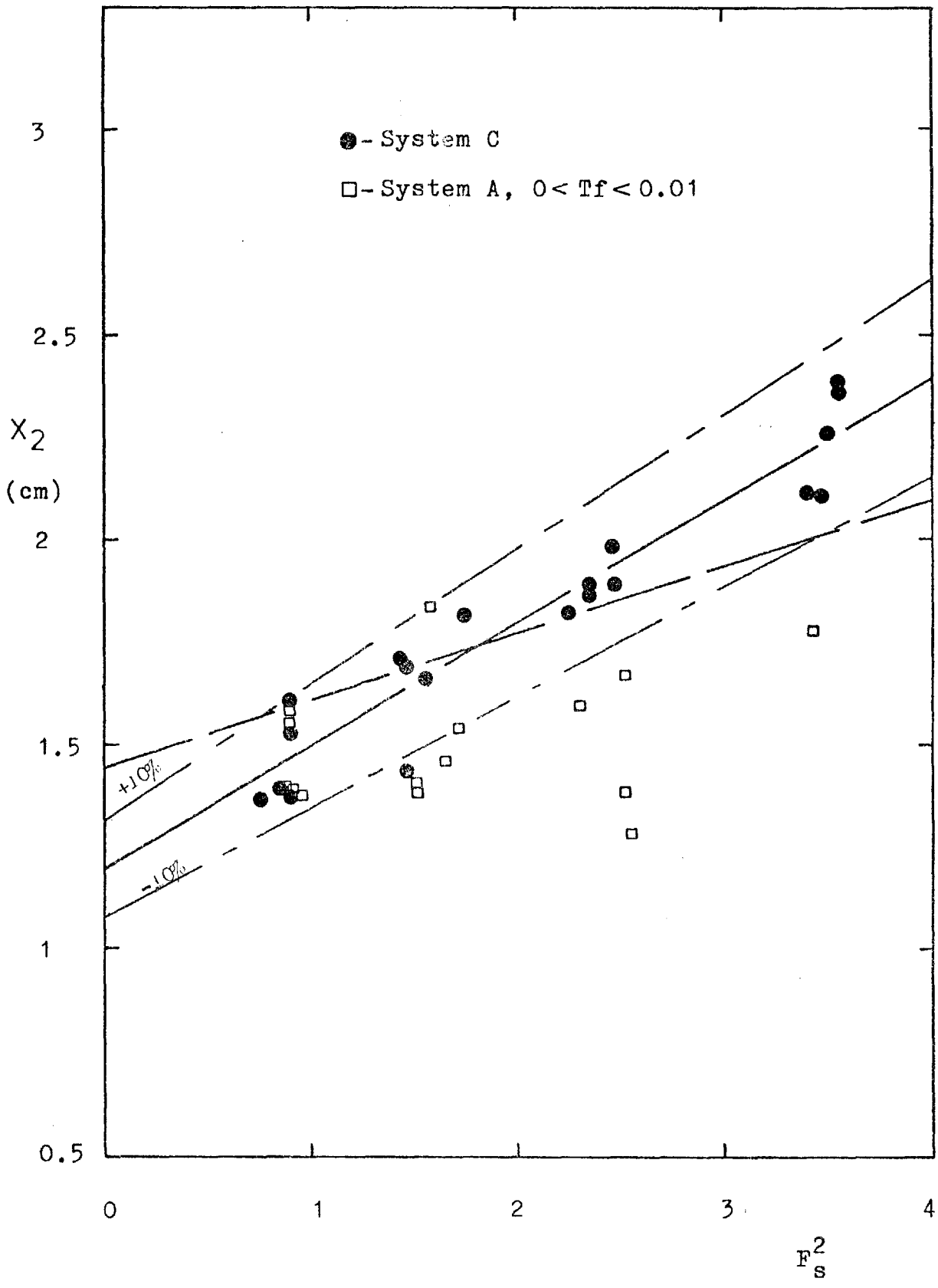

Fig. 4.24.- Variation of height of maximum dispersion density with F_s for positive systems.

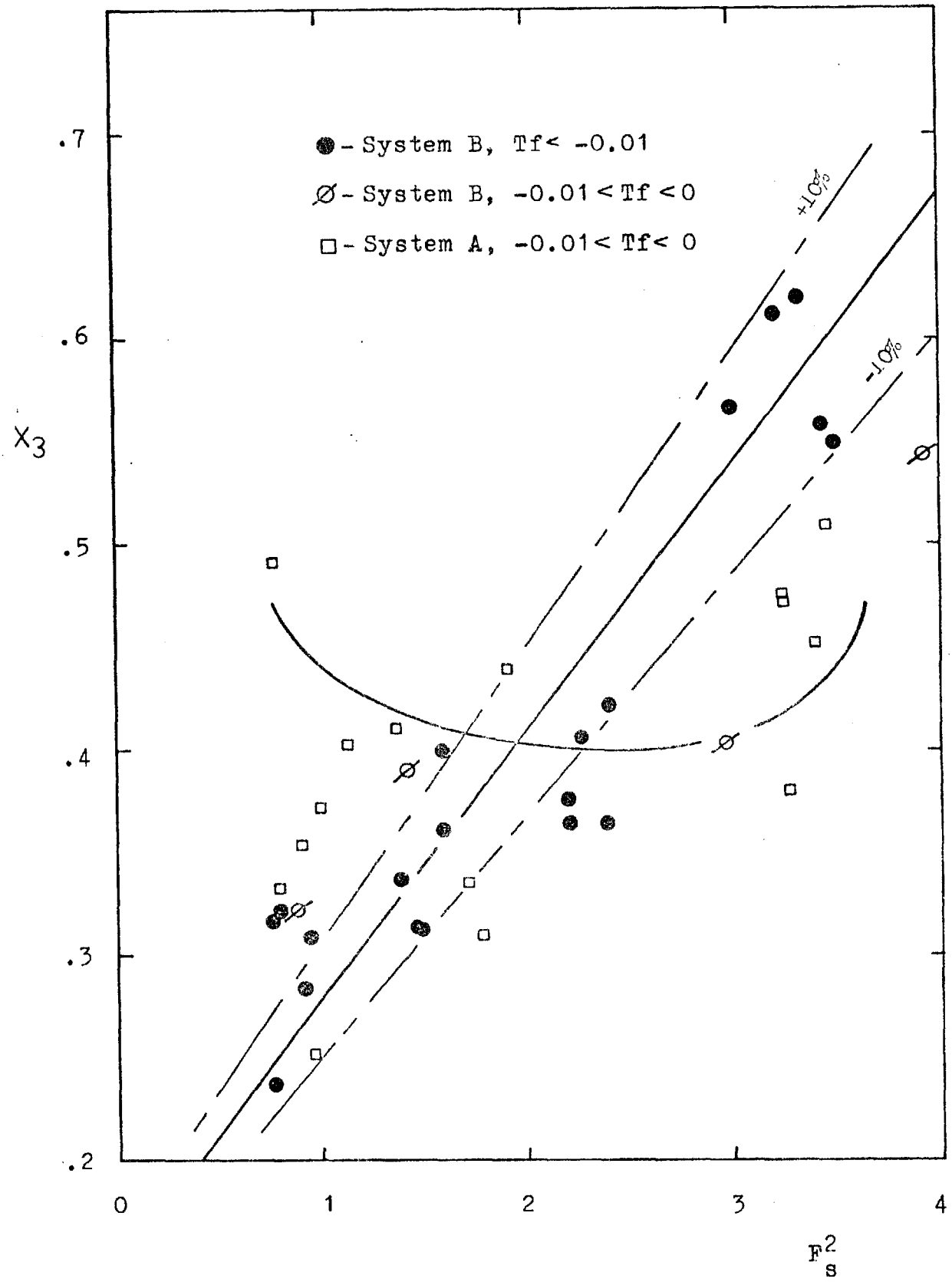

Fig. 4.25.- Variation of standard deviation of dispersion density profile with F_s for negative systems.

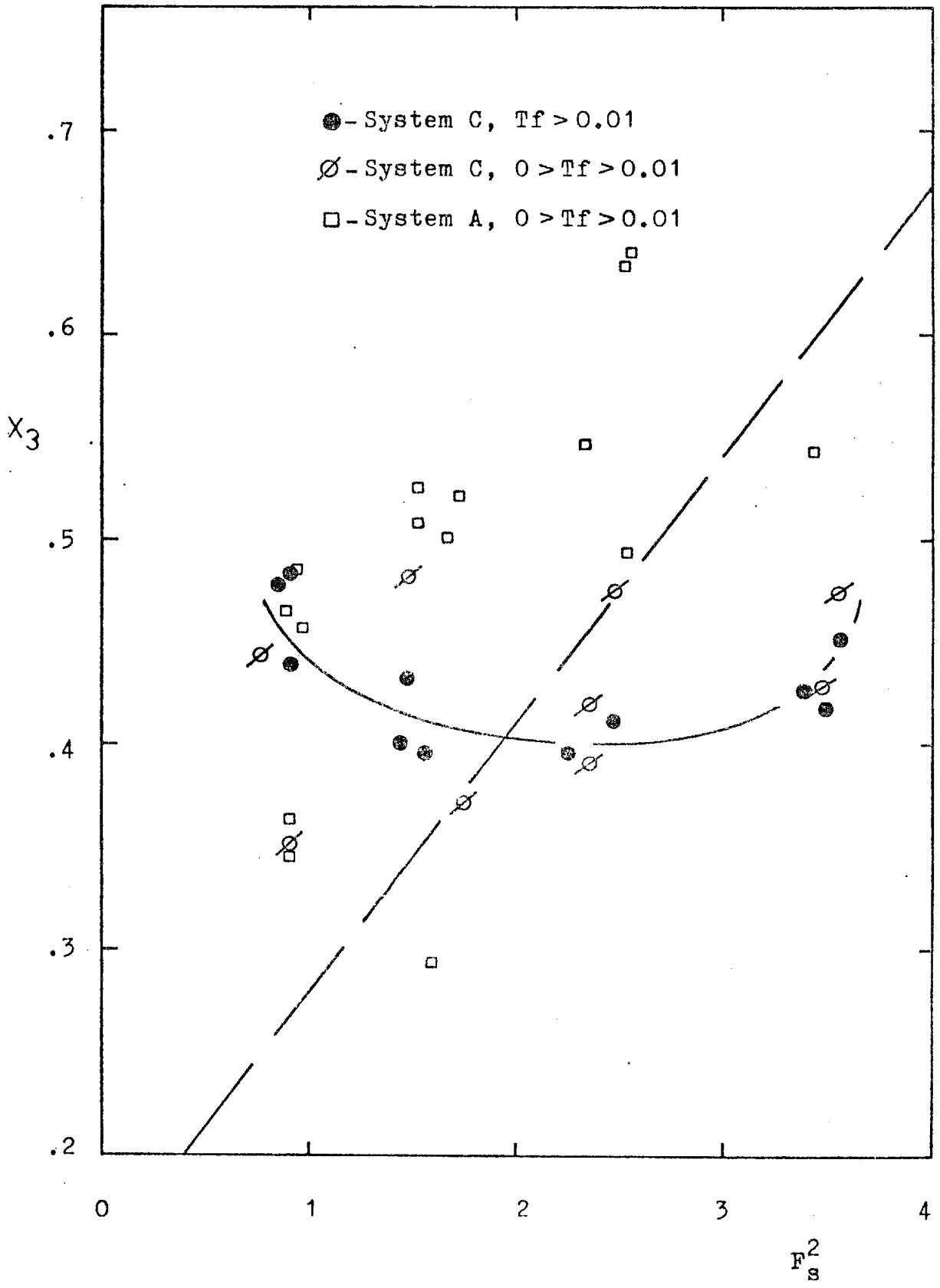

Fig. 4.26.- Variarion of standard deviation of dispersion density profile with F_s for positive systems.

(v.2) Height of maximum value of dispersion density profile

No noticeable effect of thin film stabilising number on height of maximum value of dispersion density profile (x_2) was observed. However the dependence on velocity is somewhat larger for positive systems than for negative systems. The results for the moderately positive or negative system seems to be in general slightly lower and more scattered.

The results for negative and positive systems can be correlated respectively by:

$$x_2^- = 1.45 + 0.16\ F_s^2 \qquad (106)$$

and

$$x_2^+ = 1.2 + 0.3\ F_s^2 \qquad (107)$$

as can be seen from Figures 4.23 and 4.24.

(v.3) Standard deviation of dispersion density profile

The results of standard deviation of dispersion are somewhat more scattered as would be expected. However, some general trends can be observed and again the effect of thin-film stabilising number is noticeable. The effect of gas velocity and of thin-film stabilising number on standard deviation of dispersion density profile (x_3) is almost the opposite to that reported on maximum value of liquid fraction. So, for the strongly negative systems it is:

$$x_3^- = 0.15 + 0.13\ F_s^2 \qquad (108)$$

and for strongly positive systems a minimum can be detected at transition. For system A, moderately positive or negative, the behaviour is rather uncertain. The results are represented in Figures 4.25 and 4.26 respectively for negative and positive systems.

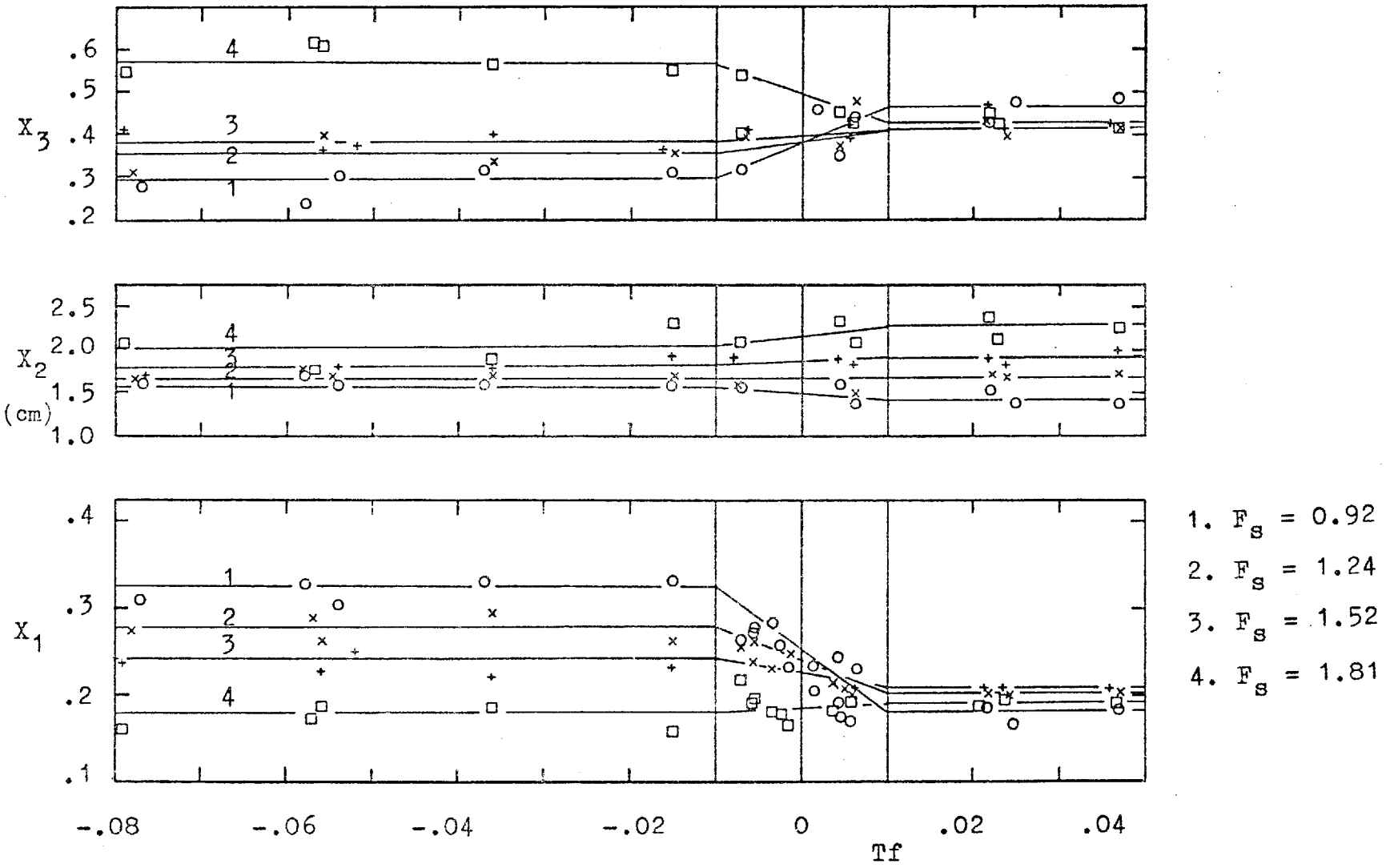

Fig. 4.27.- Effect of thin-film stabilising number on dispersion density profile parameters, for different values of F_s.

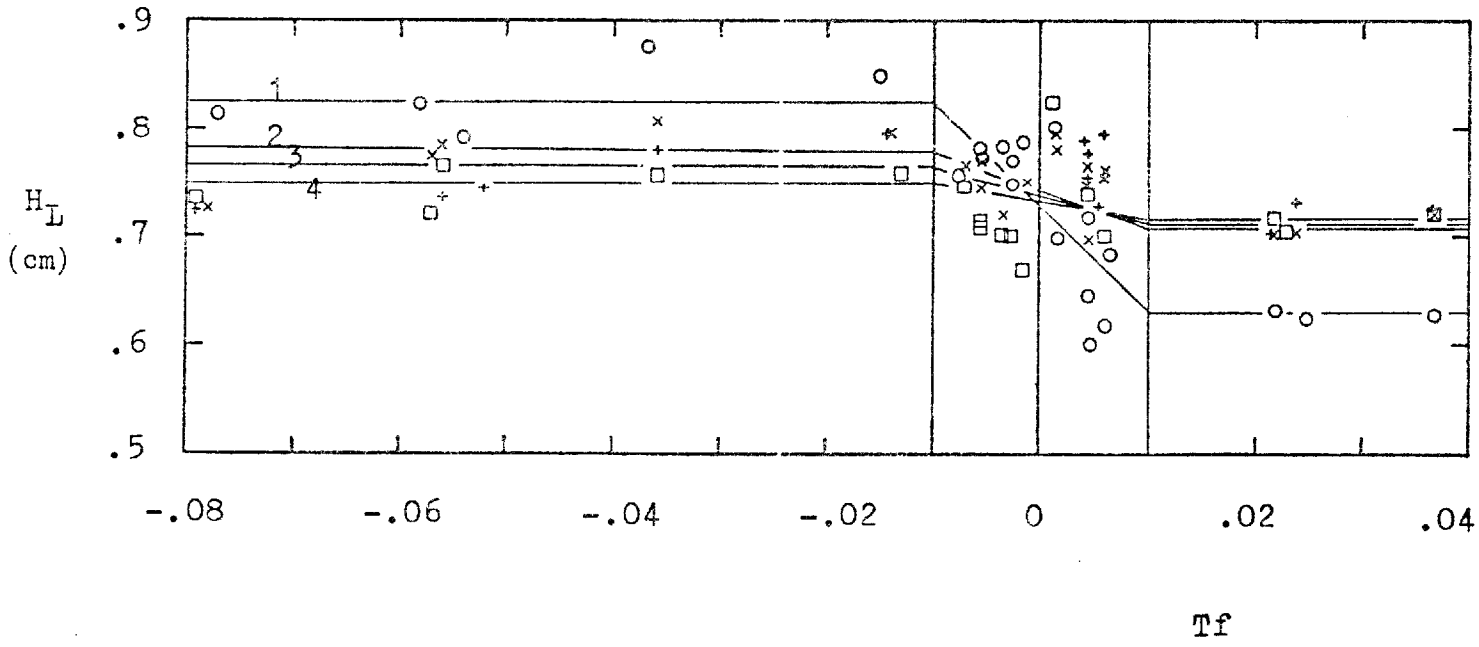

Fig. 4.28.- Effect of thin-film stabilising number on hold-up.
(1. $F_s = 0.92 \pm 0.05$, 2. $F_s = 1.24 \pm 0.08$, 3. $F_s = 1.52 \pm 0.05$,
4. $F_s = 1.81 \pm 0.09$).

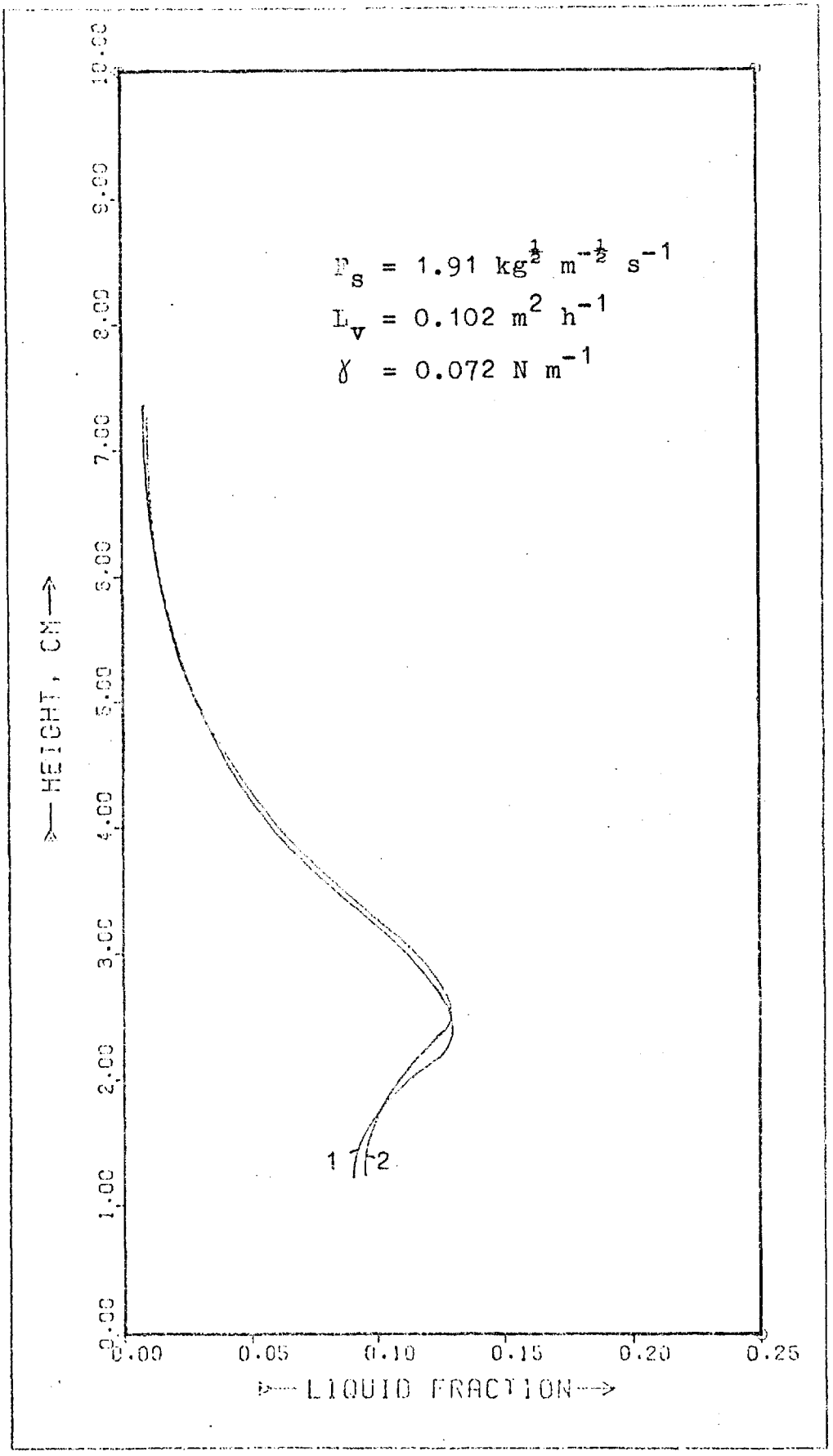

Fig. 4.29.- Effect of mass transfer on dispersion density profile in the spray regime (1. no mass transfer; 2. absorption).

(v.4) Liquid hold-up

The thin-film stabilising number is a primary factor in hold-up on plate for small values of F_s (see Figure 4.28). For strongly positive systems (Tf > 0.01) the hold-up is much smaller and the plate operates in the foaming regime. For negative systems the hold-up is bigger (also at small values of F_s) and the operating regime is represented by froth. At higher gas velocities the effect of Tf is less noticeable. Furthermore, for systems weakly negative and positive at the lowest values of F_s a general trend of decrease in hold-up when Tf increases from -0.01 to +0.01 is detected.

The results of the Marangoni effect on dispersion density parameters and on liquid hold-up are put together respectively in Figures 4.27 and 4.28. For sake of legibility, the results of system B were omitted on the first graph. The standard deviation of drop population calculated from line 4 by the simplified model were 0.31 for negative systems and 0.23 for positive systems and are thus very close to the values reported by Fane and Sawistowski[1] of 0.30 ± 0.03 and 0.19 ± 0.01 respectively.

The effect of mass transfer for the system methanol/water was very small, slightly above the experimental errors. However, if conditions of a strongly negative system are compared with neutral conditions, a somehow better spray condition can be seen for the negative system (Figure 4.29), but the differences are not really significant.

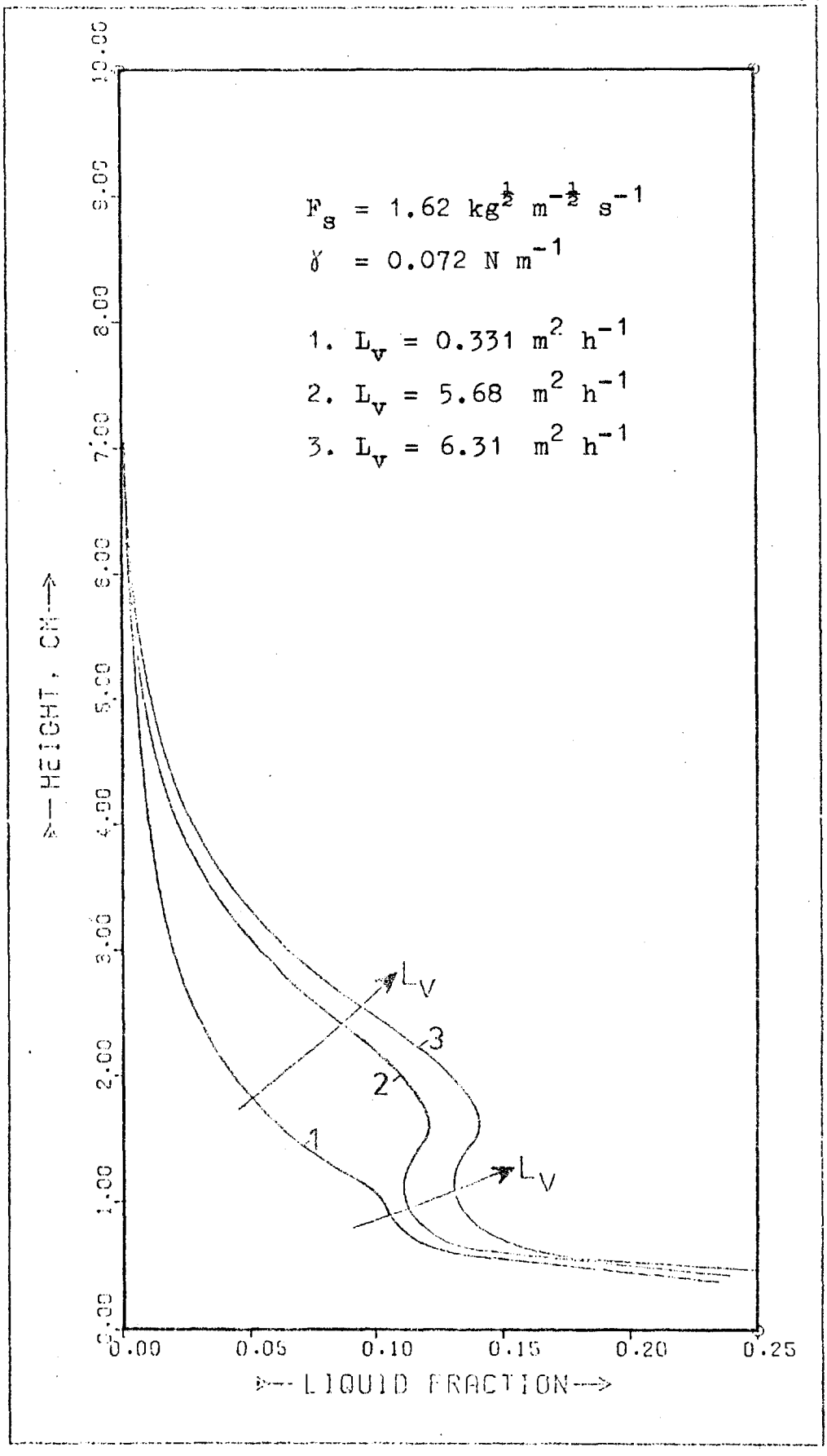

Fig. 4.30.- Effect of liquid cross-flow rate on dispersion density profile, without using a splash baffle.

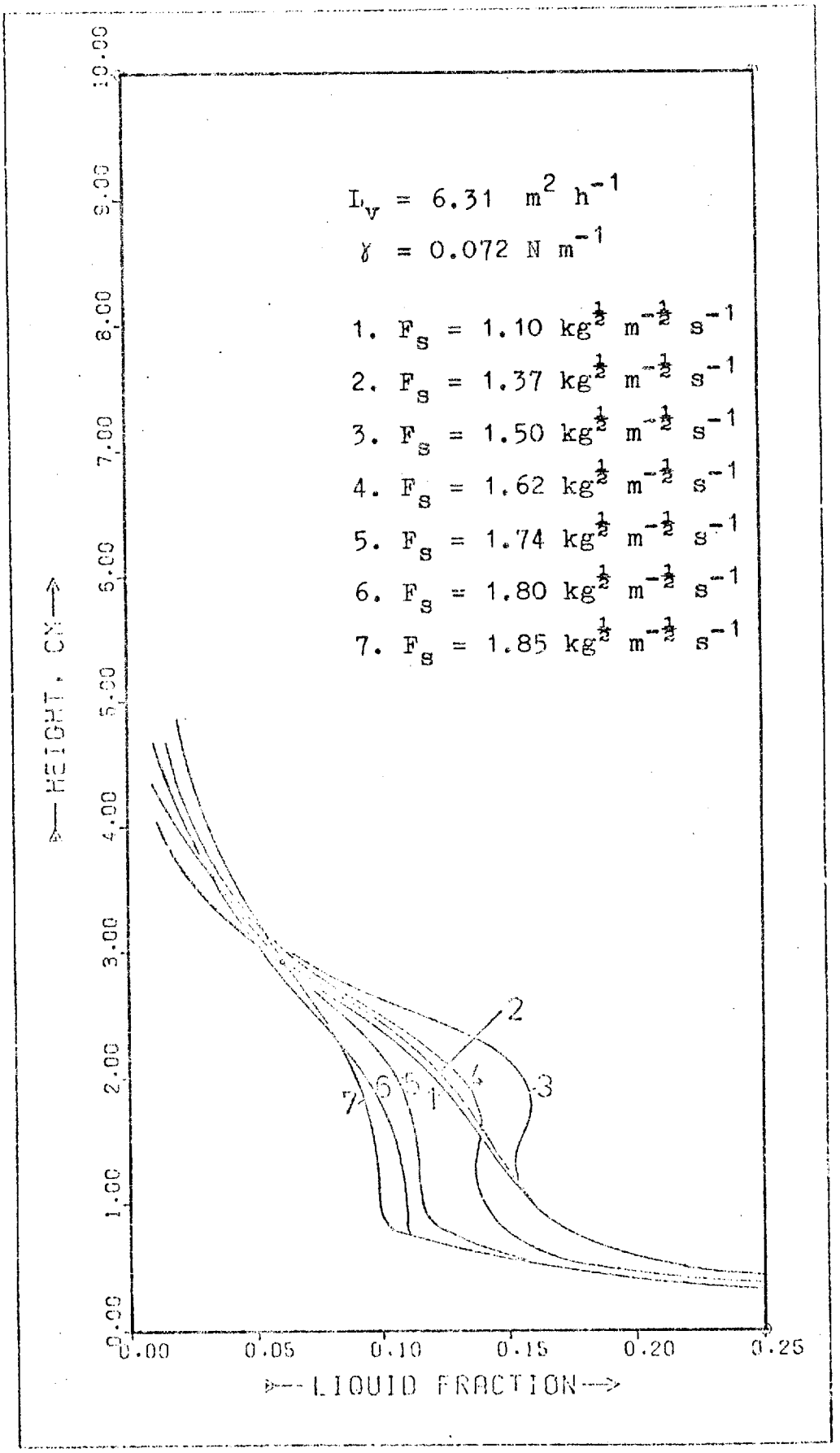

Fig. 4.31.- Effect of gas flow rate on dispersion density profile, without using a splash baffle.

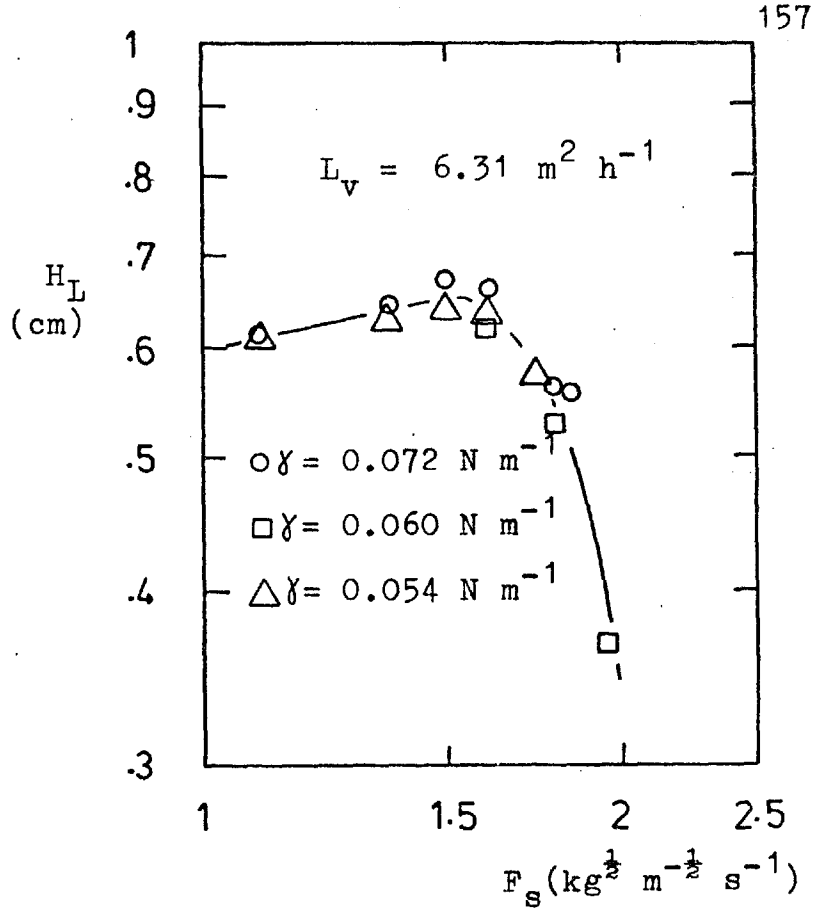

Fig. 4.32 Effect of gas flow rate on hold-up, without using a splash baffle.

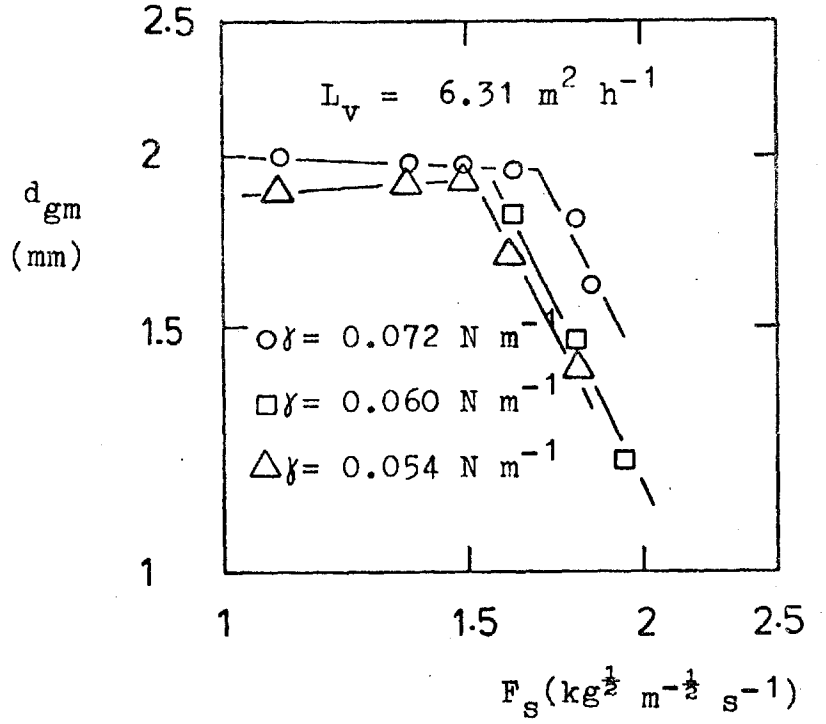

Fig. 4.33.- Effect of gas flow rate on geometric mean diameter of generated drops, without using a splash baffle.

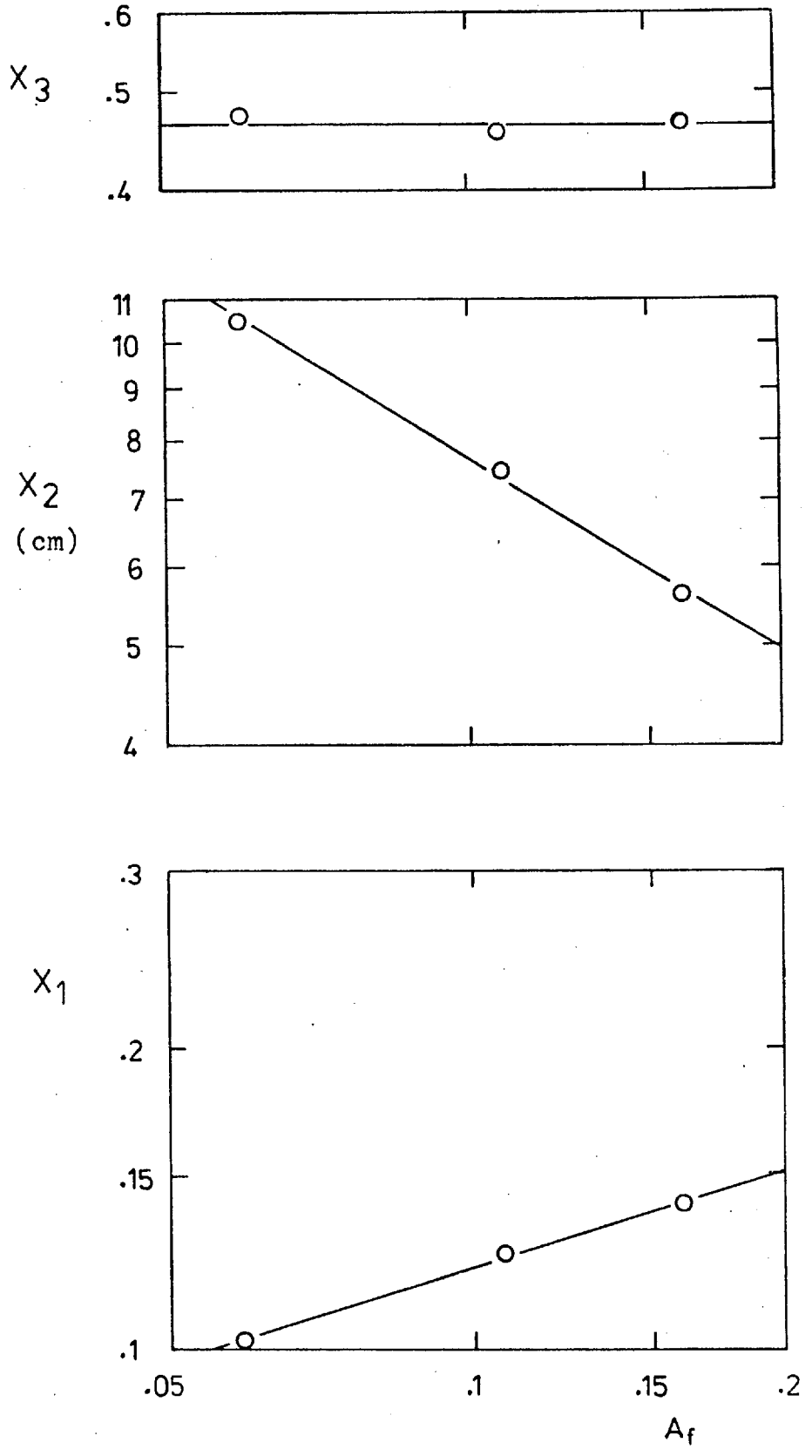

Fig. 4.34.- Effect of fractional free area on dispersion density parameters. (F_s =2.25 $kg^{\frac{1}{2}}$ $m^{-\frac{1}{2}}$ s^{-1}, L_v = 15 m^2 h^{-1}).

(vi) Effect of plate geometry

(vi. 1) Effect of a splash baffle

Some results were obtained without using any splash baffle above the outlet weir. Under these conditions some drops discharged directly into the downcomer. Dispersion density profiles obtained using a splash baffle to avoid loss of liquid by projection directly into the downcomer were quite different from the ones obtained in the absence of the baffle as can be seen by comparison of Fig. 4.9 and 4.10 with Figure 4.30 and Figures 4.12 and 4.13 with Figure 4.31. By increasing the gas rate above a certain value ($F_s \simeq 1.5$) the density profile decreases almost everywhere instead of increasing as expected. This is due to the direct projection of drops into the downcomer, producing a substantial decrease in hold-up on plate, as can be seen in Figure 4.32 and also a decrease in drop-size calculated by the "exact" model, as seen in Figure 4.33.

(vi. 2) Effect of fractional free area

Interpolation of results from Pinczewski's data for $L_v = 15\ m^3\ h^{-1}\ m^{-1}$ and $F_s = 2.25\ kg^{1/2}\ m^{-1/2}\ s^{-1}$ and hole diameter of 12.7 mm made it possible to ascertain the effect of fractional free area on parameters of the dispersion density profile. The results are presented in Figure 4.34. The maximum value of density was proportional to $Af^{0.31}$. The height of the maximum was proportional to $Af^{-0.62}$. The standard deviation of the distribution remained constant. Consequently the hold-up of drops was proportional to $Af^{-0.31}$.

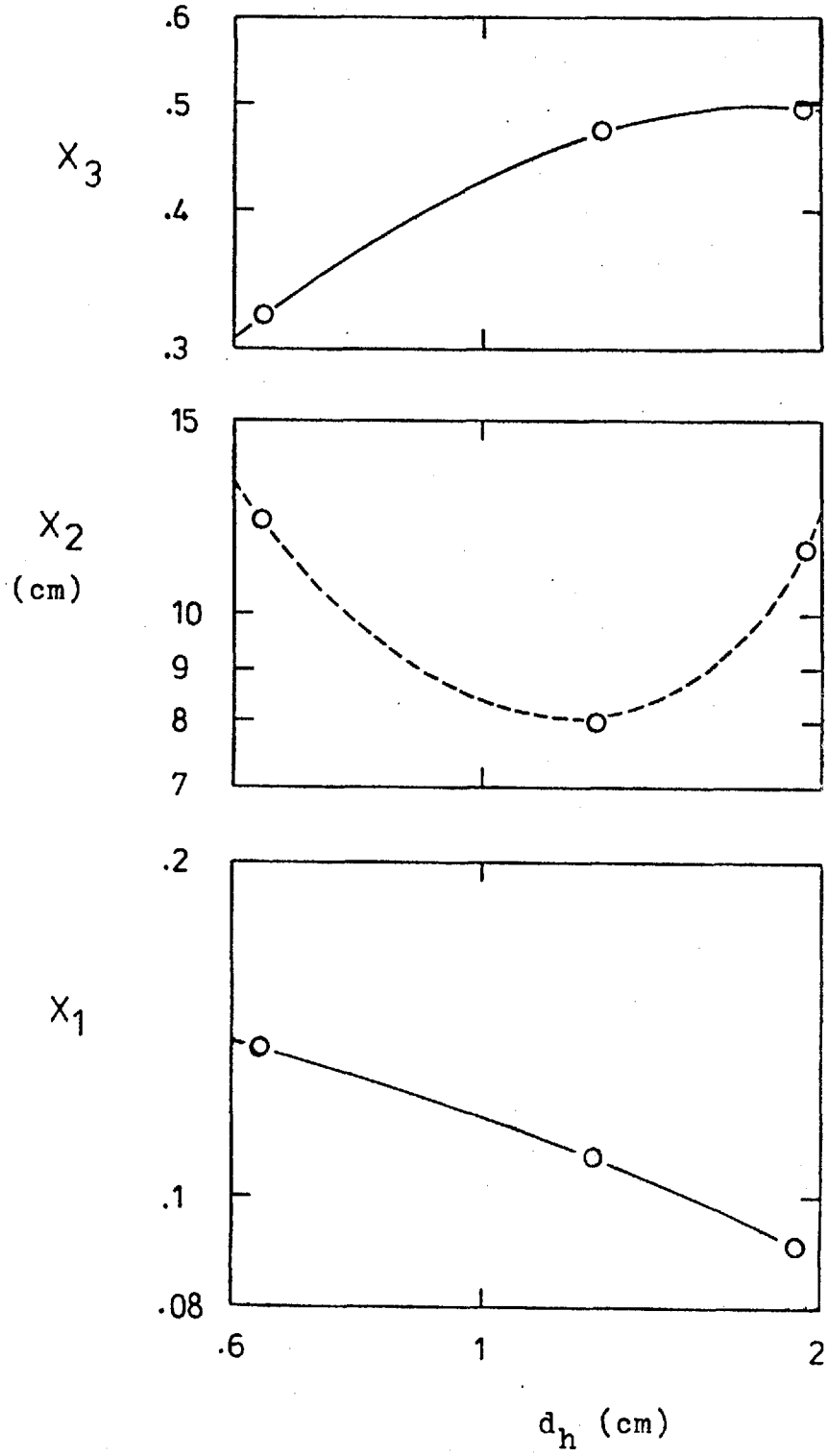

Fig. 4.35.- Effect of hole diameter on dispersion density parameters (F_s = 2.64 $kg^{\frac{1}{2}}$ $m^{-\frac{1}{2}}$ s^{-1}, L_v = 15 m^2 h^{-1}, A_f= 0.107).

(vi.3) Effect of hole diameter

The dependence of dispersion density parameters on the holes diameter when fractional free area and liquid and gas rates are the same as given by Pinczewski's profiles is somewhat strange, since the height of maximum density is always smaller for the intermediate value of the diameter. In Figure 4.35 the results are presented for F_s = 2.64 $kg^{1/2}$ $m^{-1/2}$ s^{-1}, L_v = 15 m^3 h^{-1} m^{-1} and fractional free area 0.107.

4.3 Specific Surface Area Profiles

4.3.1 Introduction

The specific surface area profiles are expected to be similar to the dispersion density profiles. In Figures 4.36 to 4.42 are presented the experimental values as well as the expected profile given by the simplified model by adjusting only the parameter A from the initial projection velocity expression

$$v_p = A\, d_p^{B} \tag{109}$$

where d_p is the diameter of the drop and B was taken as -0.93. The value of A used by Fane and Sawistowski was 0.002355. Three points calculated with this value of A are also indicated in Figures 4.36 to 4.42. The experimental values obtained for A by fitting of profiles varied from 0.0018 to 0.0045 with a mean value of 0.00265 ± 32%. The experimental conditions covered the range:

$$1.4 < F_s < 2.29 \text{ kg}^{1/2} \text{ m}^{-1/2} \text{ s}^{-1}$$

$$0.22 < L_v < 0.35 \text{ m}^3 \text{ h}^{-1} \text{ m}^{-1}$$

$$0.055 < \gamma < 0.072 \text{ N m}^{-1}$$

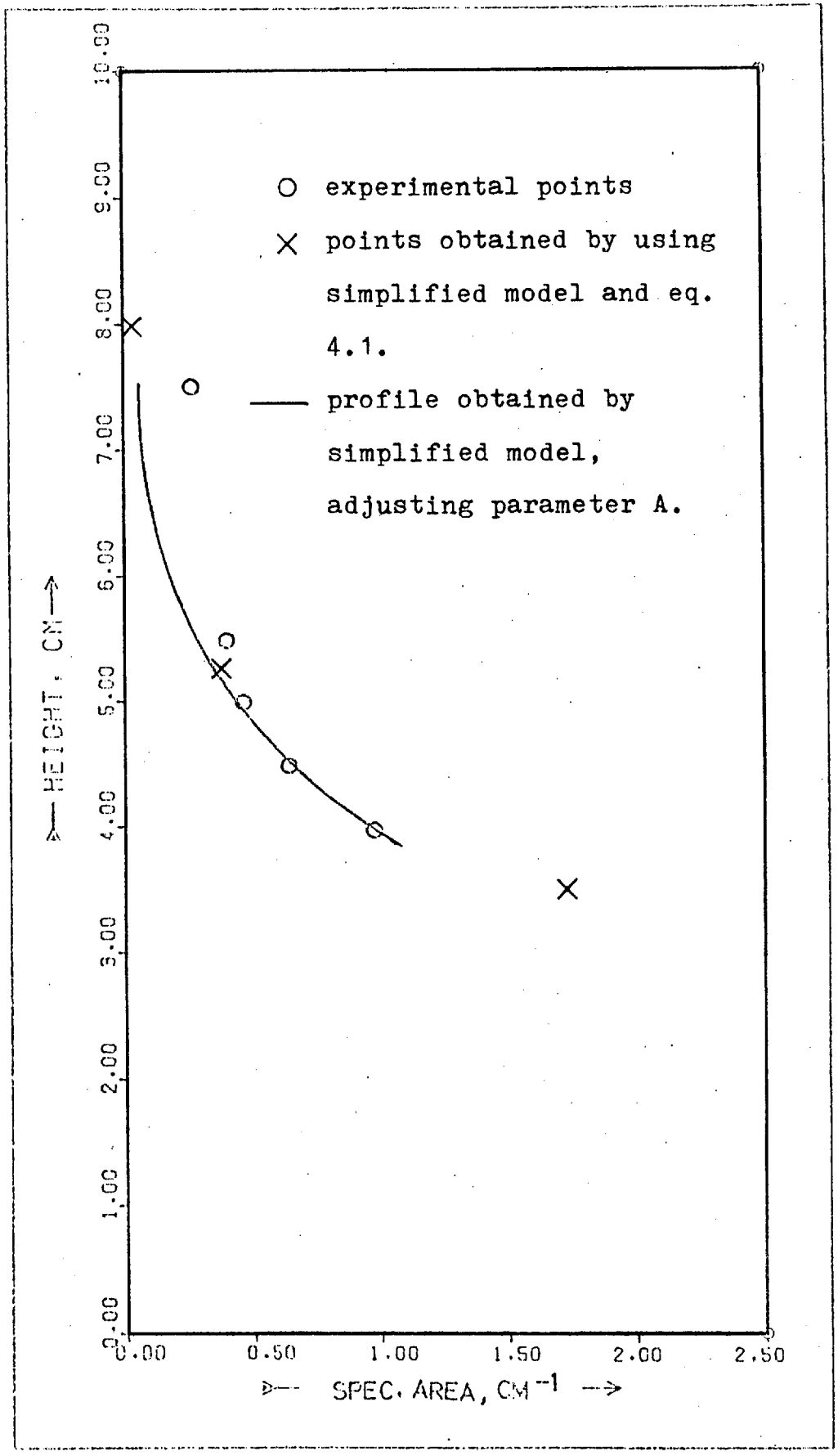

Fig. 4.36.- Specific surface area profile (F_s = 1.68 kg $^{\frac{1}{2}}$ $m^{-\frac{1}{2}}$ s^{-1}, L_v = 0.068 m^2 h^{-1}, γ = 0.055 N m^{-1}).

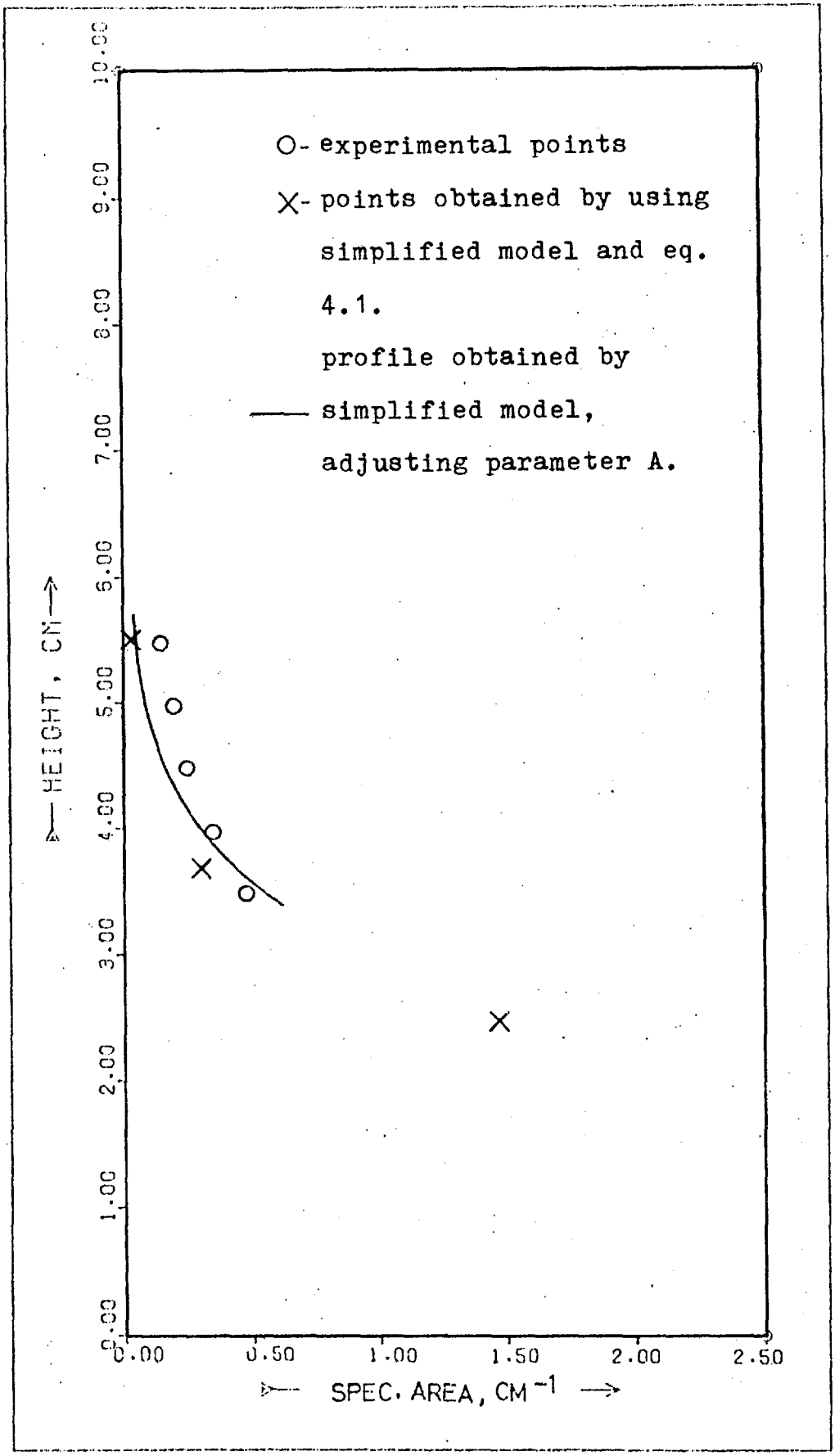

Fig. 4.37.- Specific surface area profile (F_s = 1.31 $kg^{\frac{1}{2}}$ $m^{-\frac{1}{2}}$ s^{-1}, L_v =0.068 m^2 h^{-1}, γ=0.072 N m^{-1}).

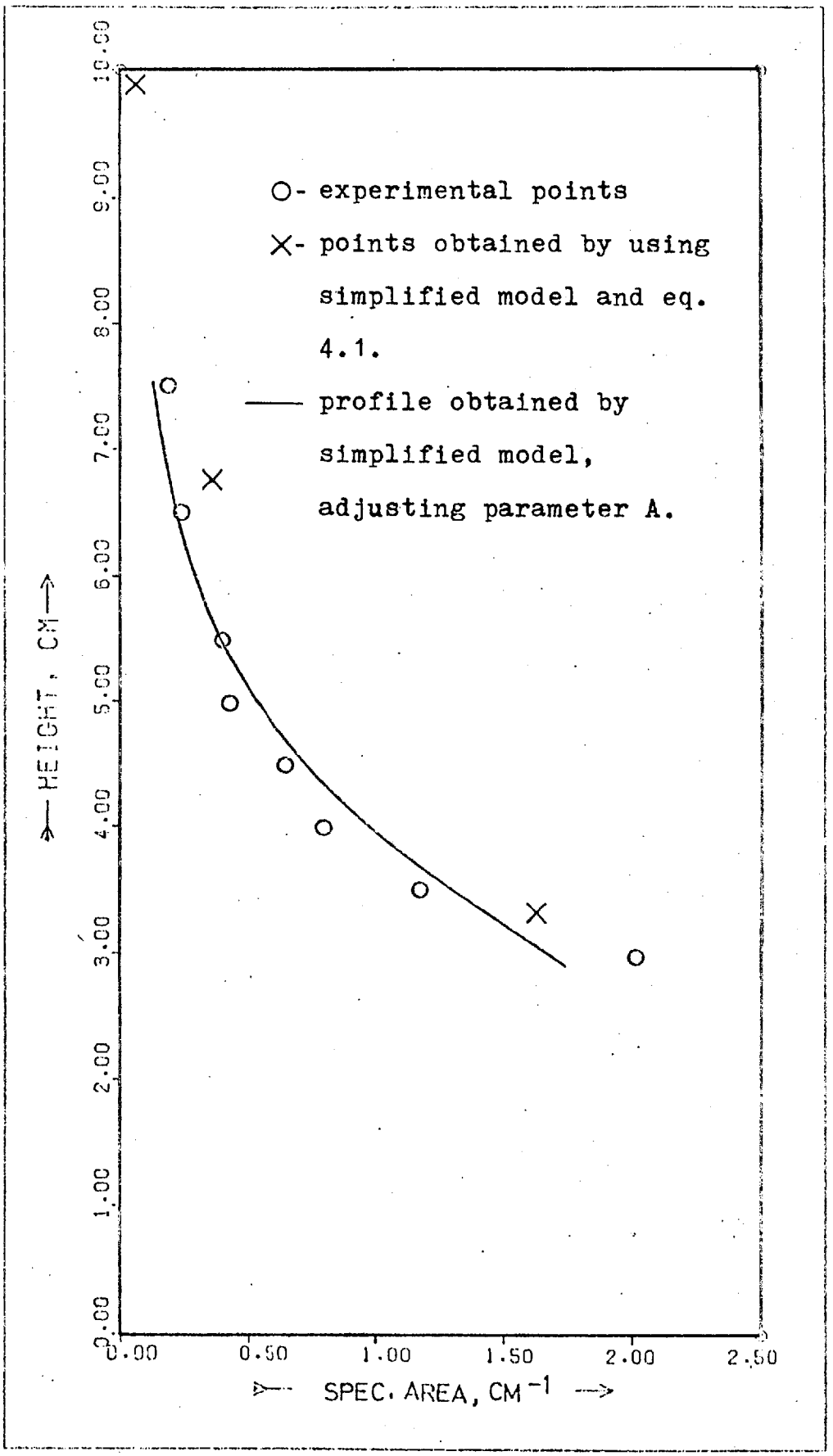

Fig. 4.38.- Specific surface area profile (F_s = 1.68 $kg^{\frac{1}{2}}$ $m^{-\frac{1}{2}}$ s^{-1}, L_v = 0.068 m^2 h^{-1}, γ =0.072 N m^{-1}).

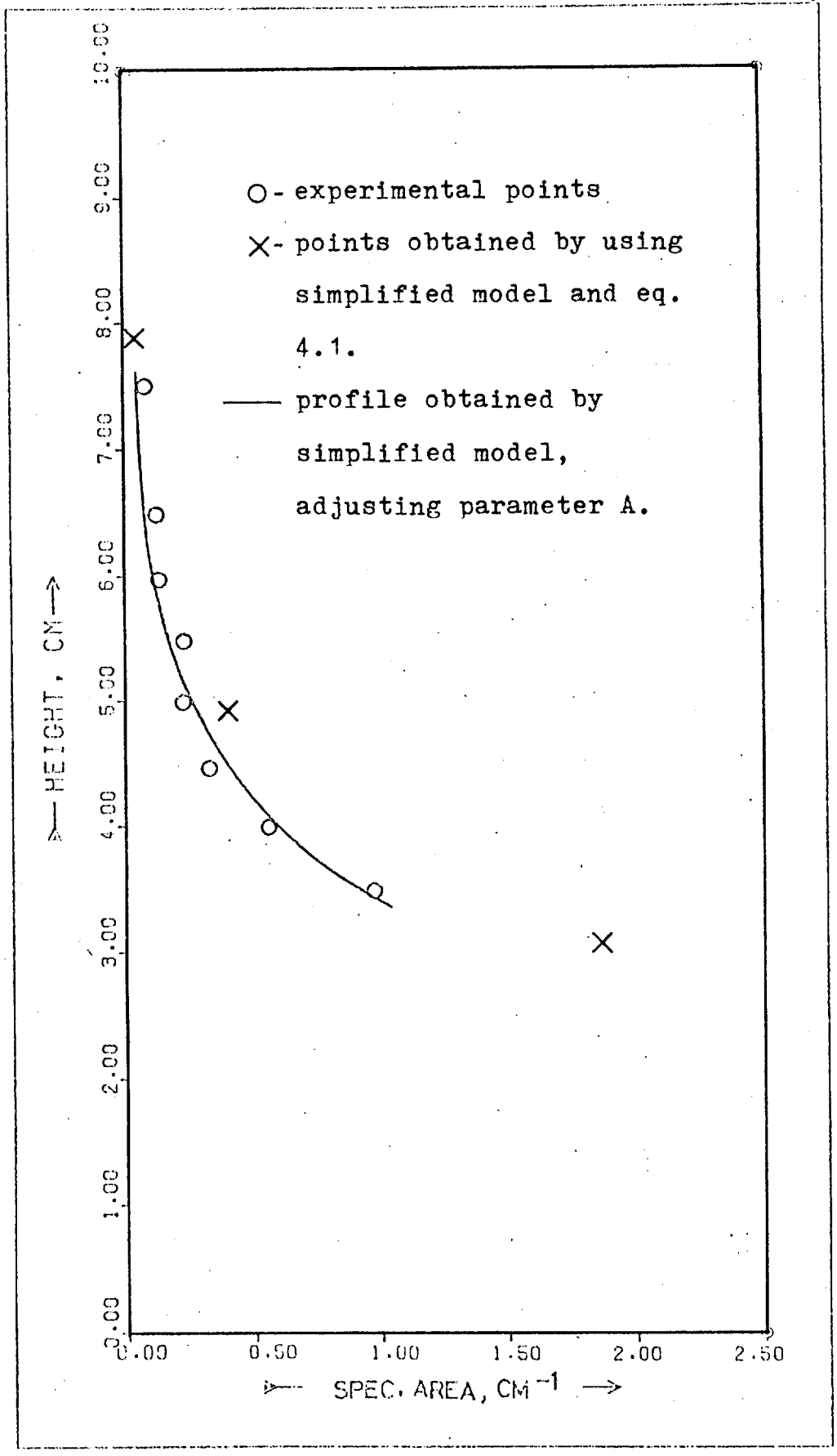

Fig.4.39.- Specific surface area profile (F_s = 1.31 $kg^{\frac{1}{2}}$ $m^{-\frac{1}{2}}$ s^{-1}, L_v = 0.102 m^2 h^{-1} γ = 0.072 N m^{-1}).

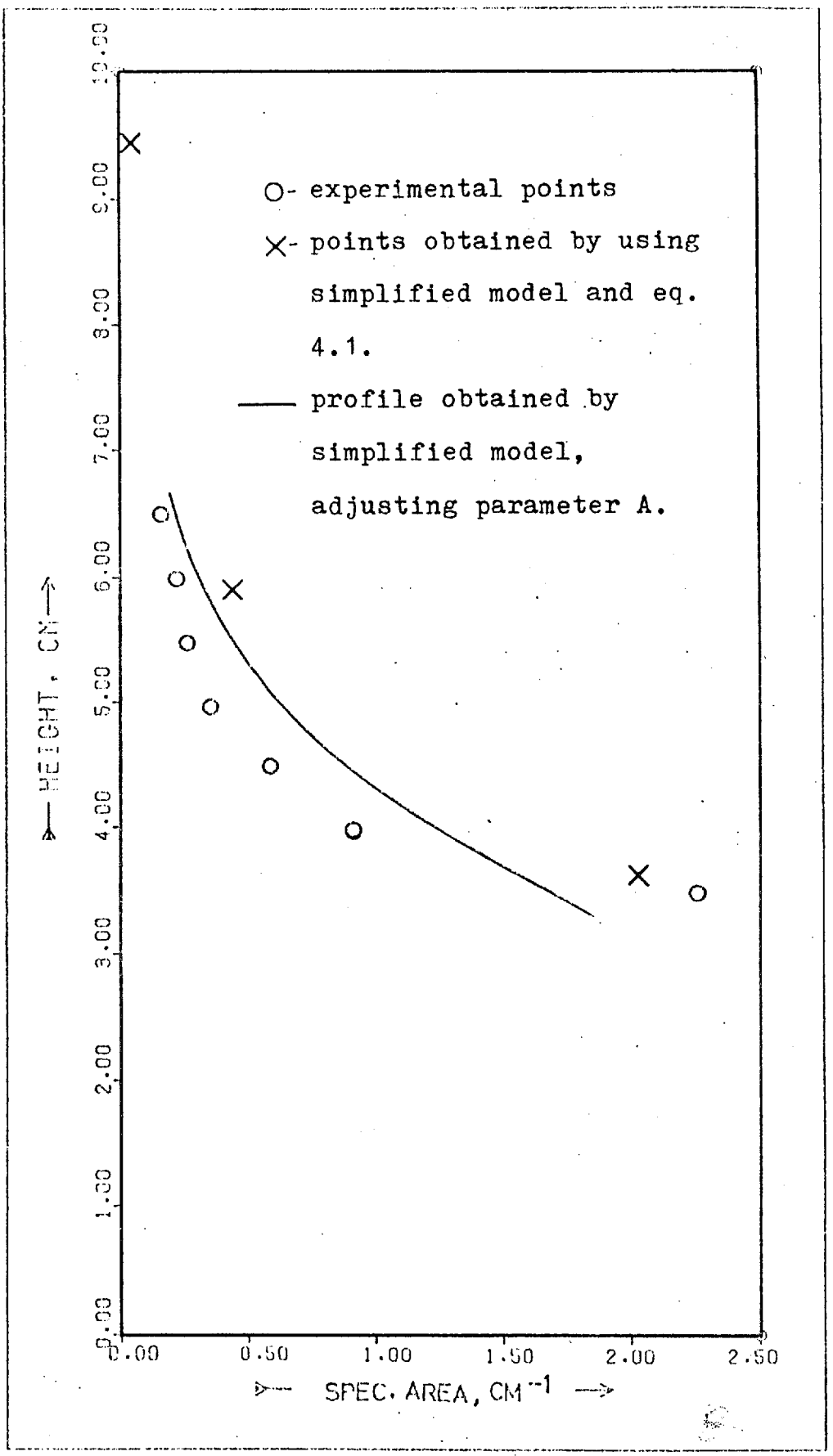

Fig. 4.40.- Specific surface area profile (F_s = 1.68 $kg^{\frac{1}{2}}$ $m^{-\frac{1}{2}}$ s^{-1}, L_v = 0.102 m^2 h^{-1}, γ = 0.072 N m^{-1}).

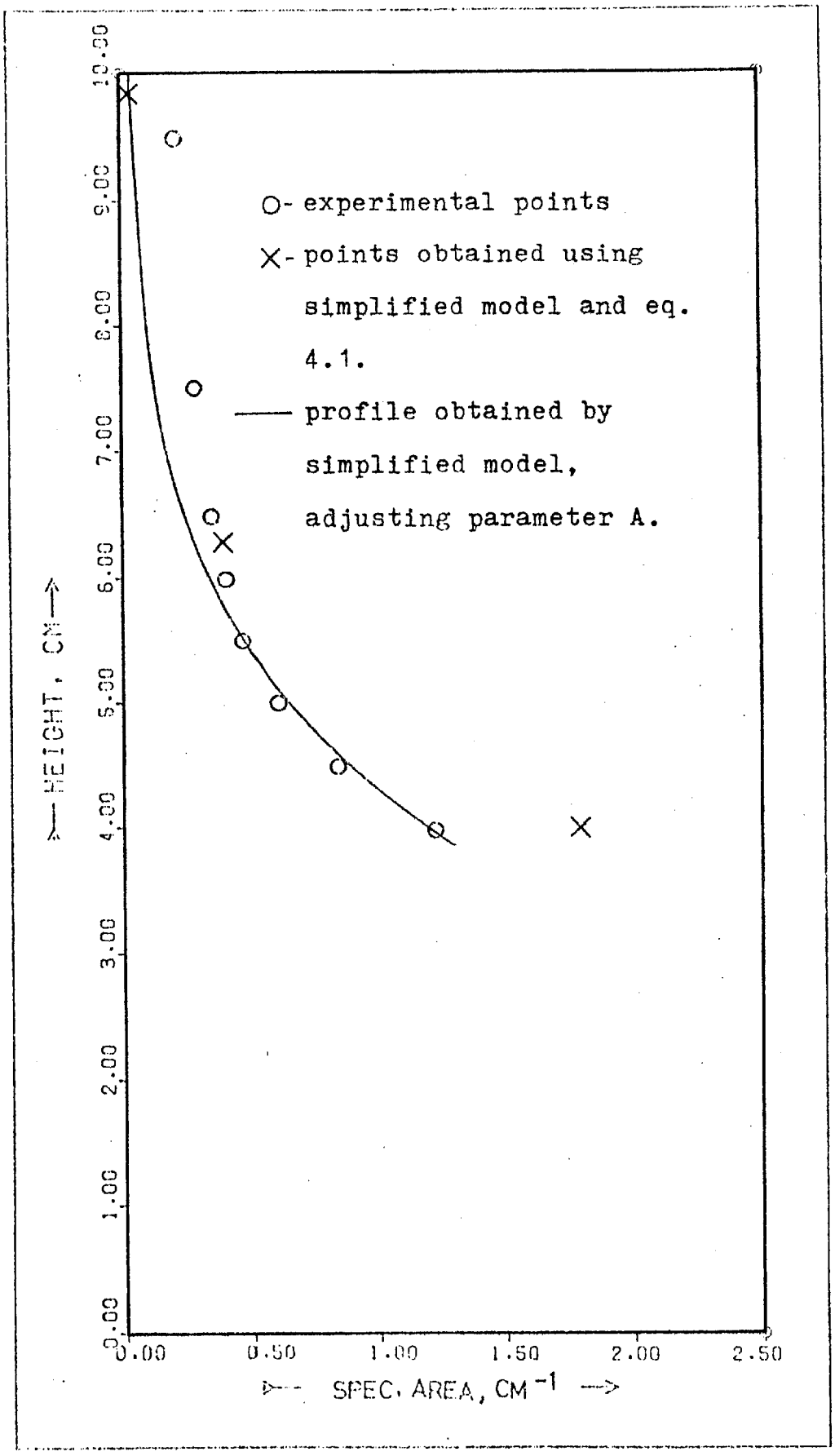

Fig. 4.41.- Specific surface area profile (F_s = 1.84 $kg^{\frac{1}{2}}$ $m^{-\frac{1}{2}}$ s^{-1}, L_v = 0.068 m^2 h^{-1}, γ = 0.072 N m^{-1}, desorption).

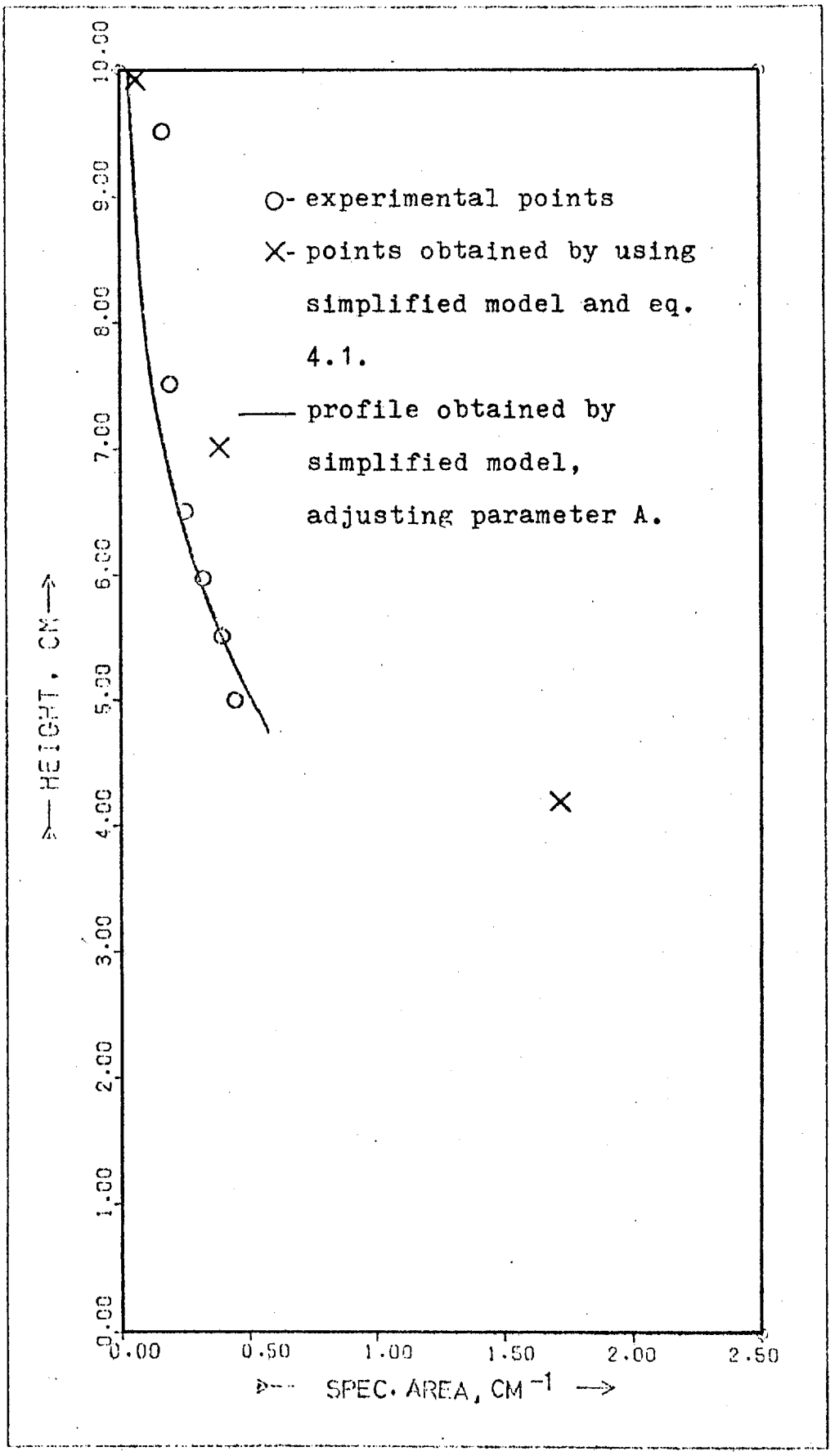

Fig. 4.42.- Specific surface area profile (F_s = 1.83 kg$^{\frac{1}{2}}$ m$^{-\frac{1}{2}}$ s^{-1}, L_v = 0.068 m^2 h^{-1}, γ = 0.072 N m^{-1}, desorption).

4.3.2 Factors affecting the specific surface area profiles

The type of factors affecting the specific surface area profiles are expected to be the same as those affecting the dispersion density profiles. Lack of time prevented a systematic study of all of these effects from being conducted. From the few experimental results it seems that the model can be used to predict the specific surface area profiles. However, it is assumed that a population of very small drops is generally being neglected. These drops seem to contribute very little to the dispersion density profile although this effect could on occasions be detected by inspection of the profiles. However, as the drops are very small they contribute significantly to the specific surface area profiles giving a general picture of systematic deviation at high levels above the plate floor.

An important limitation of this method was the fact that it was possible to measure surface area only at a level which was higher than a few centimetres above the plate floor where the density of the spray was already small. Since the error in the determination of density is almost independent of the value of the density, its relative error is high, and the expected errors in the determination of the mean Sauter diameter from experimental values of surface area and density are expected also to be high. By the same reason the errors in the determination of parameter A are also expected to be high.

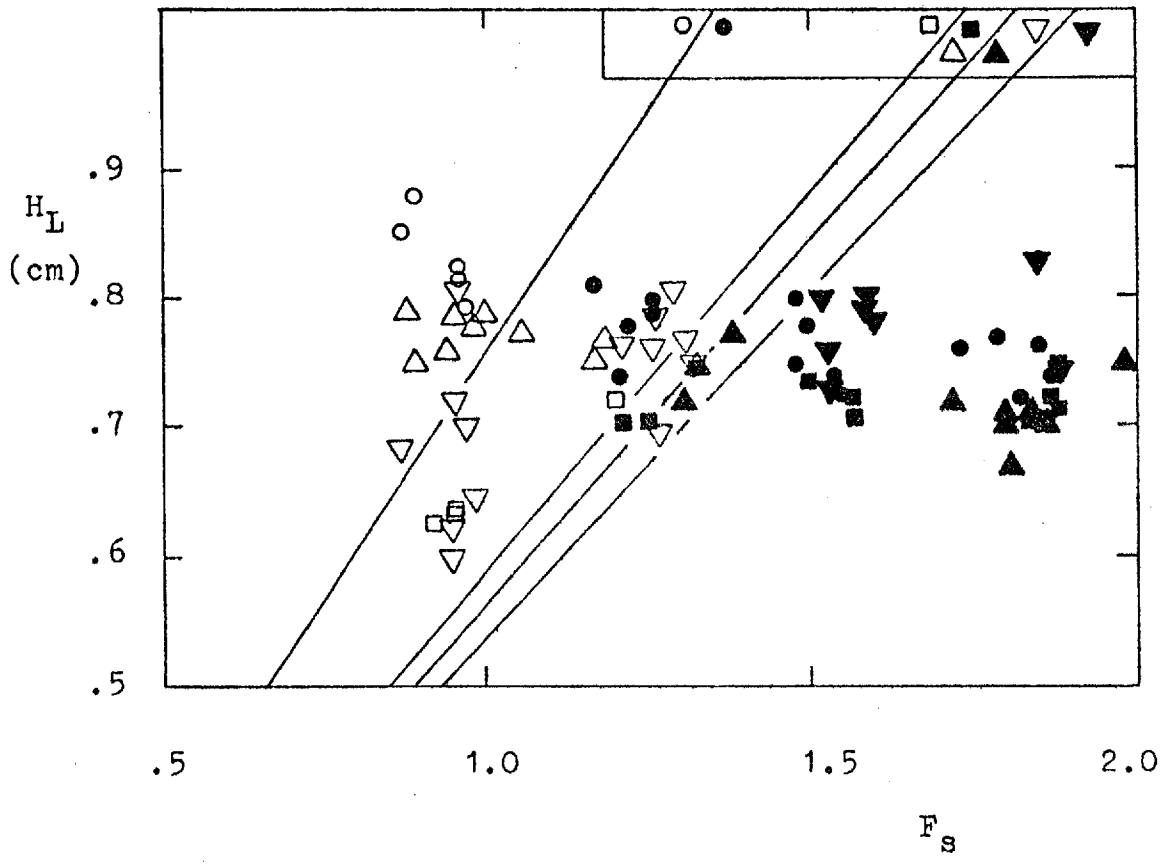

Fig. 4.43.- Froth-spray transition.

○/● - Transition for strongly negative systems

□/■ - Transition for strongly positive systems

△/▲ - Transition for weakly negative systems

▽/▼ - Transition for weakly positive systems.

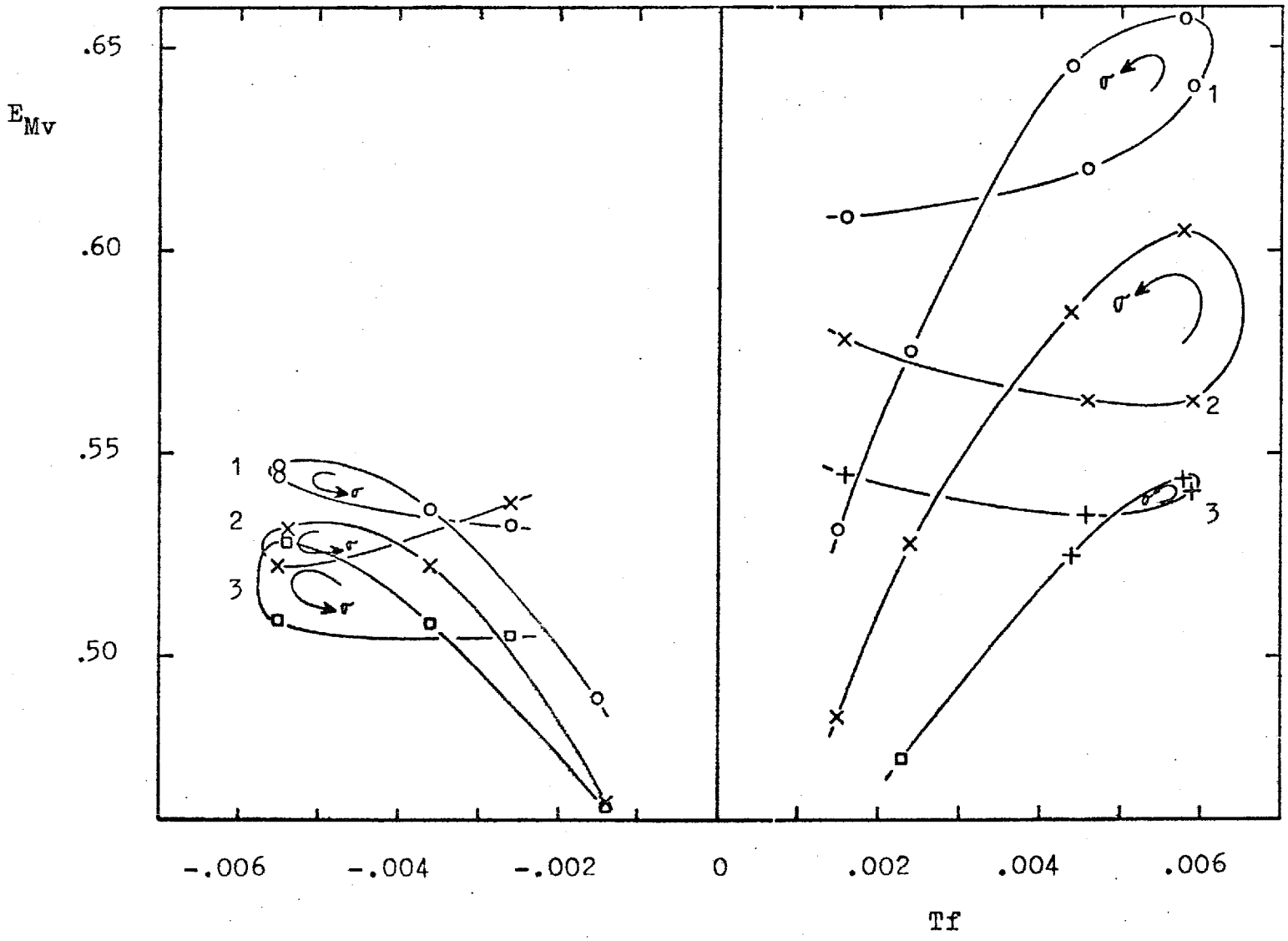

Fig. 4.44.- Mass transfer efficiency for system A in function of thin-film stabilising number.(For legend see Fig. 4.45)

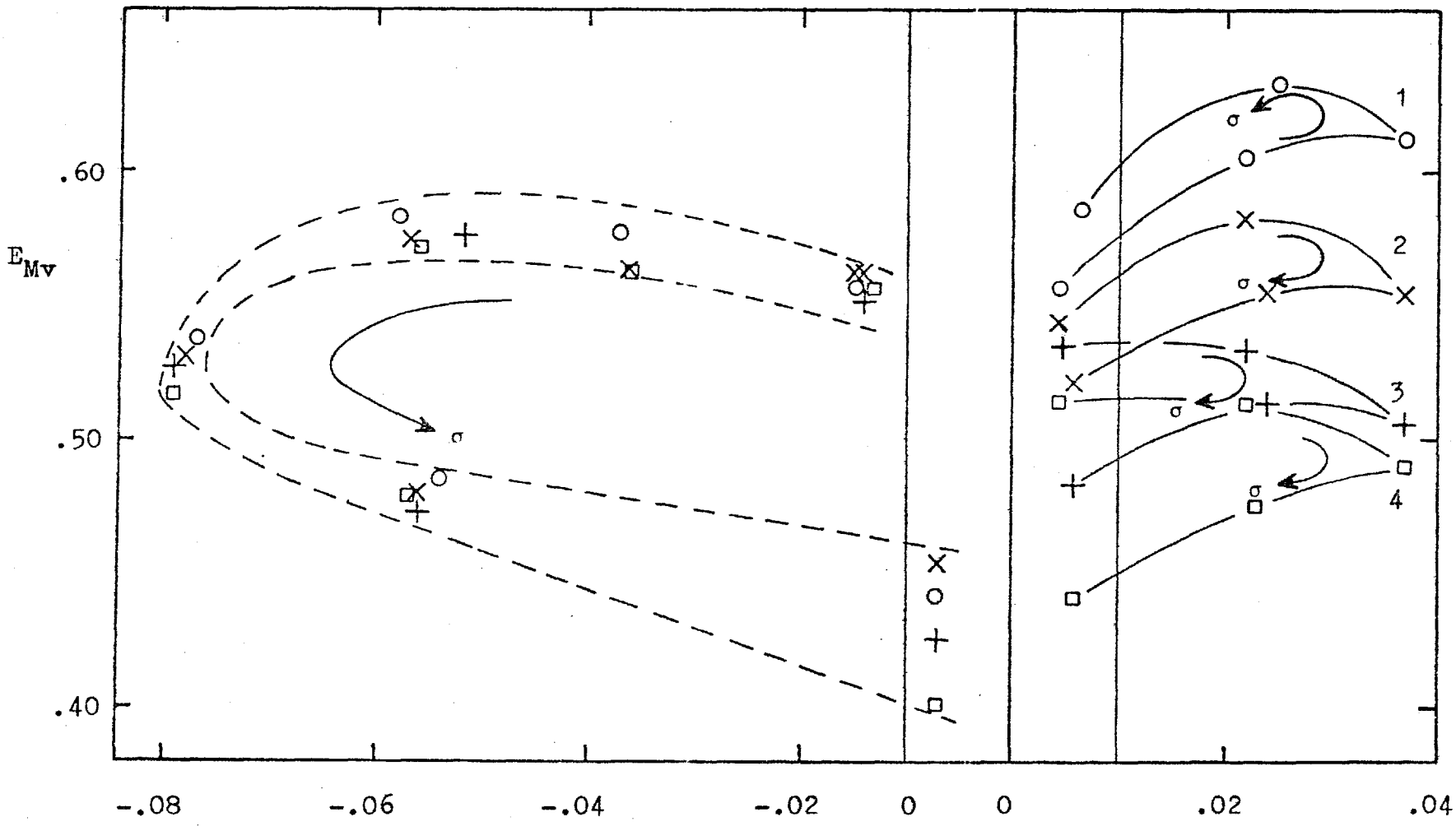

Fig. 4.45.- Mass transfer efficiency for systems B and C in function of thin-film stabilising number. (1. F_s = 0.92 ± 0.05, 2. F_s = 1.24 ± 0.08. 3. F_s = 1.52 ± 0.05, 4. F_s = 1.81 ± 0.09).

4.4 Froth-Spray Transition

The transition froth-spray also called phase inversion was the subject of a publication. The effect of mass transfer was studied from Fane's data and is represented in Figure 4.43. The differences in transition point between weakly negative, weakly positive and strongly positive systems are meaningless. However, the gas velocity for transition of the strongly negative system is about 25% below the transition for the other systems.

4.5 Mass Transfer Efficiency

Mass transfer efficiency depends on the product of the mass transfer coefficient and the area of transfer. Thus, all the variables affecting either of these will influence the efficiency.

Figures 4.44 and 4.45 are presented as an attempt to demonstrate the effect of Tf on efficiency. The graphs, as expected, are rather complicated. It is evident that the effect of gas velocity in positive systems is more important than in negative systems. The surface tension increases in the direction shown by the arrows (but it is within ±8% of the medium value for system A). It is not easy to explain the way efficiency changed with physical properties and/or mass transfer. However, in system A the change in surface tension is small, the vapour diffusivity is almost constant and the ratio of the liquid diffusivity to the gas diffusivity is small. Under these conditions the surface-renewal Marangoni effect is expected to become noticeable as an increase of efficiency when Tf becomes positive. This is in fact so and can be seen in Figure 4.44.

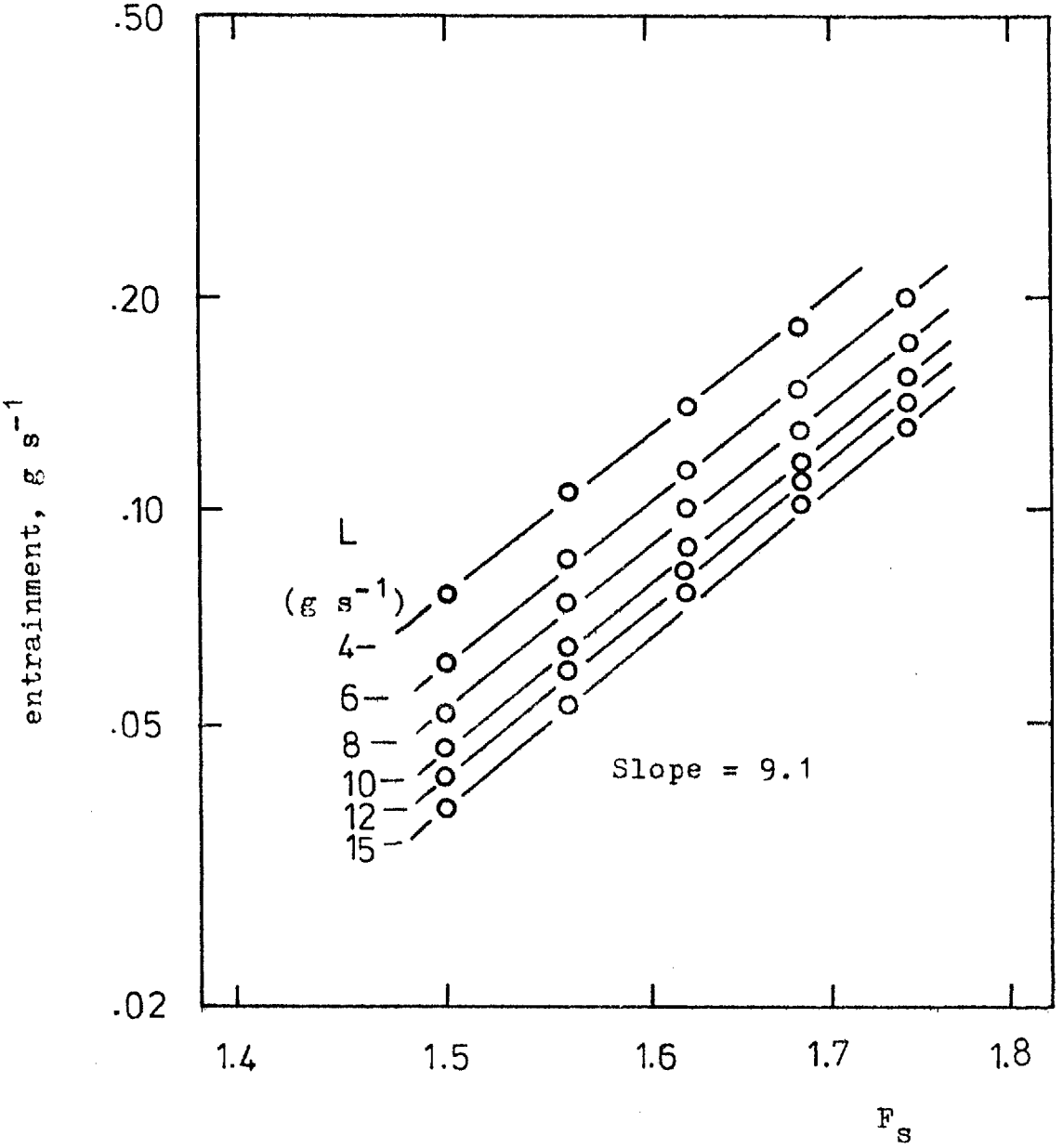

Fig. 4.46.- Effect of gas rate on entrainment (spray regime).

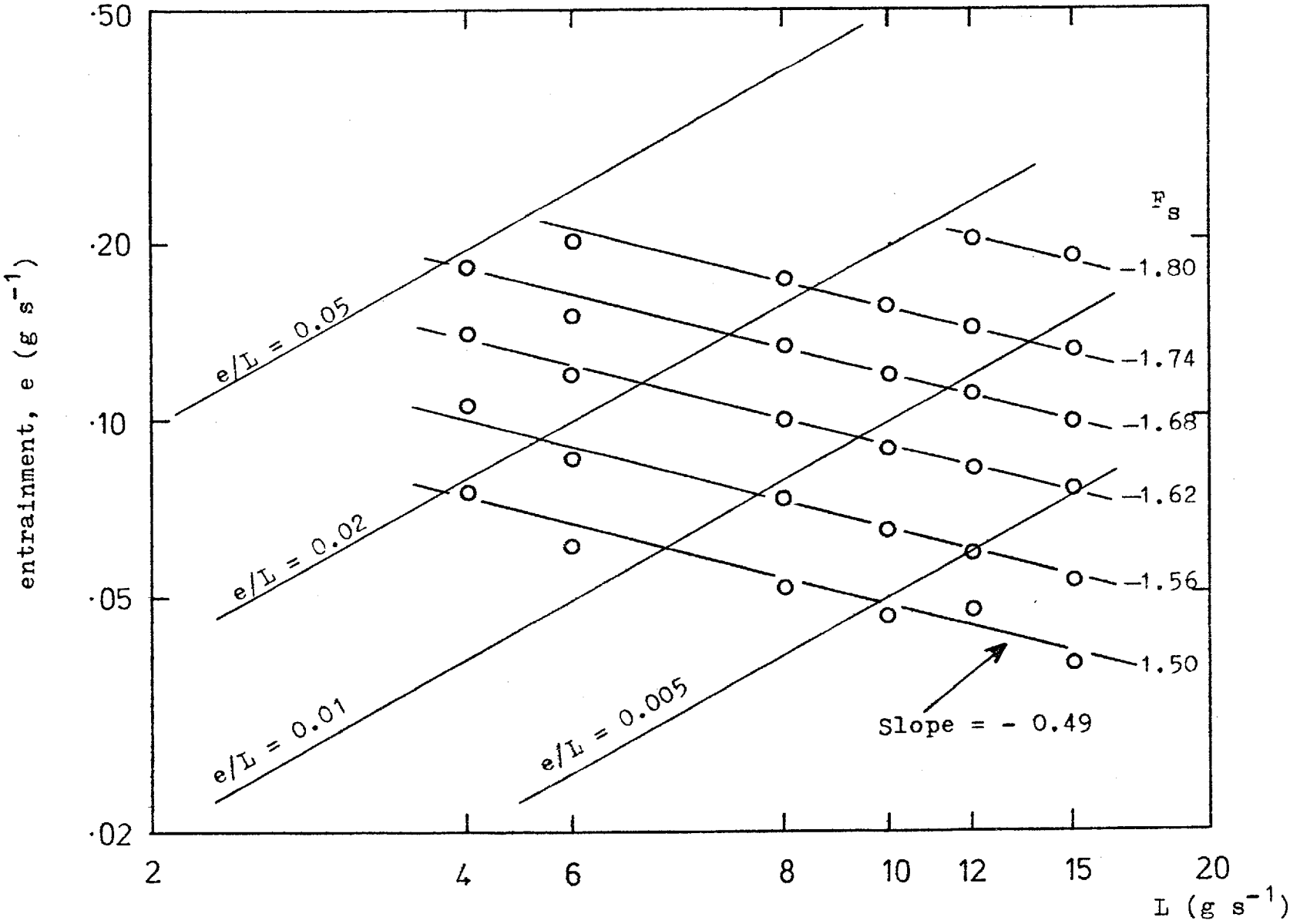

Fig. 4.47.- Effect of liquid rate on entrainment (spray regime).

4.6 Entrainment

The data on entrainment for the system air/water are summarized in Figures 4.46 and 4.47.

Available data[67] for entrainment in the spray regime for operation of a perforated plate, show that for a single orifice:

$$E \propto u_o^{4.44} \tag{110}$$

and that the dependence on the velocity increases with multiple orifices. With 13 orifices (maximum number used by the authors) it becomes

$$E \propto u_o^{6.66} \tag{111}$$

The data now obtained show a higher dependence on hole velocity. The results show that the absolute value of entrainment is not very high and can be correlated by:

$$E \propto F_s^{9.1} L_v^{-0.49} \tag{112}$$

Chapter Five

Discussion

5.1 Introduction

Various aspects of the spray regime and its boundaries have been studied in the course of this work.

In Chapter 2 problems were discussed relating to the transition froth-spray in the light of available published results. In Chapter 4 it was necessary to introduce into the analysis of the results the effect of gradients of surface tension induced in the interface by the mass transfer process, that is phenomena generally known as the Marangoni effect. The systems were classified according to the intensity and direction of action of these effects. The setting-up of criteria used there will be the subject of section 5.2.

Prediction of mass transfer taking place on the plate is the final objective of the present study. However, this aim can only be successfully achieved with a very good knowledge of the hydrodynamics of the spray regime. Once the hydrodynamics is known, the rate of mass transfer can be predicted by using any reliable methods. For this reason most of the present effort was devoted to the hydrodynamic aspects of the problem.

The effect of mass transfer on transition will be discussed in section 5.3. Dispersion density profiles are easily determined and there is already a large number of them available in literature. In Chapter 4 a method was obtained which proved to be very effective to express the results of the dispersion density profiles in terms of three parameters. Furthermore, these parameters could be related to the characteristics of the spray. The influence of the most important

factors affecting the dispersion density profiles was also observed in Chapter 4 and will be discussed in section 5.4. A tentative prediction of plate behaviour will be given in section 5.5.

5.2 Influence of Mass-Transfer-Induced Marangoni Effect on Hydrodynamics and Performance of Sieve Plates

5.2.1 Introduction

Interphase mass transfer involves three steps:

1. Mass transport from the bulk of one phase to the interface,
2. Transfer across the interface, and
3. Transport into the bulk of the second phase. Usually no resistance is assumed to the transfer of the diffusing component across the interface.

Marangoni effect is a general term for surface flow phenomena resulting from the appearance in the interface of an interfacial tension gradient. These phenomena can be described on the basis of Marangoni's finding[77,136] that a liquid of lower surface tension will always spread over a liquid of higher surface tension. This effect can result from several causes, but for the moment only concentration gradients will be considered. The local interfacial concentration can be affected mainly by two different types of phenomena:

1. Surface renewal phenomena
2. Thin-film phenomena

The first phenomena predominate when the depth of the liquid is much larger than the depth of penetration of surface movement and the

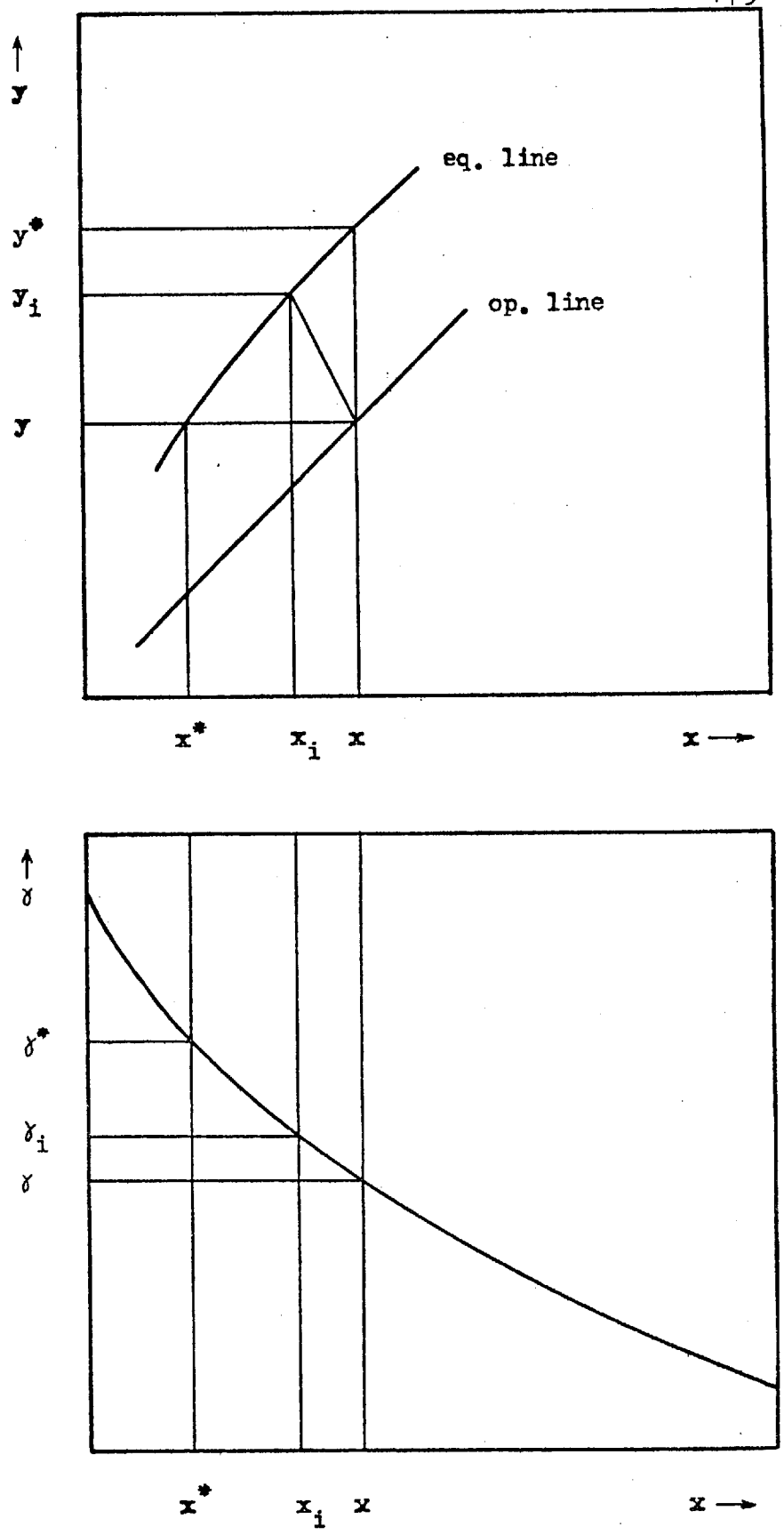

Fig. 5.1.- Effect of interface composition on surface tension.

second are important when the two depths are comparable. In the first case the affected process parameter is the mass transfer coefficient and in the second case the interfacial area. Following the findings of Marangoni[77,136] the fundamental aspect to consider is the change of static surface tension with the ageing of an interface element. If the static surface tension increases with the ageing of the element, the system is called positive. If it decreases, the system is called negative. If dynamic surface tension is to be considered, then Maxwell's relaxation law has to be used.

5.2.2 Thin-film Marangoni phenomena

Consider that the composition of the bulk of the liquid phase is x and that of the gas phase is y. Let the distribution of resistances in the phases for mass transfer be such that x_i is the interfacial composition (Figure 5.1) and γ_i the relevant surface tension. When the liquid film is very thin its composition tends to x* and the surface tension to γ^*. By making the normal assumption that the surface tension is the equilibrium value with respect to the surface composition, $(\gamma^* - \gamma_i)$ can be regarded as the thin-film stabilising force. A thin-film stabilising dimensionless number, Tf, can be defined by the ratio of the surface stabilising force to the surface tension force. Then:

$$Tf = \frac{\gamma^* - \gamma_i}{\gamma_i} \qquad (1)$$

For a positive system $Tf > 0$; for a negative one $Tf < 0$.

However

$$\frac{d\gamma}{dx} = -\frac{\gamma^* - \gamma_i}{x_i - x^*}, \qquad (2)$$

$$m = \frac{y_i - y}{x_i - x^*} \tag{3}$$

and $$K_G(y_i - y) = K_{OG}(y^* - y) \tag{4}$$

where:

K_G is the gas phase mass transfer coefficient

K_{OG} is the over-all mass transfer coefficient based on the gas phase and

m is the slope of the equilibrium line.

The substitution of equations (2), (3) and (4) into equation (1) gives

$$Tf = -\frac{K_{OG}}{mK_G}\frac{1}{\gamma_i}\frac{d\gamma}{dx}(y^* - y) \tag{5}$$

Special cases:

a) No liquid-phase resistance-gas phase control.

$$K_{OG} = K_G, \quad y_i = y^*, \quad x_i = x \text{ and } \gamma_i = \gamma$$

Then:

$$Tf = -\frac{1}{\gamma}\frac{d\gamma}{dx}(x - x^*) \tag{6}$$

b) No gas-phase resistance-liquid phase control

$$y_i = y \qquad x_i = x^* \qquad \text{and} \quad \gamma_i = \gamma^*$$

Then by (1): $$Tf = 0 \tag{7}$$

This means that no Marangoni effect is present if there is no gas-phase resistance. This result is the consequence of regarding the Marangoni

effect as a thin-film phenomenon.

If Tf > 0.01 the system will be called strongly positive and if Tf < -0.01 the system will be regarded as strongly negative. Otherwise the systems will be called weakly positive or negative. Thus at total reflux, system A (benzene-cyclohexane) is weakly negative for benzene concentrations below the azeotrope (53.2% of benzene) and it is weakly positive for higher concentrations of benzene. System B (benzene-n-heptane) is strongly negative for concentrations of n-heptane between 5% and 93%. System C (n-heptane-toluene) is strongly positive for concentrations of toluene between 10% and 86%.

5.2.3 Surface-renewal Marangoni phenomena

Surface renewal phenomena can appear as a result of:

1. Spontaneous interfacial convection, usually in the form of roll-cells,
2. Eddies coming from a turbulent bulk and arriving at the interface, or
3. Macro-scale flow under the influence of longitudinal surface tension gradients. This case was considered to be dominant in a pool column.[88]

For visualisation of the effects of surface renewal phenomena, consider the two-film model due to Whitman[137] (Figure 5.2) corresponding to the system shown in Figure 5.1. The composition of the bulk of the liquid phase is $\underline{x}$ and the corresponding composition of the interface is x_i. If, at a point of the interface, the surface is renewed with liquid from the bulk its composition tends to x and the surface tension to γ.

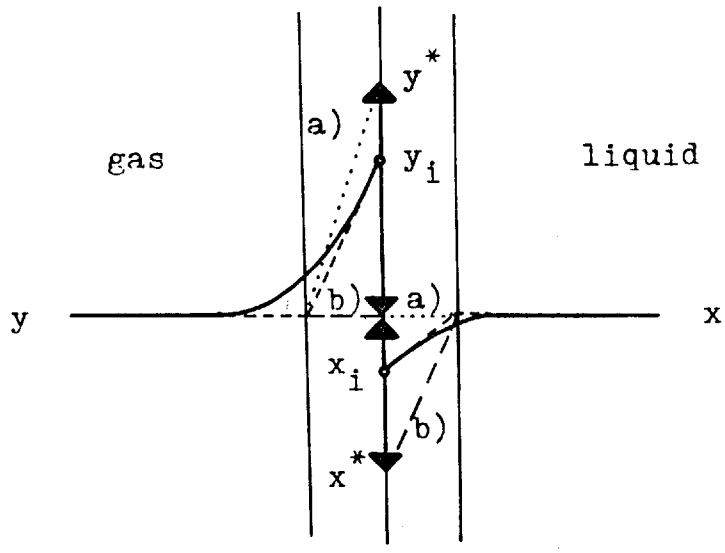

Fig. 5.2.- Composition gradients between two contacting phases. Case a) ···· gas-film control.
Case b) ---- liquid-phase control.

Thus ($\gamma_i - \gamma$) can be regarded as a surface renewal force. If the system is positive (according to the previously given definition), the surface renewal force is positive and the mass transfer coefficient increases as a result of increase in surface renewal due to the Marangoni effect. If the system is negative, Marangoni effect opposes surface renewal and this can decrease the mass transfer coefficient.

Special cases:

a) No liquid-phase resistance - gas phase control

$$x_i = x \quad \text{and} \quad \gamma_i = \gamma$$

Then:

Surface renewal force = 0 and no Marangoni effect results.

b) No gas-phase resistance - liquid phase control

$x_i = x^*$ and $\gamma_i = \gamma^*$. Then:

Surface renewal force = $\gamma^* - \gamma$ or $= -\frac{d\gamma}{dx}(x - x^*)$

Comments on Marangoni effect

1. A stabilising-index, not dimensionless, has been used by Hart and Haselden,[117] Sawistowski[118] and Moens[86-88] in order to form a measurement of differences in surface tension due to the Marangoni effect. However, it seems more realistic to distinguish separately between the effects on surface renewal and on thin-films. In the latter case it seems important to compare the differences in surface tension due to Marangoni effect with the normal value of the surface tension existing at interface since the hydrodynamic effect of interaction of both phases must consider all the forces which are present. In this way a dimensionless number was obtained satisfying the intuitive idea of stronger Marangoni effect on thin-films for systems with smaller surface tension.

2. The stabilising-index defined by:

$$M = \frac{d\gamma}{dx}(x - x^*)$$

was used by Moens[88] to analyse the surface renewal effects in a pool column. In this sense, the name given to the index is misleading since a positive value of the index is an indication of destabilising forces due to Marangoni effect, resulting in increasing surface renewal effects.

However, it is interesting to note that the classification of systems according to the Marangoni effect, that is

strongly positive for $Tf > 0.01$

" negative " $Tf < -0.01$

weakly positive " $0 < Tf < 0.01$

" negative " $0 > Tf > -0.01$

neutral for $Tf = 0$

according to the intensity of thin-film stabilising Marangoni effect agrees with the findings of Moens on the intensity of promoting or inhibition of surface renewal by Marangoni effect. In fact, Moens[88] found that the efficiency of a pool column remains unchanged, if the absolute value of the stabilising index > 0.15 dyn/cm, which was reported to be in agreement with the investigation of Ellis *et al.*[85]. The efficiency increases if the stabilising index is raised from -0.15 to +0.15 dynes/cm (see Figure 5.3). But as the values of surface tension were about 15 dynes/cm, the thin-film stabilising number, corresponding to M = 0.15 dynes/cm, was Tf = 0.01. If this agreement was not fortuitous

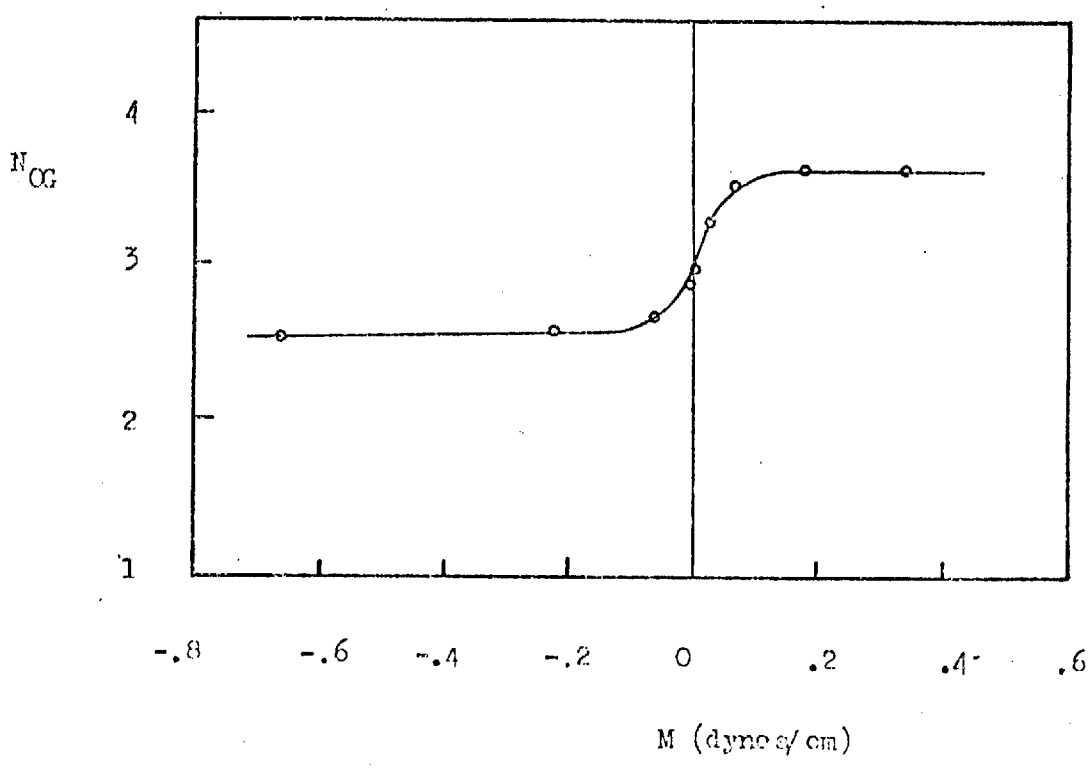

Fig. 5.3.-N_{OG} as a function of M on a pool column (i.e. with a fixed interfacial area)[88].

then a strongly positive system would be one giving strong stabilising effects on thin films and strong surface renewal effects on thick films. Similar conclusions could be applied to the other types of systems. However, this does not seem feasible, since:

a) When the system is gas-phase controlled only thin-film Marangoni-induced phenomena can occur, and

b) When the system is liquid-phase controlled only surface renewal Marangoni-induced phenomena can occur. For this reason it seems necessary to define two different criteria for the two different phenomena. The criterion for thin-film stabilisation based on $(\gamma^* - \gamma_i)$ and the criterion for surface renewal based on $(\gamma_i - \gamma)$ (in this case, Marangoni number seems to be preferred).

In the experiments reported by Moens,[88] the number of transfer units of the liquid and of the gas phases were the same (= 0.3) and this can explain the reported coincidence of the criteria.

5.3 Effect of Mass Transfer on Transition

The results reported in section 4.4 for the transition froth-spray confirm that the gas velocity necessary for transition was about 25% smaller for strongly negative systems than for the other systems. According to the adopted definition of transition, this means that kinetic energy of gas necessary to break up the liquid and produce dispersed droplets is smaller for such systems. Consider, for instance, the "necking" stage[66] in drop formation just prior to its detachment. According to what was said in the previous section about thin-film Marangoni phenomena, in the case of strongly negative systems, thin-films are destabilised and the break-up takes place under conditions that otherwise would not occur. On the other hand it would be expected that the

thin-film stabilising effect of strongly positive systems would be sufficient for the transition to take place at higher gas velocity than that necessary for weakly negative or positive systems. However, such effect is within the experimental errors and was not observed.

5.4 Factors affecting the dispersion density profiles

For a better understanding of the effect of several of the variables affecting the dispersion density profiles, a very simplified physical model will be presented here of the phenomena arising in the spray regime close to the hole.

For this purpose, imagine a vertical tube (Figure 5.4) open at the top and provided with a centrally located hole at the bottom. Let the ratio of the area of the hole to the internal cross-sectional area of the tube be equal to the fractional free area of the plate which the model is supposed to represent. Liquid is supplied from the circumference of the base of the tube and gas flows vertically through the hole. In Figure 5.4 the liquid present at different cross-sections is represented as a wall layer to represent the dispersion density profile and also the liquid-free section for gas flow.

From the homogeneous free jet theory,[119] velocity profiles can be deduced and a conical section defined to locate the boundaries of the jet, outside of which recirculation occurs. Entrainment by the jet, calculated as the amount entering this conical section by the sucking action of the jet, is proportional to the gas velocity, the hole area and the length of the jet deduced from a small initial length where entrainment does not occur.

The analysis of the stability of the gas-liquid interface of subsonic gas jets submerged in a liquid[120] has been done using linearized potential flow theory. The mechanism of liquid-drop entrainment at the surface of the gas jet is governed by the Kelvin-Helmoltz instability of the gas-liquid interface. The analysis showed that the pressure perturbation exerted by the gas phase on the liquid layer at the gas liquid interface was in phase with the wave amplitude. The energy was transferred to

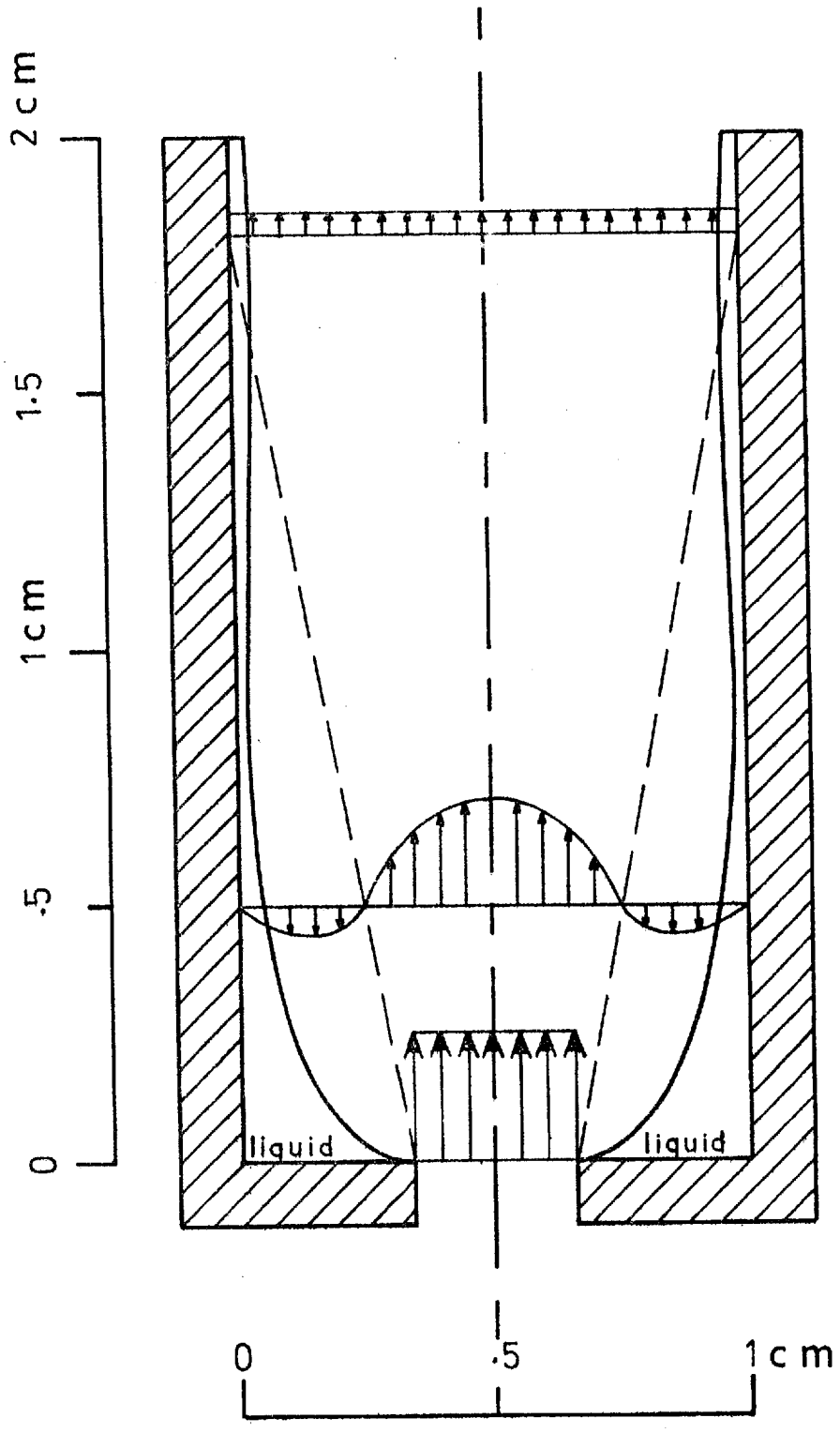

Fig. 5.4.- Scale model showing the change in mean cross sectional area available for gas flow in spray regime around each hole and mean velocity profiles.

the liquid layer predominantly through a "lift" component or by sucking in at the wave crests and pushing out at the wave troughs. The entrainment was also proportional to the gas velocity and effective length of jet.[121]

The results obtained for the dispersion density profiles will now be discussed with reference to the proposed model.

An increase in the amount of liquid fed to each hole, increases the amount of liquid in contact with the gas and thus the entrainment of liquid, explaining the effect of liquid cross-flow rate (Figures 4.9-4.11).

An increase in the gas flow-rate at constant liquid cross-flow increases the sucking effect ($\Delta p \propto F_s^2$) and thus the entrainment. However, this results in a decrease of the amount of liquid at lower levels in favour of the liquid fragmented and entrained (Figures 4.12-4.15).

Since entrainment is possible only after break-up of the liquid, an increase in surface tension makes entrainment more difficult with consequent increase of the amount of liquid at low levels (due to the lack of entrainment) and decrease at higher levels (Figures 4.16-4.17).

The effect of increase in the gas flow rate in the absence of a splash baffle is equivalent to a simultaneous decrease of liquid cross-flow rate by the effect of non-replenishment of the entrained liquid which is lost by being projected over the outlet weir (Figure 4.31).

An increase in fractional free area decreases the height of the conical section with decrease of total entrainment, of height of projection of drops and with consequent concentration of liquid at lower level leading to an increase in maximum dispersion density (Figure 4.34).

The effect of increase in hole diameter at constant fractional free area corresponds to scaling-up of all dimensions of the model tube shown in Figure 5.4. But at constant F_s and L_v, different hydrodynamic conditions arise and a proper analysis becomes complicated. Let us assume, for instance,

that the diameter is doubled. The cross-sectional area thus increases four times but the liquid flow rate only twice. So the result will be affected by the relatively smaller liquid flow rate, with decrease of dispersion density at all levels and thus of maximum dispersion density. A decrease in height of the maximum in dispersion density would be expected, due to the relative lack of liquid (as in Figure 4.9). However, the height of the maximum dispersion density, x_2, is more sensitive to liquid cross-flow for higher values of this parameter. Thus it may be possible that initially x_2 decreases when the diameter is increased, but this effect will be overtaken by the influence of scale when substantial decrease in liquid flow rate no longer affects x_2 (Figure 4.35).

5.5 Prediction of dispersion parameters in spray regime

The hydrodynamic behaviour of the plate in the spray regime is affected by so many variables that, at present, any confident prediction is difficult unless comparison with existing results is possible.

In chapter 4 it was proved that the hydrodynamic state of the plate in the spray regime could be defined by the value of five independent parameters. The dispersion density profiles allow the determination of three of them. Surface area profiles make it possible to determine the remaining two parameters and also to confirm one of those previously obtained. For the plate used in this work experimental results support the validity of equation (4.1) so that the remaining two parameters (A and B) are known and the state of the system can be fully identified. The parameters used for the computation of mass transfer are d_{gm}, σ and H_D (other than A and B).

Once parameter B is known, the standard deviation of the population of generated drops can be obtained from standard deviation of experimental profiles. From the available experimental results it seems that they depend mainly on ratio of actual gas velocity, as expressed by the F_s-factor, to the transition F_s-factor. For negative or neutral systems σ is 0.36 ± 0.06 at transition, increasing approximately with power 1.5 of F_s. For positive systems it increases only slightly with F_s and is usually in the range 0.45 ± 0.09.

Hence, the standard deviation of population of generated drops can be predicted from

$$\sigma = 0.19 \left(\frac{F_s}{F_{st}}\right)^{1.5} \tag{8}$$

where F_{st} is the F_s-factor for transition.

Since usually $F_s \leq 1.5\ F_{st}$ (entrainment is largely dependent on F_s), it seems that $0.19 < \sigma < 0.35$ for negative systems. For positive systems, it will be

$$\sigma = 0.24 \pm 0.05 \tag{9}$$

Geometric mean diameters of populations of generated drops were calculated from parameters, which defined the dispersion density profiles, using equation (4.1) by

$$d_{gm} = \frac{0.003587}{\exp(1.136\sigma_{FL}^2)\,(z_{gm}^{FL})^{0.5376}} \tag{10}$$

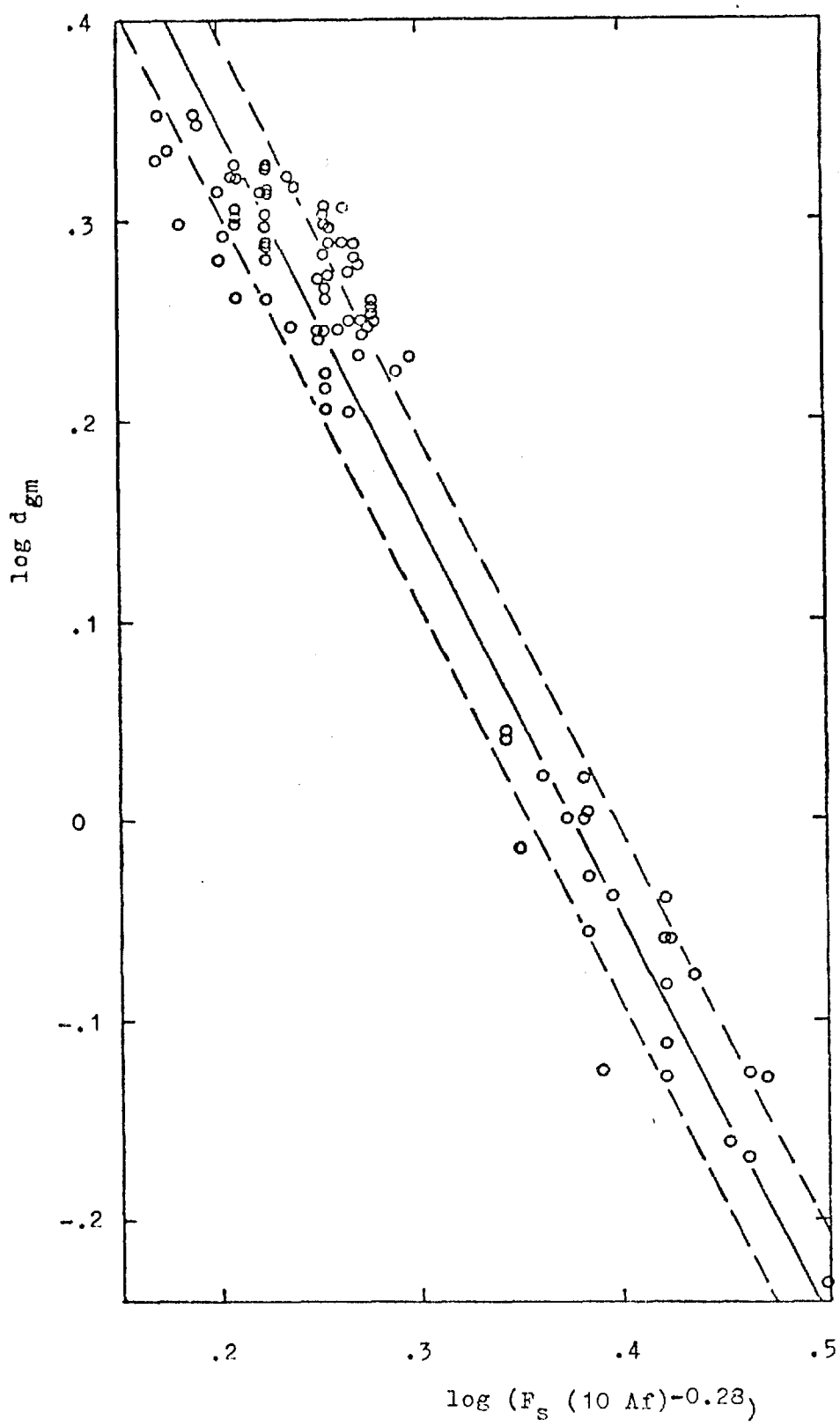

Fig. 5.5.- Determination of the functional dependence between the geometric mean diameter, the fractional free area and the F-factor.

and subsequently analysed. It was found that they depend mainly on the F_s-factor and on the fractional free area of the plate. An exponent of 0.56 on Af suitably accounted for variation in plate geometry. Hence, from Figure 5.5:

$$d_{gm} = 6 \times 10^{-3} \, (10 \, Af)^{0.56} \, F_s^{-2} \qquad (11)$$

The applicability of equation (4.1) for the condition of Pinczewski's results was not checked and is questionable since geometric mean diameters predicted seem to be too small. However, parameter z_{gm} can be calculated instead, since it does not depend on projection velocity.

It is worth noting that Fane's experimental conditions were very different from those used in the present work as far as physical properties of the systems were concerned. Thus, surface tension in his work was

$$0.013 < \gamma < 0.020 \ Nm^{-1}$$

while in present experiments

$$0.055 < \gamma < 0.072 \ Nm^{-1}$$

Since surface tension is roughly four times higher in the present experiments than in Fane's work, it was to be expected that significantly larger drops would be formed with the system air-water than with Fane's systems. This prediction will be examined with the help of possible applicable theories.

Once gas flow is turbulent, it seems reasonable to apply Kolmogorov's turbulence theory to the fragmentation of liquid by turbulent gas stream. Using the equation obtained by Levich:[122]

$$d_{Cr} \propto L^{0.4} \left(\frac{\rho_G}{\rho_L}\right)^{0.4} \gamma^{0.6} F_s^{-1.2} \qquad (12)$$

the following can be deduced:

a) drop diameters predicted for system air-water should be 40% higher than drop diameters predicted for Fane's systems A, B and C at equal F_s-factor values.

b) drop diameters in system A should be independent of composition.

c) drop diameters in the negative system B should increase by about 11% when x changes from 0 to 1 (experimental results show an increase of 16%).

d) drop diameter in the positive system C should decrease by 8% when x changes from 0 to 1 (experimental results show a decrease of 10%).

If the expression for prediction of drop sizes in venturi atomizers is used,[123] the predicted drop diameters for the system air/water should be 20% higher than those predicted for systems A, B.and C (these being approximately equal).

Finally, if the expression deduced from the theory for twin fluid atomizers[124] is used instead, predicted diameters for the system air-water will be only 4 to 6% higher than those predicted for systems B and C. For system A the predicted diameters will be about 2% higher than those for systems B and C.

The dependence of drop size on gas velocity given by all three theories is similar ($d_{gm} \propto F_s^{-1 \text{ to } -1.27}$) and is close to the experimentally obtained relation for the negative system B and for the results of

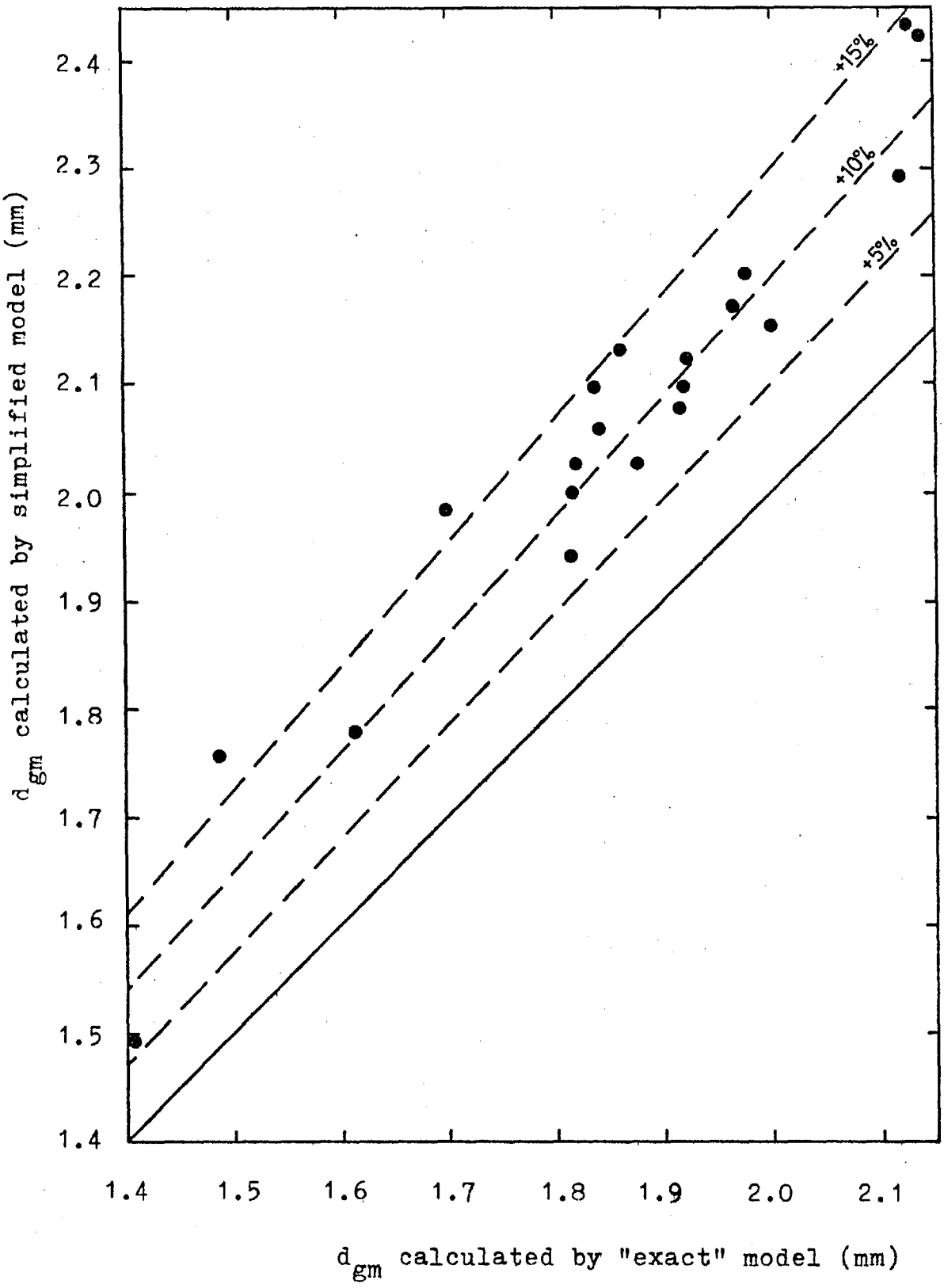

Fig. 5.6.- Comparison of geometric mean diameters calculated by simplified model and by "exact" model.

present work. If this dependence is confirmed, predicted diameters for Pinczewski's experimental conditions should be higher than those given by eq. (11) and consequently also projection velocity of drops.

Comparison of diameters calculated from a simplified model with those obtained by the "exact" model used by Fane and Sawistowski show a systematic deviation around 10% as seen in Figure 5.6.

The last parameter which needs to be predicted can be the maximum value of liquid dispersion density, x_l. In spray regime x_l is proportional to F_s^{-2}. The effect of fractional free area can be taken into account (see Figure 4.34) by the factor $Af^{0.31}$. The effect of hole diameter obtained from Figure 4.35 is represented by $x_l \propto d^{-0.37}$.

Adjusting Pinczewski's data to apply to conditions of d_h = 3.17 mm, and Af = 0.10 and all available results to F_s = 2 $kg^{1/2}\ m^{-1/2}\ s^{-1}$ by the previously mentioned relations, the effect of L_v can be isolated. Hence from Figure 5.7

$$x_l = 0.17 + 0.07 \log L_v \tag{13}$$

If the effect of F_s, Af and d_h is taken into consideration then

$$x_l = (0.17 + 0.07 \log L_v)\ (\frac{F_s}{2})^{-2} (\frac{d_h}{0.00317})^{-0.37} (10Af)^{0.31} \tag{14}$$

This expression predicts the experimental results obtained from Pinczewski's data and those obtained from the present work when a splash baffle was used. In the absence of the baffle it was found that a much larger liquid rate was necessary to reach similar dispersion density profiles. By an analogous process the derived value of x_l under the above mentioned conditions was only about 34% of that given by

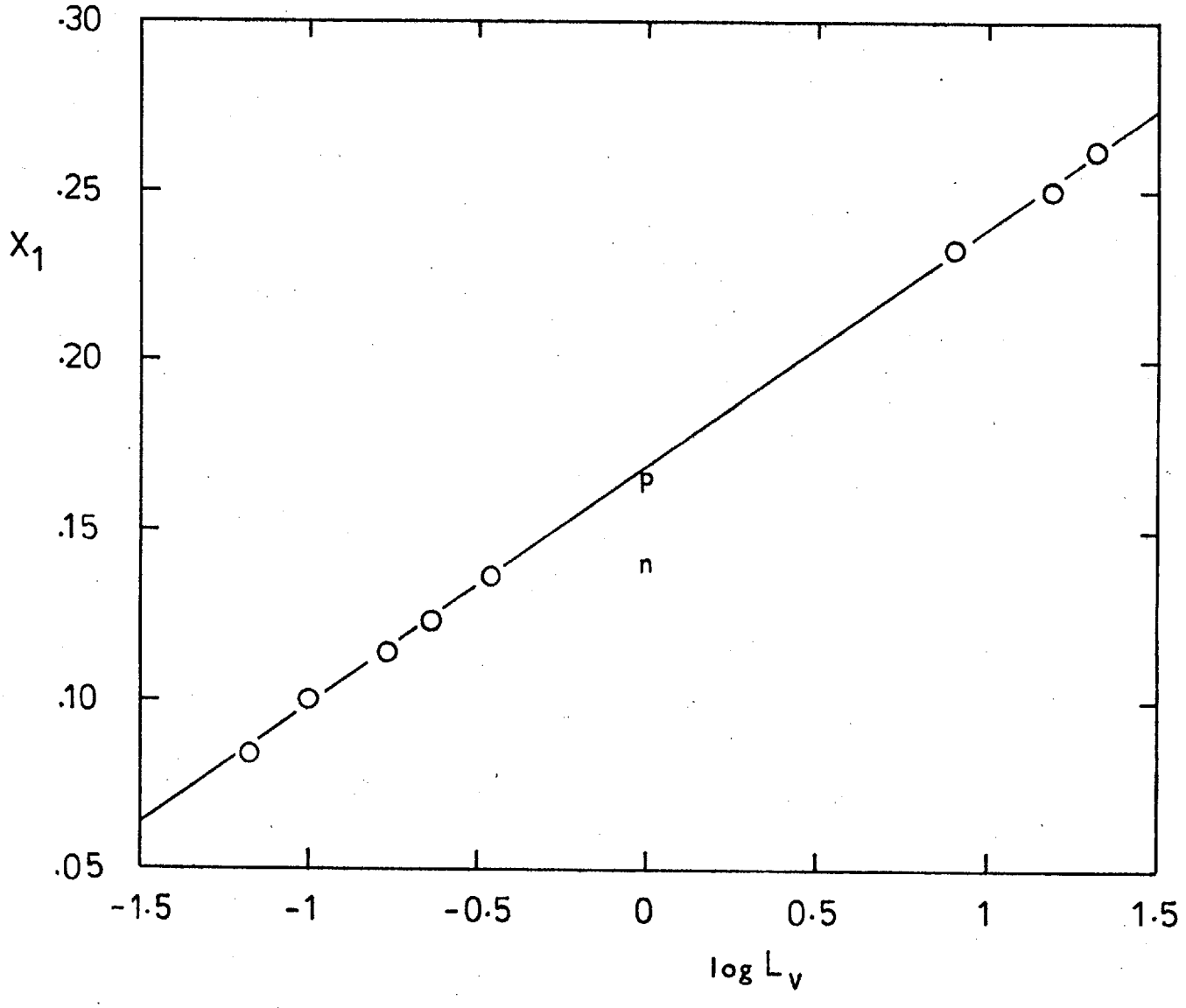

Fig. 5.7.- Effect of liquid cross-flow rate on maximum value of dispersion density.

equation (14). If Fane's data are worked out in a similar way, x_1 is about 82% and about 97% of the value given by equation (14) for the negative system B and positive system C respectively.

The value of x_1 corresponding to $F_s = 2\ kg^{1/2}\ m^{-1/2}\ s^{-1}$, $L_v = 1\ m^2\ h^{-1}$, $d_h = 3.17$ mm and Af = 0.10, represented by $\langle x_1 \rangle$ and called normalised x_1, is shown in Figure 5.8 as function of the thin-film stabilising number.

The difference between the values of $\langle x_1 \rangle$ obtained by Fane and those obtained in this work in the absence of the splash baffle are assumed to be due to the fact that smaller quantities of liquid are fragmented when surface tension is high.

Conclusion: the normalised value of x_1 is

$\langle x_1 \rangle = 0.17$ for large plate used by Pinczewski, or small plate used in this work if a splash baffle is used and surface tension is about $0.055 \div 0.072\ Nm^{-1}$.

$\langle x_1 \rangle = 0.05$ for the small plate used in this work if a splash baffle is absent and surface tension is within $0.055 \div 0.072\ Nm^{-1}$

$\langle x_1 \rangle = 0.14$ for negative systems with surface tension $0.013 \div 0.020\ Nm^{-1}$ (no splash baffle).

$\langle x_1 \rangle = 0.165$ for positive systems with surface tension $0.013 \div 0.020\ Nm^{-1}$ (no splash baffle).

The range of operating variables, physical properties and plate parameters used for these predictions are given in Table 5.1.

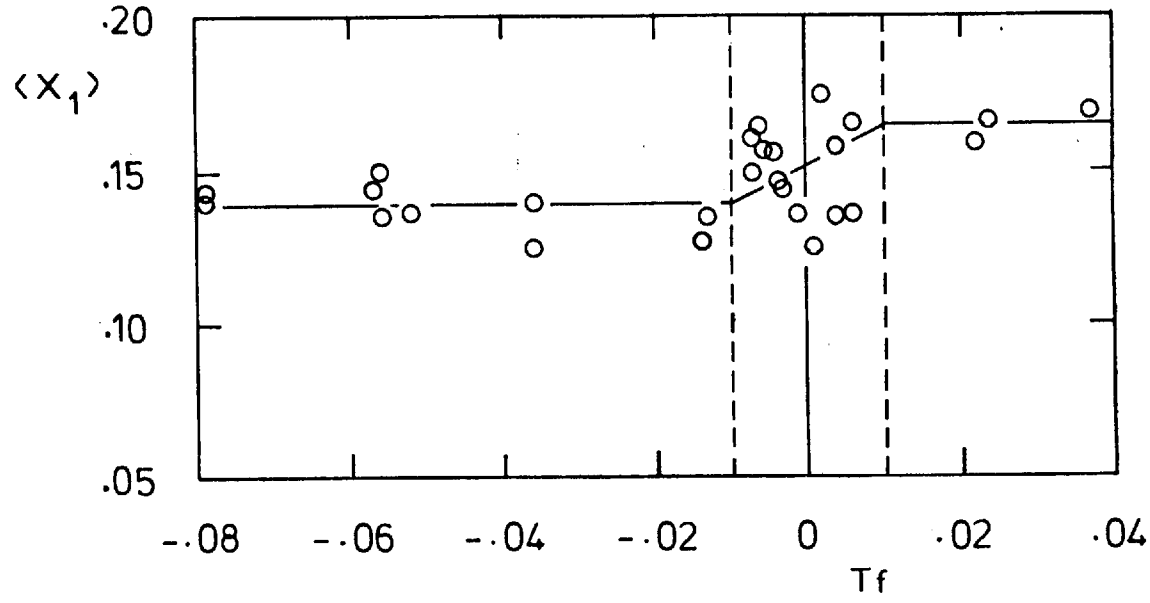

Fig. 5.8.- Effect of thin-film stabilising number on maximum value of dispersion density.

Table 5.1

Range of Operating Variables, Physical Properties and Plate Data

Hole diameter, d_h (mm)	3 - 19
Fractional free area, Af	0.059 - 0.161
F_s-factor, $kg^{1/2}\ m^{-1/2}\ s^{-1}$	1.48 - 3.16
Liquid flow-rate, L_v ($m^2\ h^{-1}$)	0.068 - 21
Surface tension, γ (Nm^{-1})	0.013 - 0.072
Gas density, ρ_G ($kg\ m^{-3}$)	1.1 - 3.3
Liquid density, ρ_L ($kg\ m^{-3}$)	620 - 1000

Chapter Six

Conclusions

Investigations carried out in this work were concerned either with the boundaries of the spray regime or with the spray regime itself.

In connection with the delineation of the spray regime a definition of the froth-spray transition was introduced in Chapter Two and the different available methods used for transition determination were compared mutually and also in relation to that definition. It was concluded that if the criterion of transition for the light transmission technique was changed so that the transition was located at a point somewhere midway of the sudden increase in transmittivity and if the criterion of frequency of bridging was changed so that the transition was located at the point where bridging frequency starts to decrease rapidly, all transition results would be very similar and would comply approximately with the adopted definition based on the availability of interfacial area for mass transfer.

The effect of mass transfer on transition was not very noticeable except that transition gas velocity for a strongly negative system was about 25% lower than for the other systems.

Entrainment was found to be proportional to the power 9.1 of gas velocity, so that practical limits of gas velocity in the spray regime will be imposed by entrainment considerations.

The free trajectory model of the spray regime was used to show that dispersion density profiles could be defined in terms of three parameters. Furthermore, these parameters could be related to the characteristics of the spray.

The total number of independent variables necessary to define the hydrodynamic state in the spray regime was deduced and found to be

number five under the assumed conditions. Since only three can be obtained from dispersion density profiles, the remaining two need to be determined independently. For this purpose a light probe was used and the value of the remaining two parameters determined. In this way the validity of the expression used by Fane and Sawistowski[1] for projection velocity of drops in spray regime could be confirmed. However, doubts exist about generalization of the use of this equation to plates of much larger hole diameters similar to those used by Pinczewski and Fell.[116] Drop diameters calculated from it for the latter case seem to be smaller than expected and theoretically predicted.

Among the different factors affecting the behaviour of the plate, the influence of mass-transfer-induced Marangoni effect was studied.

The phenomena arising from this effect were classified under two different headings:

1. Surface renewal phenomena
2. Thin-film phenomena

The effect of the second type of phenomena was described in terms of a dimensionless number, Tf, defined by the ratio of the surface stabilising force to the surface tension force. It was proved to be more important for gas-phase controlled systems and to become equal to zero when liquid-phase controls the mass transfer process. On the other hand, surface renewal phenomena due to Marangoni effect are non-existent for gas-phase controlled systems and are more important if the process is liquid-phase controlled.

Independently of the type of mass transfer operation taken into consideration, the intensification of surface renewal phenomena or of thin-film stabilization is positive if surface (or interfacial) tension increases with contact time, in which case the system is called positive. If the opposite is true, the system is called negative. This definition

is in agreement with the classification usually employed in various mass transfer operations. A subdivision of the classification into weakly or strongly positive or negative systems, allowed for an improvement in differentiation of system behaviour. The adopted classification was as follows:

strongly negative systems	$Tf < -0.01$
weakly negative systems	$-0.01 < Tf < 0$
weakly positive systems	$0 < Tf < 0.01$
strongly positive systems	$0.01 < Tf$

Physical properties apart, the hydrodynamic behaviour of a plate depends on type of system. This effect is more important in froth and foam regimes, decreasing in general when the system approaches the froth-spray transition and some times reversing in spray regime.

In relation to the effect of operating variables it is worth noting that:

1) Increasing liquid rate increases the maximum value of dispersion density and the height of this maximum above plate floor, as well as the drop hold-up. The standard deviation of the dispersion density profile is almost unchanged by the liquid rate.

2) Increasing gas flow rate decreases the maximum value of the dispersion density but increases the height of the maximum above plate floor. The standard deviation of the dispersion density profile and the hold-up of drops have a minimum at the froth-spray transition, increasing with gas flow rate in the spray regime.

LIST OF SYMBOLS

A	constant in eq. (4.7)
Ac	acceleration number (= $(d/v^2)(dv/dt)$)
A_D	total area of drops per unit cross sectional area of column
Af	fractional free area of the plate
a	characteristic dimension (in section 2.1.4.2), or surface area of dispersion per unit volume, also called specific surface area.
B	constant in eq. (4.7)
Bo	Bond number (= $gd^2\Delta\rho/\gamma$)
B_s	dimensionless number (= $u_s \varepsilon h_d \rho_G/(gD^3\rho_L\overline{F}_L)$)
b	constant in eq. (2.1)
C_o	orifice coefficient
c_D	drag coefficient
D	column diameter, or jet diameter in eq. (2.35), or diffusivity
D_E	effective diffusivity
d	volume average diameter of bubbles in eq. (2.16).
d_A	equivalent diameter of a monodispersed distribution giving the same surface area with the same number of generated drops.
d_{gm}	geometric mean diameter
d_h	hole diameter
d_p	drop diameter
d_{Sauter}	Sauter mean diameter at height z.
d_{Sauter}^{Disp}	Sauter mean diameter of dispersion on plate
d_v	equivalent diameter of a monodispersed distribution giving the same hold-up with the same number of generated drops
$\overline{d}$	Sauter mean diameter at height z.

E_{M_v} Murphree plate efficiency based on gas phase

F objective function to be minimized

F_C correction factor for crossflow of liquid

F_L volumetric liquid fraction

$\overline{F}_L$ mean volumetric liquid fraction on plate

F_{L_p} volumetric liquid fraction at projection level

Fr Froude number ($= u_s^2/(gH_L)$)

F_s factor F ($= u_s \rho_G^{1/2}$) based on superficial velocity

$\underline{f}$ body force per unit mass of fluid

$f_\sigma(x)$ Gaussian distribution function

($= 1/(\sigma\sqrt{2\pi})\ \exp(-x^2/(2\sigma^2))$).

g gravitational acceleration (9.81 m s^{-2})

H distance between plates

H_D hold-up of drops

H_L liquid hold-up

h_d mean dispersion height

I intensity of radiation after absorption

I_o incident intensity of radiation

K constant in eq. (2.14), (2.16) or (2.17)

$K_L(t)$ instantaneous liquid-phase mass-transfer coefficient

K_G gas-phase mass-transfer coefficient

K_{OG} overall mass-transfer coefficient based on the gas-phase

L length of jet break-up, or characteristic dimension, or

volumetric liquid flow-rate

L_v volumetric liquid flow-rate per unit length of weir

M value of the maximum in the profile, or stabilising-index

m slope of the equilibrium line

N	wave number ($= 2\pi h_d/\lambda$), or cumulative number distribution function of generated drops
N_T	maximum value of N
N_{OG}	number of overall gas-phase transfer units
N_p	number of drops projected per unit time and unit area of plate
P	value of F_L or a
p	pressure
p_O	pressure at z = 0
p_H	pressure at z = H
R	dependent variable (eq. 3.5)
Re	Reynolds number (eq. 2.35, 2.39 and 2.40)
Sc	Schmidt number ($= \mu/\rho D$)
Sh_G	Sherwood number ($K_G d_p/D$)
Su	surface tension number ($\gamma d\rho_O/\mu_O^2$)
T	period of motion
Tf	thin-film stabilizing number ($= (\gamma^* - \gamma_i)/\gamma_i$)
t	time
t_b	break-up time
t_d	dead time
t_{life}	life time
u_G	gas velocity
u_s	superficial gas velocity
v	upwards velocity of drop at level z.
$\underline{v}$	velocity vector
v_A	initial projection velocity of drop of size d_A
v_p	initial projection velocity of drop of size d_p
v_R	relative velocity
v_V	initial projection velocity of drop of size d_V

We	Weber number ($= D\rho u^2/\gamma$)
We_t	Weber number at transition ($= d\rho_G u_t^2/\gamma$)
X	molar ratio methanol/water in liquid phase
x	molar fraction in liquid-phase, or
	$= \ln(d_p/d_{gm})$ or
	$= \ln (z/z_{gm})$
x_1	value of the maximum dispersion density of the profile
$<x_1>$	normalised value of x_1 (value of x_1 for $F_s = 2$ kg$^{1/2}$ m$^{-1/2}$ s^{-1}, $L_v = 1$ m^2 h^{-1}, $d_h = 3.17$ mm, Af = 0.1)
x_2	height corresponding to x_1
x_3	standard deviation of profile
y	mole fraction in gas-phase
z	height above plate floor
z_{gm}	maximum height reached by a drop of size d_{gm}
z_{gm}^a	geometric mean height of specific surface area profile
z_{gm}^{FL}	" " " " dispersion density profile
z_{gm}^P	" " " " any profile
z_{max}	maximum height reached by a drop of size d_p.
γ	surface tension
Δ	angular deviation of an incident ray
$\Delta\rho$	$= \rho_L - \rho_G$
ε	gas void fraction
ε_0	" " " for z = 0
$\bar{\varepsilon}$	mean void fraction
ε_f	liquid hold-up fraction in the films (eq. 2.17)
ε_b	" " " " " the borders (eq. 2.17)
λ	wavelength
μ	fluid viscosity, or mass absorption coefficient (in chapter 3)
ρ	fluid density

ρ_m	mean dispersion density
σ	standard deviation of population of generated drops
σ_a	standard deviation of specific surface area profile
σ_{FL}	" " " dispersion density profile
σ_p	" " " any profile

Subscripts

a	specific surface area profile
FL	dispersion density profile
G	gas phase
i	discontinuous phase or at interface
i,j	running indices
l	liquid phase
o	continuous phase

Superscripts

C	calculated
E	experimental
u	for upwards movement
*	at equilibrium conditions

BIBLIOGRAPHY

1. Fane, A.G. and Sawistowski, H. In "Distillation-1969", I.Chem.E.Symp.Ser. No.32, Session 1, p.8. (London: The Institution of Chemical Engineers).
2. Lindsey, J.K., Ph.D. Thesis. University of London, 1972.
3. Fane, A.G., Lindsey, J. and Sawistowski, H., Indian Chem. Engr, 1973, 15(4), p.15.
4. Zuiderweg, F.J. and Harmens, A., Chem. Engng Sci., 1958, 9, p.89.
5. Wallis, G.B. in "Proceedings of Heat Transfer Conference, Boulder - 1961", Paper 38, p.319, (New York: Am. Soc. of Mech. Engineers).
6. Ho, G.E., Muller, R.L. and Prince, R.G.H., in "Distillation - 1969", I.Chem.E.Symp.Ser. No.32, Session 2, 10. (London: The Institution of Chemical Engineers).
7. Macmillan, W.P., Ph.D. Thesis. University of London, 1962.
8. Bernard, J.D.T. and Sargent, R.W.H. Trans. Instn chem. Engrs, 1966, 44, p.314.
9. Pinczewski, W.V. and Fell, C.J.D., Trans. Instn chem. Engrs, 1972, 50, p.102.
10. Shakhov, Yu.A., Noskov, A.A., and Romankov, P.G., Zh. Prikl. Khim., 1964, 37, p.2074.
11. Biddulph, M.W. and Stephens, D.J., AIChE Journal, 1974, 20, p.60.
12. Biddulph, M.W., AIChE Journal, 1975, 21, p.41.
13. Shoukry, E.S., Čermák, J. and Kolář, V., The Chem. Engng Journal, 1974, 8, p.27.
14. Shoukry, E.S. and Kolář, V., The Chem. Engng Journal, 1974, 8, p.41.

15. Pinczewski, W.V., Benke, N.D. and Fell, C.J.D., AIChE Journal, 1975, 21, p.1210.

16. Leroy, P. and Cohen de Lara, G., Revue de Metallurgie, 1958, 55, p.186.

17. Pinczewski, W.V. and Fell, C.J.D., AIChE Journal, 1975, 21, p.1019.

18. Luhning, R.W. and Sawistowski, H. in "Proceedings of Intl Solvent Extraction Conf.", 1971, p.873. (London: Society of Chemical Industry).

19. Hinze, J.O., in "Symp. on Two-Phase Flow", 1965, p. F101. (Exeter: University of Exeter).

20. Beek, W.J., in "Symp. on Two-Phase Flow", 1965, p.F401. (Exeter: University of Exeter).

21. Azbel, D.S., Khim. prom., 1962, 1, p.854.

22. Kim, S.K., International Chem. Eng., 1966, 6, p.634.

23. Takahashi, T., Matsuno, R. and Miyahara, T., J. of Chem. Engng of Japan, 1973, 6, p.38.

24. Takahashi, T., Miyahara, T. and Shimizu, K., J. of Chem. Engng of Japan, 1974, 7, p.75.

25. Steiner, L. and Kolář, V., Colln Czech. chem. Commun. Engl. Edn., 1968, 33, p.2207.

26. Kolář, V., Chem. Engng Sci., 1969, 24, p.1285.

27. Cervenka, J. and Kolář, V., The Chem. Engng. J., 1973, 6, p.45.

28. Čermak, J. and Rosenbaum, M., Colln Czech. chem. Commun. Engl. Edn, 1974, 39, p.1823.

29. McCann, D.J. and Prince, R.G.H., Chem. Engng Sci., 1969, 24, p.801.

30. Bhatia, V.K., AIChE Journal, 1969, 15, p.466.

31. Muller, R.L. and Prince, R.G.H., Chem. Engng Sci., 1972, 27, p.1583.

32. Khurana, A.K. and Kumar, R., Chem. Engng Sci., 1969, 24, p.1711.

33. Kumar, R., Chem. Engng Sci., 1971, 26, p.177.

34. Ho, G.E. and Prince, R.G.H. in "Proceedings of Symposium on Bubbles and Foams", 1971. (Nuremberg: Verein deutscher Ingenieure).

35. Hartland, S. and Barber, A.D., Trans. Instn chem. Engrs, 1974, 52, p.43.

36. Calderbank, P.H. and Moo-Young, M.B. in "Distillation", Rottenburg, P.A. (Ed.), 1960, p.59. (London: The Institution of Chemical Engineers).

37. Rennie, J. and Smith, W. in "Transport Phenomena", Rottenburg, P.A. (Ed.), 1965, p.67. (London: The Institution of Chemical Engineers).

38. Nicklin, D.J., Wilkes, J.D. and Davidson, J.F., Trans. Instn chem. Engrs, 1962, 40, p.61.

39. Ellis, J.E. and Lloyd Jones, E. in "Proceedings of the Symposium on Two-Phase Flow, 1965", Paper B1. (Exeter: University of Exeter).

40. Porter, K.E. and Wong, P.F.Y., in " Distillation-1969", I.Chem.E. Symp. Ser. No.32, Session 2, p.22. (London: The Institution of Chemical Engineers).

41. Andrew, S.P.S., in "Distillation-1969", I.Chem.E. Symp. Ser. No.32. Session 2, p.49. (London: The Institution of Chemical Engineers).

42. Newitt, D.M., Dombrowski, N. and Kuelman, F.H., Trans. Instn chem. Engrs, 1954, 32, p.244.

43. Gleim, V.G., Shelomov, I.K. and Shidlovskii, B.R., J. Appl. Chem., USSR, 1959, 32, p.222 (Eng. Transl.).

44. Rayleigh Lord, Proc. Lond. Math. Soc., 1878/9, 10, p.4.

45. Teller, A.J. and Rood, R.E., AIChE Journal, 1962, 8, p.369.

46. Jeronimo, M.A. da S., and Sawistowski, H., Trans. Instn chem. Engrs, 1974, 52, p.291.

47. Payne, G.J. and Prince, R.G.H., Trans. Instn chem. Engrs, 1975, 53, p.209.

48. Azbel, D.S., Teor. Osnovy. Khim. Tekh., 1971, 5, p.708.

49. Nielsen, R.D., Ph.D. dissertation. University of Michigan, 1965.

50. Pinczewski, W.V. and Fell, C.J.D., The Can. J. of Chem. Eng., 1971, 49, p.548.

51. Levich, V.G., in "Physicochemical Hydrodynamics", 1962, p.661, (New Jersey: Prentice Hall).

52. Lane, W.R., Ind. Eng. Chem., 1951, 43, p.1312.

53. Eisenklam, P., J. Inst. F., 1961, 37, p.130.

54. Chawla, T.E., Argonne National Lab., III. Rept ANL-7949, June 1972.

55. Grant, R.P. and Middleman, S., AIChE Journal, 1966, 12, p.669.

56. Hughes, R.R. and Gilliland, E.R., Chem. Eng. Prog., 1952, 48, p.497.

57. Jeronimo, M.A. da S., not published.

58. Gal-Or, B., The Canadian J. Chem. Engng, 1970, 48, p.526.

59. Harper, J.F., Advances in Applied Mechanics, 1972, 12, 59.

60. Wallis, G.B., Int. J. Multiphase Flow, 1974, 1, p.491.

61. Steiner, L., Balmer, J.F. and Hartland, S., The Chem. Engng Journal, 1975, 10, p.35.

62. Sawistowski, H., private communication.

63. de Goederen, C.W.J., Chem. Engng Sci., 1965, 20, p.115.

64. Ditneiski, Yu.I., Chem. Storow., 1965, No.3B, p.309. also in Intl Chemical Engng, 1966, 6, p.204.

65. Quigley, L.J., Johnson, A.I. and Harris, B.Z., Chem. Engng Prog. Symp. Series, 1955, 16, p.31.

66. Bainbridge, G.S. and Sawistowski„ H., Chem. Engng Sci., 1964, 19, p.992.

67. Banerjee, T.S., Roy, N.K. and Rao, M.N., Indian Journal of Technology, 1969, 7, p.308.

68. Banerjee, T.S., Murti, P.L.N., Roy, N.K. and Rao, M.N., Indian Journal of Technology, 1970, 8, p.32.

69. Banerjee, T.S., Roy, N.K. and Rao, M.N., Indian Journal of Technology, 1969, 7, p.301.

70. Davies, B.T. and Porter, K.E., in "Symp. on Two-Phase Flow", 1965, p.F301. (Exeter: University of Exeter).

71. Jeronimo, M.A. da S. and Sawistowski, H., Trans. Instn chem. Engrs, 1973, 51, p.265.

72. Kutateladze, S.S. and Sorokin, Y.L., in "Problems of Heat Transfer and Hydraulics of Two-Phase Media", 1969, p.385 (Oxford: Pergamon Press).

73. Murphree, E.V., Ind. Eng. Chem., 1925, 17, p.747.

74. Hausen, H., Chemie-Ingr. Tech., 1953, 25, p.595.

75. Standart, G.L., Chem. Engng Sci., 1965, 20, p.611.

76. Colburn, A.P., Ind. Eng. Chem., 1936, 28, p.526.

77. Marangoni, C., in "Sull' espansione delle goccie di un liquido galleggiante sulla superficie di altro liquido" Fusi, Pavia, 1865.

78. Bird, R.B., Stewart, W.E. and Lightfoot, E.N., "Transport Phenomena", Wiley, New York, 1960, 656-676.

79. Sawistowski, H., Chemie-Ing-Techn., 1973, 45, p.1114.

80. Sawistowski, H., Chemie-Ing-Techn., 1973, 45, p.1093.

81. Fane, A.G. and Sawistowski, H., Chem. Engng Sci., 1968, 23, p.943.

82. Boyles, A.P. and Ponter, A.B., Chem. Engng Sci., 1970, 25, p.1952.

83. Burkholder, H.C. and Berg, J.C., AIChE Journal, 1974, 20, p.863.

84. Danckwerts, P.V., Smith, W. and Sawistowski, H. in Rottenburg, P.A. (Ed.). "International Symposium on Distillation", p.7. (London: The Institution of Chemical Engineers).

85. Ellis, S.R.M. and Biddulph, M.W., Trans. Instn chem. Engrs, 1967, 45, p.T223.

86. Moens, F.P., Chem. Engng Sci., 1972, 27, p.275.

87. Moens, F.P., Chem. Engng Sci., 1972, 27, p.285.

88. Moens, F.P. and Bos, R.G., Chem. Engng Sci., 1972, 27, p.403.

89. Block, M.J., Nature, 1958, 178, p.650.

90. Pearson, J.R.A., J. Fluid Mech., 1958, 4, p.489.

91. Sternling, C.V. and Scriven, L.E., AIChE Journal, 1959, 5, p.514.

92. Nield, D.A., J. Fluid Mech., 1964, 19, p.341.

93. Scriven, L.E. and Sternling, C.V., J. Fluid Mech., 1964, 19, p.321.

94. Ruckeinstein, E. and Berbente, C., Chem. Engng Sci., 1964, 19, p.329.

95. Berg, J.C. and Acrivos, A., Chem. Engng Sci., 1965, 20, p.737.

96. Smith, K.A., J. Fluid Mech., 1966, 24, p.401.

97. Brian, P.L.T., Vivian, J.E. and Mayr, S.T., Ind. Eng. Chem. Fundam., 1971, 10, p.75.

98. Brian, P.L.T., AiChE Journal, 1971, 17, p.765.

99. Brian, P.L.T. and Smith, K.A., AIChE Journal, 1972, 18, p.231.

100. Brian, P.L.T. and Ross, J.R., AIChE Journal, 1972, 18, p.582.

101. Shah, Y.T. and Szeri, A., Int. J. Heat Mass Transfer, 1974, 17, p.1419.

102. Berg, J.C., Acrivos, A. and Bourdart, M., Adv. Chem. Eng., 1966, 6, p.61.

103. Heines, H. and Westwater, J.W., Intern. J. Heat Mass Transfer, 1972, 15, p.2109.

104. Zeren, R.W. and Reynolds, W.C., J. Fluid Mech., 1972, 53, p.305.

105. Sawistowski, H. and Perez de Ortiz, E.S., Chem. Engng Sci., 1973, 28, p.2051.

106. Davidson, C.M. and Evans, R.D., Review of Modern Physics, 1952, 24, p.79.

107. Fane, A.G., Ph.D. Thesis, University of London, 1968.

108. McLaughlin, C.M. and Rushton, J.H., AIChE Journal, 1973, 19, p.817.

109. Nielsen, R.D., Tek, M.R. and York, J.L., in "Proceedings of Symposium on Two-Phase Flow", 1965 (Exeter: University of Exeter), p. F.2 (1st vol.).

110. Aiba, S. and Yamada, T., AIChE Journal, 1959, 5, p.506.

111. Cheng, S.I. and Teller, A.J., AIChE Journal, 1961, 7, p.282.

112. Akselrod, L.S. and Yusova, G.M., Zh. Prikl. Khimy, Leningr., 1957, 30, p.697.

113. Pinczewski, W.V., Ph.D. Thesis, 1973. University of New South Wales.

114. Dix, M.J., Sawistowski, H. and Tyley, L.R.T., in "High Speed Photography", 1974, p.404, (London: Chapman and Hall).

115. Powell, M.J.D., The Computer Journal, 1964, 7, p.155.

116. Pinczewski, W.V. and Fell, C.J.D., Trans. Instn chem. Engrs, 1974, 52, p.294.

117. Hart, D.J. and Haselden, G.G., in "Distillation-1969", I. Chem. E. Symp. Ser. No.32, Session 1, p.8. (London: The Institution of Chemical Engineers).

118. Sawistowski, H., in "Distillation-1969", I. Chem. E. Symp. Ser. No.32, Session 1, p.64. (London: The Institution of Chemical Engineers).

119. Rouse, H., in "Advanced Mechanics of Fluids", 1959, p.382. (New York: John Wiley & Sons Inc.).

120. Chawla, T.C., Argonne National Laboratory, Rept. ANL-8094, 1974.

121. Chawla, T.C., Nuclear Science and Engineering, 1975, 56, p.1.

122. Levich, V.G., in "Physicochemical Hydrodynamics", 1962, p.465. (New Jersey: Prentice Hall).

123. Mugele, R.A., AIChE Journal, 1960, 6, p.3.

124. Nukiyama, S. and Tanasawa, Y., Trans. Soc. Mech. Engrs (Japan), 1938, 4, S13, 86: S24, 138 and 1939, 4, S14, 63: S15, 68.

125. Levich, V.G., in "Physicochemical Hydrodynamics", 1962, p.649 (New Jersey: Prentice Hall).

126. Dulitskaya, K.A., Zh. Ob. Khim., 1945, 15, p.9.

127. Butler, J.A.V., Thomson, D.W. and Maclennan, W.H., J. Chem. Soc., 1933, p.674.

128. Breatg., B. and Bayer, R., Z. phys. Chem., 1927, 130, p.1.

129. Renon, H. and Prausnitz, J.M., AIChE Journal, 1968, 14, p.135.

130. Hougen, O.A., Watson, K.M. and Ragatz, R.A., in "Chemical Process Principles", Part I, 1966, p.92 (New York: John Wiley & Sons, Inc.).

131. "Handbook of Chemistry and Physics", 1972, p.F-29 (Cleveland: CRC Publ. Co.).

132. Bowden, S.T. and Butler, E.T., J. Chem. Soc., 1939, p.79.

133. Carr, J.G. and Riddick, J.A., IEC, 1951, 43, p.692.

134. Lemonde, H., Ann. Phys., 1938, 9, p.539.

135. Welty, J.R., Wilson, R.E. and Wicks, C.E., in "Fundamentals of Momentum, Heat and Mass Transfer", 1969, p.458 (New York: John Wiley & Sons, Inc.).

136. Marangoni, C., Ann. Phys. (Leipzig), 1871, 143, p.337.

137. Whitman, W.G., Chem. Met., 1923, 29, p.147.

APPENDICES

APPENDIX I

CALIBRATIONS

Nomenclature

ρ - liquid density (g/cm^3)

μ - liquid viscosity (cpoise)

TABLE I.1

LIQUID ROTAMETER - 2 PLATE COLUMN ($m^3 s^{-1} x 10^6$)

	.0	.1	.2	.3	.4	.5	.6	.7	.8	.9
0	1.859	1.899	1.938	1.978	2.018	2.058	2.098	2.138	2.178	2.218
1	2.259	2.299	2.340	2.381	2.422	2.463	2.504	2.545	2.586	2.628
2	2.669	2.711	2.753	2.795	2.837	2.879	2.921	2.963	3.006	3.048
3	3.091	3.134	3.177	3.220	3.263	3.306	3.349	3.393	3.436	3.480
4	3.524	3.568	3.612	3.656	3.700	3.744	3.789	3.833	3.878	3.923
5	3.967	4.012	4.058	4.103	4.148	4.194	4.239	4.285	4.330	4.376
6	4.422	4.468	4.515	4.561	4.607	4.654	4.701	4.747	4.794	4.841
7	4.888	4.935	4.983	5.030	5.079	5.125	5.173	5.221	5.269	5.317
8	5.365	5.414	5.462	5.511	5.559	5.608	5.657	5.706	5.755	5.804
9	5.853	5.903	5.952	6.002	6.052	6.102	6.152	6.202	6.252	6.302
10	6.353	6.403	6.454	6.504	6.555	6.606	6.657	6.709	6.760	6.811
11	6.863	6.914	6.966	7.018	7.070	7.122	7.174	7.227	7.279	7.331
12	7.384	7.437	7.490	7.543	7.596	7.649	7.702	7.756	7.809	7.863
13	7.917	7.970	8.024	8.078	8.133	8.187	8.241	8.296	8.350	8.405
14	8.460	8.515	8.570	8.625	8.680	8.736	8.791	8.847	8.903	8.959
15	9.015	9.071	9.127	9.183	9.239	9.296	9.353	9.409	9.466	9.523
16	9.580	9.637	9.695	9.752	9.810	9.867	9.925	9.983	10.041	10.099
17	10.157	10.215	10.274	10.332	10.391	10.449	10.508	10.567	10.626	10.685
18	10.745	10.804	10.864	10.923	10.983	11.043	11.103	11.163	11.223	11.283
19	11.343	11.404	11.465	11.525	11.586	11.647	11.708	11.769	11.831	11.892
20	11.953	12.015	12.077	12.139	12.201	12.263	12.325	12.387	12.449	12.512
21	12.574	12.637	12.700	12.763	12.826	12.889	12.952	13.016	13.079	13.143
22	13.206	13.270	13.334	13.398	13.462	13.527	13.591	13.656	13.720	13.785
23	13.850	13.915	13.980	14.045	14.110	14.175	14.241	14.306	14.372	14.438
24	14.504	14.570	14.636	14.702	14.769	14.835	14.902	14.968	15.035	15.102
25	15.169	15.236	15.304	15.371	15.438	15.506	15.574	15.641	15.709	15.777
26	15.846	15.914	15.982	16.051	16.119	16.188	16.257	16.326	16.395	16.464
27	16.533	16.602	16.672	16.741	16.811	16.881	16.951	17.021	17.091	17.161
28	17.232	17.302	17.373	17.443	17.514	17.585	17.656	17.727	17.798	17.870
29	17.941	18.013	18.084	18.156	18.228	18.300	18.372	18.444	18.517	18.589

Example:

Reading: 12.4

Liquid flow rate:

$7.596\ 10^{-6} m^3\ s^{-1}$

TABLE I.2

AIR ROTAMETER - 2 PLATE COLUMN ($ft^3\ min^{-1}$)

	.0	.1	.2	.3	.4	.5	.6	.7	.8	.9
0	5.842	6.033	6.224	6.414	6.604	6.794	6.983	7.172	7.361	7.550
1	7.738	7.926	8.114	8.302	8.489	8.676	8.862	9.049	9.235	9.421
2	9.606	9.791	9.976	10.161	10.345	10.529	10.713	10.897	11.080	11.263
3	11.446	11.628	11.810	11.992	12.174	12.355	12.536	12.717	12.897	13.077
4	13.257	13.437	13.616	13.795	13.974	14.152	14.331	14.508	14.686	14.863
5	15.040	15.217	15.394	15.570	15.746	15.922	16.097	16.272	16.447	16.621
6	16.796	16.970	17.143	17.317	17.490	17.663	17.835	18.007	18.179	18.351
7	18.523	18.694	18.865	19.035	19.206	19.376	19.545	19.715	19.884	20.053
8	20.221	20.390	20.558	20.726	20.893	21.060	21.227	21.394	21.560	21.726
9	21.892	22.058	22.223	22.388	22.553	22.717	22.881	23.045	23.208	23.372
10	23.535	23.697	23.860	24.022	24.184	24.345	24.507	24.668	24.829	24.989
11	25.149	25.309	25.469	25.628	25.787	25.946	26.104	26.262	26.420	26.578
12	26.735	26.892	27.049	27.205	27.362	27.518	27.673	27.829	27.984	28.139
13	28.293	28.448	28.602	28.755	28.909	29.062	29.215	29.367	29.519	29.671
14	29.823	29.975	30.126	30.277	30.427	30.578	30.728	30.877	31.027	31.176
15	31.325	31.474	31.622	31.770	31.919	32.065	32.212	32.359	32.506	32.652
16	32.799	32.944	33.090	33.235	33.380	33.525	33.669	33.813	33.957	34.101
17	34.244	34.387	34.530	34.672	34.814	34.956	35.098	35.239	35.380	35.521
18	35.661	35.801	35.941	36.081	36.220	36.359	36.498	36.637	36.775	36.913
19	37.050	37.188	37.325	37.462	37.599	37.734	37.870	38.006	38.141	38.276
20	38.411	38.546	38.680	38.814	38.948	39.081	39.214	39.347	39.480	39.612
21	39.744	39.876	40.007	40.138	40.269	40.400	40.530	40.660	40.790	40.920
22	41.049	41.178	41.306	41.435	41.563	41.690	41.818	41.945	42.072	42.199
23	42.325	42.451	42.577	42.703	42.828	42.953	43.078	43.202	43.326	43.450
24	43.574	43.697	43.820	43.943	44.065	44.187	44.309	44.431	44.552	44.673
25	44.794	44.914	45.034	45.154	45.274	45.393	45.512	45.631	45.750	45.868
26	45.986	46.103	46.221	46.338	46.455	46.571	46.687	46.803	46.919	47.034
27	47.150	47.264	47.379	47.493	47.607	47.721	47.834	47.947	48.060	48.173
28	48.285	48.397	48.509	48.620	48.732	48.843	48.953	49.063	49.174	49.283
29	49.393	49.502	49.611	49.720	49.828	49.936	50.044	50.151	50.259	50.366

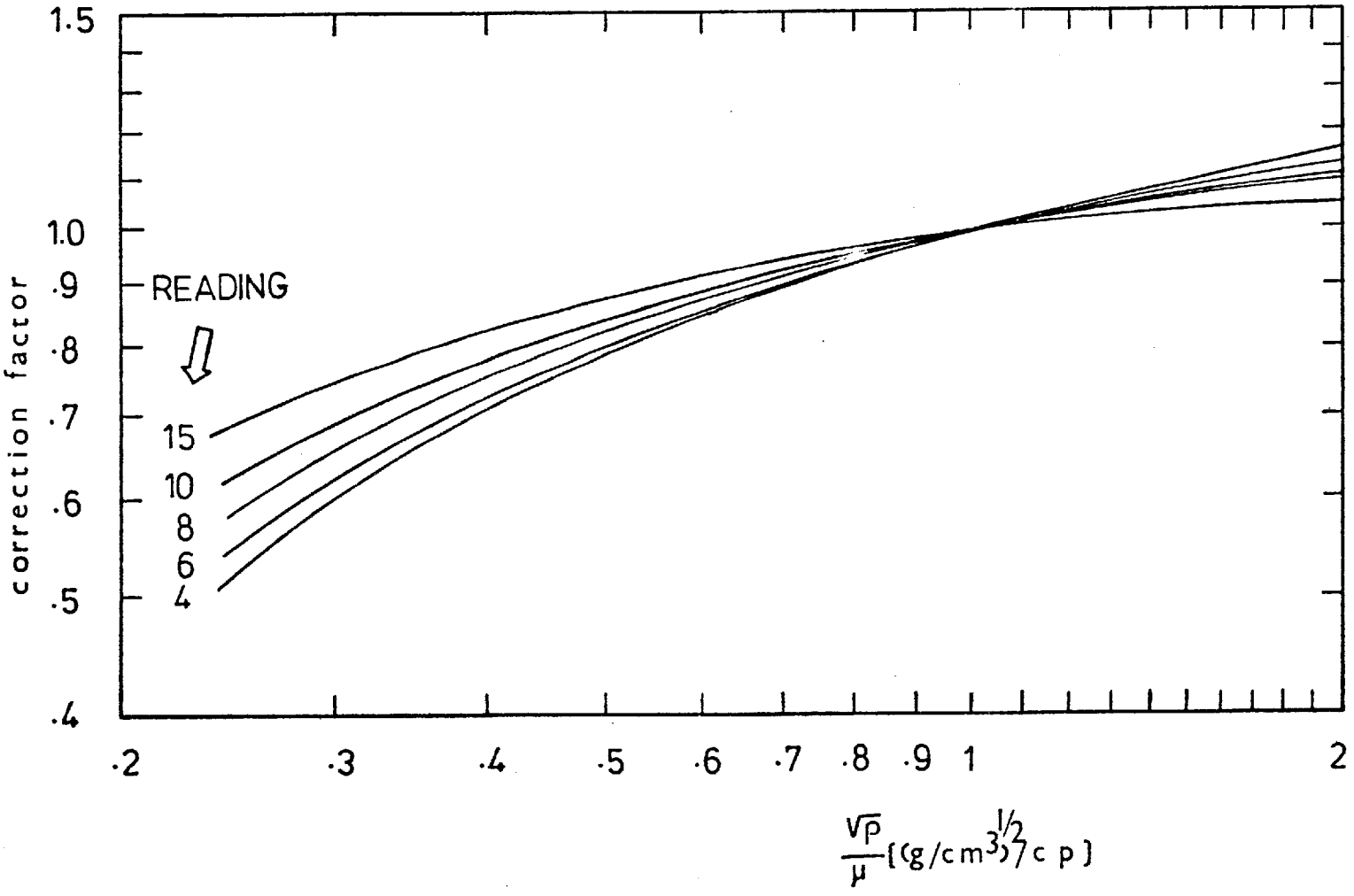

Fig. I.1.- Liquid rotameter - 2 plate column. Correction for physical properties.

APPENDIX II

PHYSICAL PROPERTIES

SYSTEM AQUEOUS METHANOL / AIR

CONTENTS

APPENDIX II

PHYSICAL PROPERTIES

SYSTEM AQUEOUS METHANOL/AIR

1. Equilibrium and vapour pressure data

Available data for partial pressures of water and methanol over aqueous solutions of methanol between the temperatures 25 and 62.5 ^{o}C were used[126-128] and correlated by the NRTL equation.[129]

The summation of standard deviations of vapour molar fractions together with the standard relative deviations of vapour pressures was minimized, as suggested by Renon and Prausnitz.[129] The minimization routine due to Powell[115] was employed.

The NRTL equation is an equation for the molar excess of Gibbs energy, G^E, of a binary mixture as a function of the mole fractions x_1 and x_2 and the absolute temperature T:

$$\frac{G^E}{RT} = x_1 x_2 \frac{\tau_{21} G_{21}}{x_1 + x_2 G_{21}} + \frac{\tau_{12} G_{12}}{x_2 + x_1 G_{12}} \qquad (1)$$

where: $G_{12} = \exp(-\alpha_{12}\,\tau_{12})$

$G_{21} = \exp(-\alpha_{12}\,\tau_{21})$

$\tau_{12} = (g_{12} - g_{21})/RT$

$\tau_{21} = (g_{21} - g_{12})/RT$

with $g_{12} = g_{21}$ and, when

$$\left| \frac{G^E}{RT} \right| < 0.35,$$

it can be assumed that $\alpha_{12} = 0.30$.

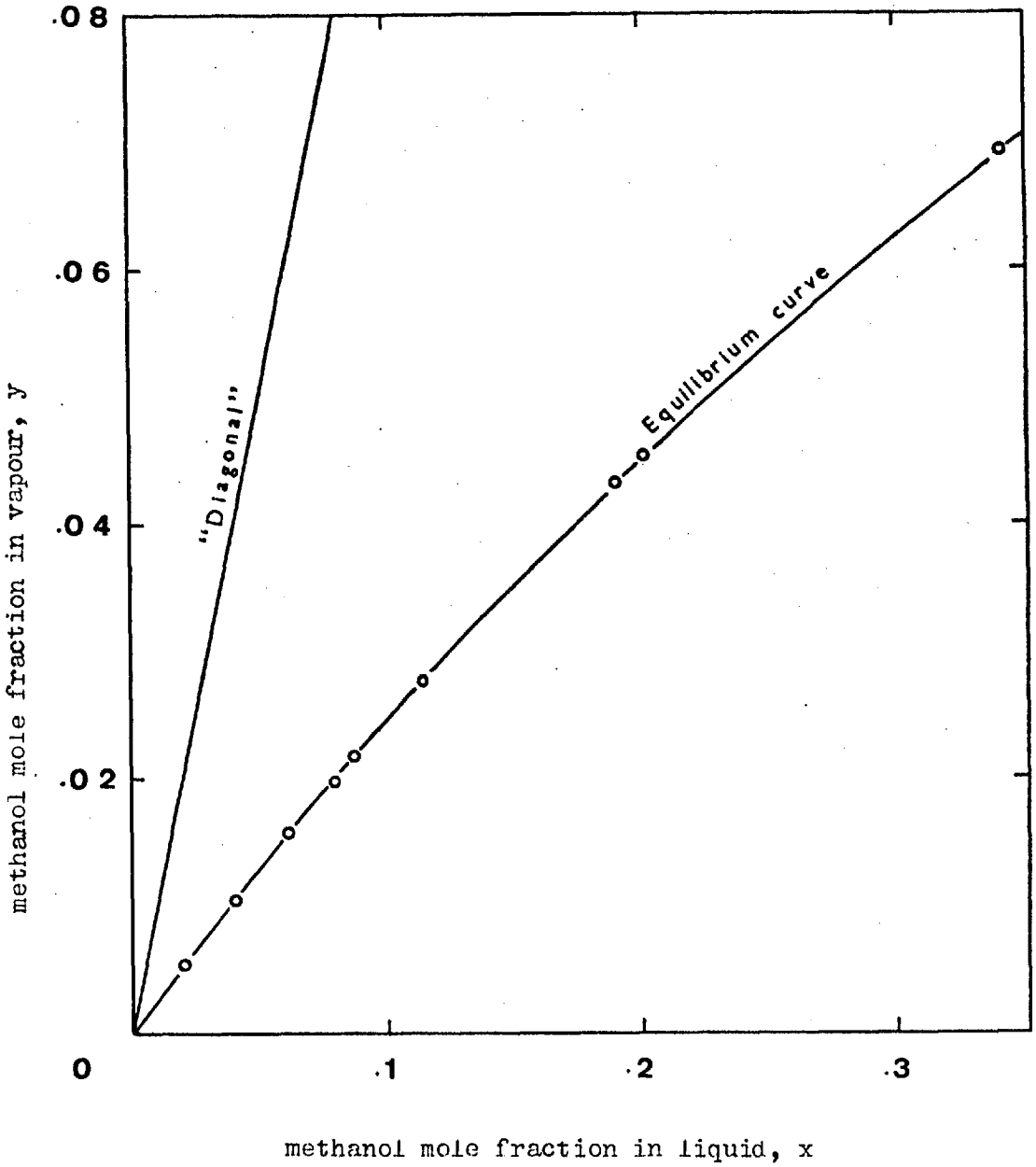

Fig.II.1.- Equilibrium curve for system aqueous methanol / air at 298 K and normal atmospheric pressure.

Equation (1) contains two temperature-dependent parameters, $(g_{12} - g_{22})$ and $(g_{21} - g_{11})$, in addition to a nonrandomness parameter, α_{12}, which is supposed to be independent of temperature. As suggested by Renon and Prausnitz, $(g_{21} - g_{11})$ and $(g_{12} - g_{22})$ were supposed to be linear functions of temperature. By differentiation of equation (1), the activity coefficients γ_1 and γ_2 can be obtained:

$$\ln \gamma_1 = x_2^2 \left\{ \frac{\tau_{12} \exp(-\alpha_{12} \tau_{12})}{[x_1 \exp(-\alpha_{12} \tau_{12}) + x_2]^2} + \frac{\tau_{21} \exp(-2\alpha_{12} \tau_{21})}{[x_1 + x_2 \exp(-\alpha_{12} \tau_{21})]^2} \right\} \tag{2}$$

$$\ln \gamma_2 = x_1^2 \left\{ \frac{\tau_{12} \exp(-2\alpha_{12} \tau_{12})}{[x_1 \exp(-\alpha_{12} \tau_{12}) + x_2]^2} + \frac{\tau_{21} \exp(-\alpha_{12} \tau_{21})}{[x_1 + x_2 \exp(-\alpha_{12} \tau_{21})]^2} \right\} \tag{3}$$

The data correlated by the NRTL equation need not be tested for consistency, since that equation is a solution of the Gibbs-Duhem equation.

The vapour pressures of the pure components, water and methanol, were estimated by the empirical expression[130]

$$\log p = -A/T_r + B - \exp[-20(T_r - b)^2] \tag{4}$$

where:

p is the vapour pressure, in mm Hg,

T_r is the reduced temperature, T/T_c,

T is the actual temperature, and

T_c is the critical temperature.

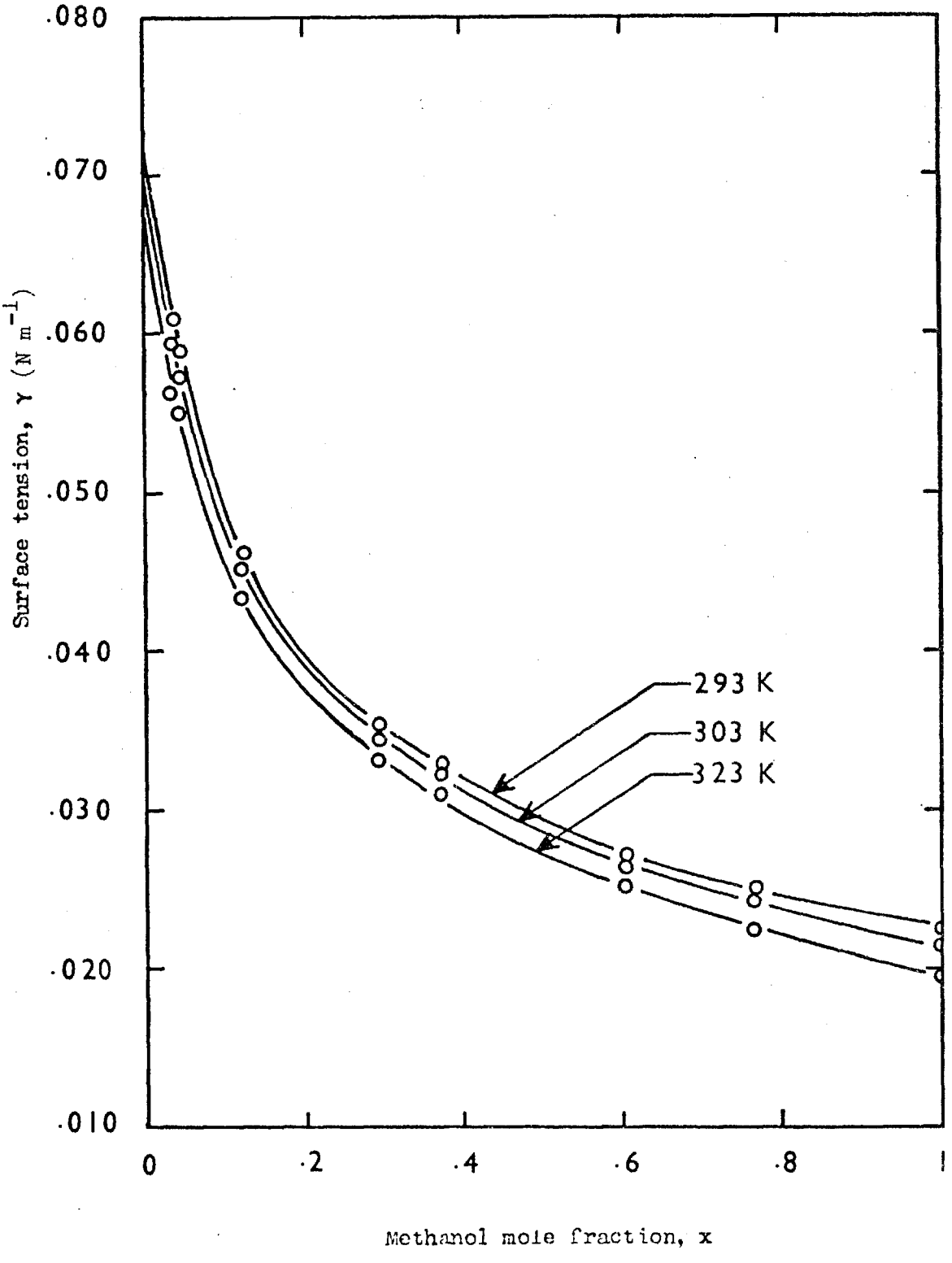

Fig.II.2.- Surface tension of aqueous methanol solutions at 293, 303 and 323 K.

For water:

A = 3.1423

B = 8.3610 T_c = 647.3 K

b = 0.163

For methanol:

A = 3.5876

B = 8.3642 T_c = 513.2 K

b = 0.243

2. Liquid properties

2.1 Surface tension

Surface tension for the system methanol/water at 293, 303 and 323 K is plotted in Figure II.2.

When only the surface tensions of the pure components are known, the following interpolation expression[132] was suggested for low pressures and quick evaluation

$$\frac{1}{\gamma} = \frac{x_1}{\gamma_1} + \frac{x_2}{\gamma_2} \qquad (5)$$

where γ is the surface tension of the solution, and x_1, x_2 are the molar fractions of components 1 and 2, respectively.

Hence, the inverse of the surface tension would be a linear function of composition. This is not exactly true for the present system but can be useful for purposes of temperature interpolation.

The effect of temperature on surface tension of pure component, i, can be expressed by:

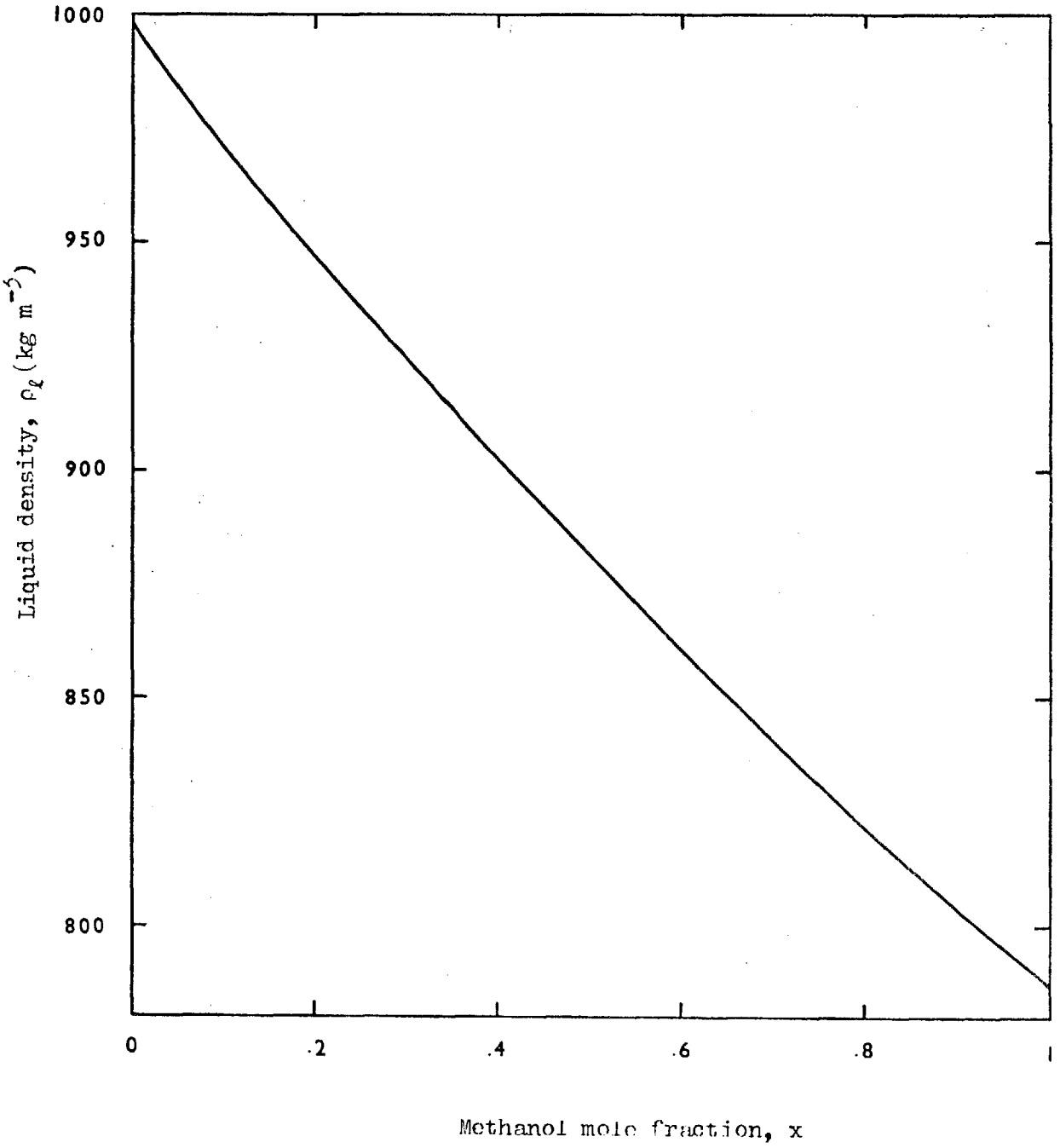

Fig. II.3.- Density of aqueous methanol solutions at 298 K

$$\frac{\gamma_{i\ ref}}{\gamma_i} = \exp[B_i(\frac{1}{T} - \frac{1}{T_{ref}})] \tag{6}$$

where the subscript i refers to the pure component i and B_i is constant over a limited range of temperatures. The subscript ref refers to the reference temperature. Usually the temperature effect is not large. Thus, equation (5) and (6) can be assumed to apply for temperature correction at any composition. Thus:

$$\frac{\gamma_{ref}}{\gamma} = \frac{\frac{x_1}{\gamma_{1ref}}}{\frac{x_1}{\gamma_{1ref}} + \frac{x_2}{\gamma_{2ref}}} \exp[B_1(\frac{1}{T} - \frac{1}{T_{ref}})] +$$

$$\frac{\frac{x_2}{\gamma_{2ref}}}{\frac{x_1}{\gamma_{1ref}} + \frac{x_2}{\gamma_{2ref}}} \exp[B_2(\frac{1}{T} - \frac{1}{T_{ref}})] \tag{7}$$

2.2 Liquid density

Density of methanol-water solutions at 298 K[133] is plotted in Figure II.3.

2.3 Liquid viscosity

Viscosity of methanol-water solutions at 288 K[134] is shown in Figure II.4.

2.4 Diffusivity in liquid phase

Diffusivity of methanol-water solutions at 288 K[134] is plotted in Figure II.5.

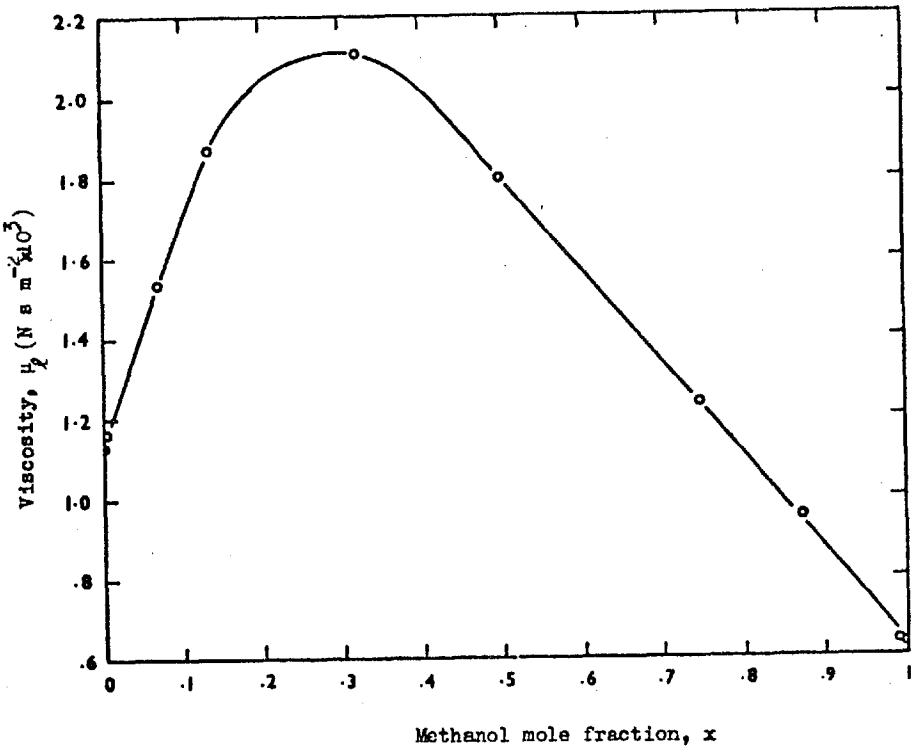

Fig.II.4.- Viscosity of aqueous methanol solutions at 288 K.

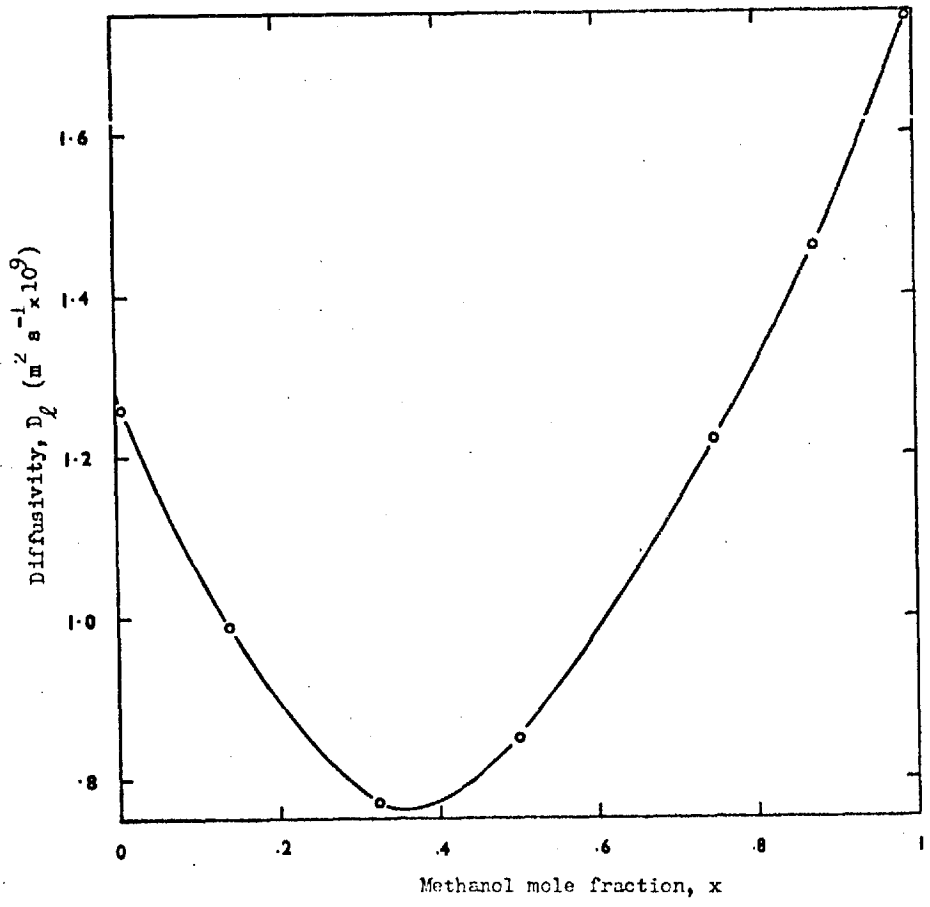

Fig.II.5.- Diffusivity of aqueous methanol solutions at 288 K.

3. Gas properties

3.1 Gas density

Gas density can be calculated from the ideal gas law.

3.2 Kinematic viscosity of air

Kinematic viscosity of air for the temperature range of 273 to 373 K is given approximately by

$$\nu_{air} = 0.15 \left(\frac{T}{293}\right)^{1.7} \ (cm^2\ s^{-1})$$

3.3 Gas diffusivity

Diffusivity of methanol in air at 298 K is given by:[135]

$$D_G P = 0.162\ cm^2\ atm\ s^{-1},$$

where P is the atmospheric pressure (in atm.).

APPENDIX III

DISPERSION DENSITY DATA AND DERIVED RESULTS

Table III.1.- Dispersion density data for system aqueous methanol / air (experimental conditions in Table III.2).

Table III.2.- Dispersion density parameters and calculated values of drops hold-up and size for system aqueous methanol / air.

Table III.3.- Dispersion density parameters and calculated values of drops hold-up and size for Fane's data with the system A (benzene / cyclohexane) at total reflux.

Table III.4.- Idem for system B (benzene / n-heptane).

Table III.5.- Idem for system C (n-heptane / toluene).

Table III.6.- Dispersion density parameters and calculated values of drops hold-up and size for Pinczewski's data with system air / water.

Figs III.1 to III.58 - Dispersion density profiles and the fitting curves.

Nomenclature

Af	fractional free area of plate
CR	counting rate
d_{gm}	geometric mean diameter of population of projected drops (mm)
d_h	hole diameter (inch)
F	summation of squares of deviations between experimental and calculated dispersion densities

F_s F_s- factor

H_D drops hold-up (cm)

INIT. COUNTING - counting rate in absence of liquid

LEVEL Level reading (cm).Plate floor at reading of 60.69

L_v liquid cross flow rate per weir length.

Tf Thin-film stabilising number

x_1 maximum value of dispersion density

x_2 height above plate floor of point of maximum dispersion density

x_3 standard deviation of dispersion density profile

γ surface tension (Nm^{-1})

TABLE III.1

DISPERSION DENSITY DATA

SYSTEM AQUEOUS METHANOL / AIR

EXP. 1 DATA POINTS (LEVEL,CR) INIT. COUNTING= 238 00

60.60 12.04 60.71 86.29 60.81 89.77 60.90 122.44 61.00 141.29 61.10 159.78
61.20 172.00 61.30 179.03 61.40 182.35 61.50 185.57 61.60 191.10 61.70 188.89
61.81 192.71 61.91 193.39 62.00 192.29 62.11 194.47 62.20 198.11 62.30 199.77
62.40 200.21 62.50 200.29 62.61 202.49 62.70 201.48 62.80 207.25 62.90 211.30
63.00 211.46 63.10 216.54 63.21 214.38 63.30 218.33 63.42 220.54 63.50 222.17
63.60 224.86 63.71 225.22 63.80 226.16 63.90 229.59 64.01 229.30 64.20 230.80
64.40 232.91

EXP. 2 DATA POINTS (LEVEL,CR) INIT. COUNTING= 235 00

60.61 14.48 60.70 82.95 60.80 82.33 60.90 121.93 61.00 139.93 61.10 156.97
61.20 174.16 61.30 179.72 61.40 183.30 61.51 185.84 61.61 190.12 61.71 192.17
61.81 193.48 61.91 193.58 62.00 190.32 62.11 194.17 62.20 194.73 62.40 196.23
62.50 199.92 62.60 202.01 62.81 206.14 63.00 214.40 63.20 215.60 63.40 222.63
63.60 224.95 63.80 222.92 64.00 230.40 64.10 232.56 64.20 229.74 64.30 230.12
64.40 230.33

EXP. 3 DATA POINTS (LEVEL,CR) INIT. COUNTING= 234 30

60.60 12.29 60.68 86.55 60.82 83.28 60.90 115.72 61.00 134.61 61.10 160.42
61.20 172.23 61.30 182.87 61.40 186.41 61.50 188.22 61.62 188.69 61.72 191.82
61.80 192.91 61.90 192.08 62.00 192.89 62.10 192.28 62.20 190.74 62.40 198.51
62.62 205.30 62.80 207.49 62.90 209.87 63.10 214.47 63.30 219.51 63.51 222.62
63.70 223.69 63.90 226.58 64.12 228.32 64.30 232.36 64.50 232.06

EXP. 4 DATA POINTS (LEVEL,CR) INIT. COUNTING= 235.20

60.60 11.28 60.72 53.71 60.80 79.48 60.91 122.50 61.00 147.99 61.10 164.11
61.20 176.58 61.30 180.00 61.40 192.15 61.50 196.92 61.60 197.81 61.70 197.98
61.80 200.00 61.92 202.45 62.01 204.02 62.10 207.12 62.22 206.90 62.35 213.80
62.51 215.25 62.72 218.16 62.91 220.19 63.10 223.71 63.32 223.31 63.50 223.04
63.70 226.93 63.90 226.59 64.10 226.00 64.30 225.94 64.50 227.80 64.80 228.09
65.10 229.00 65.60 229.57 66.00 229.98 67.00 231.53

EXP. 5 DATA POINTS (LEVEL,CR) INIT. COUNTING= 234.50

60.59 10.80 60.70 43.88 60.80 77.93 60.90 114.17 61.00 137.68 61.10 158.37
61.20 174.85 61.30 184.48 61.40 187.15 61.52 194.04 61.71 189.13 61.90 195.63
62.10 193.75 62.30 192.80 62.50 193.40 62.70 194.92 62.90 200.76 63.10 201.97
63.40 207.56 63.60 212.71 63.80 218.13 64.00 221.93 64.20 224.57 64.70 226.75
65.00 229.71 65.50 227.72 66.02 232.80 66.50 231.63

EXP. 6 DATA POINTS (LEVEL,CR) INIT. COUNTING= 234.90

60.60 10.50 60.69 39.43 60.81 84.78 60.90 112.68 61.04 150.49 61.10 159.96
61.21 173.47 61.35 184.80 61.50 187.86 61.70 192.34 61.90 191.90 62.00 192.70
62.15 192.50 62.20 189.55 62.30 193.73 62.50 191.81 62.70 191.89 62.75 192.15
62.90 197.11 62.91 194.41 63.20 199.91 63.52 206.51 64.00 216.32 64.50 224.71
65.00 229.54 65.50 228.50

EXP. 11 DATA POINTS (LEVEL,CR) INIT. COUNTING= 230.00

60.60 6.60 60.73 42.80 60.91 110.25 61.00 132.79 61.20 168.96 61.45 184.67
61.59 184.91 61.73 192.24 61.80 189.89 61.93 190.57 62.02 191.90 62.17 190.73
62.28 190.71 62.40 190.83 62.50 189.58 62.60 188.68 62.70 190.39 62.80 192.09
62.92 192.39 63.03 195.82 63.20 196.82 63.45 202.13 63.70 207.76 63.93 210.43
64.20 213.37 64.50 216.75 64.80 222.00 65.07 224.82 65.50 225.91 66.00 226.60
67.08 226.22 67.50 227.60

EXP. 12 DATA POINTS (LEVEL,CR) INIT. COUNTING= 221.87

60.60 7.42 60.71 32.38 60.82 79.25 60.91 119.35 61.02 146.44 61.15 168.61
61.27 176.26 61.37 187.13 61.50 194.36 61.62 193.51 61.71 199.74 61.82 197.74
61.99 200.08 62.11 196.43 62.24 198.11 62.37 195.66 62.50 196.67 62.61 195.50
62.73 199.29 62.90 199.38 63.05 198.36 63.23 201.81 63.40 202.87 63.60 204.30
63.71 202.52 63.90 205.34 64.10 205.57 64.14 209.94 64.28 211.30 64.30 211.09
64.70 212.92 65.05 216.49 65.55 217.94 65.80 217.44 66.10 217.52 66.40 217.44
66.80 218.64 67.10 218.62 67.40 218.74 67.70 217.49 68.00 219.81 68.38 216.55
68.80 220.14 69.10 215.67 69.60 219.86 70.00 217.83 70.40 218.78 71.10 218.64
72.11 220.02

EXP. 13 DATA POINTS (LEVEL,CR) INIT. COUNTING= 228.40

60.60 6.44 60.71 34.53 60.82 107.02 61.00 198.35 61.18 215.77 61.40 219.24
61.60 221.92 61.80 222.28 62.00 221.53 62.20 222.71 62.50 222.20 62.80 224.94
63.10 223.09 63.50 221.97 64.00 222.79 64.50 223.06 65.00 225.53 65.50 224.43
66.00 220.94 66.50 226.39 67.00 223.24 67.50 224.00 68.00 222.77 68.50 222.36
69.00 223.26 69.50 225.33 70.00 224.67 71.00 222.71 72.00 224.22 73.00 224.37
74.00 224.84 75.00 225.53 76.00 225.32 77.00 227.01

EXP. 14 DATA POINTS (LEVEL,CR) INIT. COUNTING= 228.00

60.60 7.54 60.70 20.05 60.80 59.37 60.90 96.57 61.00 133.78 61.19 165.45
61.30 176.16 61.40 182.52 61.60 189.17 61.70 187.12 61.90 189.99 62.10 189.04
62.30 190.26 62.50 188.66 62.70 191.23 63.00 195.46 63.20 196.43 63.40 199.07
63.60 205.64 63.80 206.91 64.00 212.97 64.50 221.59 65.00 220.60 65.50 220.33
66.00 223.42 66.50 225.98 67.10 225.93 67.50 226.34 68.00 225.82 68.50 226.01
69.00 226.01 69.50 226.10 70.00 225.13 70.50 227.09 71.00 225.38 71.50 225.32
72.00 225.95 72.50 227.01

EXP. 15 DATA POINTS (LEVEL,CR) INIT. COUNTING= 228.04

60.60 7.14 60.70 18.35 60.80 63.01 60.90 109.53 61.00 135.79 61.20 173.79
61.30 183.09 61.50 190.00 61.70 194.18 61.90 200.77 62.00 196.84 62.10 199.30
62.20 198.97 62.30 202.95 62.40 200.56 62.50 201.73 62.60 203.13 62.70 204.11
62.80 203.07 62.90 203.56 63.00 204.65 63.10 205.88 63.30 205.52 63.50 205.15
63.70 209.28 63.90 213.19 64.10 215.08 64.30 217.46 64.50 213.42 65.00 221.98
65.50 218.47 66.00 221.83 66.50 223.20 67.00 221.72 67.50 225.47 68.00 223.09
69.00 223.22 70.00 227.94 71.00 224.60 73.00 227.28

EXP. 16 DATA POINTS (LEVEL,CR) INIT. COUNTING= 224.45

60.70 23.14 60.80 57.95 60.90 93.17 61.00 119.29 61.10 136.34 61.20 155.09
61.30 165.12 61.45 175.60 61.60 181.52 61.70 182.21 61.85 184.62 62.00 184.18
62.15 182.10 62.30 182.51 62.50 182.29 62.51 183.94 62.65 184.69 62.80 181.98
62.90 186.17 63.00 188.38 63.10 188.53 63.20 191.53 63.30 197.21 63.40 196.67
63.50 195.10 63.60 199.29 63.70 207.24 63.90 205.73 64.10 210.58 64.30 213.64
64.50 213.19 64.80 220.98 65.10 217.72 65.50 220.59 66.00 220.85 67.00 223.05

EXP. 17 DATA POINTS (LEVEL,CR) INIT. COUNTING= 221.50

60.70 29.14 60.80 60.32 60.90 94.54 61.00 119.34 61.10 132.42 61.20 151.52
61.30 158.00 61.40 167.01 61.50 177.10 61.60 178.64 61.70 177.80 61.80 179.00
61.90 179.32 62.00 179.31 62.10 179.72 62.20 181.15 62.30 178.84 62.40 182.81
62.50 181.58 62.60 182.61 62.70 183.95 62.80 185.17 62.90 186.80 63.00 189.37
63.10 190.21 63.20 190.28 63.30 194.13 63.40 193.71 63.50 198.40 63.60 199.10
63.70 203.07 63.80 205.07 63.90 205.38 64.00 206.75 64.10 208.60 64.20 212.38
64.40 211.28 64.60 215.22

EXP. 18 DATA POINTS (LEVEL,CR) INIT. COUNTING= 221.43

60.70 38.34 60.80 65.35 60.90 105.34 61.02 129.50 61.11 141.07 61.20 153.69
61.30 163.52 61.40 167.10 61.50 171.70 61.60 174.62 61.70 175.74 61.80 177.11
61.90 177.08 62.01 177.31 62.20 177.05 62.40 180.19 62.50 180.92 62.60 181.09
62.70 181.24 62.80 185.12 62.90 185.12 63.00 186.86 63.20 188.61 63.40 192.24
63.60 197.08 63.80 200.70 64.00 204.70 64.20 208.27 64.40 210.05 64.60 209.98
64.80 212.47 65.00 217.41

EXP. 19 DATA POINTS (LEVEL,CR) INIT. COUNTING= 222.80

60.70 27.63 60.81 71.66 60.90 110.10 61.02 140.71 61.11 159.06 61.21 171.37
61.30 175.12 61.41 185.55 61.50 184.27 61.60 185.25 61.70 186.30 61.80 185.49
61.90 182.93 62.01 182.64 62.11 184.91 62.20 186.65 62.35 187.58 62.50 182.32
62.65 189.46 62.80 190.55 62.95 192.23 63.11 195.11 63.26 196.14 63.40 195.91
63.55 200.95 63.70 204.48 63.85 203.52 64.00 207.28 64.15 207.89 64.30 210.05
64.45 212.81 64.60 212.26 64.75 213.88 64.90 212.75 65.05 214.93 65.20 218.27

EXP. 20 DATA POINTS (LEVEL,CR) INIT. COUNTING= 220 42

60.60 8.40 60.70 20.42 60.80 63.05 60.90 101.05 61.00 122.01 61.10 137.70
61.20 149.18 61.30 161.03 61.40 163.59 61.55 173.78 61.70 168.09 61.85 170.06
62.00 172.53 62.17 171.37 62.40 170.87 62.60 178.77 62.76 170.89 62.90 171.06
63.05 176.66 63.20 181.75 63.40 194.19 63.60 196.85 63.80 201.45 64.00 201.19
64.20 198.98 64.40 210.04 64.60 215.94 64.80 215.10 65.00 217.25

EXP. 21 DATA POINTS (LEVEL,CR) INIT. COUNTING= 223 65

60.71 34.47 60.80 65.03 60.90 102.88 61.00 125.92 61.10 140.03 61.20 153.45
61.30 159.61 61.40 166.11 61.50 170.83 61.60 172.78 61.70 173.98 61.85 175.73
62.00 177.32 62.15 177.49 62.30 178.42 62.45 181.37 62.60 180.97 62.75 183.68
62.90 185.62 63.10 188.69 63.30 194.22 63.50 197.87 63.70 202.48 63.90 208.51
64.10 212.80 64.30 216.03 64.50 220.06 64.70 218.49 64.90 220.41 65.10 218.81
65.30 220.04 66.00 221.73

EXP. 22 DATA POINTS (LEVEL,CR) INIT. COUNTING= 223 14

60.69 26.99 60.80 72.51 60.90 102.32 61.00 131.17 61.10 145.28 61.20 150.83
61.30 158.18 61.40 163.63 61.50 170.86 61.60 171.32 61.70 173.19 61.80 172.87
61.90 174.58 62.10 174.44 62.30 179.72 62.45 179.74 62.60 183.12 62.75 182.85
62.90 184.08 63.10 190.85 63.25 194.57 63.40 196.79 63.55 199.76 63.70 203.09
63.85 207.32 64.00 208.21 64.15 209.86 64.35 213.58 64.50 217.73 64.70 219.68

EXP. 23 DATA POINTS (LEVEL,CR) INIT. COUNTING= 221.23

60.70 30.57 60.80 61.33 60.90 96.33 61.00 119.94 61.10 142.77 61.20 157.22
61.30 165.14 61.40 172.35 61.50 173.96 61.60 176.79 61.70 174.44 61.85 178.58
62.00 175.75 62.15 177.13 62.30 177.83 62.45 175.62 62.60 177.49 62.75 179.11
62.90 181.87 63.05 183.65 63.20 186.39 63.35 192.30 63.50 193.83 63.67 196.52
63.80 202.54 63.97 204.49 64.10 205.28 64.26 207.99 64.40 210.29 64.55 209.85
64.70 212.54 64.86 212.84 65.00 214.60 65.40 215.00

EXP. 24 DATA POINTS (LEVEL,CR) INIT. COUNTING= 218.71

60.70 31.33 60.80 65.52 60.90 101.40 61.00 128.93 61.10 148.27 61.20 161.72
61.30 171.33 61.40 178.18 61.50 177.96 61.60 180.67 61.70 180.39 61.85 185.24
62.00 182.00 62.15 184.46 62.30 180.63 62.47 182.78 62.60 180.31 62.75 184.28
62.90 185.52 63.05 187.21 63.20 187.94 63.35 192.55 63.50 195.60 63.65 197.87
63.80 200.01 63.95 202.75 64.10 204.68 64.25 208.48 64.40 207.10 64.55 207.74
64.70 211.02 64.85 212.16 65.00 211.92 65.20 215.55 65.40 215.98

EXP. 25 DATA POINTS (LEVEL,CR) INIT. COUNTING= 218.71

60.70 31.50 60.80 66.60 60.90 106.88 61.00 140.52 61.10 156.15 61.20 166.59
61.30 173.90 61.40 180.03 61.50 184.79 61.60 186.26 61.70 186.06 61.85 187.49
62.00 184.76 62.15 186.34 62.30 189.75 62.45 187.58 62.60 186.60 62.75 189.35
62.90 189.85 63.07 191.69 63.20 193.73 63.35 192.57 63.50 196.04 63.65 195.97
63.80 199.17 63.95 201.93 64.10 202.61 64.25 204.85 64.40 204.31 64.60 205.71
64.70 209.25 64.85 210.98 65.00 208.88 65.20 209.52 65.40 210.43

EXP. 32 DATA POINTS (LEVEL,CR) INIT. COUNTING= 220 55

60.61 8.68 60.70 27.27 60.80 64.20 60.90 101.62 61.00 131.27 61.10 154.64
61.20 162.52 61.30 176.08 61.41 169.94 61.50 172.14 61.60 171.05 61.70 175.41
61.80 176.89 61.90 178.16 62.00 189.42 62.10 187.26 62.30 189.76 62.50 188.23
62.70 188.42 62.90 189.29 63.10 189.00 63.30 191.26 63.50 195.97 63.70 197.36
63.90 200.48 64.10 191.83 64.30 193.60 64.50 194.97 64.70 197.91 64.90 197.21
65.10 201.54 65.30 206.27 65.50 198.83 65.70 200.47 65.90 215.71

EXP. 33 DATA POINTS (LEVEL,CR) INIT. COUNTING= 273.00

60.71 39.55 60.80 75.75 60.90 128.99 61.00 158.96 61.10 187.83 61.20 198.71
61.30 211.58 61.40 218.50 61.50 221.31 61.60 230.62 61.70 227.47 61.82 232.38
62.00 229.61 62.20 237.34 62.40 229.06 62.60 228.14 62 80 234.37 63.00 234.23
63.20 238.42 63.40 244.74 63.60 247.24 63.80 252.84 64.00 256.49 64.20 256.46
64.40 258.49 64.60 260.22 64.80 263.86 65.00 265.85 65.20 270.13 65.40 268.30
65.63 268.60 65.80 267.19 66.00 269.77 66.50 267.06 67.00 268.63 67.50 269.92
68.00 268.60 69.00 272.79 70.05 269.78 71.50 268.55 93.00 268.82 93.05 269.08

EXP. 34 DATA POINTS (LEVEL,CR) INIT. COUNTING= 276.70

60.70 29.05 60.80 74.28 60.91 125.05 61.00 159.09 61.10 185.10 61.20 199.97
61.30 213.33 61.40 220.97 61.50 221.57 61.60 228.99 61.70 228.87 61.80 228.51
61.91 232.48 62.00 232.76 62.20 231.46 62.40 229.17 62.60 231.81 62.80 233.80
63.00 236.04 63.20 241.01 63.40 246.34 63.60 251.76 63.80 258.76 64.00 261.50
64.20 264.30 64.40 265.72 64.60 266.85 64.80 269.32 65.00 269.75 65.20 272.10
65.40 273.78 65.60 271.49 65.80 273.51

EXP. 35 DATA POINTS (LEVEL,CR) INIT. COUNTING= 276.70

60.70 32.28 60.80 62.17 60.90 122.71 61.00 157.86 61.10 184.26 61.20 197.27
61.30 214.82 61.40 221.24 61.50 223.74 61.65 230.19 61.80 236.16 62.00 234.71
62.20 232.35 62.40 231.53 62.60 234.00 62.80 234.24

EXP. 36 DATA POINTS (LEVEL,CR) INIT. COUNTING= 276.70

60.71 42.43 60.80 50.65 60.90 127.38 61.00 158.54 61.10 186.73 61.20 206.14
61.30 215.98 61.40 222.43 61.50 228.48 61.60 228.65 61.70 235.83 61.80 234.91
61.90 235.69 62.00 233.49 62.10 230.62 62.20 232.83 62.32 231.20 62.40 232.60
62.50 226.94 62.60 229.00 62.80 232.22 63.00 234.45 63.20 235.09 63.40 237.49
63.60 239.65 63.80 247.85 64.00 246.94 64.20 255.86 64.40 257.42 64.60 258.34
64.80 259.89 65.00 265.74 65.20 265.62 65.50 268.51 66.00 270.76 66.50 270.52
67.00 270.34 68.10 272.40 69.50 275.10

EXP. 37 DATA POINTS (LEVEL,CR) INIT. COUNTING= 278.70

60.70 35.03 60.86 107.93 61.00 159.98 61.14 192.45 61.30 221.00 61.46 228.99
61.60 234.03 61.80 237.30 62.00 236.98 62.20 233.84 62.40 232.17 62.60 235.37
62.80 233.87 63.00 245.97 63.20 237.38 63.50 243.50 64.00 250.56 64.50 257.54
65.00 264.08 65.50 264.86 66.00 273.87 66.50 271.83 67.00 274.27 67.50 271.80
68.00 275.30 68.50 273.44 70.00 275.28

EXP. 38 DATA POINTS (LEVEL,CR) INIT. COUNTING= 276.81

60.70 37.22 60.80 80.61 60.90 120.99 61.00 157.03 61.10 177.64 61.20 193.32
61.30 205.66 61.40 215.36 61.60 224.53 61.70 225.11 61.90 221.98 62.10 225.06
62.30 225.99 62.50 225.16 62.70 228.08 62.90 231.58 63.20 242.69 63.42 246.66
63.60 250.95 63.80 252.73 64.00 258.83 64.20 261.55 64.40 264.52 64.60 268.49
64.80 266.78 65.00 270.55 65.20 269.17 65.40 269.50 65.60 267.59 65.80 271.07
66.00 271.05 66.30 271.11 66.60 269.89 67.60 276.33 68.60 277.00

EXP.118 DATA POINTS (LEVEL,CR) INIT. COUNTING= 247.00

61.00 136.76 61.50 203.85 62.00 206.15 62.50 207.37 63.00 205.80 63.50 211.34
64.00 222.42 65.00 236.33 66.00 243.58 68.00 244.21 70.00 246.87

EXP.119 DATA POINTS (LEVEL,CR) INIT. COUNTING= 247.00

61.00 132.25 61.50 200.90 62.00 206.77 62.50 207.41 63.00 216.25 63.50 222.08
64.00 235.92 65.00 241.34 66.00 245.50 68.00 243.14 70.00 244.89

EXP.120 DATA POINTS (LEVEL,CR) INIT. COUNTING= 247.00

61.00 133.23 61.50 198.92 62.00 204.53 62.50 207.59 63.00 213.51 63.50 219.28
64.00 232.44 65.00 241.11 66.00 243.25 68.00 243.29 70.00 245.99

EXP.121 DATA POINTS (LEVEL,CR) INIT. COUNTING= 247.00

61.00 132.55 61.50 203.51 62.00 206.96 62.50 207.15 63.00 206.51 63.50 213.41
64.00 221.66 65.00 236.93 66.00 239.96 68.00 245.51 70.00 244.96

EXP.122 DATA POINTS (LEVEL,CR) INIT. COUNTING= 247.00

61.00 132.33 61.50 196.31 62.00 202.80 62.50 205.71 63.00 208.93 63.50 212.46
64.00 217.87 64.50 226.50 65.00 234.48 66.00 241.13 68.00 247.08 70.00 245.79

EXP.123 DATA POINTS (LEVEL,CR) INIT. COUNTING= 247.00

61.00 132.23 61.50 203.05 62.00 206.34 62.50 202.30 63.00 201.61 63.50 202.48
64.00 206.54 65.00 230.35 66.00 238.17 67.00 243.00 68.00 243.15 70.00 243.60

EXP.124 DATA POINTS (LEVEL,CR) INIT. COUNTING= 247.00

61.50 192.60 62.00 201.45 62.50 206.33 63.00 218.60 63.50 232.32 64.00 239.15
65.00 244.74 66.00 245.54 68.00 244.78 70.00 246.90

EXP.125 DATA POINTS (LEVEL,CR) INIT. COUNTING= 247.00

61.50 200.42 62.00 205.46 62.50 203.73 63.00 208.42 63.50 217.61 64.00 226.49
65.00 236.89 66.00 240.97 68.00 243.31 70.00 246.00

EXP.126 DATA POINTS (LEVEL,CR) INIT. COUNTING= 247.00

62.00 195.22 62.50 198.00 63.00 203.54 63.50 216.30 64.00 226.23 64.50 233.00
65.00 237.75 66.00 244.41 68.00 245.31 70.00 246.70

EXP.127 DATA POINTS (LEVEL,CR) INIT. COUNTING= 247.00

61.50 197.72 62.00 201.38 62.50 199.35 63.00 200.56 63.50 206.33 64.00 214.70
64.50 227.20 65.00 232.14 66.00 239.47 68.00 245.47 70.00 245.13

EXP.128 DATA POINTS (LEVEL,CR) INIT. COUNTING= 247.00

61.00 164.33 61.50 213.55 62.00 214.80 62.50 210.83 63.00 207.20 63.50 207.80
64.00 214.84 64.50 222.86 65.00 230.15 66.00 240.87 68.00 244.18 70.00 245.10

EXP.129 DATA POINTS (LEVEL,CR) INIT. COUNTING= 247.00

61.00 153.80 61.50 213.00 62.00 213.94 62.50 208.45 63.00 207.86 63.50 209.92
64.00 216.48 64.50 220.07 65.00 229.97 66.00 240.43 68.00 242.51 70.00 245.50

EXP.130 DATA POINTS (LEVEL,CR) INIT. COUNTING= 247.00

61.00 129.27 61.50 198.51 62.00 206.21 62.50 201.18 63.00 210.55 63.50 220.92
64.00 230.67 64.50 236.15 65.00 241.61 66.00 242.49 68.00 246.04 70.00 246.80

EXP.141 DATA POINTS (LEVEL,CR) INIT. COUNTING= 247.00

61.50 185.51 62.00 194.69 62.50 193.03 63.00 196.63 63.50 215.22 64.00 229.03
64.50 236.13 65.00 243.33 66.00 246.89

EXP.142 DATA POINTS (LEVEL,CR) INIT. COUNTING= 247.00

61.50 176.63 62.00 190.48 62.50 188.57 63.00 202.95 63.50 217.87 64.00 233.30
65.00 246.55 66.00 245.22

EXP.143 DATA POINTS (LEVEL,CR) INIT. COUNTING= 247.00

62.00 183.03 62.50 188.96 63.00 201.33

EXP.146 DATA POINTS (LEVEL,CR) INIT. COUNTING= 247.00

61.50 172.70 62.00 180.67 62.50 175.30 63.00 174.94 63.50 179.32 64.00 183.81
65.00 208.64 66.00 233.46 67.00 243.06 68.00 244.13 70.00 245.00

EXP.156 DATA POINTS (LEVEL,CR) INIT. COUNTING= 247.00

62.00 221.92 62.50 217.59 63.00 213.09 63.50 215.17 64.00 220.10 64.50 228.40
65.00 234.55 66.00 240.43 68.00 244.89 70.00 245.44

EXP.157 DATA POINTS (LEVEL,CR) INIT. COUNTING= 247.00

62.00 210.58 62.50 208.66 63.00 203.20 63.50 205.90 64.00 212.92 64.50 222.91
65.00 229.42 66.00 247.86 68.00 243.11 70.00 245.33

EXP.158 DATA POINTS (LEVEL,CR) INIT. COUNTING= 247.00

62.00 204.72 62.50 199.55 63.00 196.92 63.50 199.38 64.00 202.41 64.50 209.44
65.00 218.22 66.00 233.63 68.00 243.51 70.00 244.90

EXP.159 DATA POINTS (LEVEL,CR) INIT. COUNTING= 247.00

62.00 205.42 62.50 200.92 63.00 194.45 63.50 190.29 64.00 190.51 64.50 196.52
65.00 204.95 66.00 226.21 68.00 241.48 70.00 243.89

EXP.160 DATA POINTS (LEVEL,CR) INIT. COUNTING= 247.00

63.00 196.10 63.50 194.50 64.50 204.82 65.00 214.20 66.00 230.20 68.00 242.50
70.00 245.00 62.50 200.00

EXP.161 DATA POINTS (LEVEL,CR) INIT. COUNTING= 247.00

62.00 214.58 62.50 211.20 63.00 208.35 63.50 214.49 64.00 225.60 64.50 233.21
65.00 236.10 66.00 240.00 67.00 242.37 68.00 244.54 70.00 244.54

EXP.162 DATA POINTS (LEVEL,CR) INIT. COUNTING= 247.00

62.00 203.24 62.50 202.38 63.00 201.24 63.50 204.30 64.00 214.72 64.50 226.90
65.00 233.08 66.00 240.31 67.00 242.84 68.00 244.42

EXP.163 DATA POINTS (LEVEL,CR) INIT. COUNTING= 247.00

62.00 210.86 62.50 208.69 63.00 202.64 63.50 200.59 64.00 209.68 64.50 219.80
65.00 225.99 66.00 237.63 67.00 240.56 68.00 242.50 70.00 244.00

EXP.164 DATA POINTS (LEVEL,CR) INIT. COUNTING= 247.00

62.00 198.91 62.50 197.32 63.00 199.55 63.50 210.30 64.00 222.97 64.50 232.23
65.00 239.19 66.00 241.79 67.00 243.60 68.00 245.00 70.00 244.00

EXP.165 DATA POINTS (LEVEL,CR) INIT. COUNTING= 247.00

62.00 212.81 62.50 209.25 63.00 200.68 63.50 202.04 64.00 210.77 64.50 220.50
65.00 227.48 66.00 236.40 67.00 242.27 68.00 243.46

EXP.166 DATA POINTS (LEVEL,CR) INIT. COUNTING= 247.00

62.00 205.05 62.50 198.32 63.00 196.49 63.50 198.38 64.00 204.39 64.50 217.40
65.00 228.61 66.00 242.13 68.00 246.70 70.00 246.35

EXP.167 DATA POINTS (LEVEL,CR) INIT. COUNTING= 247.00

62.00 206.50 62.50 202.11 63.00 196.10 63.50 197.00 64.00 200.30 64.50 208.52
65.00 222.62 66.00 237.77 70.00 246.50

EXP.168 DATA POINTS (LEVEL,CR) INIT. COUNTING= 247.00

62.00 213.36 62.50 212.20 62.75 209.19 63.00 206.46 63.50 216.08 64.00 225.24
64.50 233.26 65.00 238.82 66.00 244.52 67.00 244.60

EXP.169 DATA POINTS (LEVEL,CR) INIT. COUNTING= 247.00

62.00 219.85 62.50 216.66 62.75 216.67 63.00 212.78 63.20 215.17 63.30 212.86
63.50 212.24 64.00 218.40 64.50 225.78 65.00 232.73 66.00 241.26

TABLE III.2

DISPERSION DENSITY PARAMETERS AND

CALCULATED VALUES OF DROPS HOLD-UP AND SIZE.

SYSTEM AQUEOUS METHANOL / AIR

Run	F_s	L_v	δ	mass transfer	$F*10^4$	x_1	x_2 (cm)	x_3	H_D (cm)	d_{gm} (mm)
1	1.10	0.34	0.072	no	5.5	0.125	1.32	0.51	0.24	2.29
2	1.37	0.34	0.072	no	4.0	0.122	1.36	0.45	0.21	2.42
3	1.46	0.34	0.072	no	2.1	0.122	1.32	0.46	0.21	2.43
4	1.62	0.34	0.072	no	2.4	0.055	1.60	0.50	0.15	2.10
5	1.62	5.68	0.072	no	3.4	0.123	1.58	0.49	0.27	2.13
6	1.62	6.31	0.072	no	6.4	0.131	1.62	0.53	0.32	2.03
11	1.62	6.31	0.060	no	4.9	0.121	1.66	0.52	0.30	2.00
12	1.80	6.31	0.060	no	8.6	0.074	1.70	0.61	0.23	1.76
13	1.96	6.31	0.060	no	3.4	0.017	0.77	2.62	2.61	1.68
14	1.62	6.31	0.055	no	8.3	0.119	1.58	0.55	0.30	1.99
15	1.80	6.31	0.055	no	8.2	0.082	1.33	0.80	0.30	1.49
16	1.50	6.31	0.054	no	9.8	0.131	1.69	0.47	0.29	2.11
17	1.37	6.31	0.055	no	8.0	0.131	1.52	0.53	0.30	2.10
18	1.10	6.31	0.054	no	5.5	0.138	1.48	0.57	0.34	2.03
19	1.80	6.31	0.072	no	7.1	0.118	1.43	0.61	0.31	1.94
20	1.50	6.31	0.072	no	27.	0.162	1.68	0.45	0.33	2.17
21	1.37	6.31	0.072	no	8.6	0.143	1.58	0.46	0.29	2.20
22	1.10	6.31	0.072	no	7.6	0.149	1.41	0.54	0.32	2.16
23	1.62	6.31	0.072	no	4.6	0.144	1.63	0.49	0.33	2.10
24	1.74	6.31	0.072	no	4.7	0.117	1.69	0.48	0.27	2.08
25	1.85	6.31	0.072	no	4.9	0.098	1.57	0.64	0.30	1.78

Note: runs 1-25 were obtained without using a splash baffle.

Table III.2 (cont.)

Run	F_s	L_v	δ	mass transfer	$F*10^4$	x_1	x_2 (cm)	x_3	H_D (cm)	d_{gm} (mm)
32	1.85	.068	0.072	no	3.4	0.108	1.07	1.24	0.77	0.61
33	1.68	.068	0.057	des.	2.7	0.113	1.62	0.51	0.27	2.06
34	1.68	.068	0.057	des.	3.0	0.117	1.62	0.48	0.26	2.13
35	1.68	.068	0.057	no	.11	0.107	1.66	0.66	0.37	1.67
36	1.79	.077	0.072	des.	7.0	0.115	1.76	0.56	0.34	1.87
37	1.79	.077	0.072	no	3.2	0.111	1.77	0.60	0.35	1.76
38	1.68	.068	0.056	abs.	6.8	0.130	1.44	0.56	0.32	2.06
118	1.68	.068	0.055	no	.47	0.115	2.08	0.42	0.28	1.98
119	1.31	.068	0.055	no	2.4	0.107	1.63	0.46	0.23	2.16
120	1.31	.068	0.060	no	1.8	0.106	1.76	0.46	0.24	2.09
121	1.68	.068	0.060	no	.68	0.112	2.00	0.46	0.29	1.94
122	1.31	.102	0.060	no	1.5	0.112	1.99	0.50	0.32	1.86
123	1.68	.102	0.060	no	.44	0.134	2.23	0.47	0.39	1.82
124	1.31	.068	0.072	no	.45	0.116	1.54	0.40	0.19	2.38
125	1.68	.068	0.072	no	.58	0.120	1.63	0.56	0.32	1.94
126	1.31	.102	0.072	no	.27	0.135	1.73	0.47	0.31	2.08
127	1.68	.102	0.072	no	.94	0.134	2.00	0.48	0.36	1.91
128	1.84	.068	0.072	des.	.90	0.112	2.29	0.45	0.32	1.83
129	1.83	.068	0.072	des.	1.9	0.110	2.16	0.51	0.35	1.76
130	1.68	.068	0.072	abs.	.38	0.129	1.55	0.50	0.28	2.14
141	1.50	.102	0.072	abs.	.44	0.155	1.89	0.35	0.27	2.22
142	1.10	.102	0.072	abs.	.99	0.174	1.20	0.37	0.28	2.31
143	1.24	.102	0.072	abs.	.00	0.172	1.47	0.36	0.38	2.27
146	1.43	.345	0.072	no	11.	0.224	2.21	0.49	0.68	1.79
156	1.80	.068	0.051	no	.41	0.092	2.28	0.44	0.26	1.84
157	1.80	.102	0.051	no	.54	0.120	2.26	0.46	0.35	1.82

Table III.2 (cont)

Run	F_s	L_v	γ	mass transfer	$F*10^4$	x_1	x_2 (cm)	x_3	H_D (cm)	d_{gm} (mm)
158	1.80	.170	0.051	no	2.5	0.144	2.31	0.52	0.50	1.78
159	1.80	.345	0.051	no	6.0	0.166	2.67	0.49	0.62	1.61
160	1.80	.227	0.051	no	2.4	0.151	2.43	0.52	0.54	1.64
161	1.81	.068	0.072	abs.	2.2	0.103	2.03	0.45	0.26	1.95
162	1.80	.102	0.072	abs.	1.3	0.131	2.12	0.44	0.34	1.92
163	1.91	.102	0.072	abs.	1.9	0.127	2.37	0.45	0.38	1.79
164	1.68	.102	0.072	abs.	1.5	0.139	1.92	0.42	0.31	2.07
165	1.91	.102	0.072	no	.46	0.127	2.35	0.44	0.36	1.82
166	1.80	.170	0.072	abs.	4.1	0.150	2.24	0.44	0.40	1.88
167	1.91	.170	0.072	abs.	4.2	0.150	2.41	0.45	0.45	1.78
168	1.80	.068	0.072	abs.	.55	0.106	2.13	0.38	0.23	2.03
169	1.91	.068	0.072	abs.	2.0	0.092	2.36	0.45	0.27	1.80

TABLE III.3

DISPERSION DENSITY PARAMETERS AND

CALCULATED VALUES OF DROPS HOLD-UP AND SIZE.

SYSTEM A: BENZENE / CYCLOHEXANE

Run	F_s	γ	$F*10^4$	x_1	x_2 (cm)	x_3	H_D (cm)	d_{gm} (mm)	$Tf*10^3$
A21V1	0.88	0.0181	4.0	0.233	1.05	0.49	0.34	2.67	-1.5
A21V2	1.17	0.0181	4.0	0.250	1.50	0.41	0.42	2.39	-1.4
A21V3	1.81	0.0181	2.4	0.164	2.23	0.38	0.38	1.98	-1.4
A22V1	0.95	0.0183	6.2	0.285	1.48	0.35	0.40	2.52	-3.6
A22V2	1.31	0.0183	3.9	0.230	1.79	0.33	0.37	2.31	-3.6
A22V3	1.86	0.0183	6.6	0.179	1.87	0.51	0.48	1.91	-3.6
A23V1	0.98	0.0185	.40	0.271	1.73	0.23	0.28	2.51	-5.5
A23V2	1.33	0.0185	1.5	0.238	1.72	0.31	0.33	2.41	-5.4
A24V1	1.00	0.0188	.54	0.279	1.49	0.37	0.42	2.48	-5.5
A24V2	1.38	0.0188	10.	0.262	1.52	0.44	0.48	2.31	-5.5
A24V3	1.80	0.0188	6.8	0.193	1.83	0.47	0.47	2.01	-5.5
A25V1	0.89	0.0193	.42	0.258	1.54	0.33	0.35	2.52	-2.6
A25V2	1.06	0.0193	4.7	0.259	1.45	0.40	0.41	2.44	-2.6
A25V3	1.80	0.0193	4.0	0.177	1.88	0.47	0.44	1.99	-2.6
A26V1	0.97	0.0197	1.4	0.201	1.39	0.49	0.38	1.30	+1.6
A26V2	1.27	0.0197	2.7	0.243	1.41	0.53	0.52	2.18	+1.6
A26V3	1.52	0.0197	3.6	0.218	1.60	0.55	0.55	1.99	+1.6
A27V1	0.95	0.0200	.15	0.173	1.58	0.36	0.27	2.41	+4.6
A27V2	1.31	0.0200	2.0	0.216	1.54	0.52	0.50	2.08	+4.6
A27V3	1.59	0.0200	1.4	0.212	1.67	0.49	0.49	2.07	+4.6
A29V1	0.95	0.0204	.46	0.167	1.56	0.35	0.24	2.47	+5.8
A29V2	1.26	0.0204	.67	0.201	1.84	0.29	0.29	2.35	+5.8
A29V3	1.59	0.0204	4.1	0.217	1.39	0.63	0.59	1.91	+5.8

Table III.3 (cont.)

Run	F_s	γ	$F*10^4$	x_1	x_2 (cm)	x_3	H_D (cm)	d_{gm} (mm)	$Tf*10^3$
A30V1	0.98	0.0207	.01	0.192	1.38	0.46	0.34	2.39	+4.4
A30V2	1.27	0.0207	.71	0.217	1.37	0.51	0.43	2.26	+4.4
A30V3	1.60	0.0207	3.6	0.247	1.29	0.64	0.63	1.97	+4.4
A31V1	0.94	0.0210	8.1	0.238	1.41	0.46	0.44	2.34	+2.4
A31V2	1.29	0.0210	1.4	0.247	1.46	0.50	0.51	2.20	+2.4
A31V3	1.85	0.0210	7.9	0.203	1.78	0.55	0.57	1.88	+2.3

TABLE III.4

DISPERSION DENSITY PARAMETERS AND

CALCULATED VALUES OF DROPS HOLD-UP AND SIZE.

SYSTEM B: BENZENE / N-HEPTANE

Run	F_s	γ	$F*10^4$	x_1	x_2 (cm)	x_3	H_D (cm)	d_{gm} (mm)	$Tf*10^3$
B10V1	0.87	0.0131	7.3	0.332	1.59	0.32	0.44	2.50	-15
B10V2	1.26	0.0131	17.	0.262	1.68	0.36	0.42	2.35	-14
B10V3	1.48	0.0131	1.3	0.232	1.95	0.36	0.44	2.16	-14
B10V4	1.85	0.0131	1.8	0.157	2.34	0.56	0.60	1.60	-13
B11V1	0.89	0.0138	8.4	0.333	1.58	0.32	0.45	2.50	-37
B11V2	1.17	0.0138	1.9	0.296	1.71	0.34	0.45	2.37	-36
B11V3	1.50	0.0138	3.1	0.221	1.79	0.41	0.44	2.18	-36
B11V4	1.73	0.0138	7.0	0.187	1.90	0.57	0.59	1.77	-36
B12V1	0.87	0.0148	.02	0.327	1.72	0.24	0.34	2.52	-58
B12V2	1.22	0.0147	1.2	0.289	1.73	0.31	0.41	2.40	-57
B12V3	1.48	0.0145	.95	0.250	1.76	0.37	0.44	2.26	-52
B12V4	1.79	0.0147	7.0	0.188	1.75	0.61	0.60	1.74	-56
B13V1	0.96	0.0168	4.3	0.307	1.62	0.28	0.37	2.53	-77
B13V2	1.21	0.0167	8.9	0.273	1.67	0.31	0.38	2.44	-78
B13V3	1.55	0.0167	2.8	0.238	1.67	0.42	0.46	2.23	-79
B13V4	1.87	0.0166	7.4	0.161	2.10	0.55	0.54	1.71	-79
B14V1	0.97	0.0180	3.2	0.302	1.60	0.31	0.39	2.51	-54
B14V2	1.26	0.0180	5.5	0.262	1.63	0.40	0.46	2.31	-56
B14V3	1.54	0.0180	4.0	0.228	1.80	0.36	0.40	2.25	-56
B14V4	1.82	0.0180	9.3	0.173	1.64	0.62	0.53	1.78	-57
B15V1	0.94	0.0198	1.1	0.264	1.56	0.32	0.35	2.52	- 7
B15V2	1.19	0.0198	2.3	0.256	1.51	0.39	0.41	2.42	- 7
B15V3	1.72	0.0198	5.9	0.217	1.92	0.40	0.45	2.11	- 7
B15V4	1.98	0.0198	4.2	0.153	2.14	0.54	0.52	1.71	- 7

TABLE III.5

DISPERSION DENSITY PARAMETERS AND

CALCULATED VALUES OF DROPS HOLD-UP AND SIZE.

SYSTEM C: N-HEPTANE / TOLUENE

Run	F_s	γ	$F*10^4$	x_1	x_2 (cm)	x_3	H_D (cm)	d_{gm} (mm)	$Tf*10^3$
C1V1	0.87	0.0182	.35	0.231	1.37	0.44	0.39	2.43	+ 7
C1V2	1.21	0.0182	1.1	0.234	1.48	0.48	0.47	2.23	+ 6
C1V3	1.53	0.0182	6.7	0.211	1.87	0.39	0.42	2.16	+ 6
C1V4	1.86	0.0182	5.2	0.192	2.11	0.43	0.48	1.95	+ 6
C2V1	0.92	0.0175	.23	0.162	1.40	0.48	0.31	2.31	+25
C2V2	1.25	0.0175	4.4	0.200	1.67	0.40	0.36	2.28	+24
C2V3	1.50	0.0175	5.3	0.208	1.83	0.40	0.41	2.17	+24
C2V4	1.84	0.0175	2.4	0.196	2.12	0.43	0.49	1.95	+23
C3V1	0.95	0.0161	3.3	0.185	1.38	0.49	0.36	2.29	+37
C3V2	1.20	0.0161	6.0	0.204	1.72	0.40	0.38	2.24	+37
C3V3	1.57	0.0161	9.9	0.208	1.99	0.41	0.47	2.05	+37
C3V4	1.87	0.0161	4.3	0.192	2.27	0.42	0.50	1.90	+37
C4V1	0.95	0.0147	3.3	0.186	1.53	0.44	0.35	2.30	+22
C4V2	1.21	0.0147	6.8	0.204	1.70	0.43	0.41	2.19	+22
C4V3	1.57	0.0147	8.2	0.208	1.90	0.48	0.53	1.97	+22
C4V4	1.88	0.0147	4.0	0.179	2.39	0.45	0.54	1.78	+22
C5V1	0.95	0.0132	6.6	0.246	1.61	0.35	0.37	2.41	+ 5
C5V2	1.32	0.0132	13.	0.233	1.82	0.37	0.42	2.22	+ 5
C5V3	1.53	0.0132	11.	0.234	1.90	0.42	0.51	2.08	+ 5
C5V4	1.88	0.0132	5.7	0.181	2.36	0.47	0.57	1.75	+ 5

TABLE III.6

DISPERSION DENSITY PARAMETERS AND

CALCULATED VALUES OF DROPS HOLD-UP AND SIZE.

SYSTEM AIR / WATER

Run	plate	d_h	Af	F_s	L_v	$F*10^4$	x_1	x_2	x_3	H_D	d_{gm}
1	1	¼	.110	2.64	15	1.8	0.135	12.5	0.32	1.44	0.82
2	1	¼	.110	2.90	15	3.8	0.105	13.9	0.37	1.47	0.75
3	1	¼	.110	3.16	15	4.4	0.073	16.1	0.49	1.62	0.59
4	5	¾	.103	2.21	15	1.3	0.119	9.2	0.37	1.09	0.93
5	5	¾	.103	2.42	15	.56	0.104	10.0	0.39	1.11	0.88
6	5	¾	.103	2.64	15	.96	0.090	11.2	0.49	1.41	0.74
7	2	½	.059	1.86	15	.42	0.146	8.8	0.30	0.99	1.01
8	2	½	.059	2.21	15	.25	0.123	9.3	0.39	1.20	0.91
9	2	½	.059	2.42	15	.43	0.108	10.0	0.44	1.31	0.84
10	3	½	.107	2.21	15	.67	0.154	6.6	0.39	1.08	1.10
11	3	½	.107	2.42	15	.49	0.132	7.3	0.42	1.12	1.01
12	3	½	.107	2.64	15	1.5	0.108	8.0	0.47	1.15	0.91
13	3	½	.107	2.96	15	1.5	0.087	9.4	0.57	1.38	0.74
14	4	½	.161	2.64	15	.62	0.119	6.2	0.51	1.08	1.00
15	4	½	.161	2.96	15	.98	0.103	6.9	0.58	1.21	0.87
16	4	½	.161	3.16	15	2.1	0.083	9.3	0.63	1.49	0.69
17	3	½	.107	2.21	8	3.4	0.143	5.4	0.48	1.08	1.11
18	3	½	.107	2.41	8	1.5	0.123	5.8	0.50	1.02	1.05
19	3	½	.107	2.64	8	1.1	0.088	6.2	0.65	1.11	0.83
20	3	½	.107	2.41	21	2.9	0.153	7.5	0.42	1.30	1.00
21	3	½	.107	2.64	21	4.0	0.128	8.6	0.48	1.47	0.87
22	3	½	.107	2.90	21	5.3	0.102	10.9	0.58	1.92	0.68
31	2	½	.059	1.40	19	15.	0.225	6.2	0.38	1.41	1.15
32	2	½	.059	1.60	19	4.4	0.187	7.7	0.31	1.18	1.07

Table III.6 (cont.).

Run	plate	d_h	Af	F_s	L_v	$F*10^4$	x_1	x_2	x_3	H_D	d_{gm}
33	2	½	.059	1.85	19	1.3	0.178	8.8	0.30	1.25	1.01
34	2	½	.059	1.98	19	.85	0.172	9.1	0.33	1.38	0.97
35	2	½	.059	2.15	19	1.1	0.165	9.4	0.35	1.46	0.97
36	3	½	.107	1.60	19	22.	0.261	4.0	0.63	1.98	1.10
37	3	½	.107	1.80	19	12.	0.212	5.1	0.46	1.39	1.17
38	3	½	.107	1.90	19	6.0	0.200	5.8	0.43	1.36	1.14
39	3	½	.107	2.30	19	1.7	0.152	6.3	0.50	1.35	1.01
40	4	½	.161	2.10	19	7.1	0.203	5.2	0.49	1.46	1.01
41	4	½	.161	2.30	19	6.6	0.187	5.2	0.53	1.48	1.08
42	4	½	.161	2.55	19	5.0	0.168	5.6	0.61	1.73	0.93
43	4	½	.161	2.74	19	3.2	0.148	5.9	0.73	2.10	0.75
44	4	½	.161	2.94	19	4.0	0.130	8.3	0.60	1.91	0.77

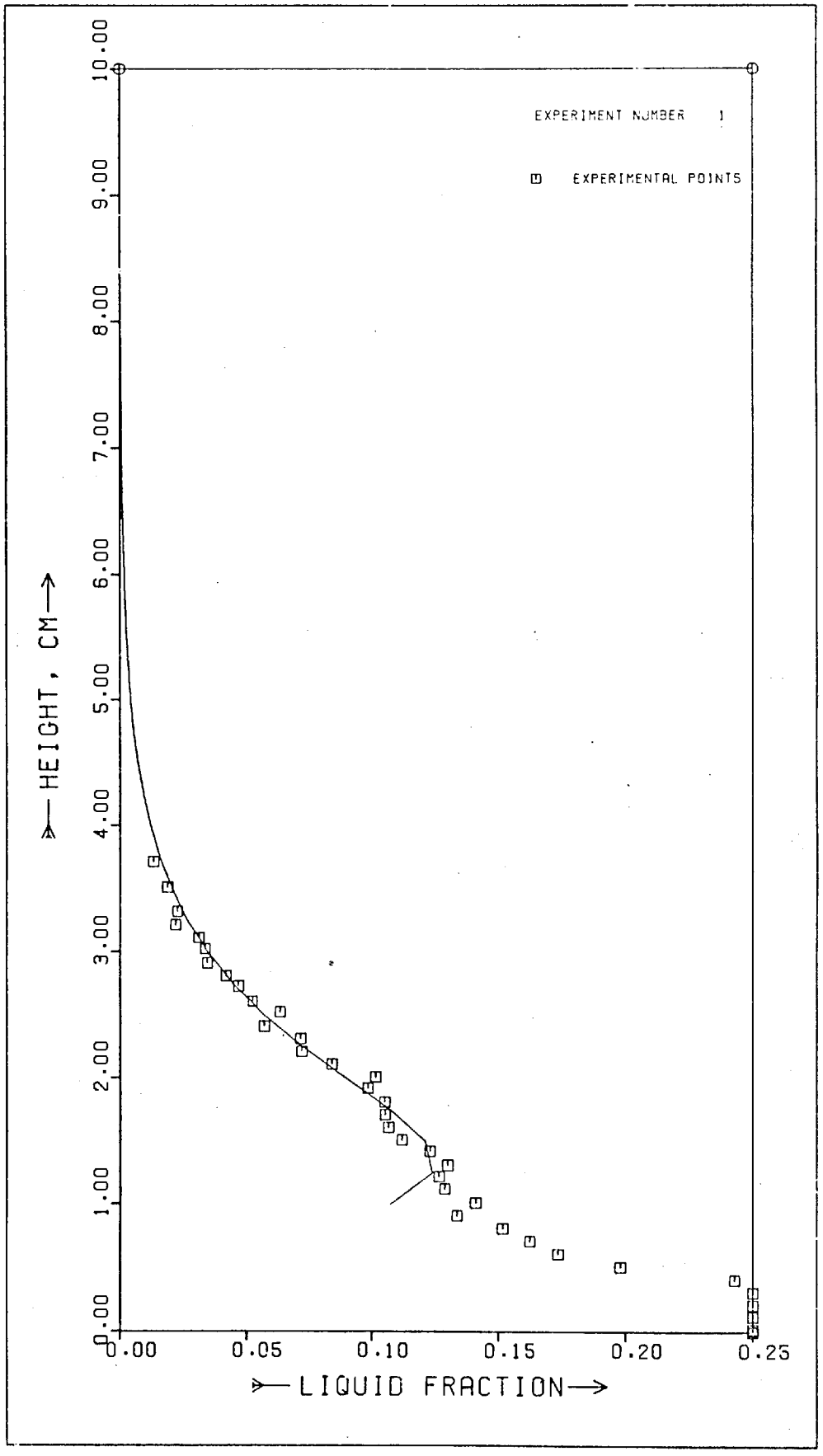

Fig.III. 1.- Dispersion density profile and fitting curve.

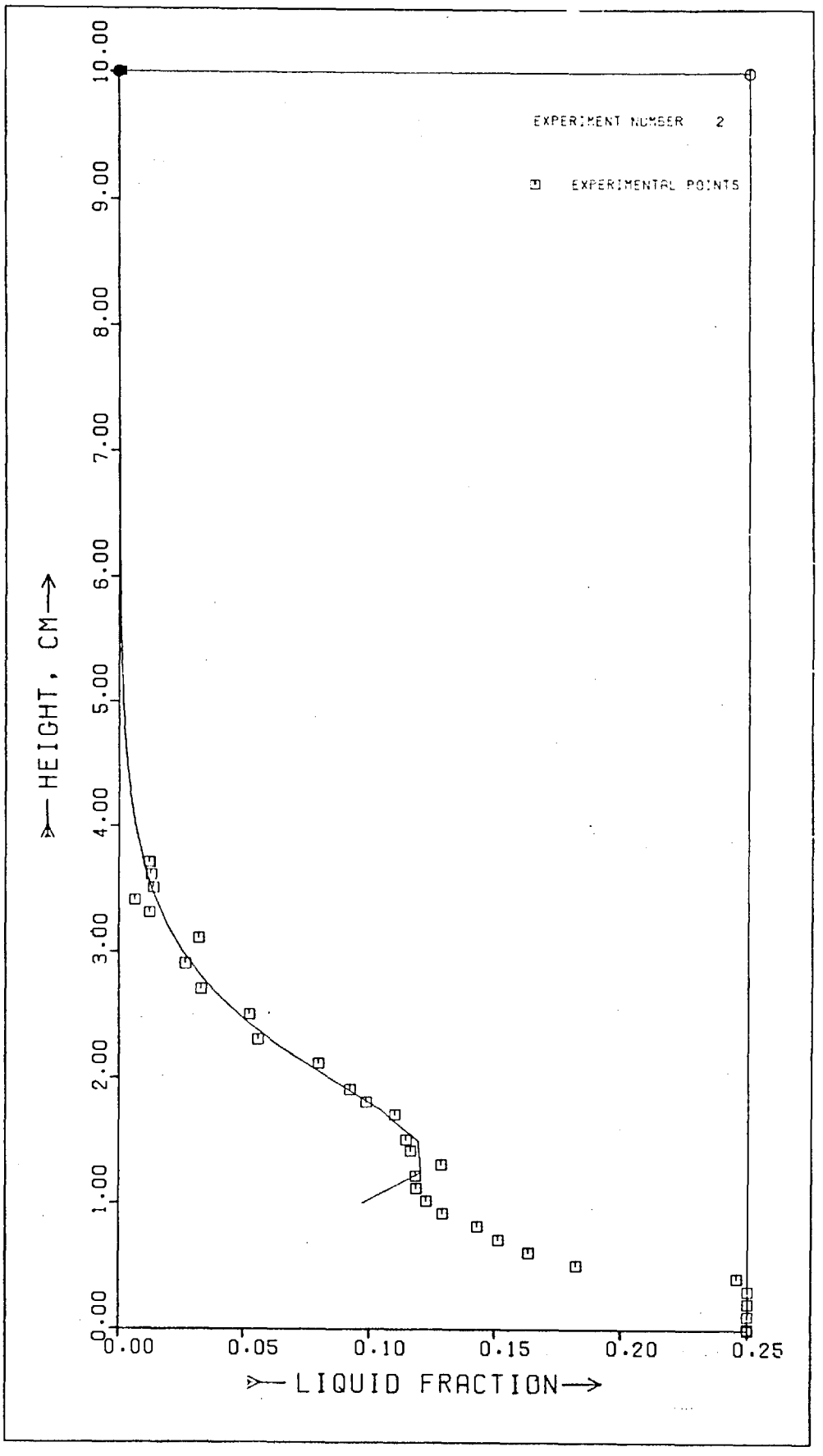

Fig.III. 2.- Dispersion density profile and fitting curve.

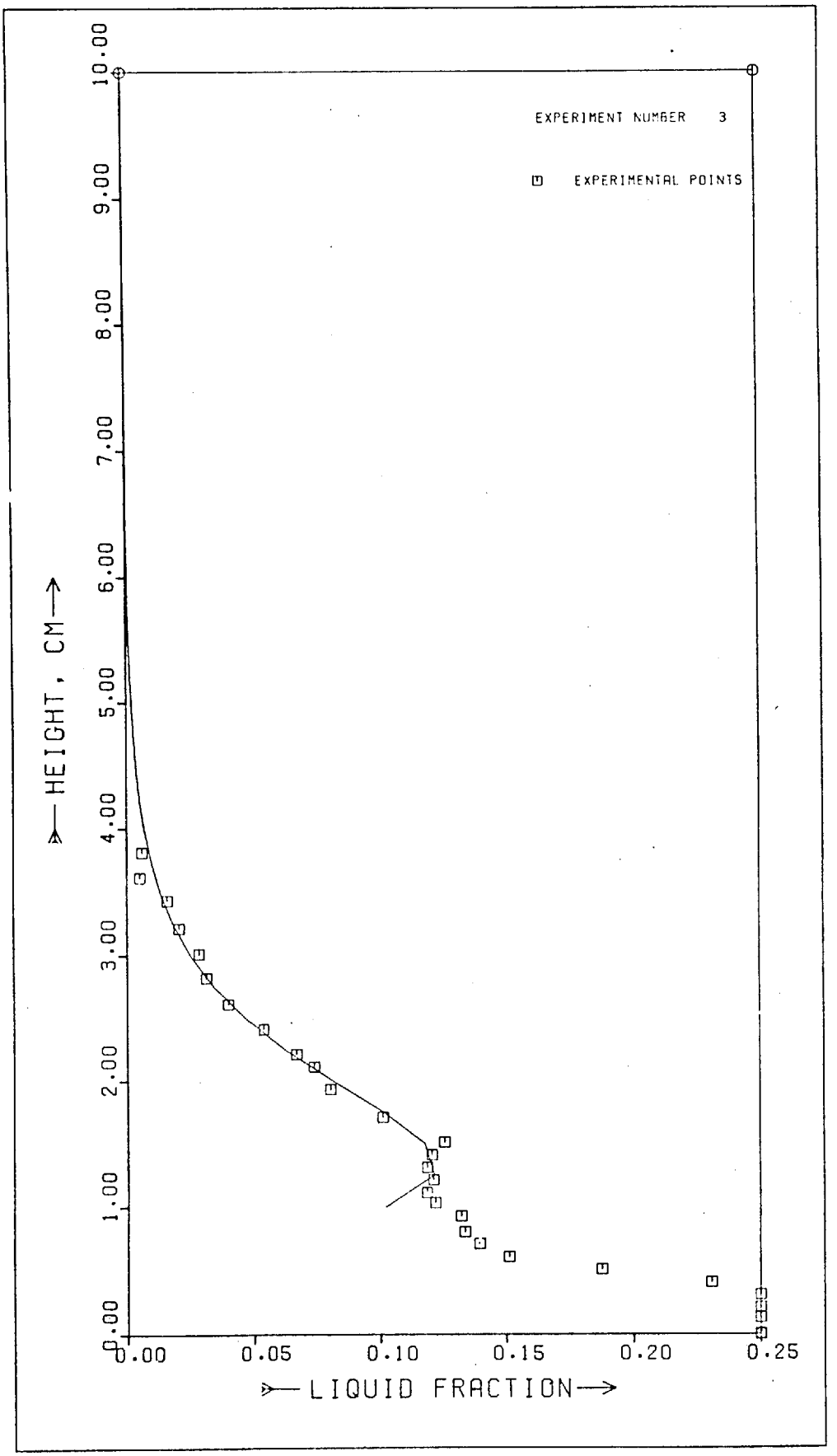

Fig.III. 3.- Dispersion density profile and fitting curve.

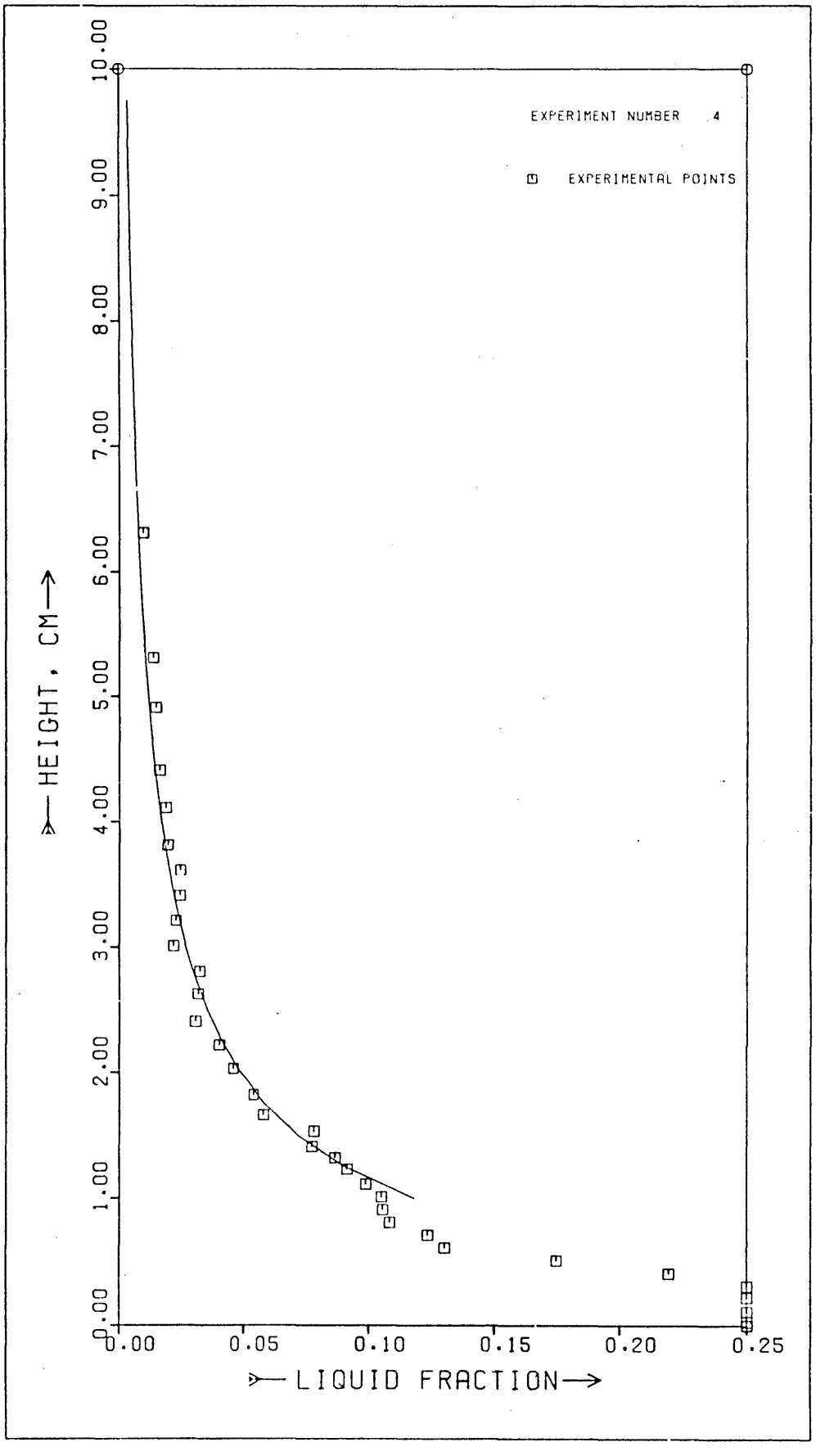

Fig.III. 4.- Dispersion density profile and fitting curve.

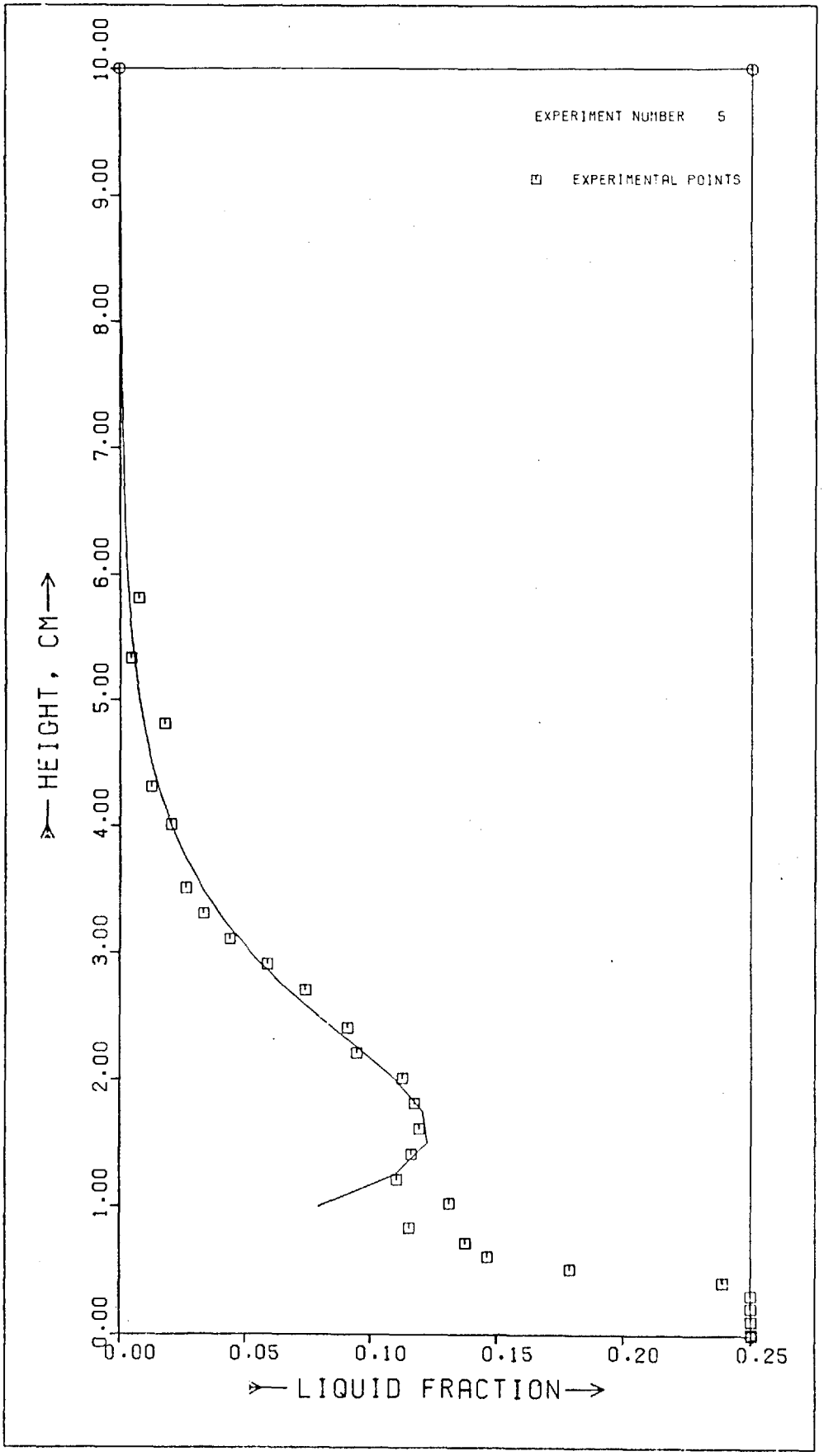

Fig.III. 5.- Dispersion density profile and fitting curve.

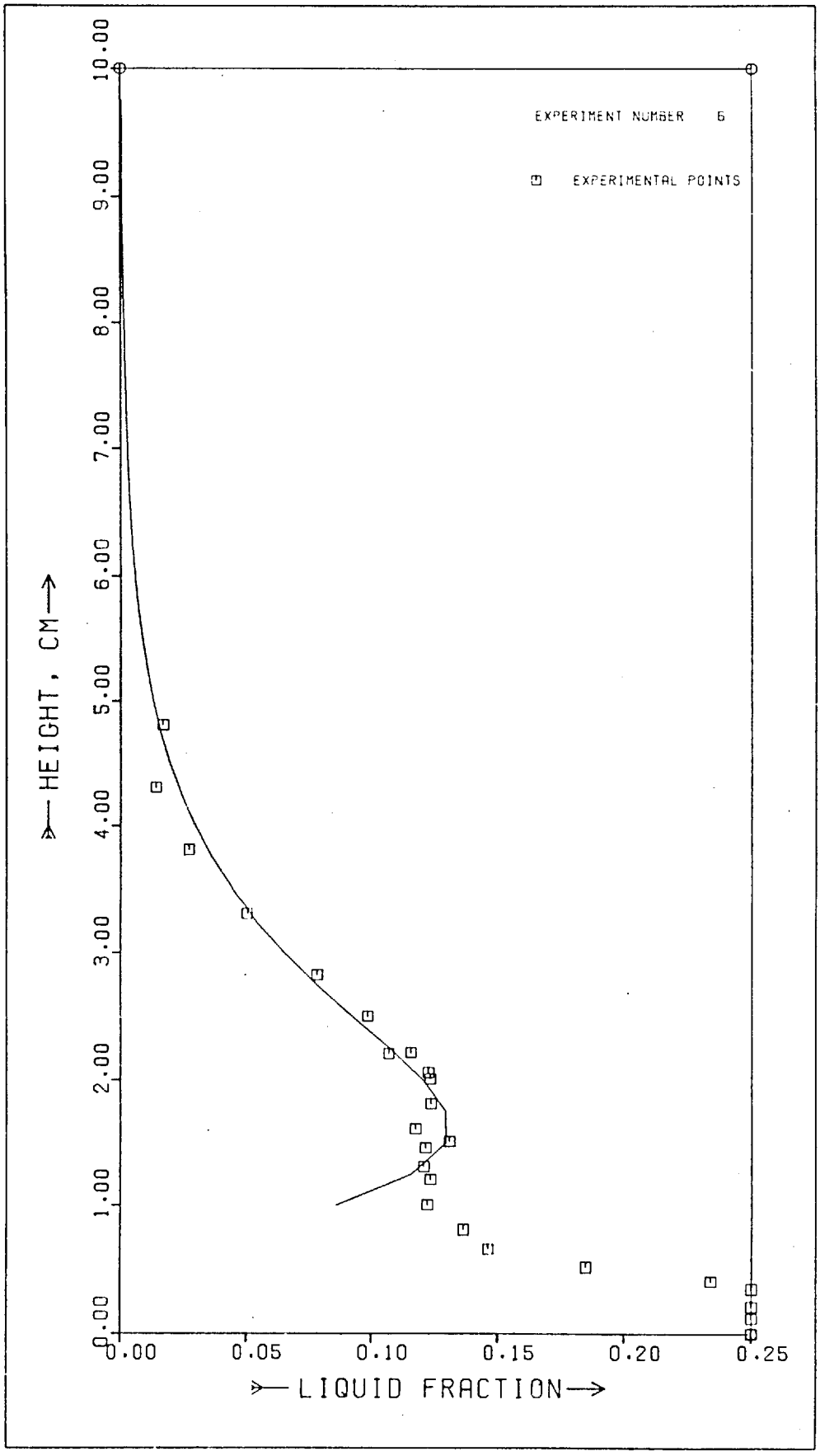

Fig.III. 6.- Dispersion density profile and fitting curve.

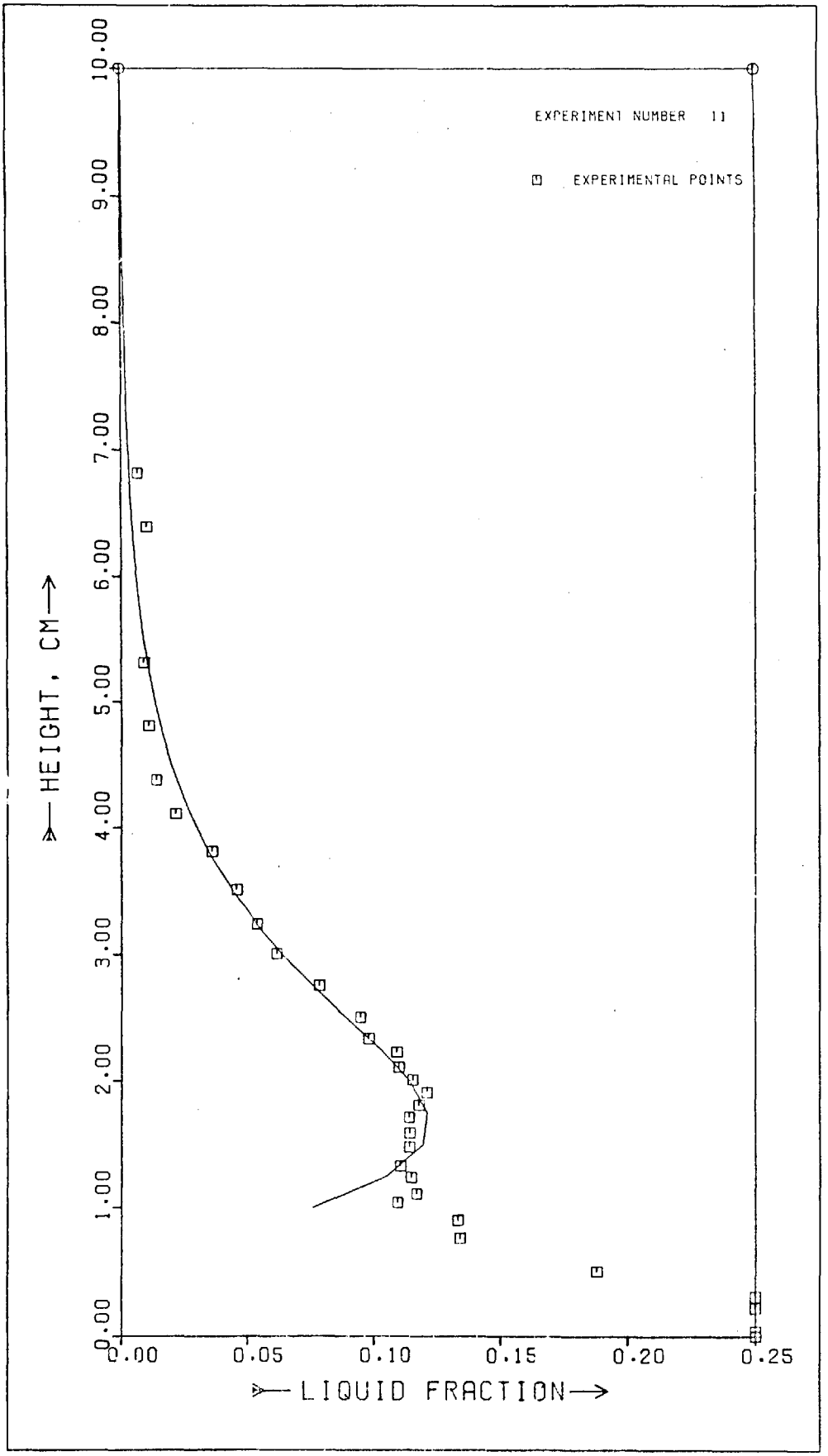

Fig.III. 7.- Dispersion density profile and fitting curve.

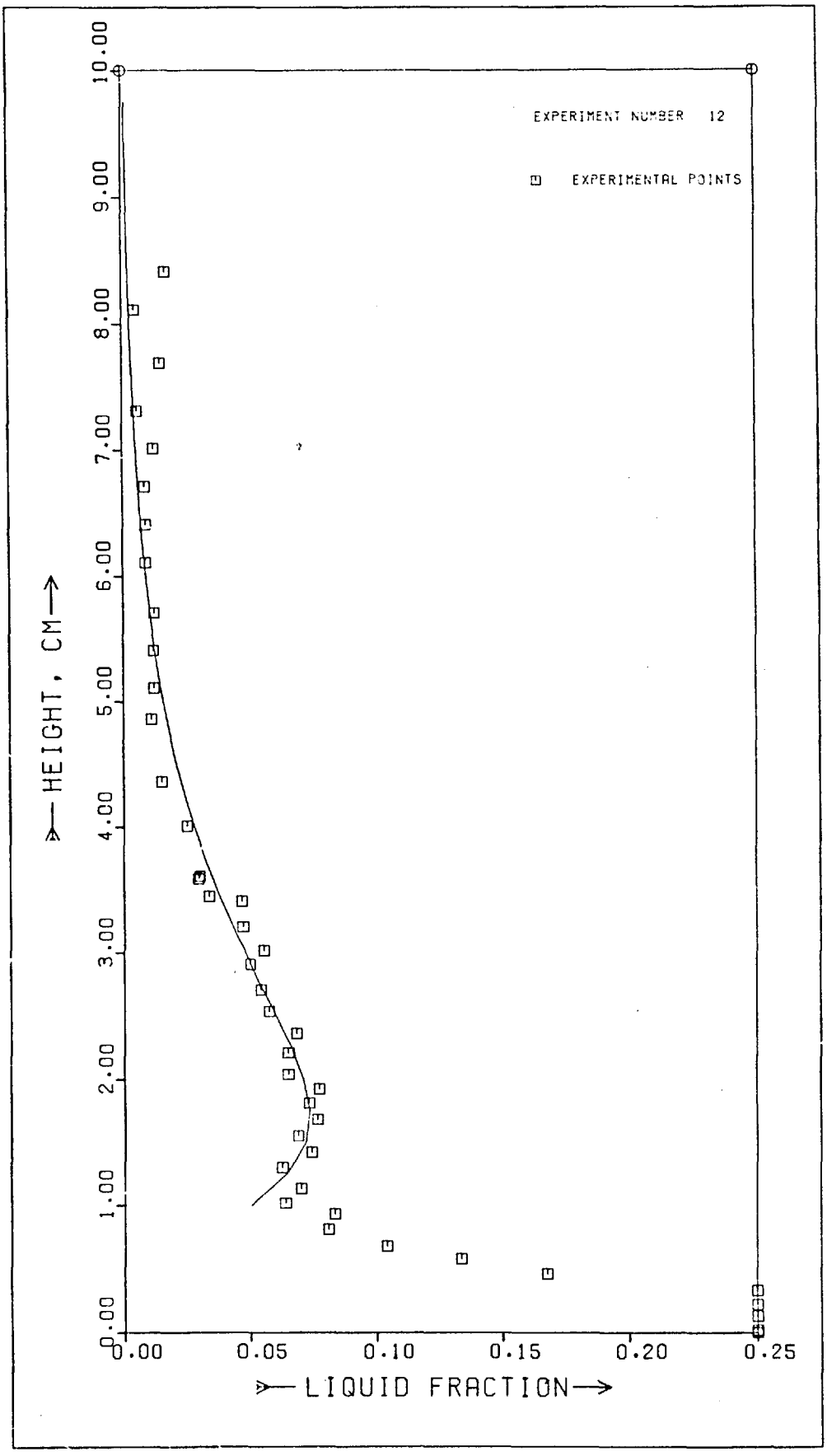

Fig.III. 8.- Dispersion density profile and fitting curve.

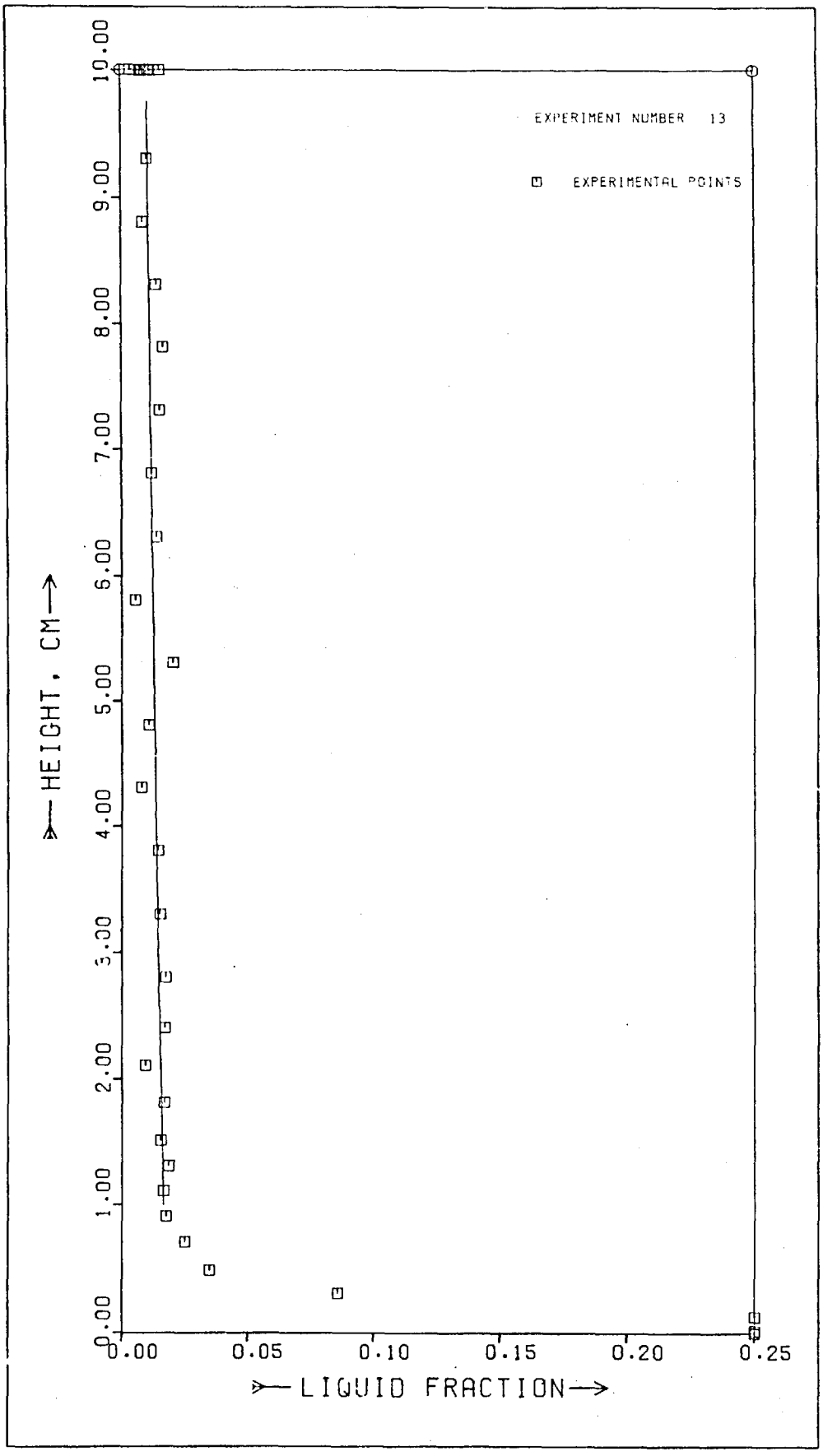

Fig.III. 9.- Dispersion density profile and fitting curve.

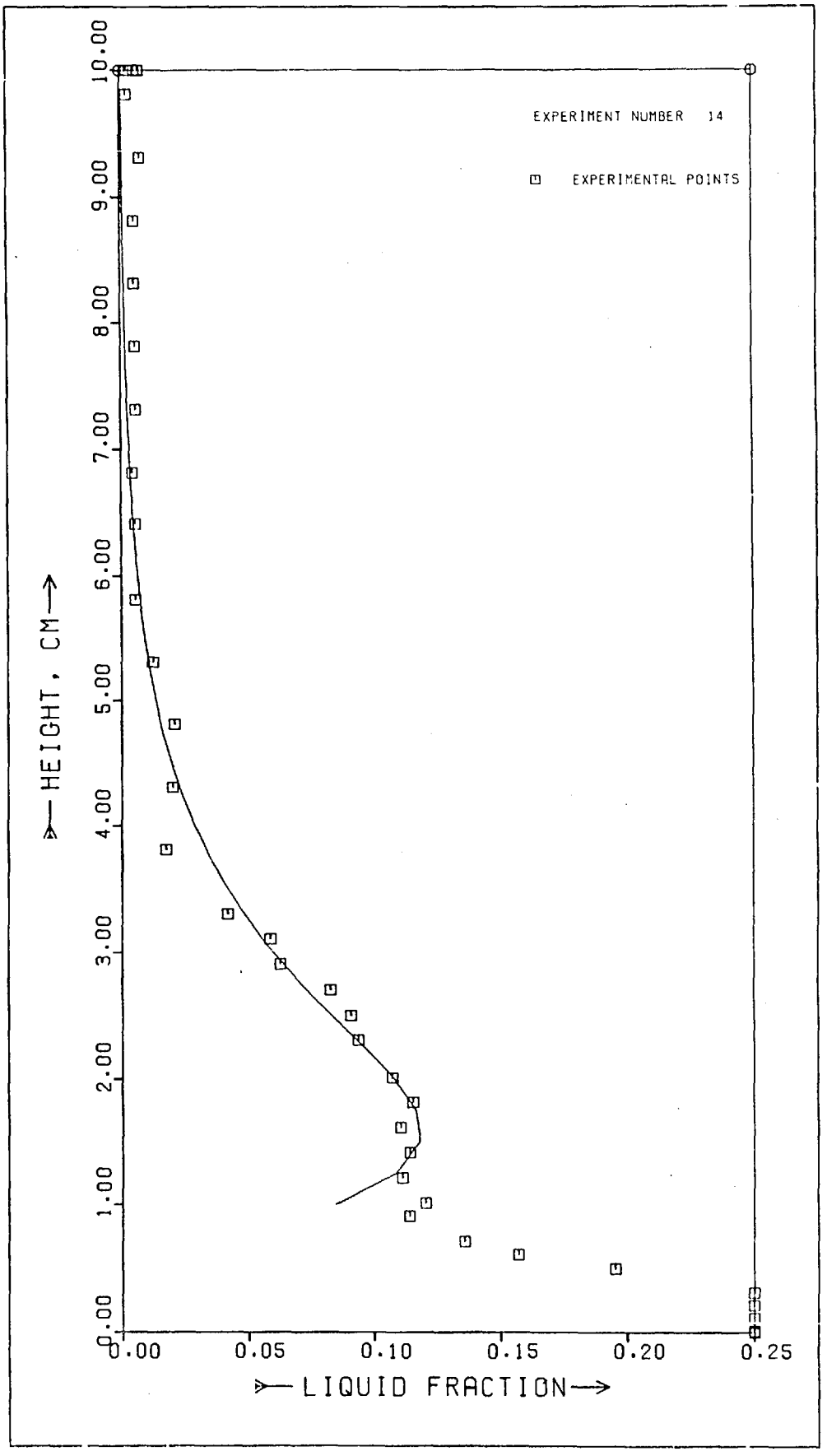

Fig.III.10.- Dispersion density profile and fitting curve.

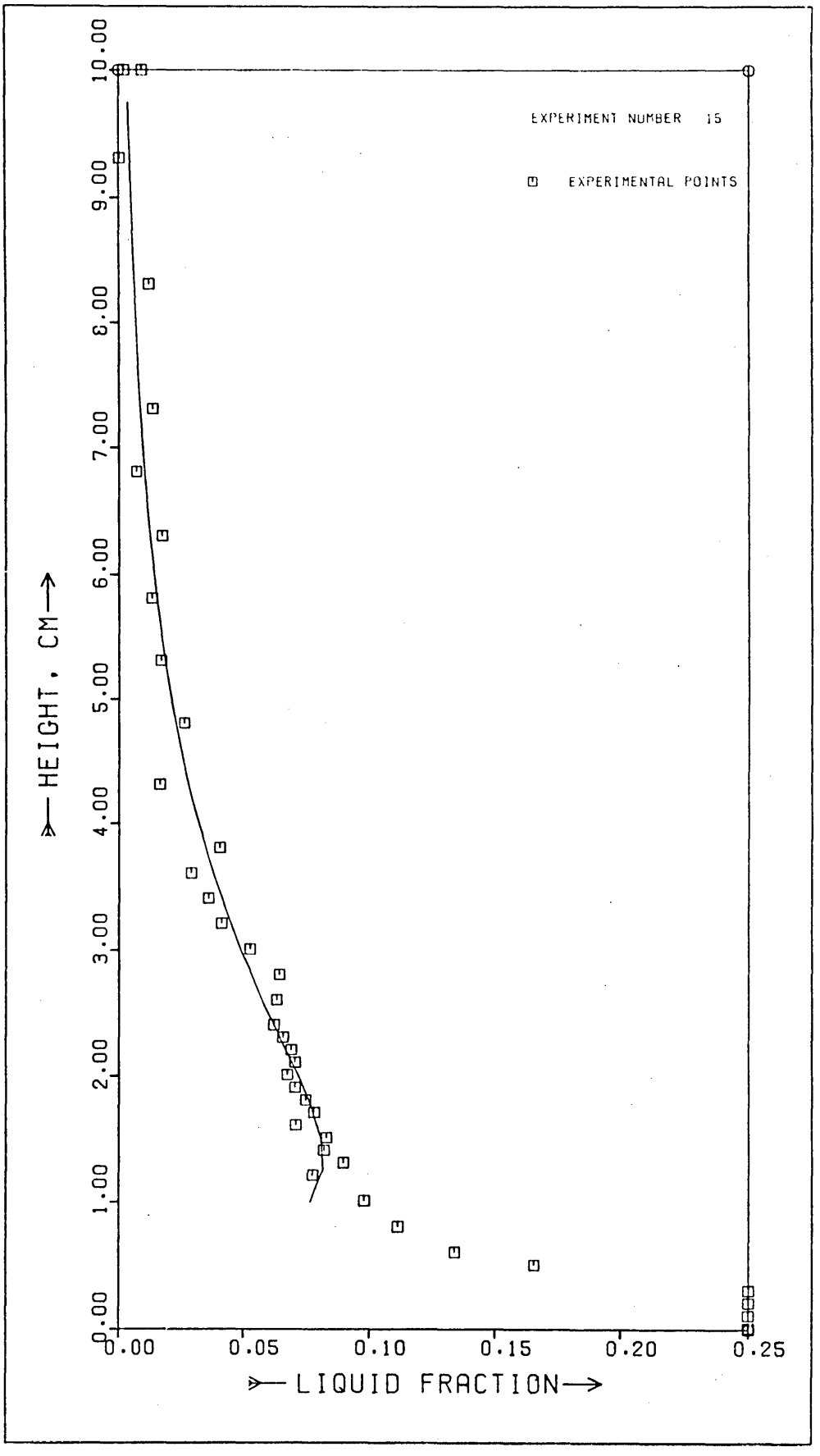

Fig.III.11.- Dispersion density profile and fitting curve.

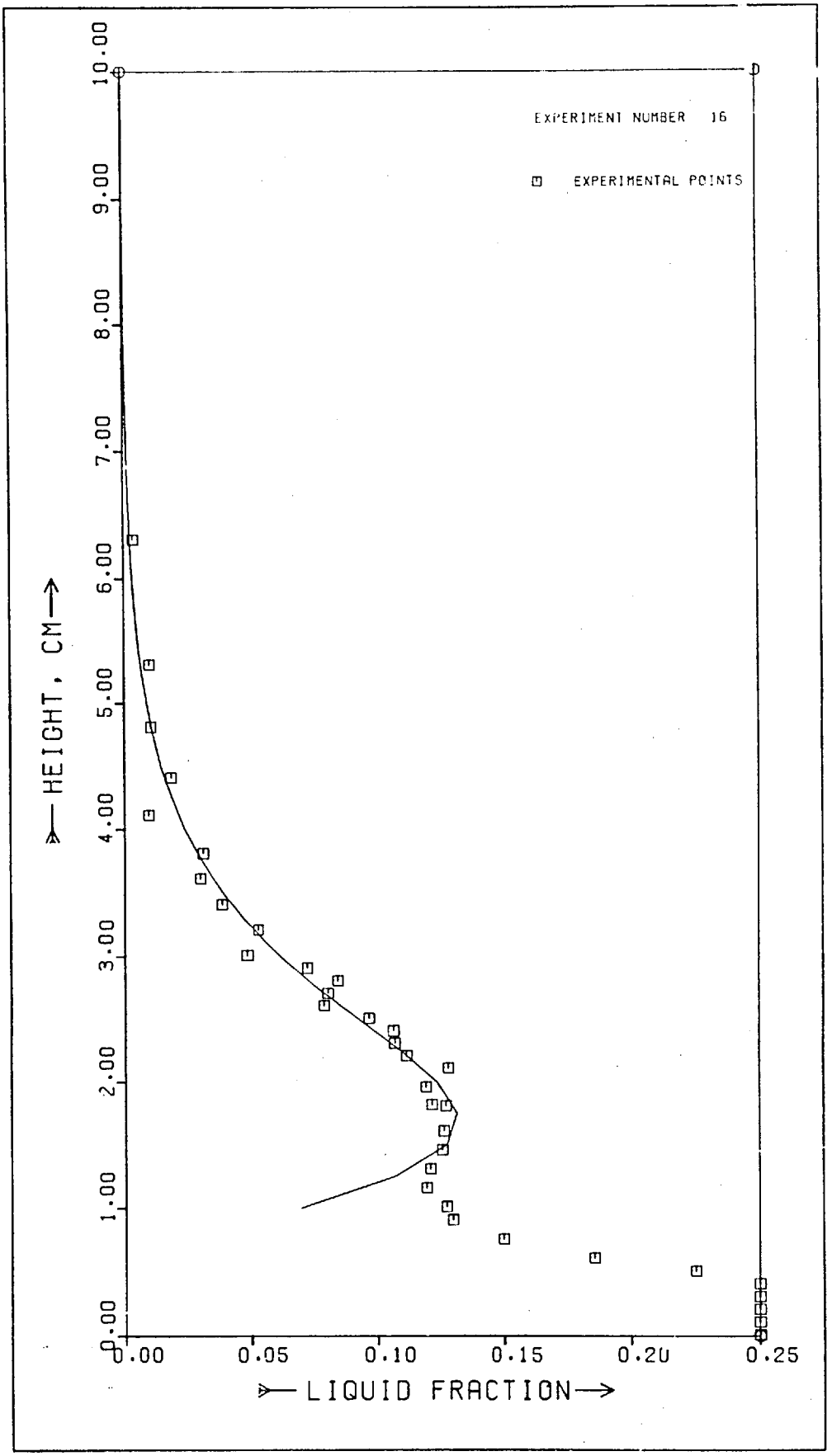

Fig.III.12.- Dispersion density profile and fitting curve.

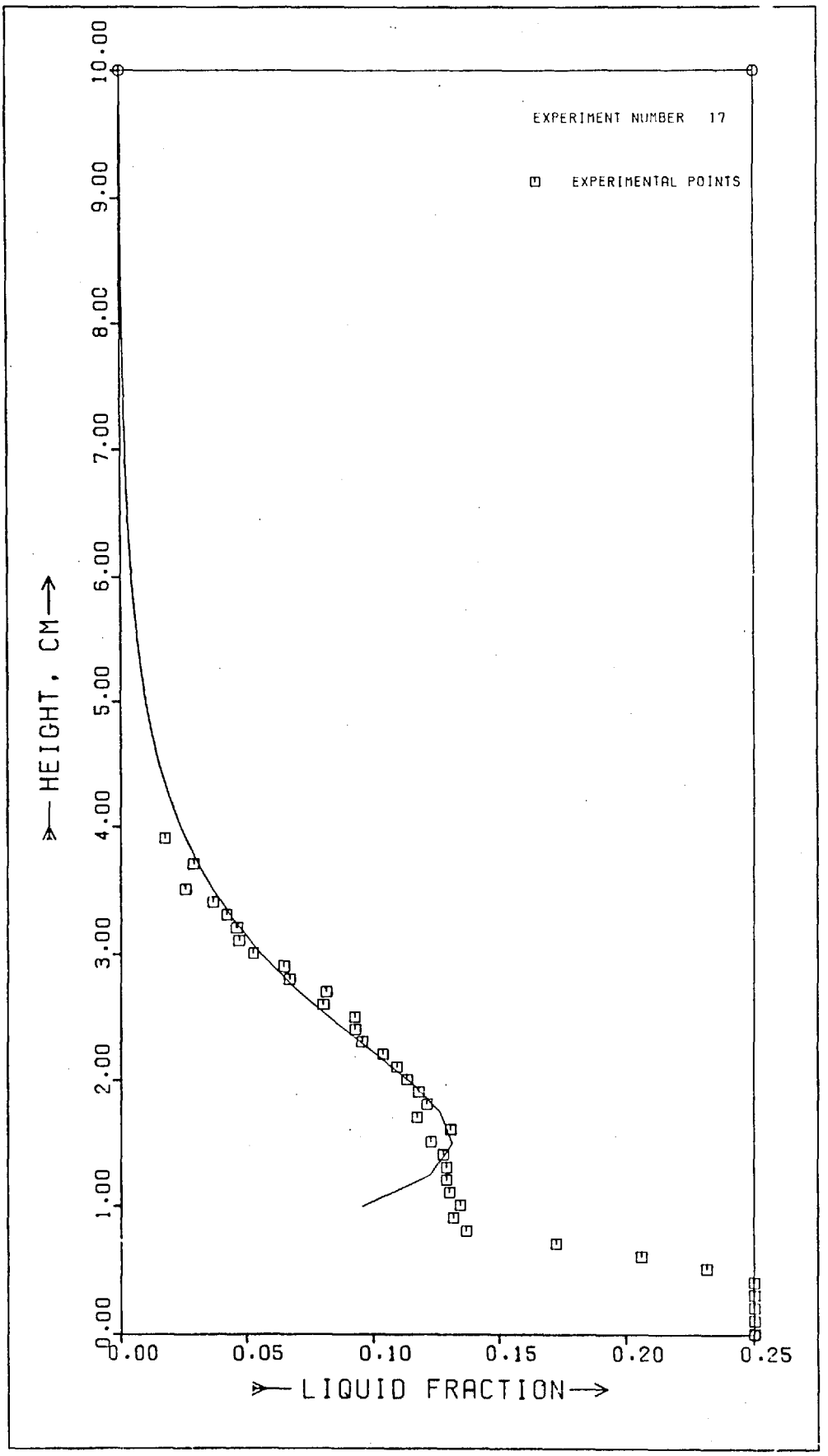

Fig.III.13.- Dispersion density profile and fitting curve.

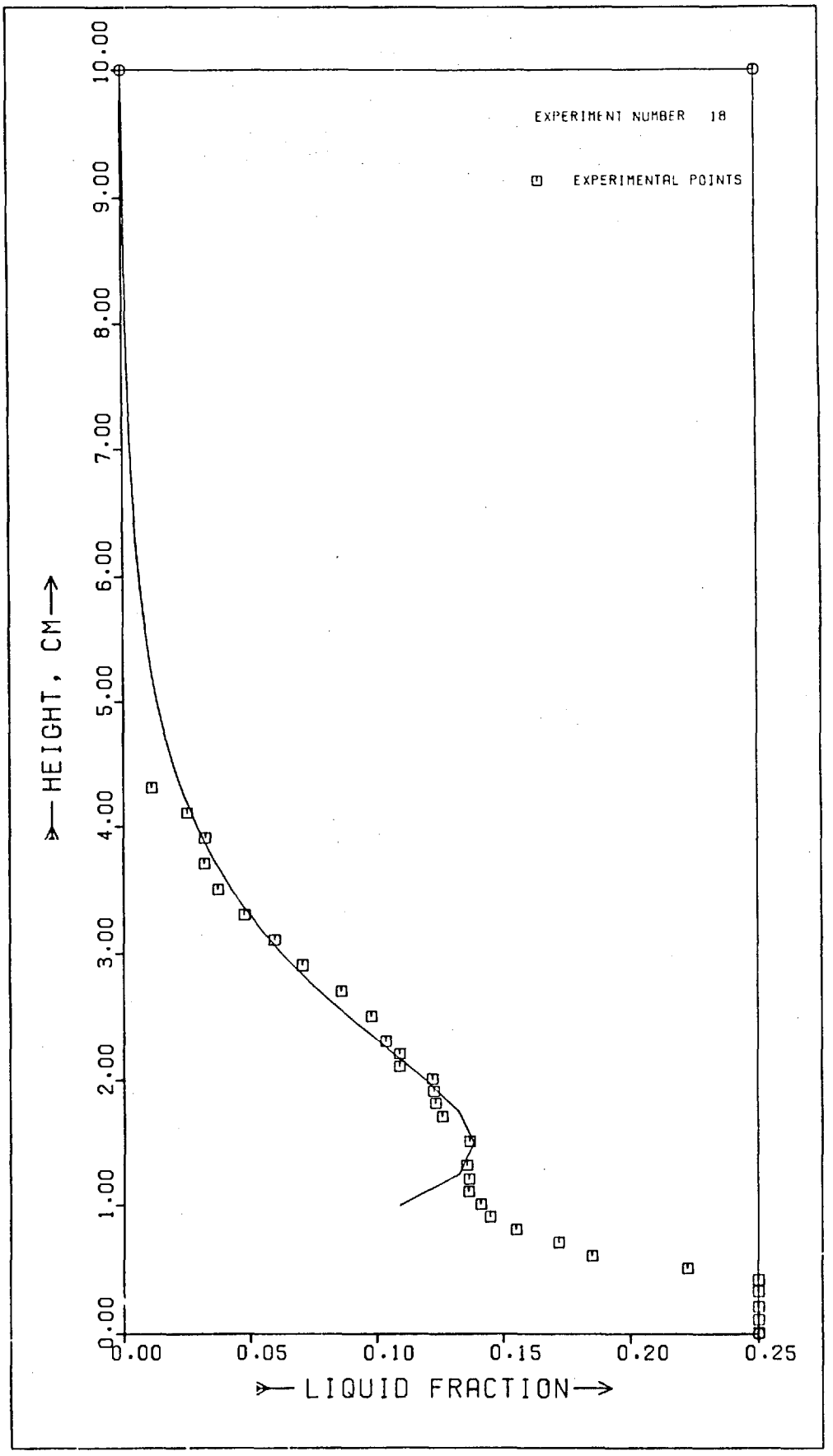

Fig.III.14.- Dispersion density profile and fitting curve.

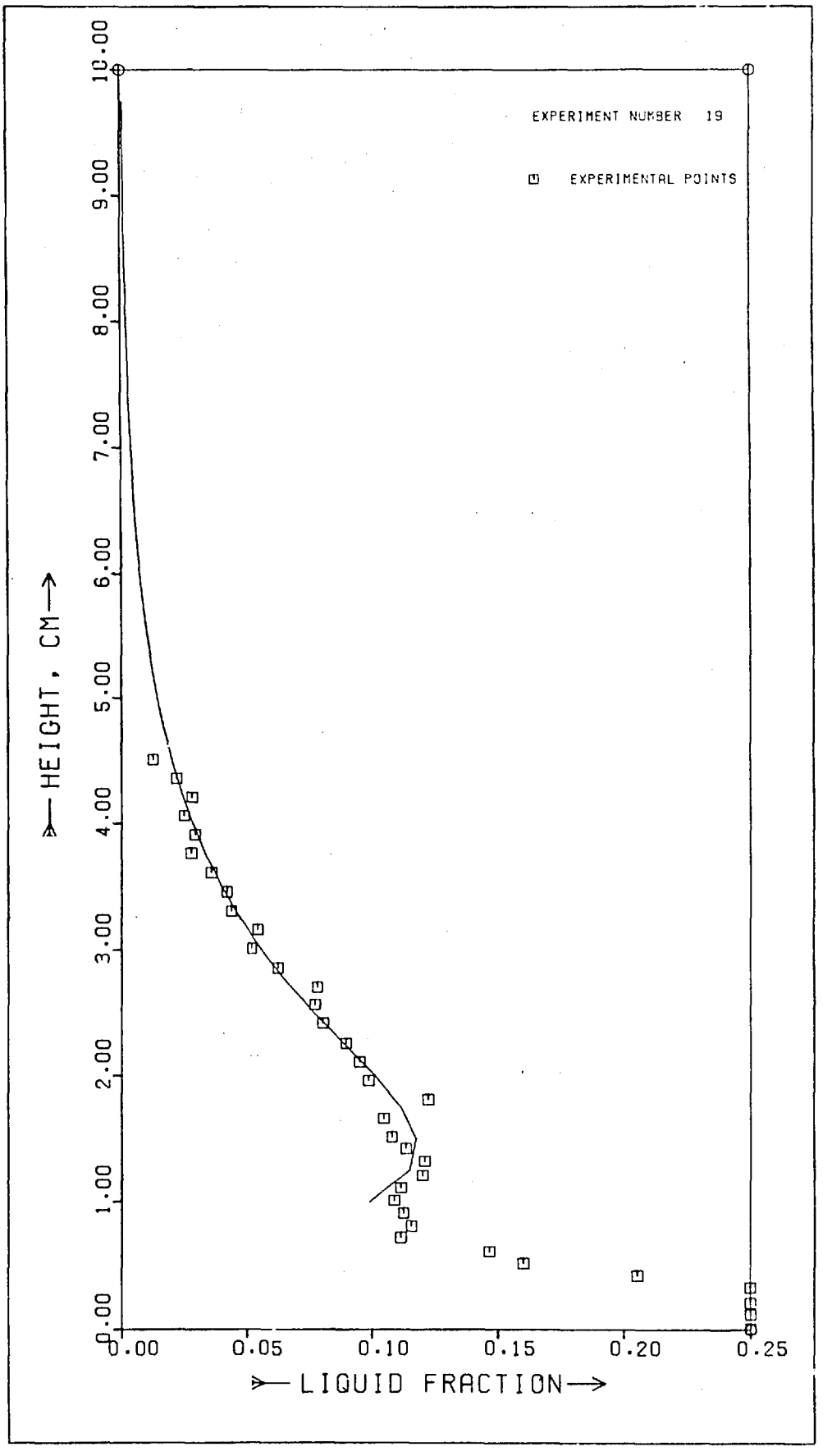

Fig.III.15.- Dispersion density profile and fitting curve.

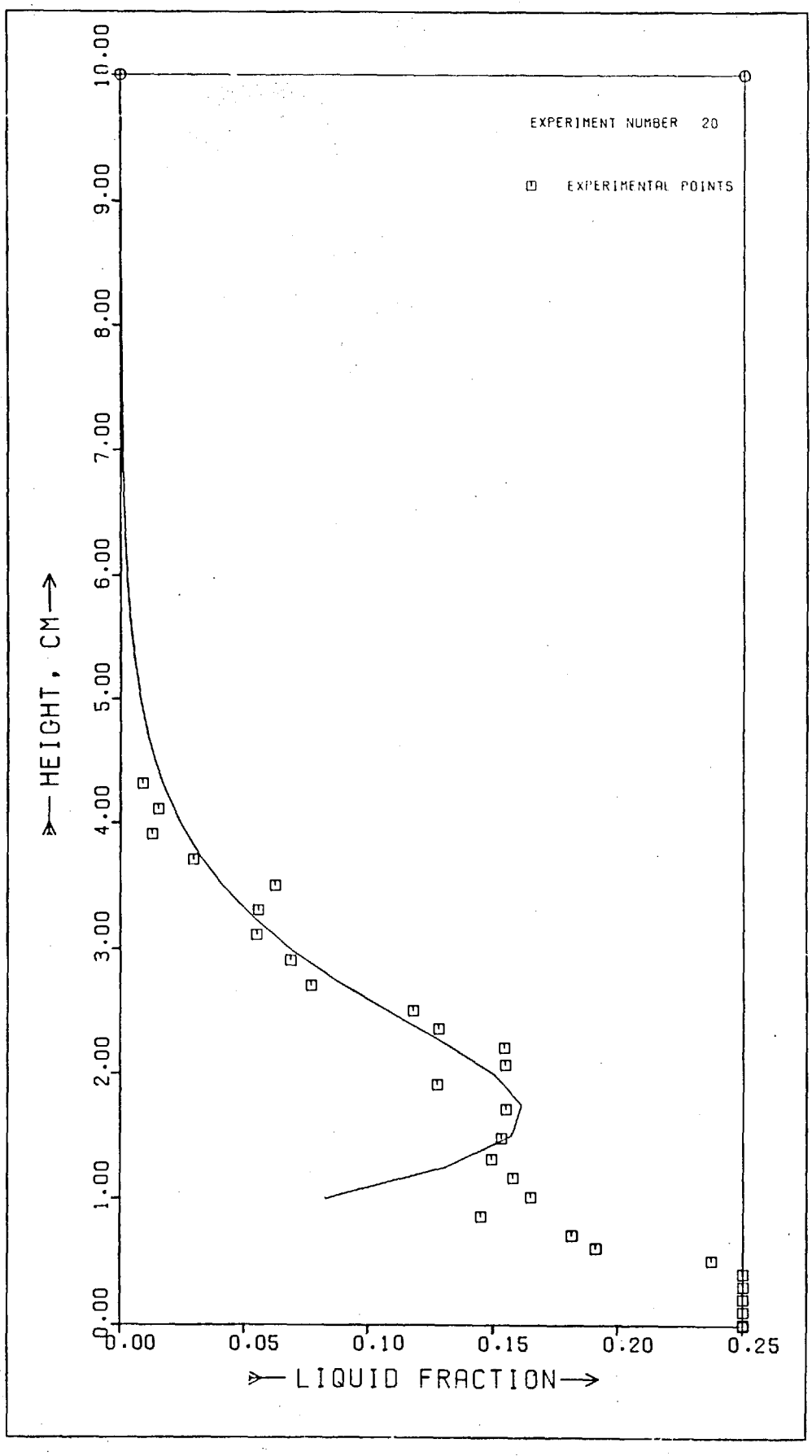

Fig.III.16.- Dispersion density profile and fitting curve.

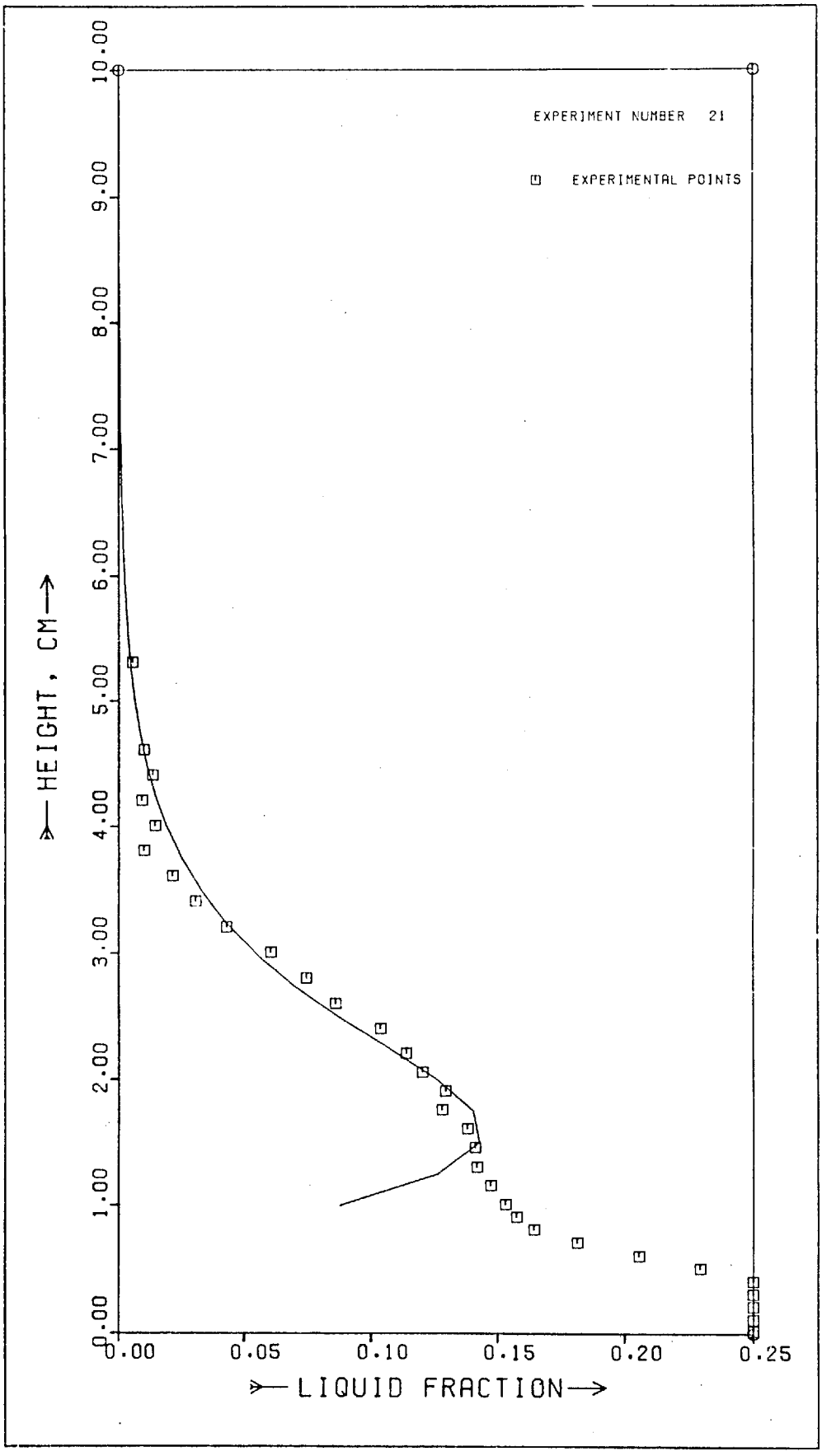

Fig.III.17.- Dispersion density profile and fitting curve.

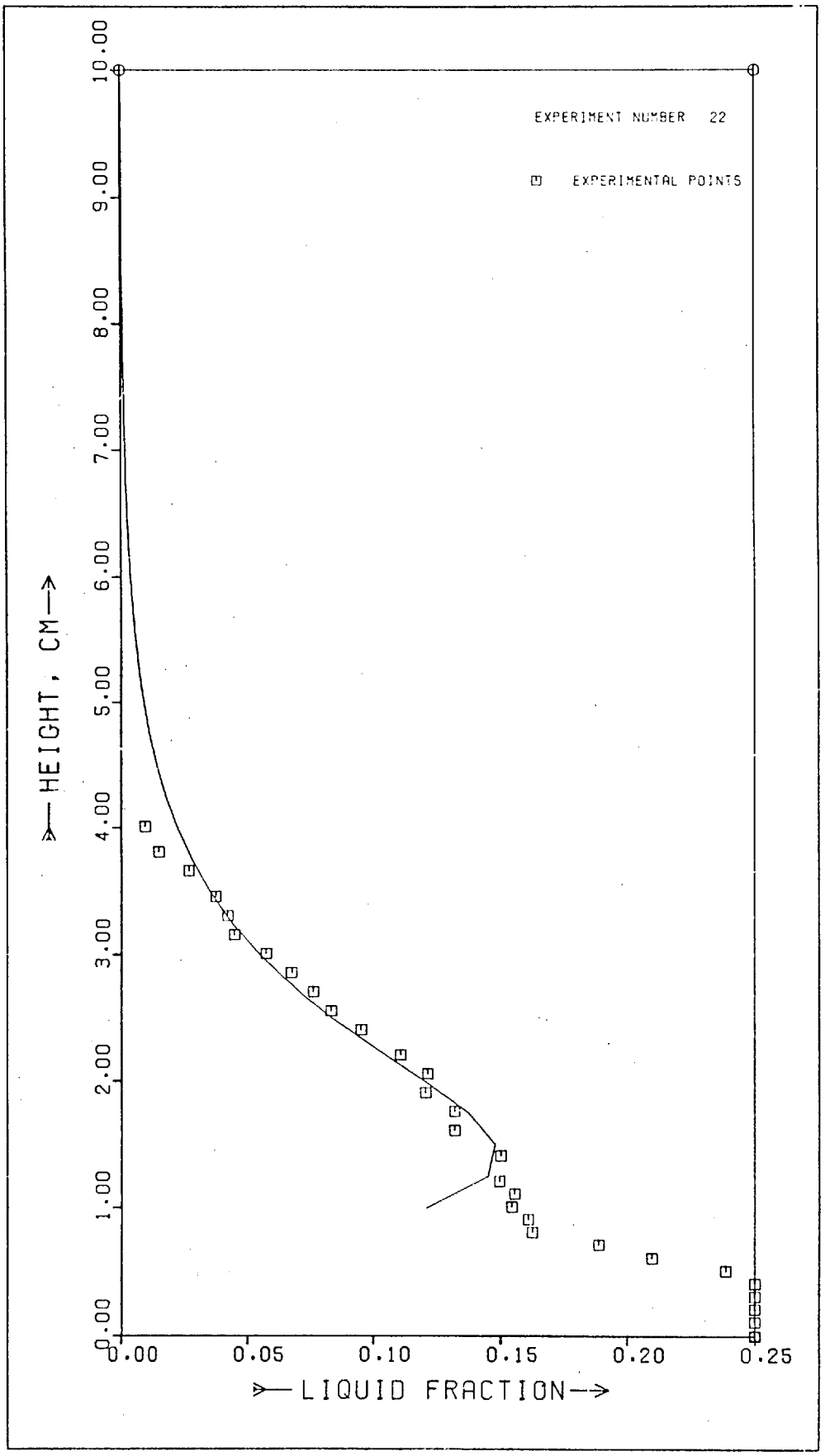

Fig.III.18.- Dispersion density profile and fitting curve.

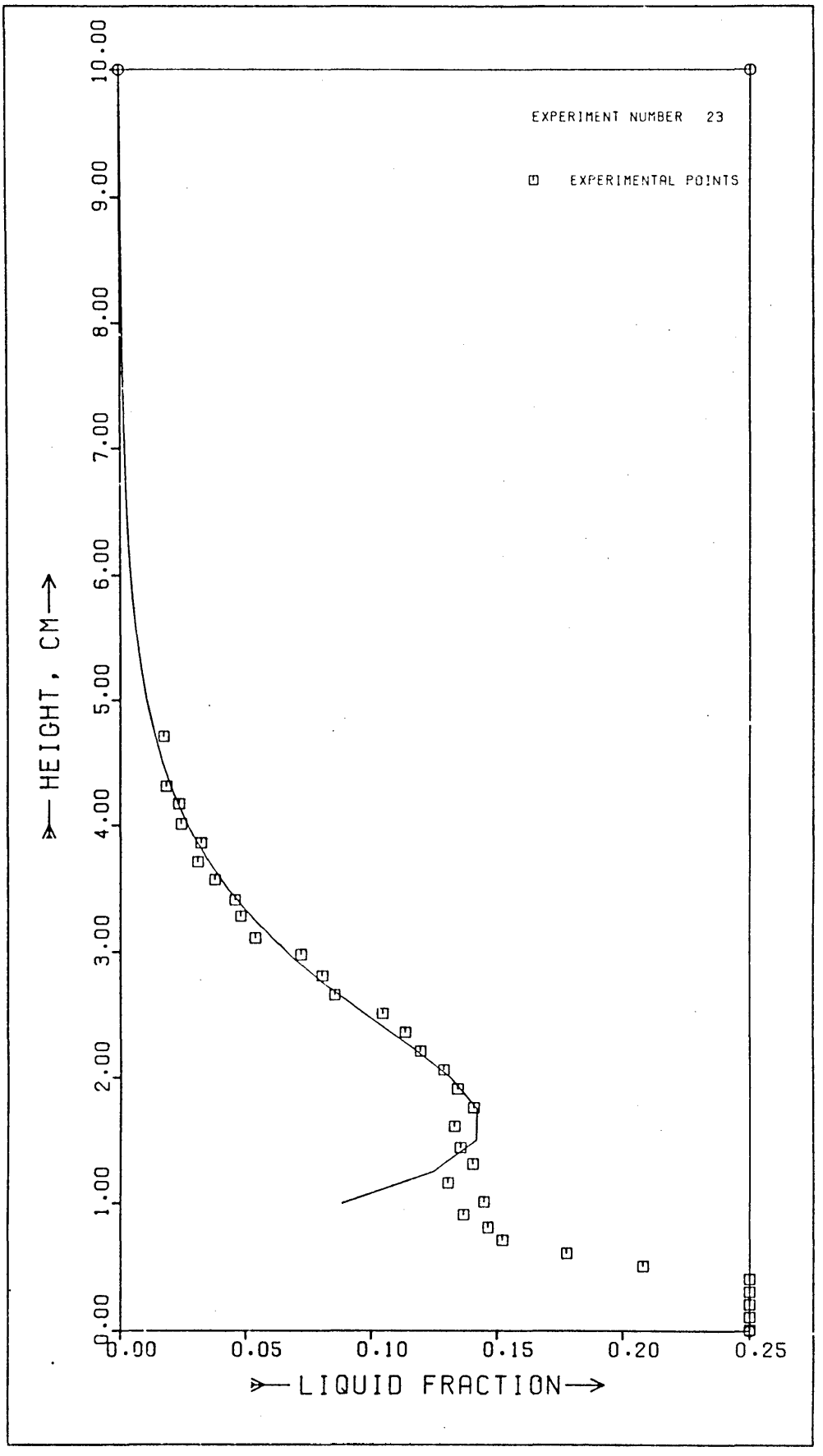

Fig.III.19.- Dispersion density profile and fitting curve.

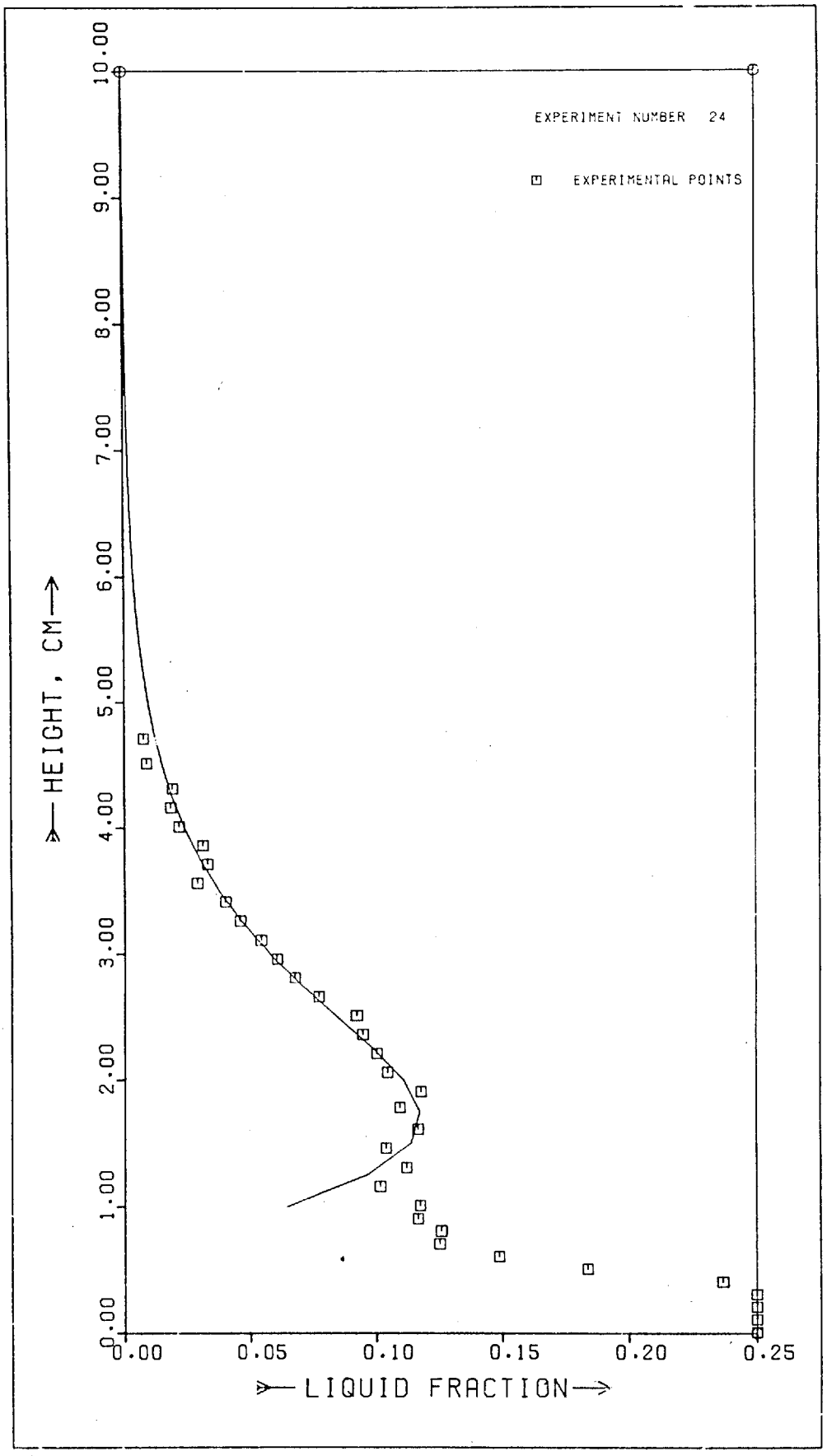

Fig.III.20.- Dispersion density profile and fitting curve.

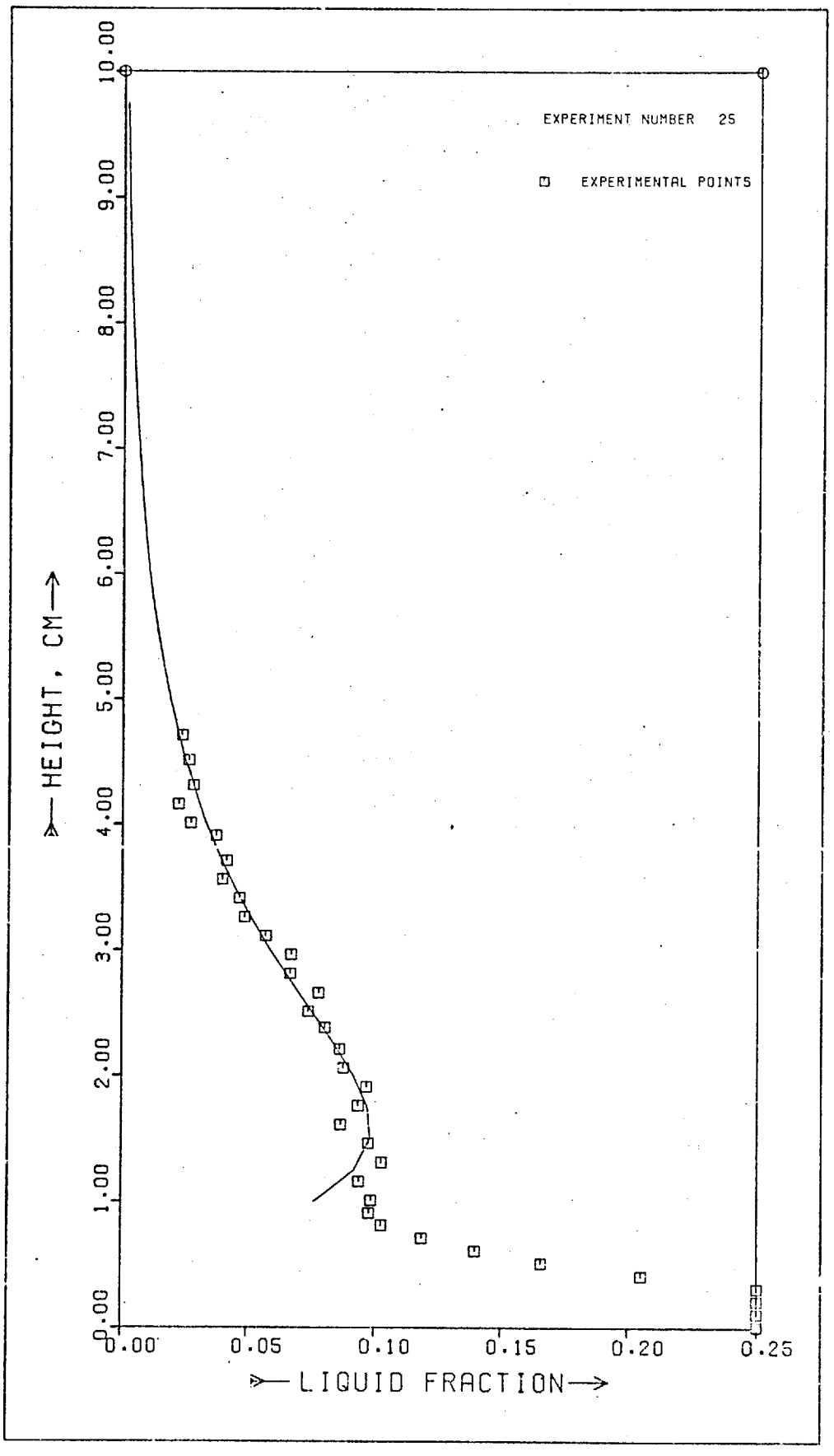

Fig.III.21.- Dispersion density profile and fitting curve.

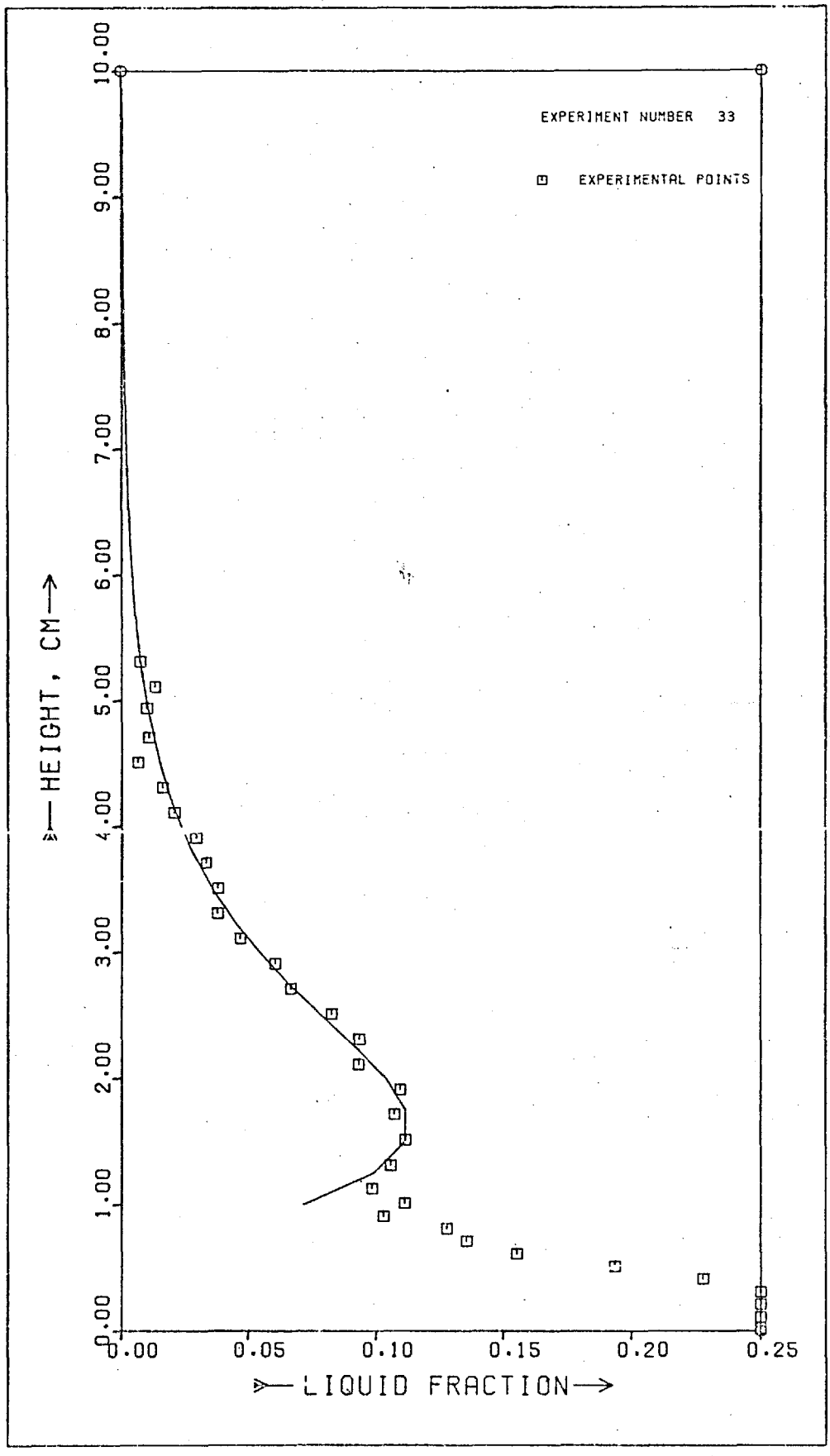

Fig.III.22.- Dispersion density profile and fitting curve.

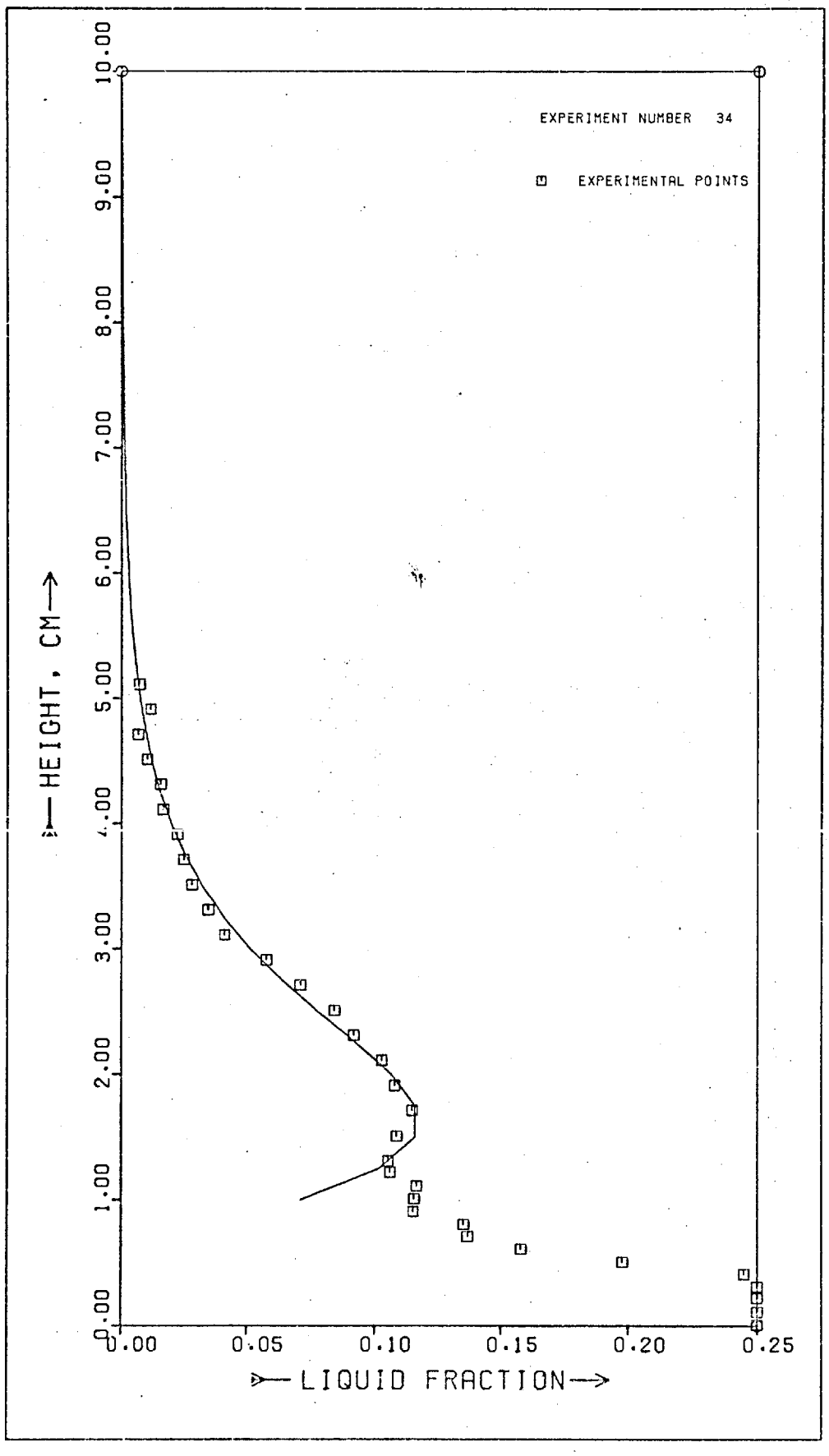

Fig.III.23.- Dispersion donsity profile and fitting curve.

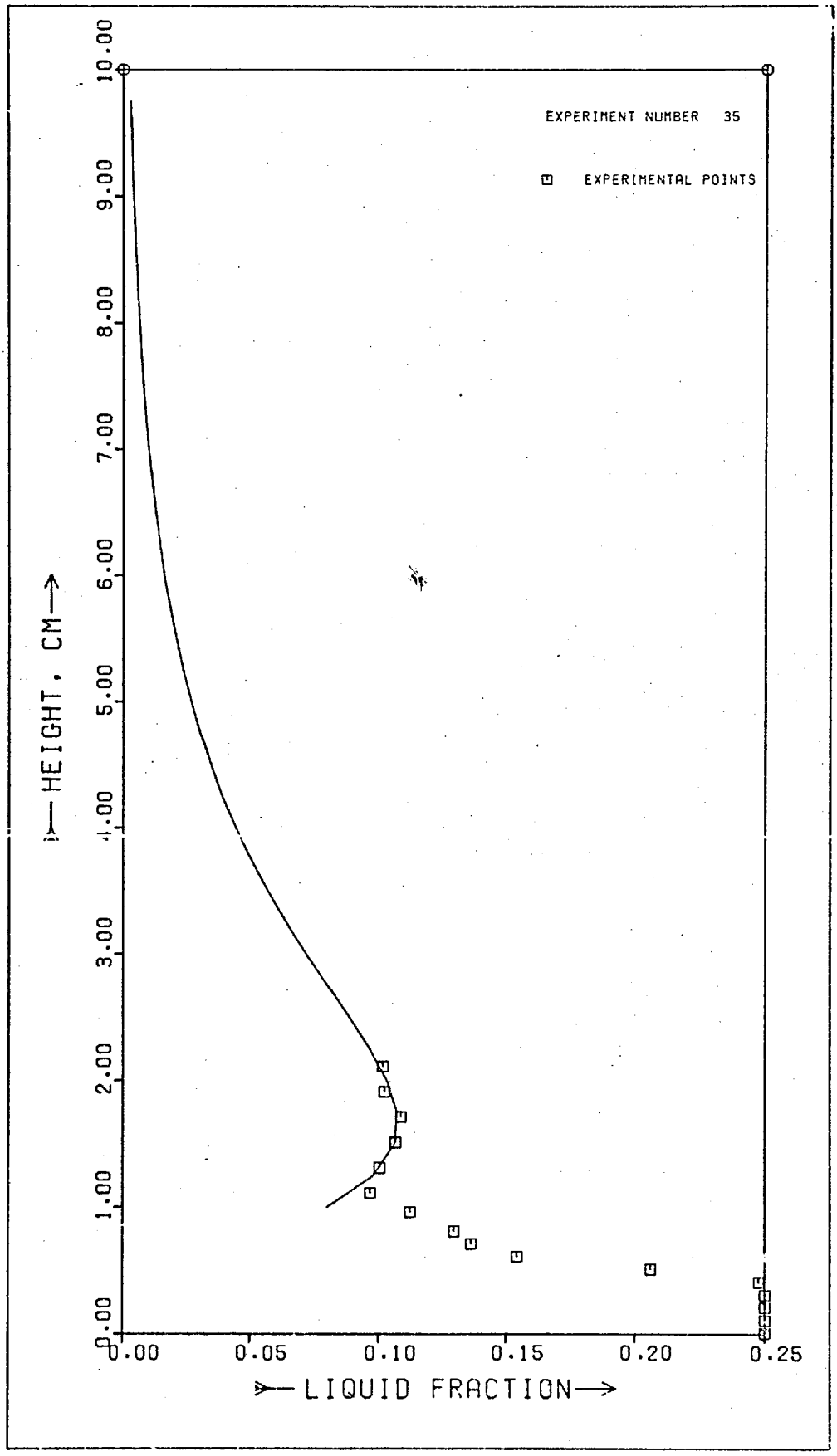

Fig.III.24.- Dispersion density profile and fitting curve.

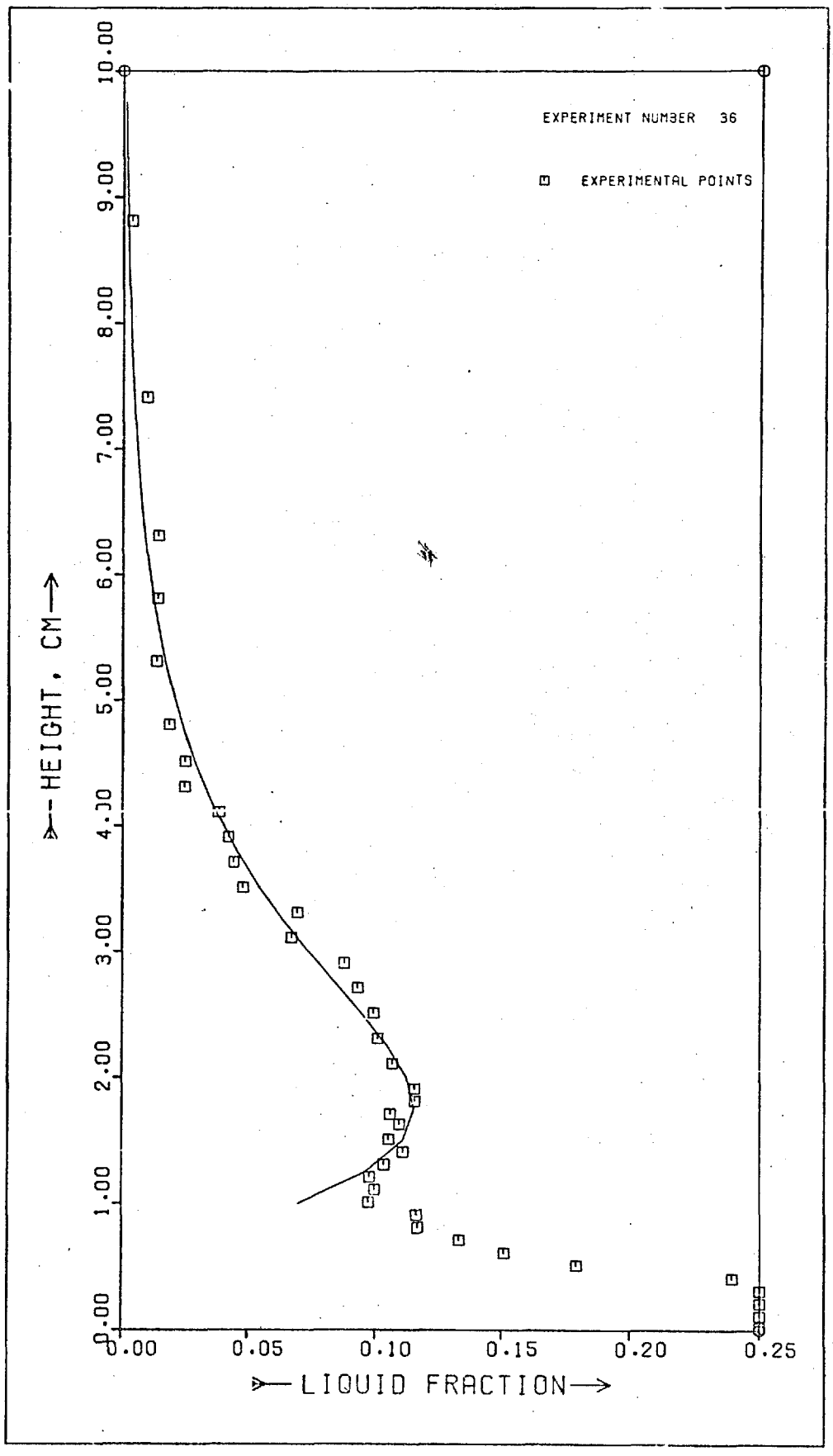

Fig.III.25.- Dispersion density profile and fitting curve.

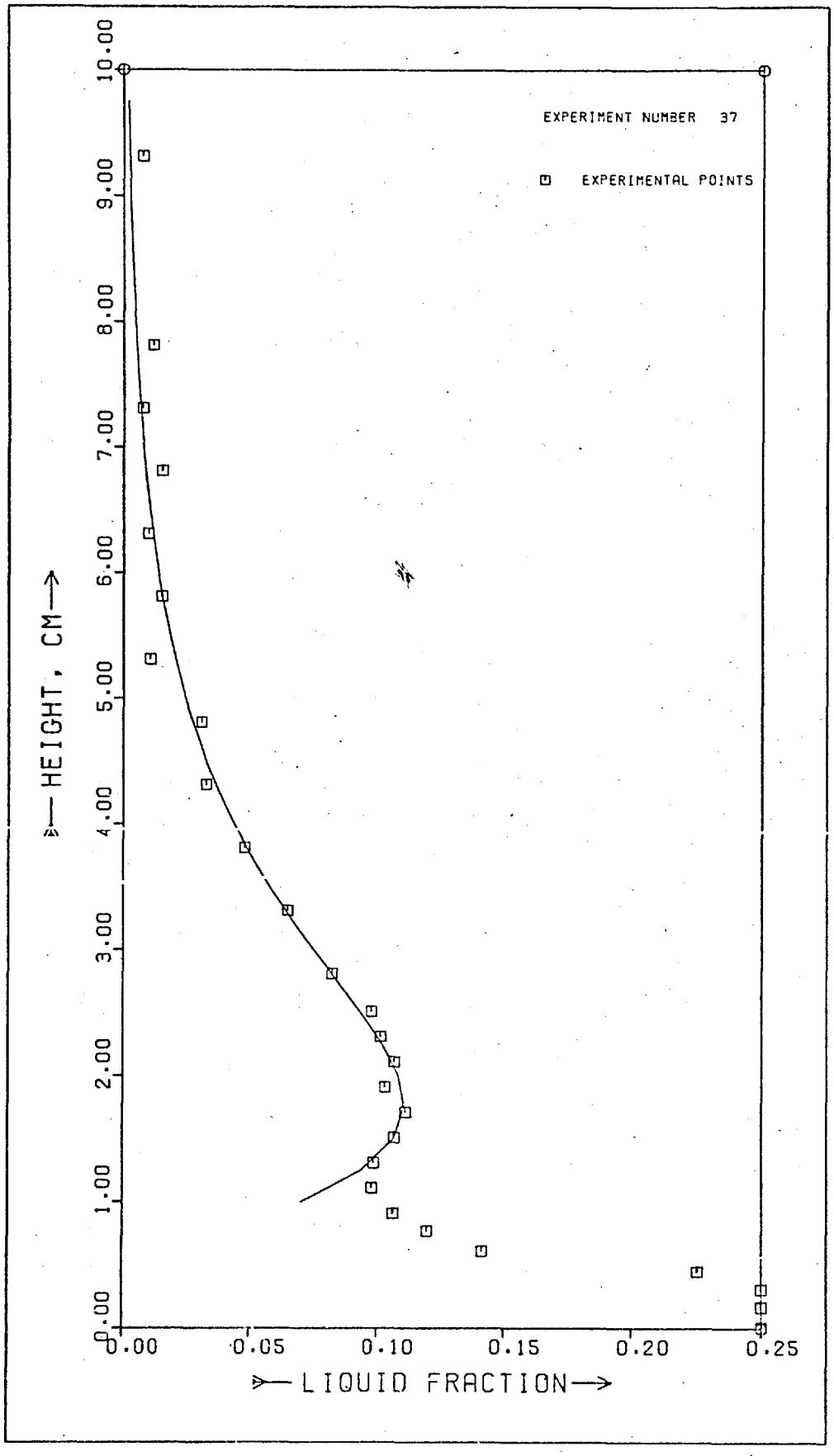

Fig.III.26.- Dispersion density profile and fitting curve.

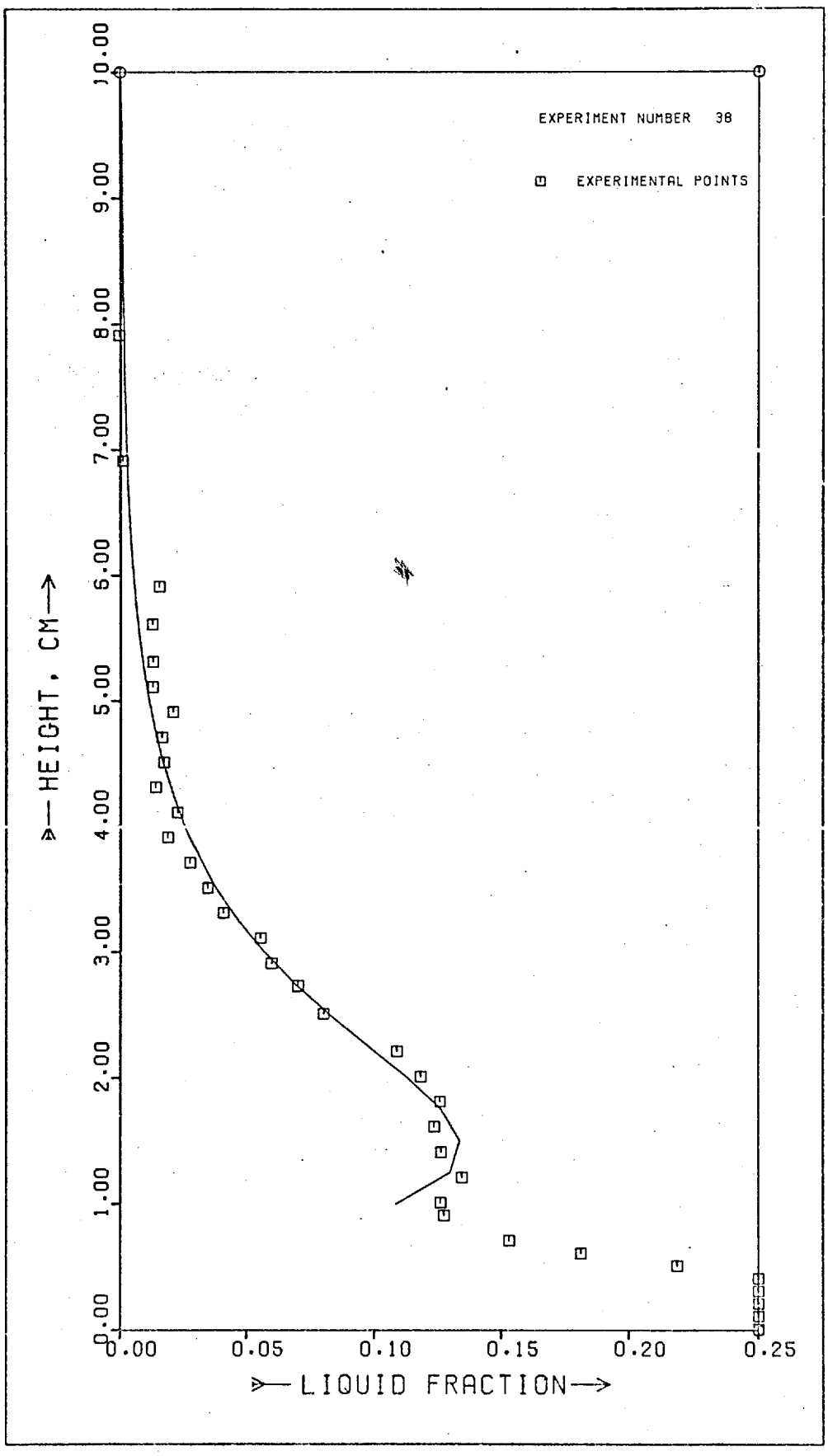

Fig.III.27.- Dispersion density profile and fitting curve.

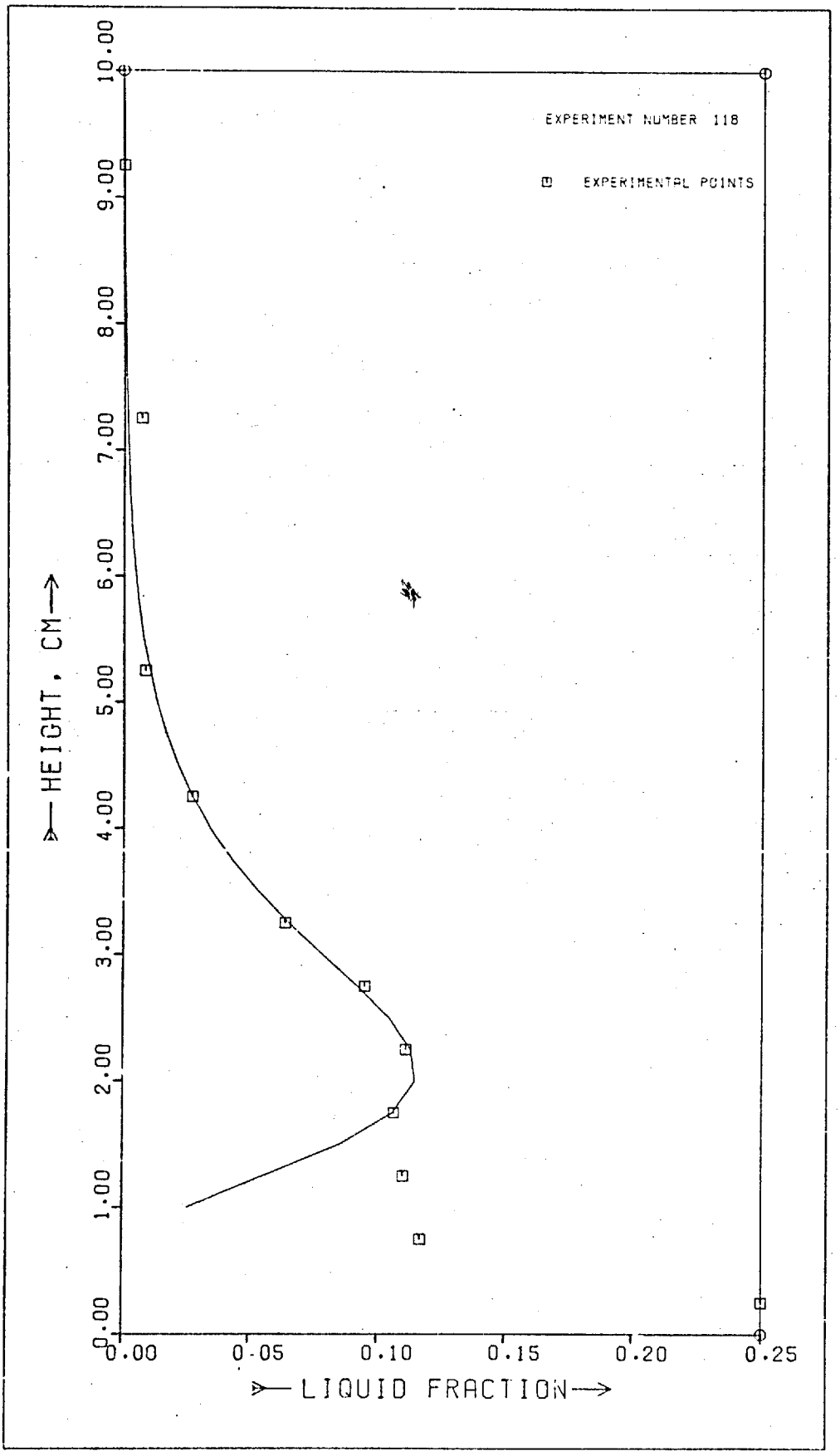

Fig.III.28.- Dispersion density profile and fitting curve.

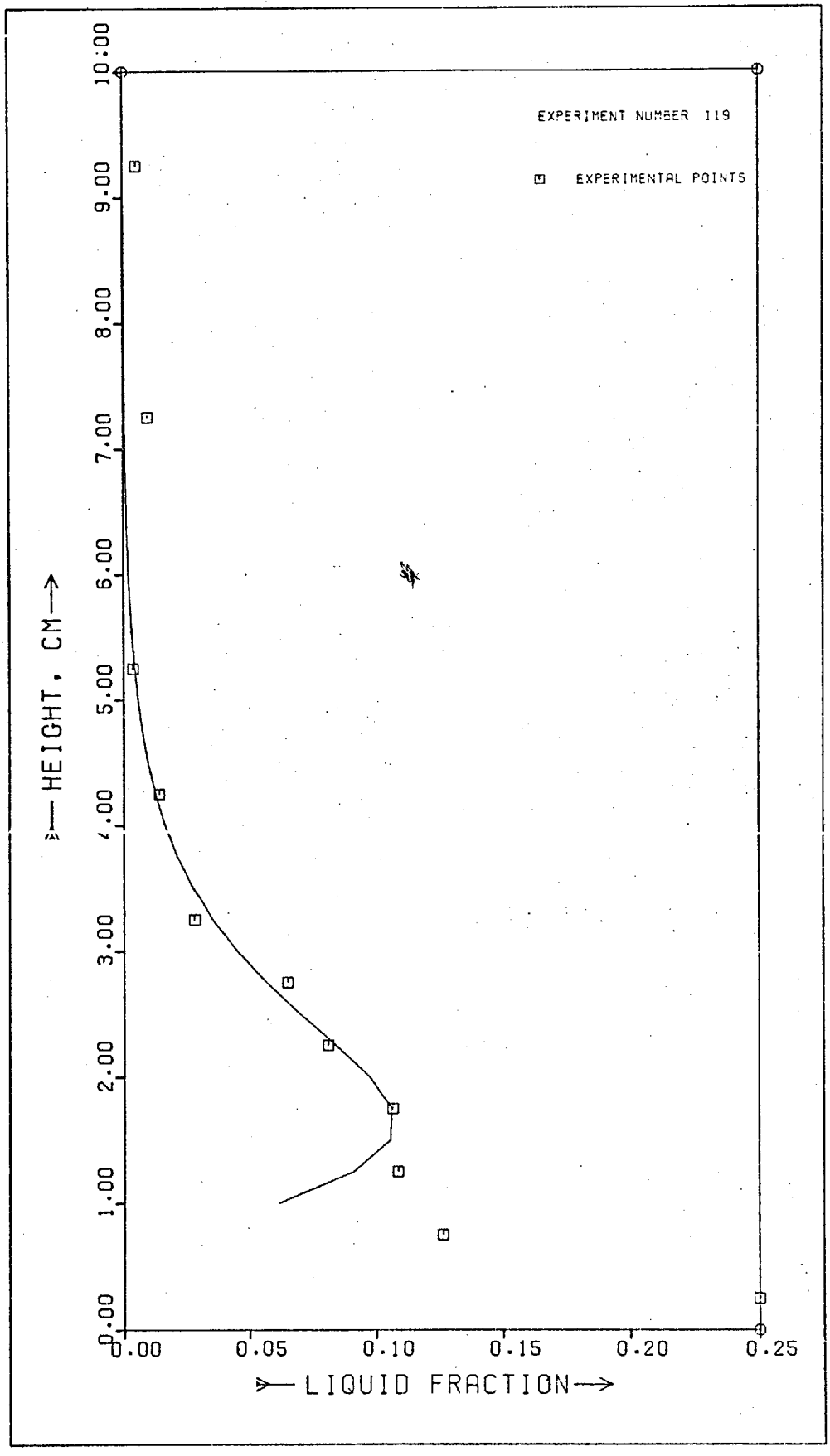

Fig.III.29.- Dispersion density profile and fitting curve.

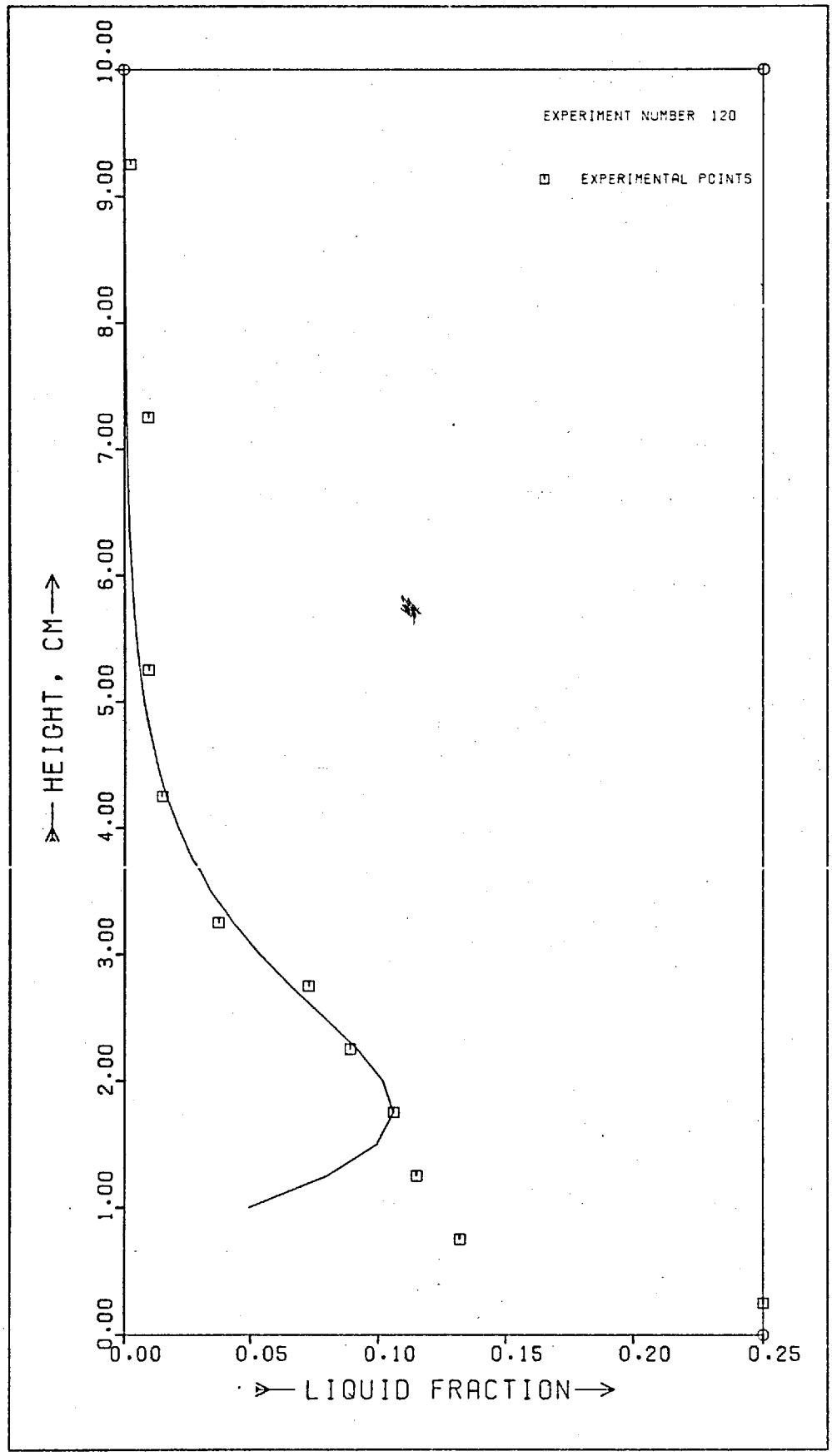

Fig.III.30.- Dispersion density profile and fitting curve.

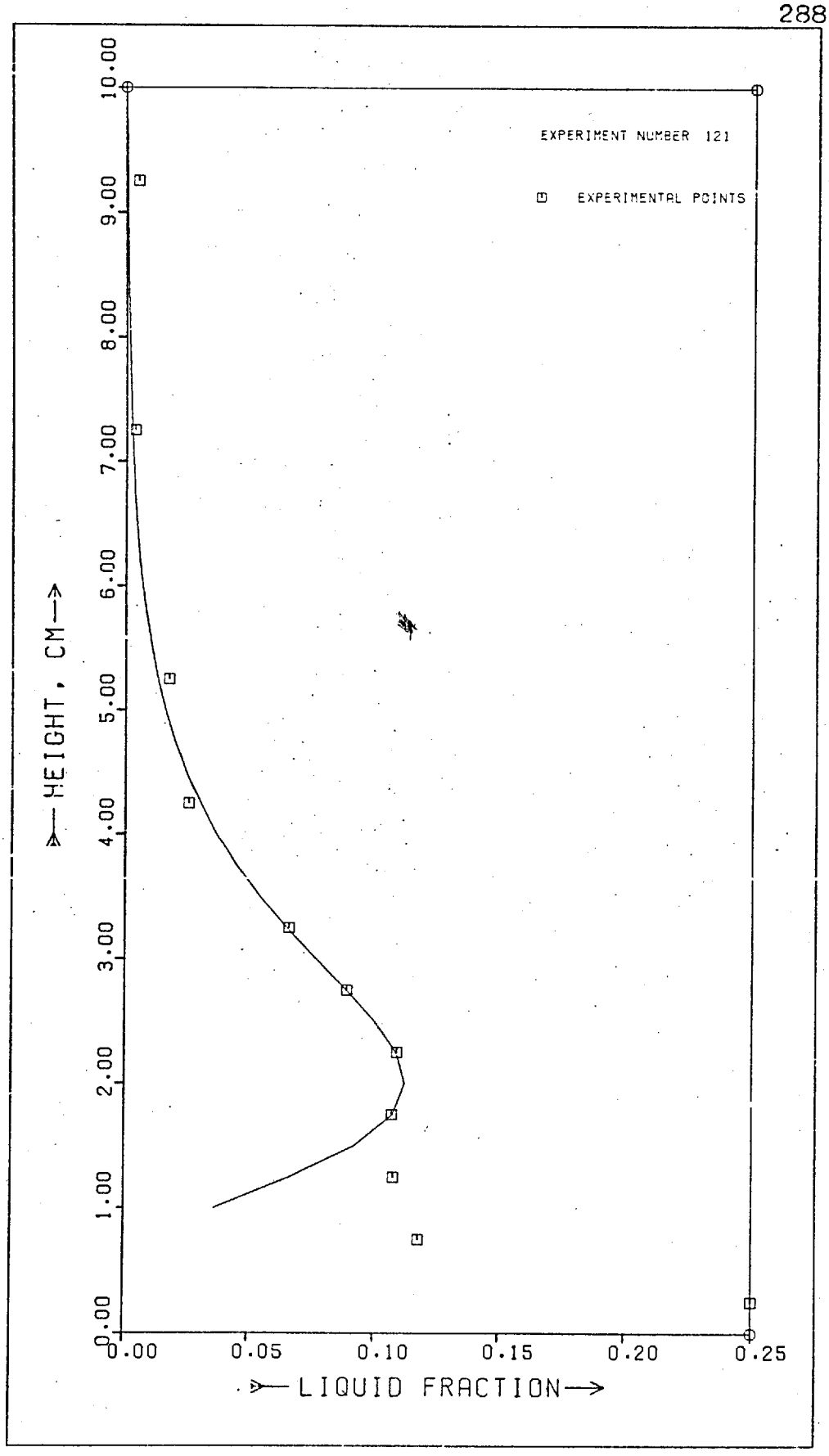

Fig.III.31.- Dispersion density profile and fitting curve.

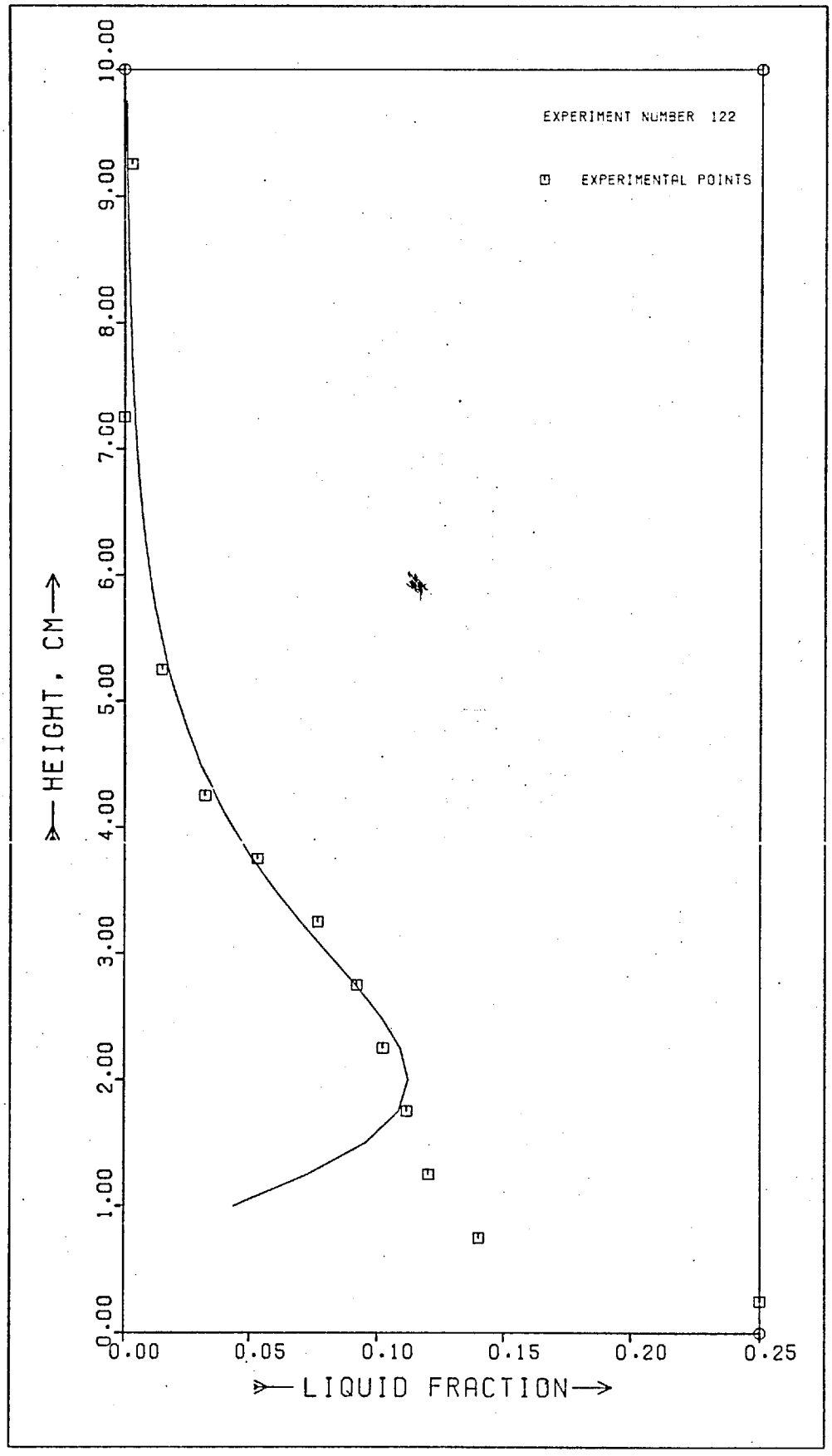

Fig.III.32.- Dispersion density profile and fitting curve.

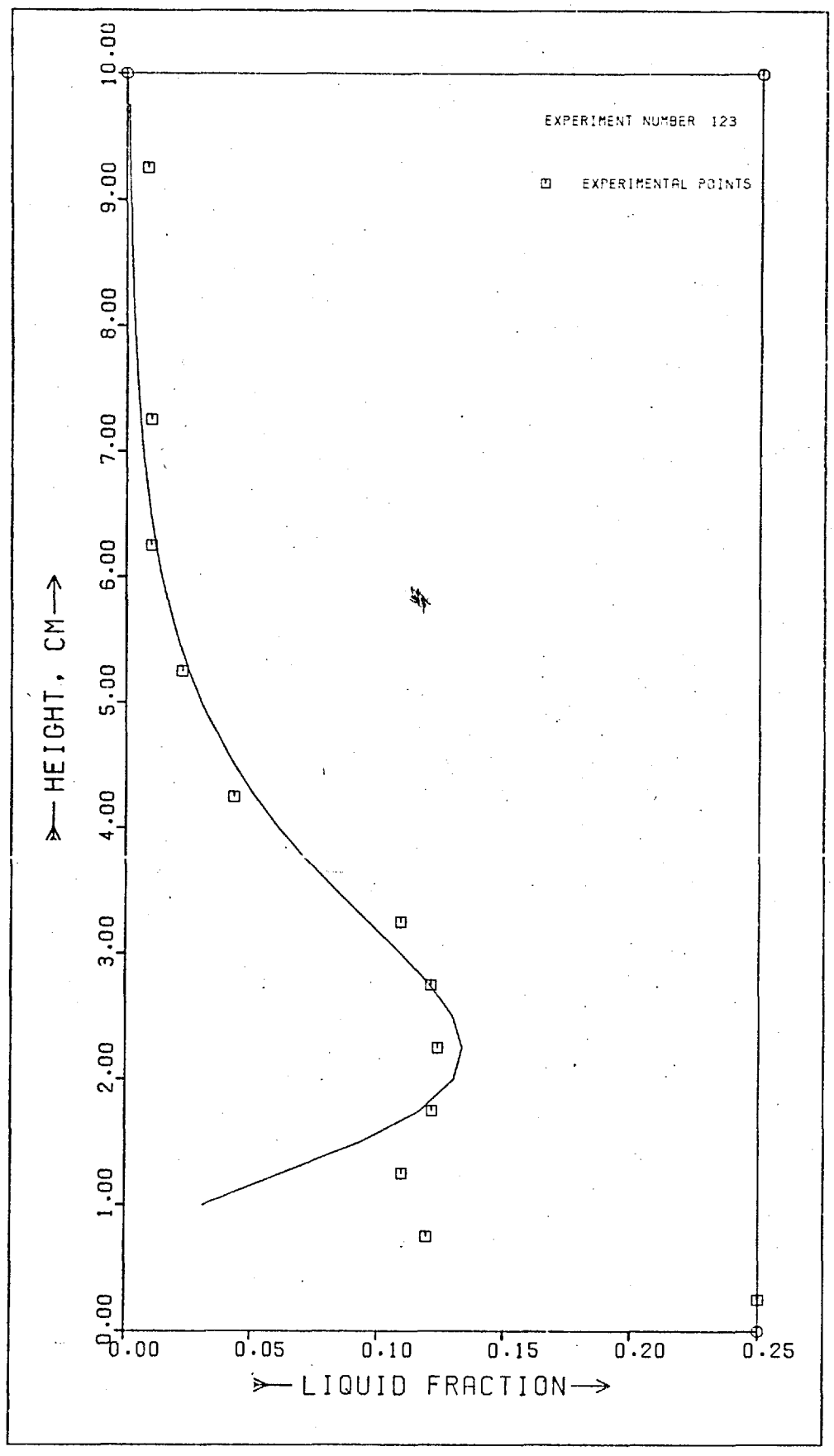

Fig.III.33.- Dispersion density profile and fitting curve.

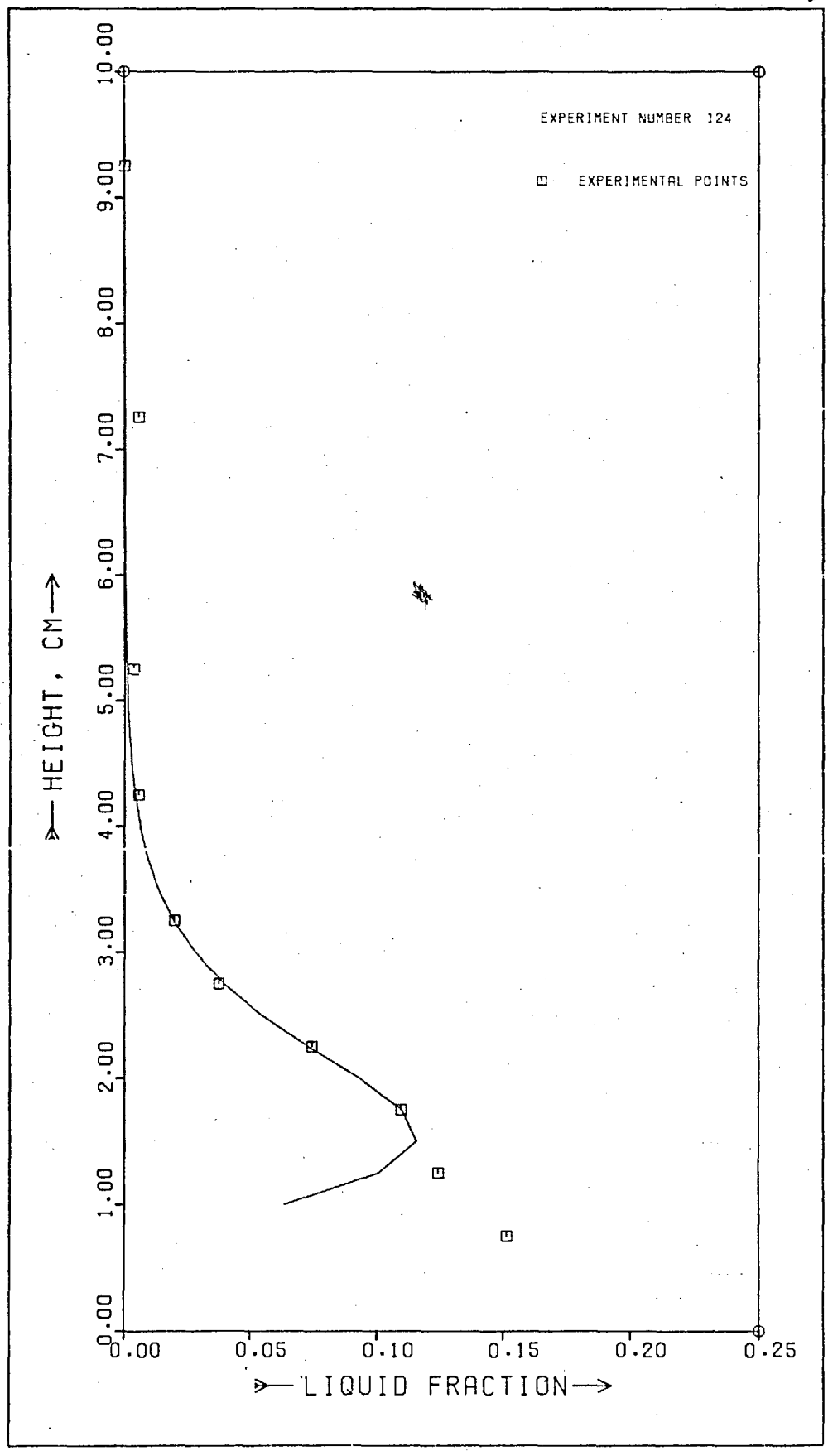

Fig.III.34.- Dispersion density profile and fitting curve.

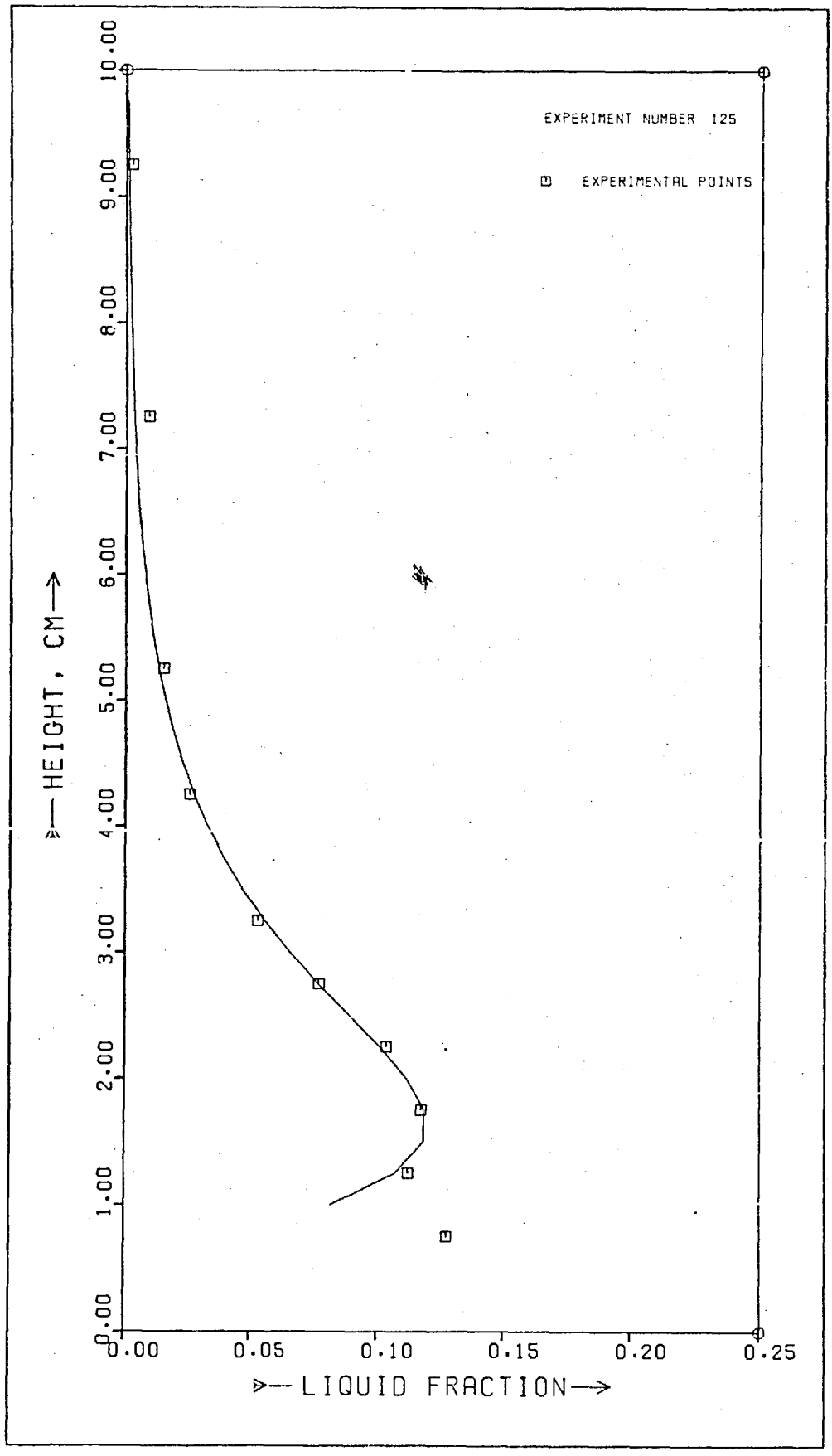

Fig.III.35.- Dispersion density profile and fitting curve.

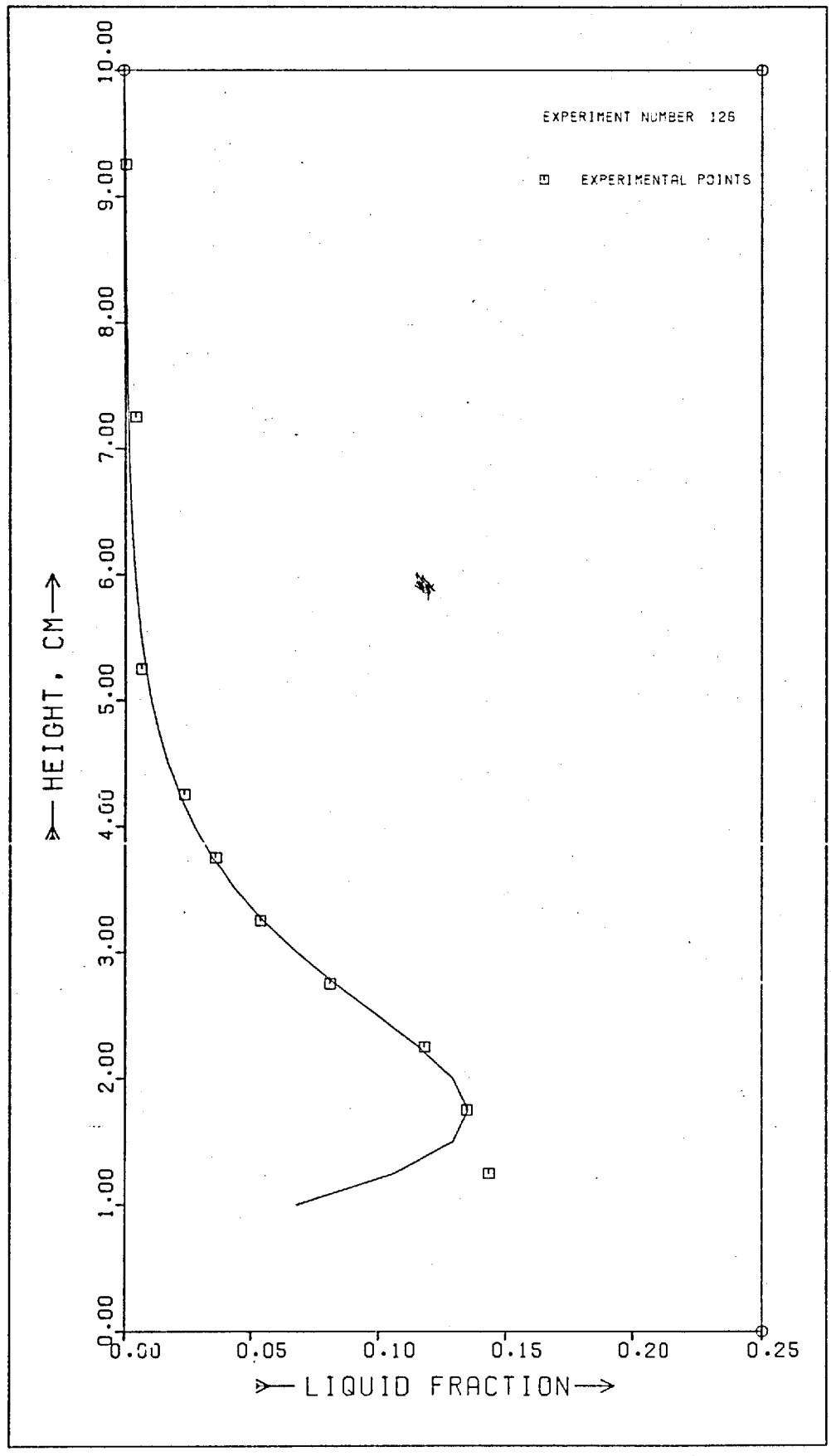

Fig.III.36.- Dispersion density profile and fitting curve.

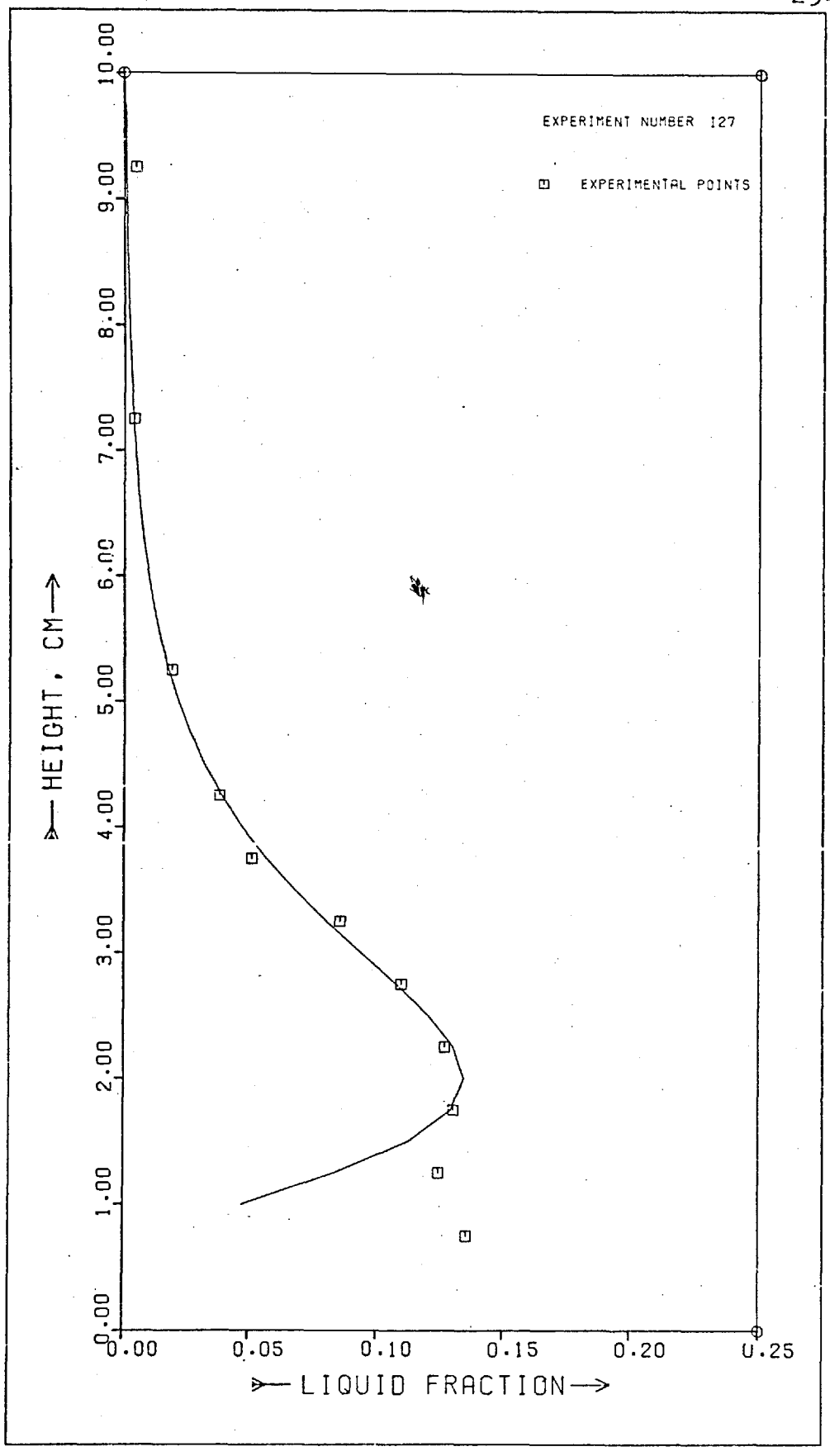

Fig.III.37.- Dispersion density profile and fitting curve.

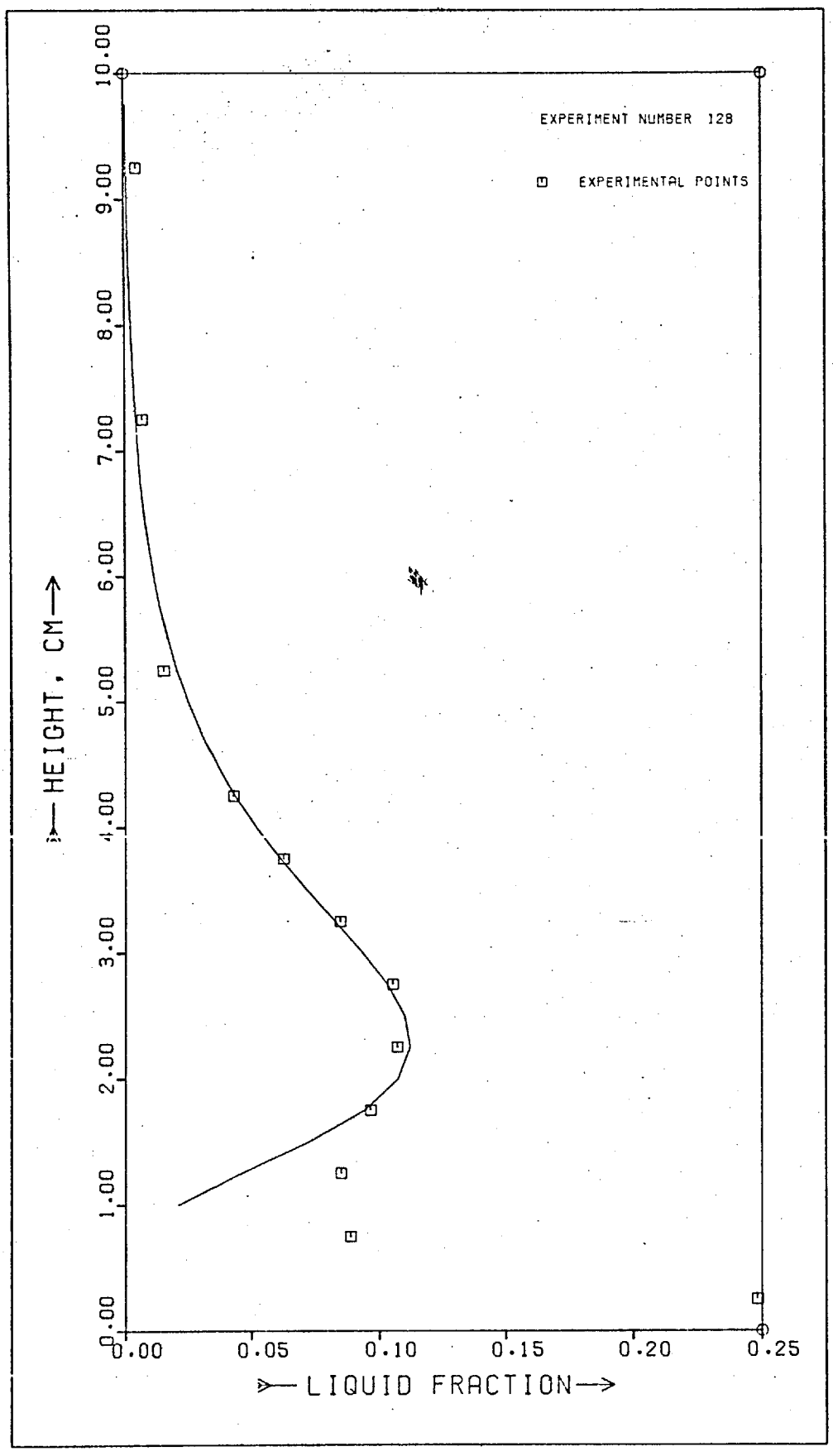

Fig.III.38.- Dispersion density profile and fitting curve.

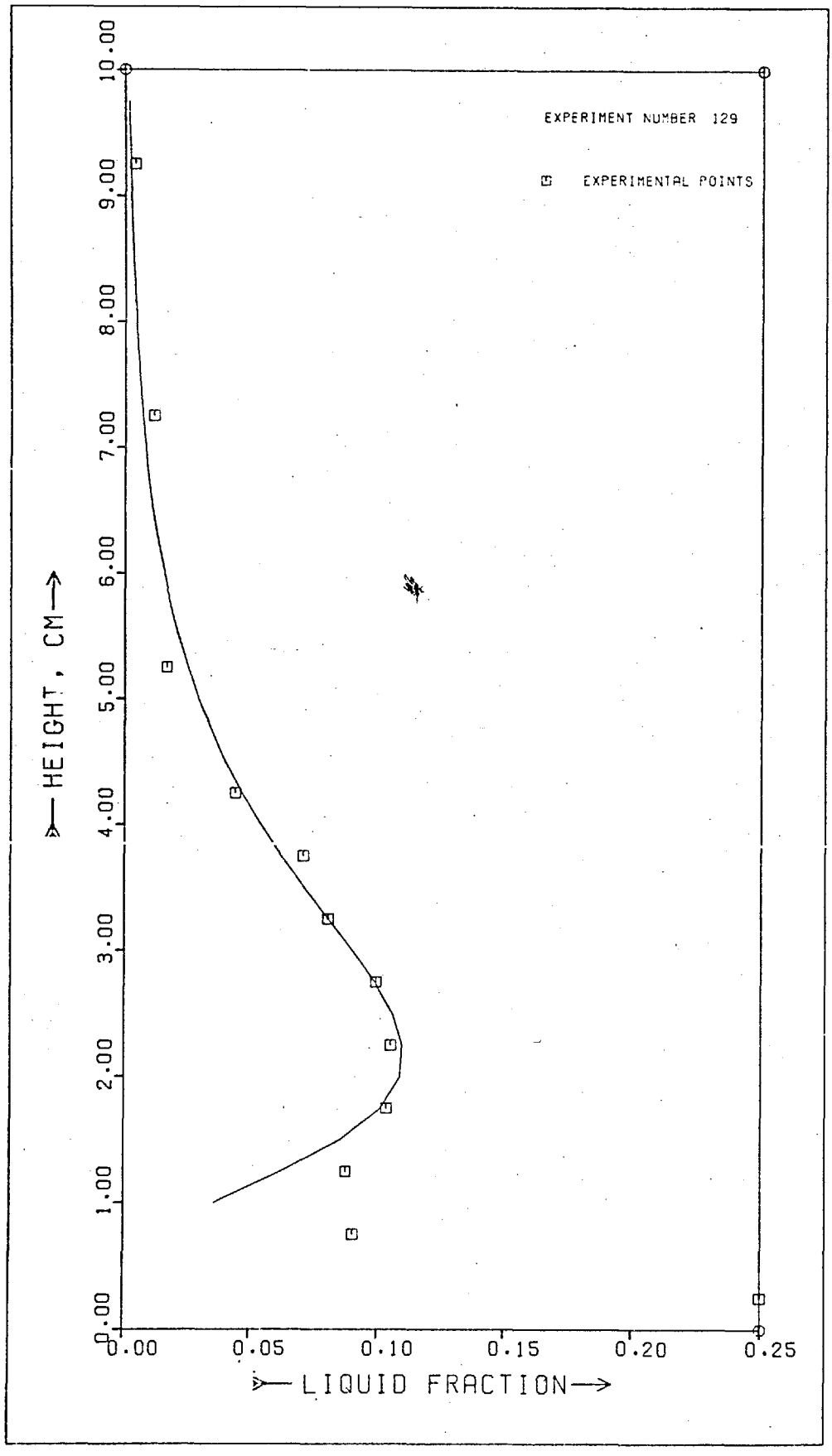

Fig.III.39.- Dispersion density profile and fitting curve.

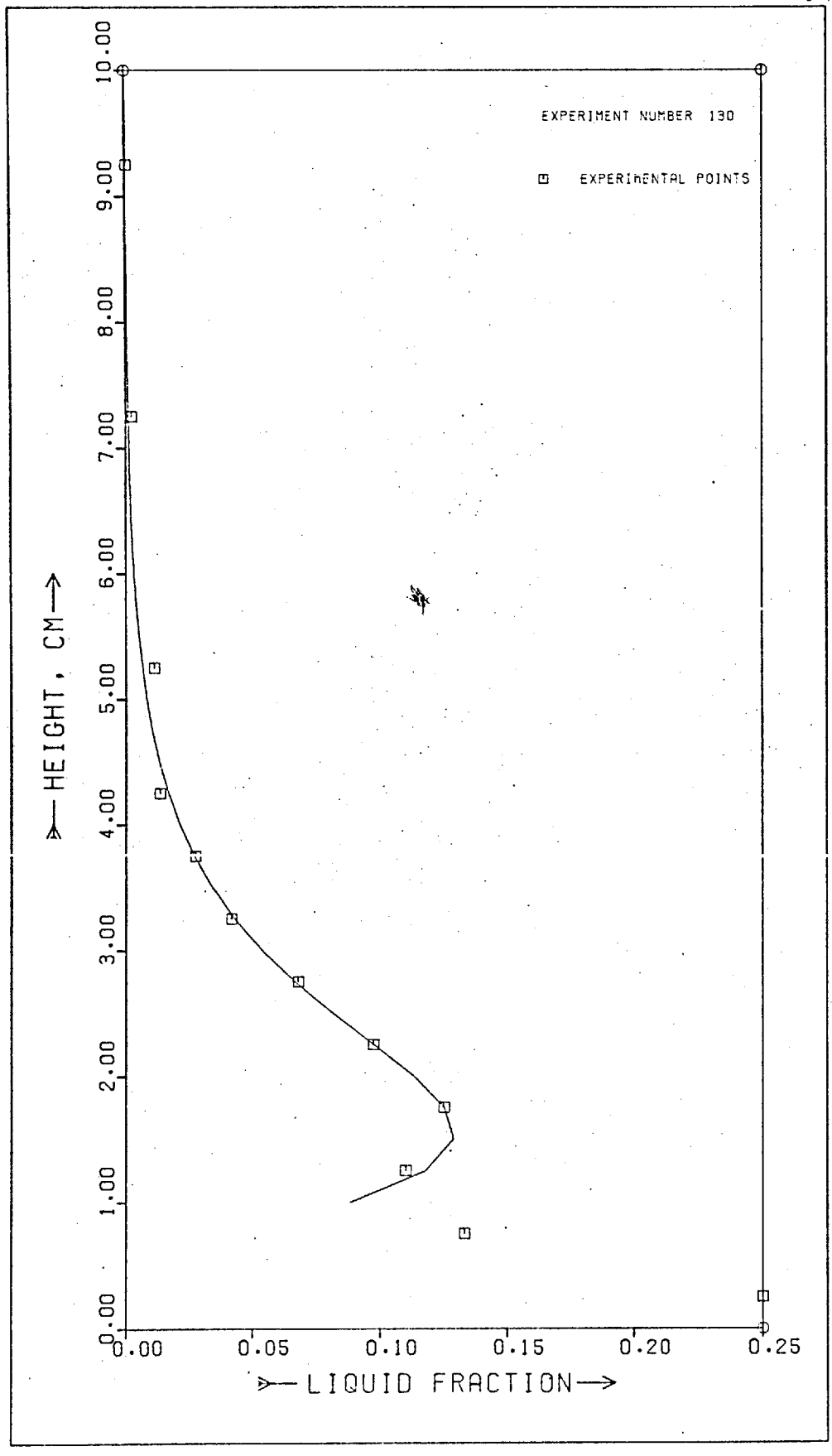

Fig.III.40.- Dispersion density profile and fitting curve.

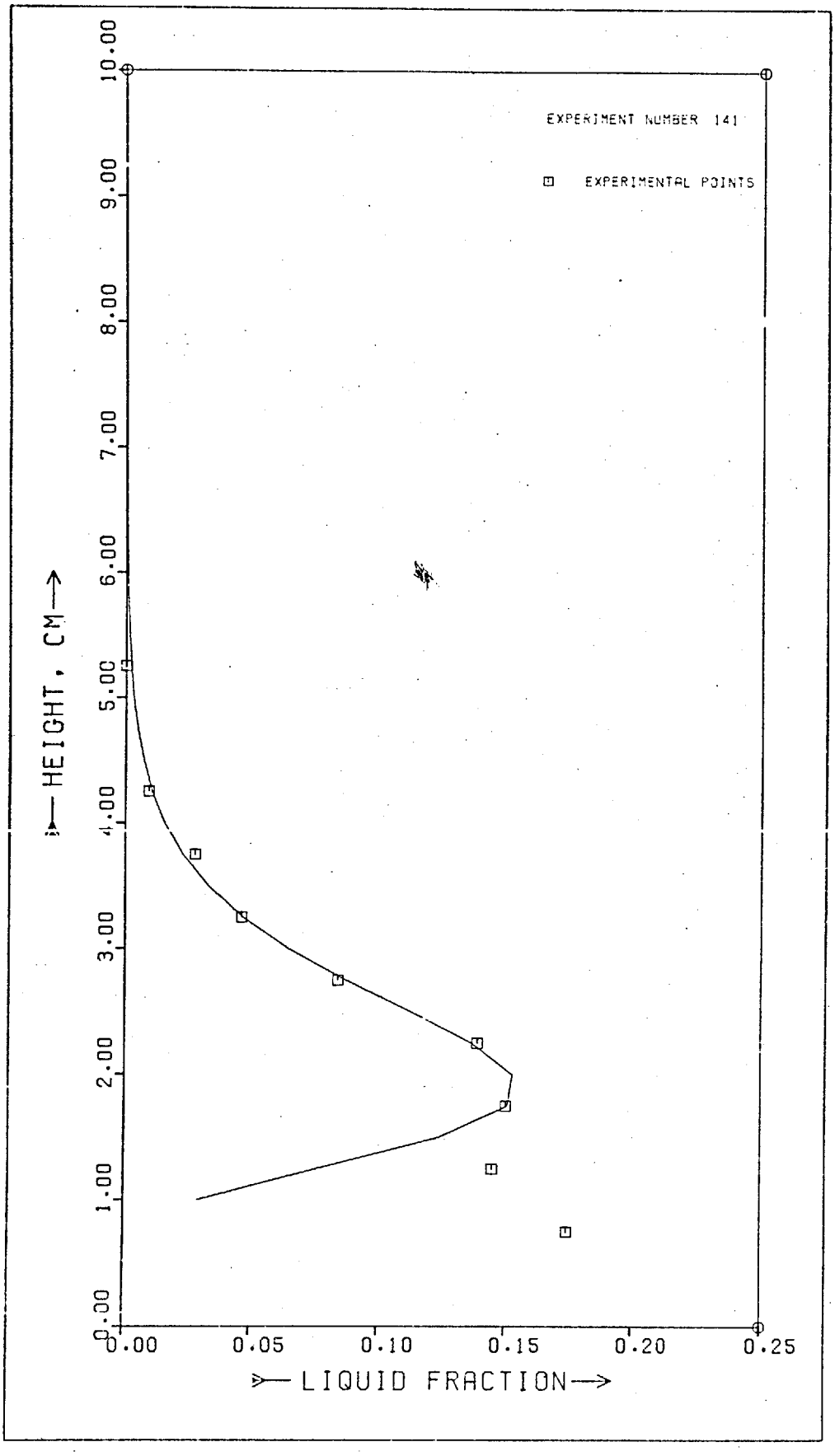

Fig.III.11.- Dispersion density profile and fitting curve.

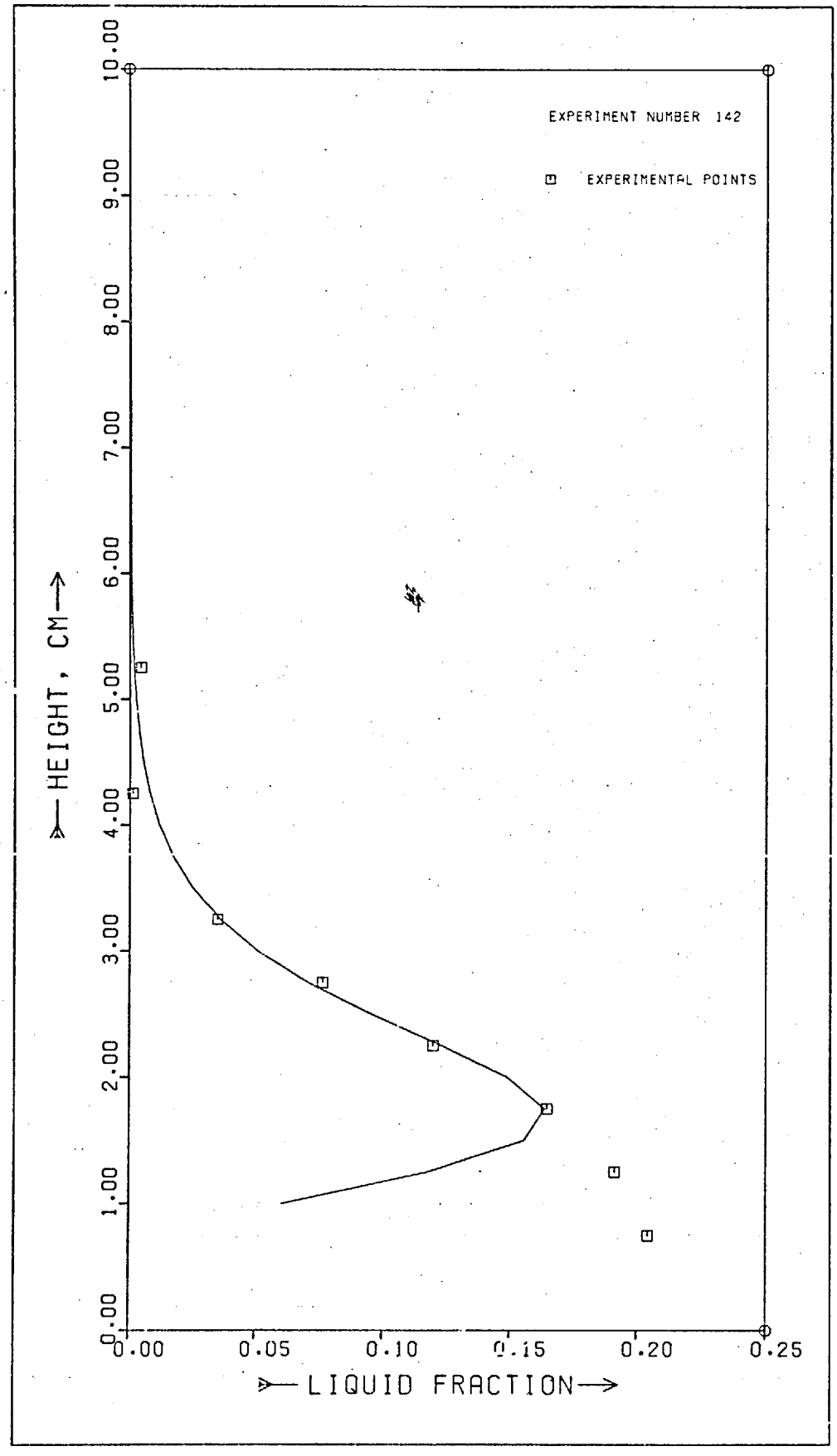

Fig.III.12.- Dispersion density profile and fitting curve.

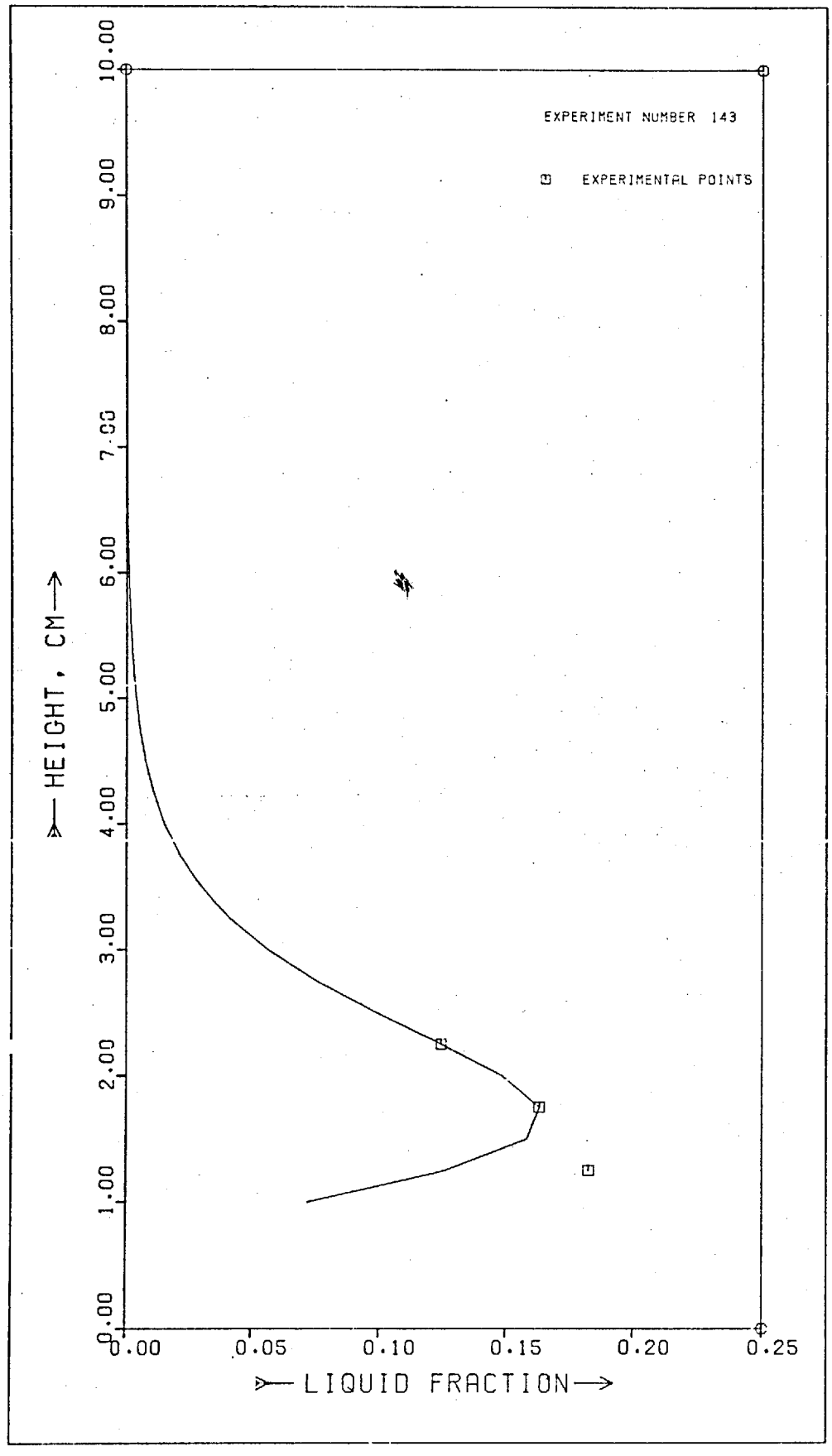

Fig.III.43.- Dispersion density profile and fitting curve.

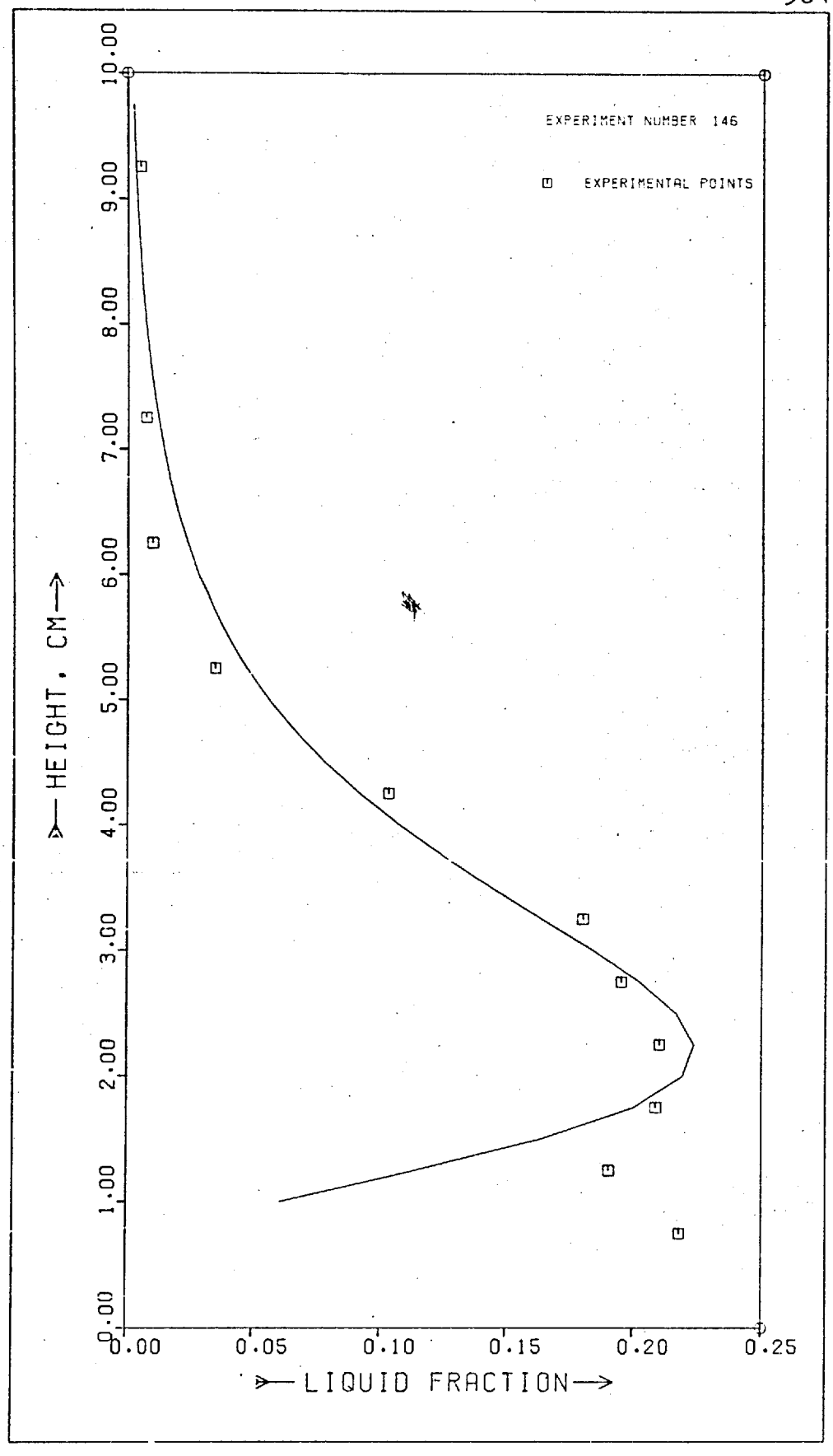

Fig.III.44.- Dispersion density profile and fitting curve.

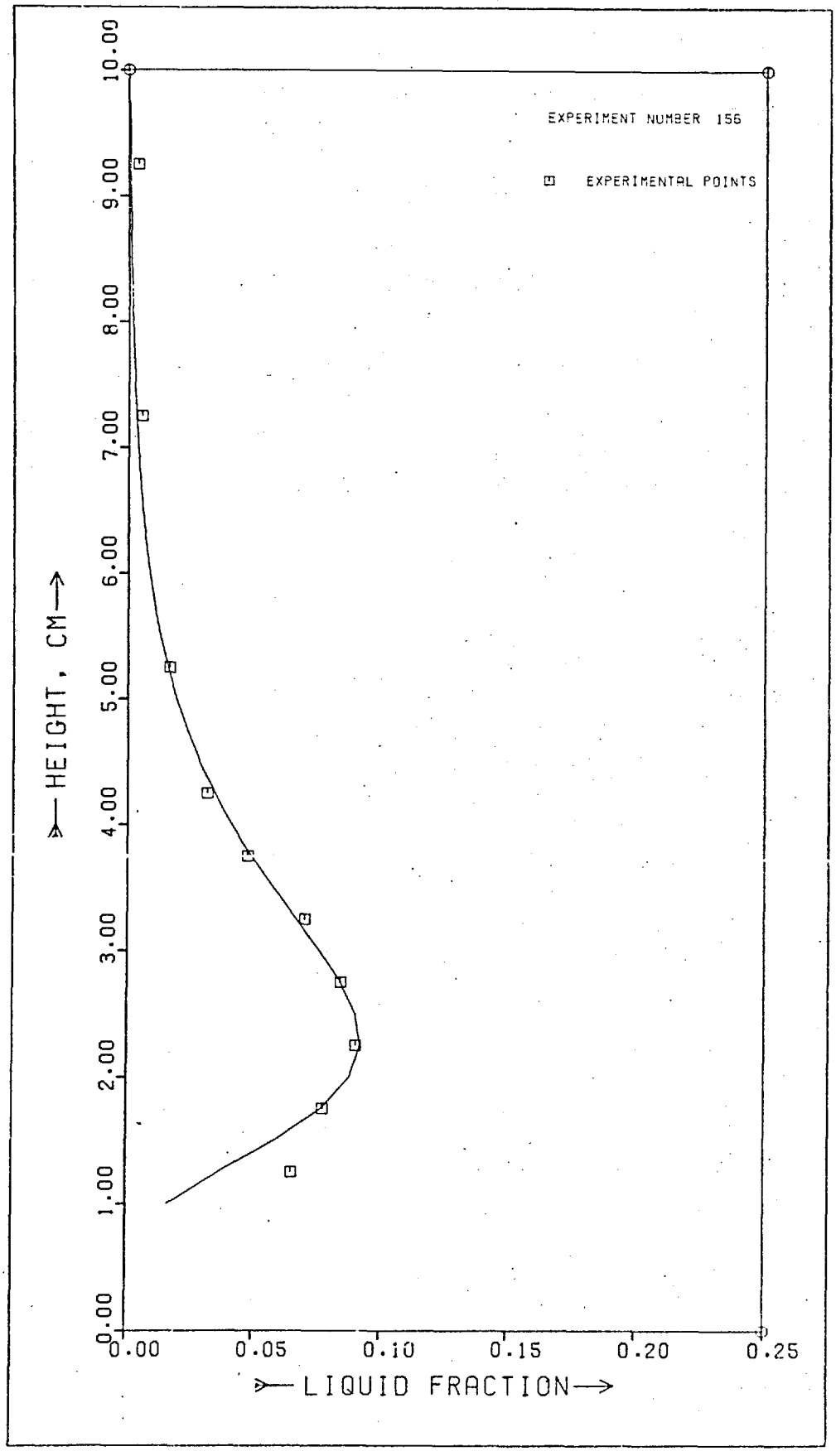

Fig.III.45.- Dispersion density profile and fitting curve.

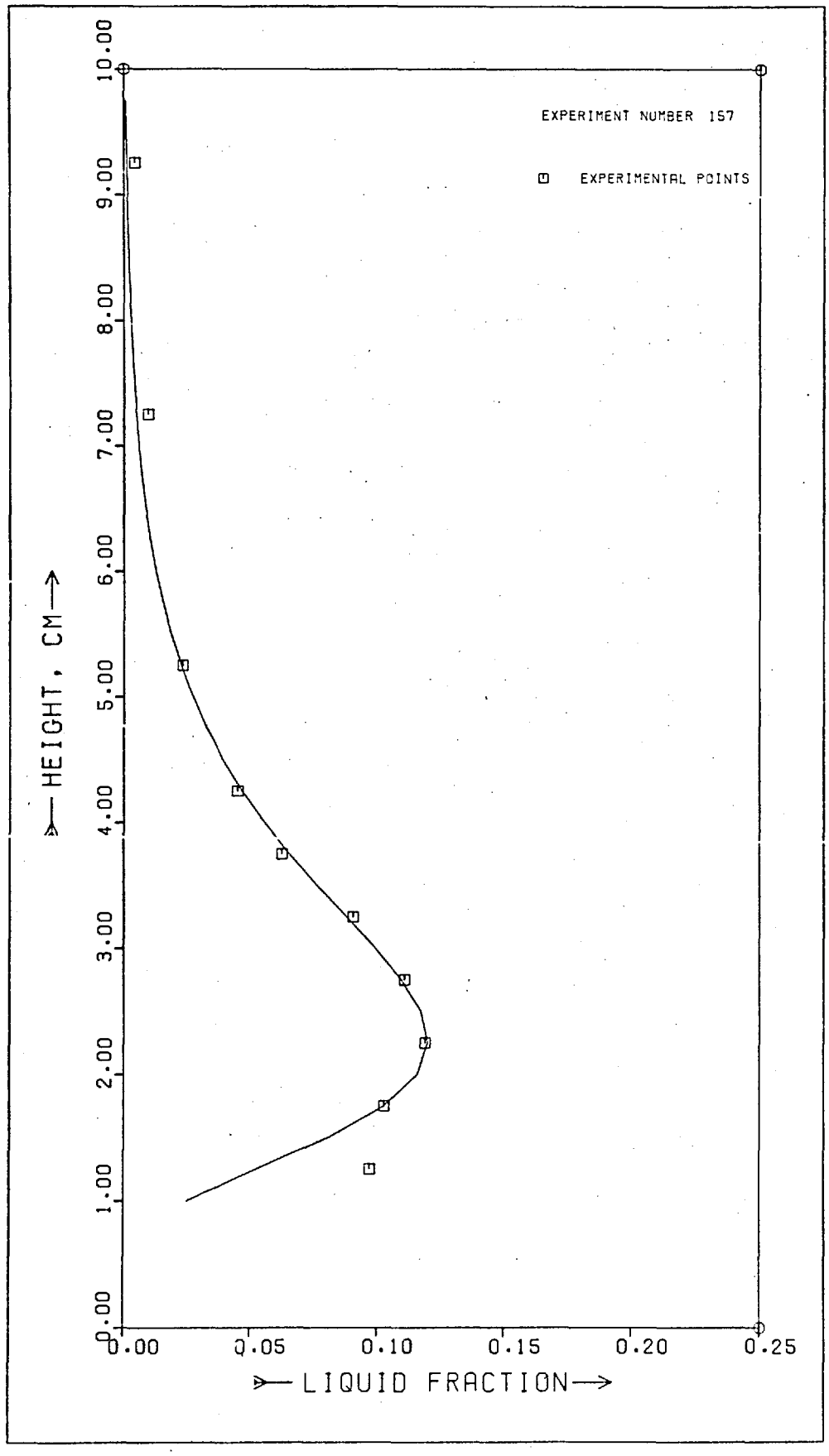

Fig.III.46.- Dispersion density profile and fitting curve.

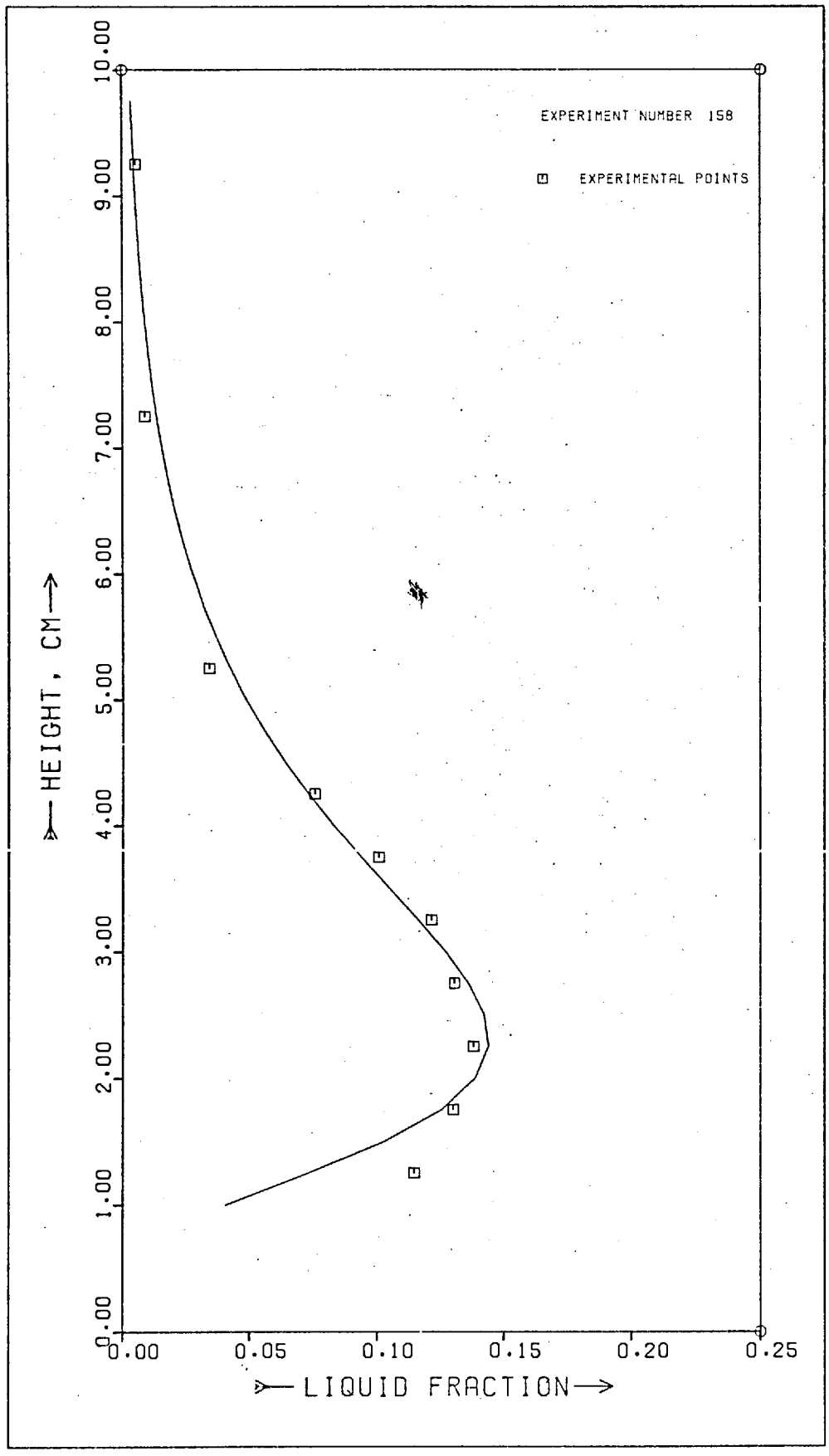

Fig.III.47.- Dispersion density profile and fitting curve.

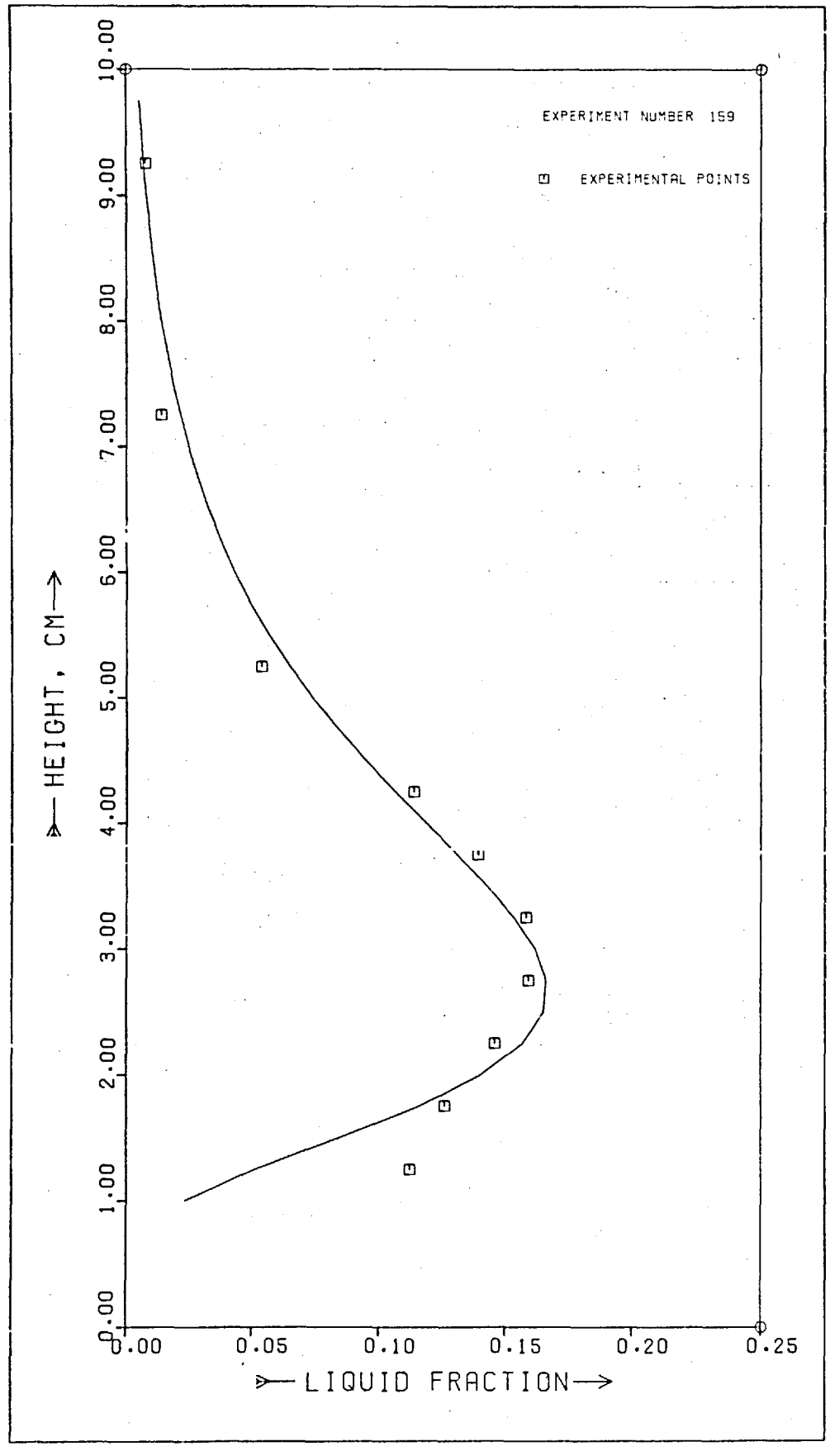

Fig.III.48.- Dispersion density profile and fitting curve.

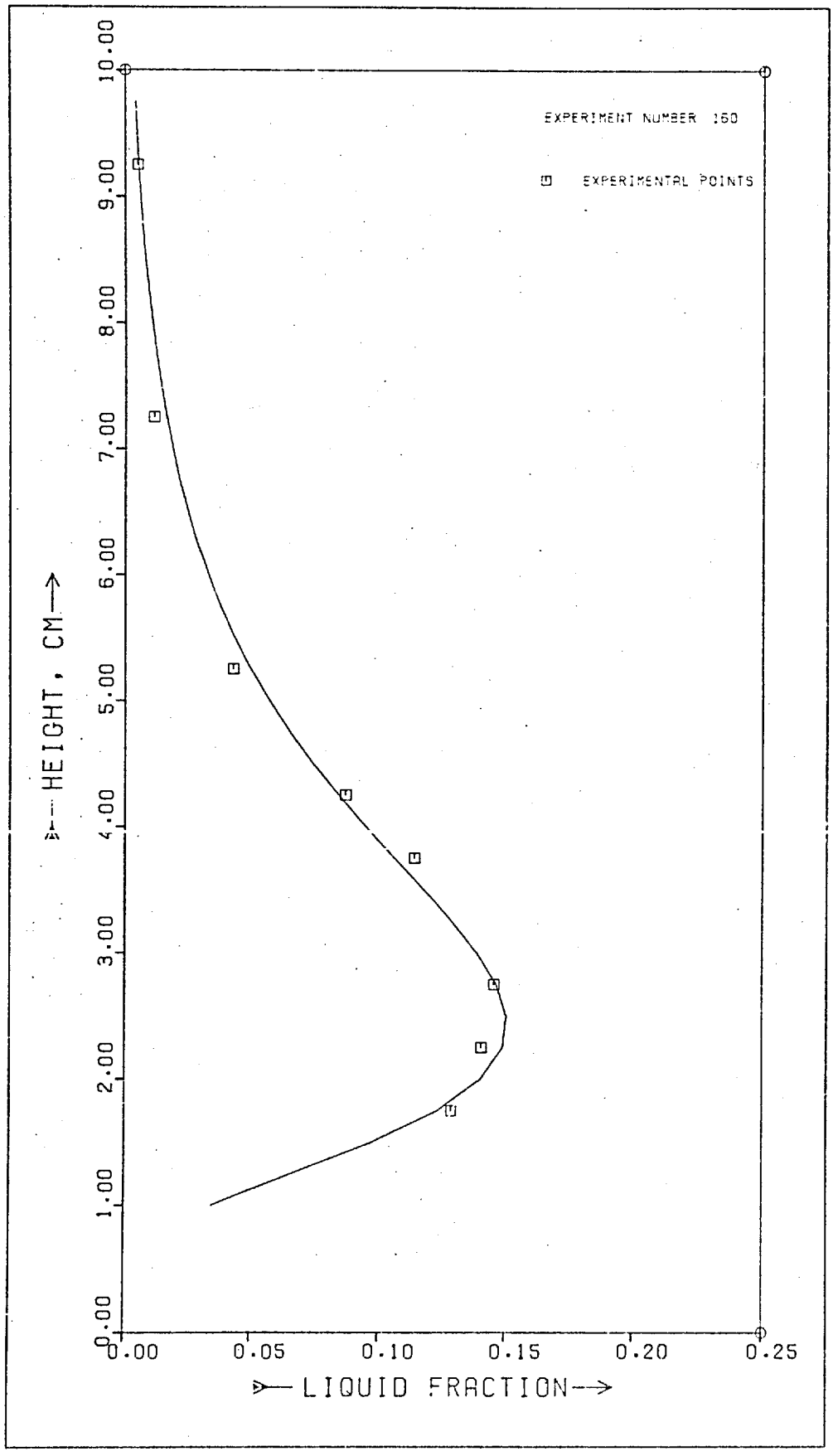

Fig.III.19.- Dispersion density profile and fitting curve.

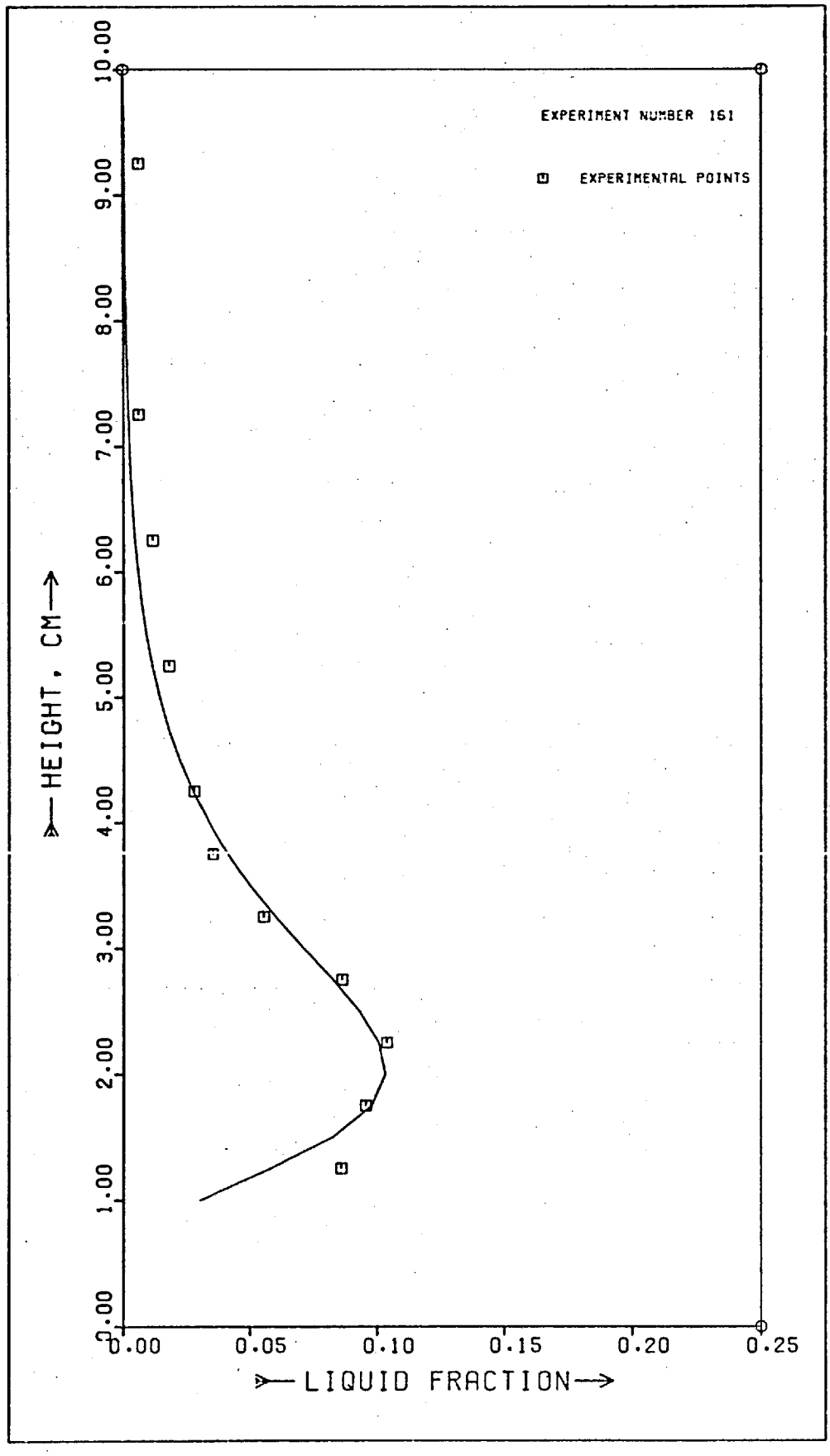

Fig.III.50.- Dispersion density profile and fitting curve.

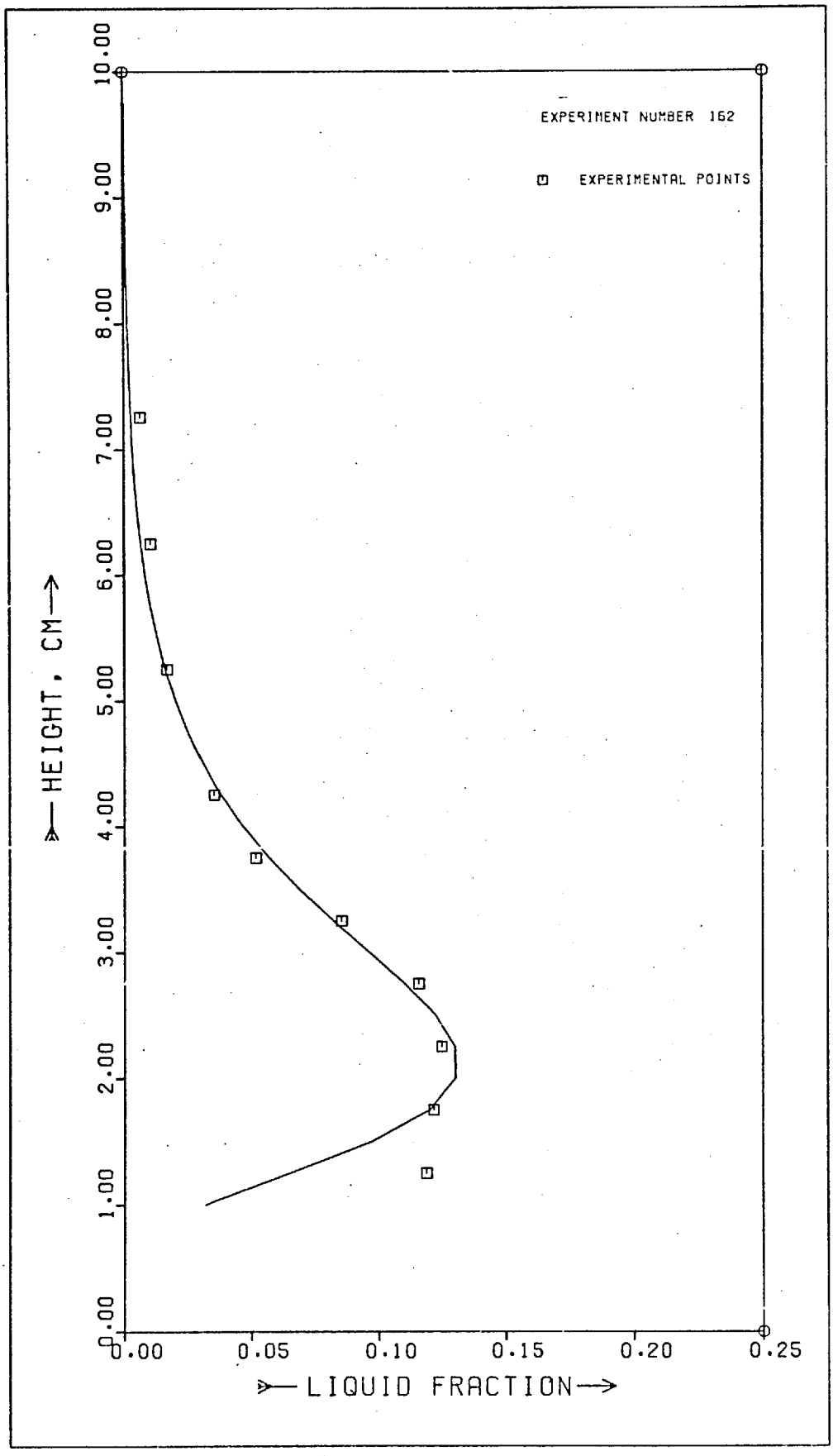

Fig.III.51.- Dispersion density profile and fitting curve.

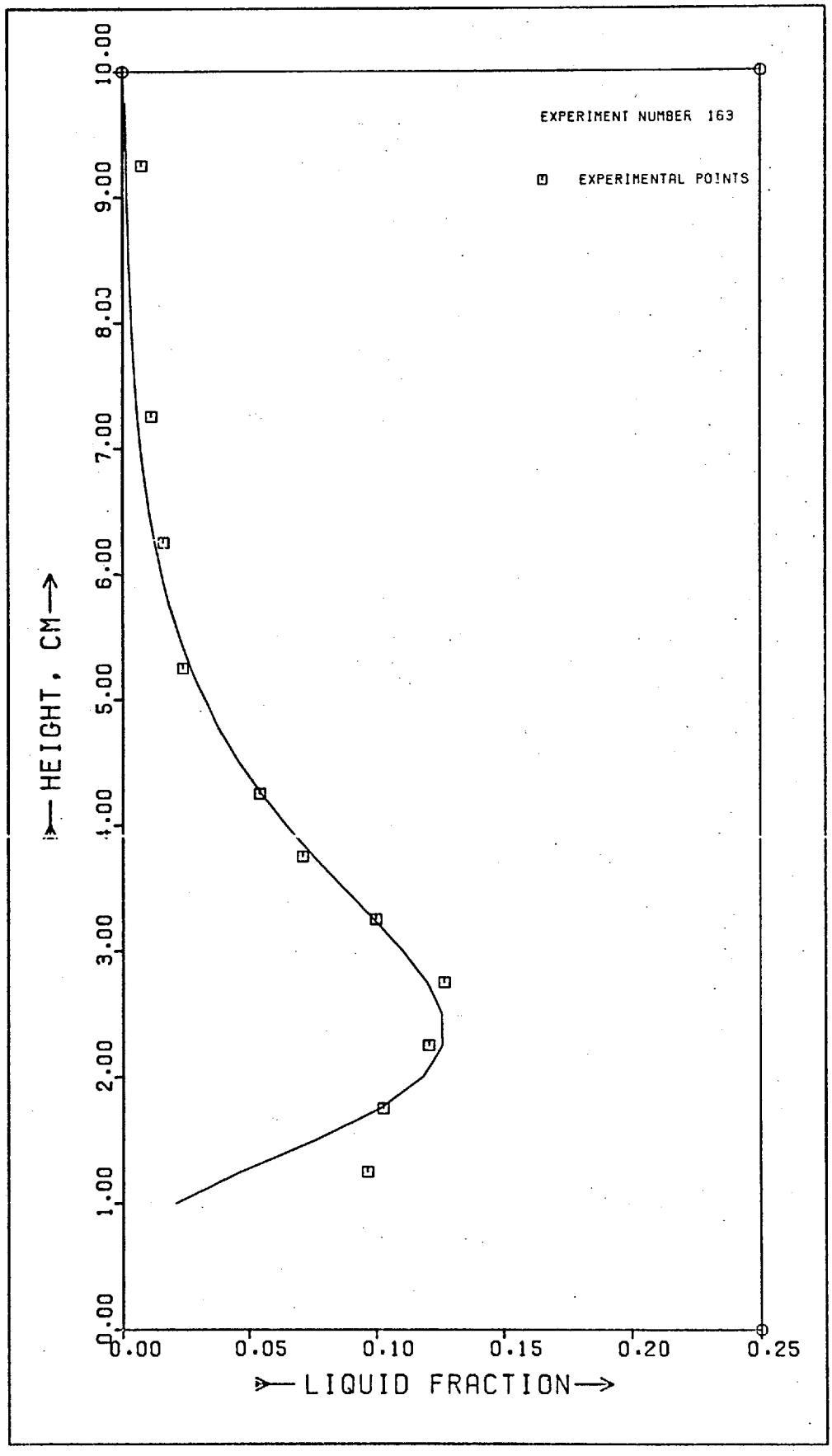

Fig.III.52.- Dispersion density profile and fitting curve.

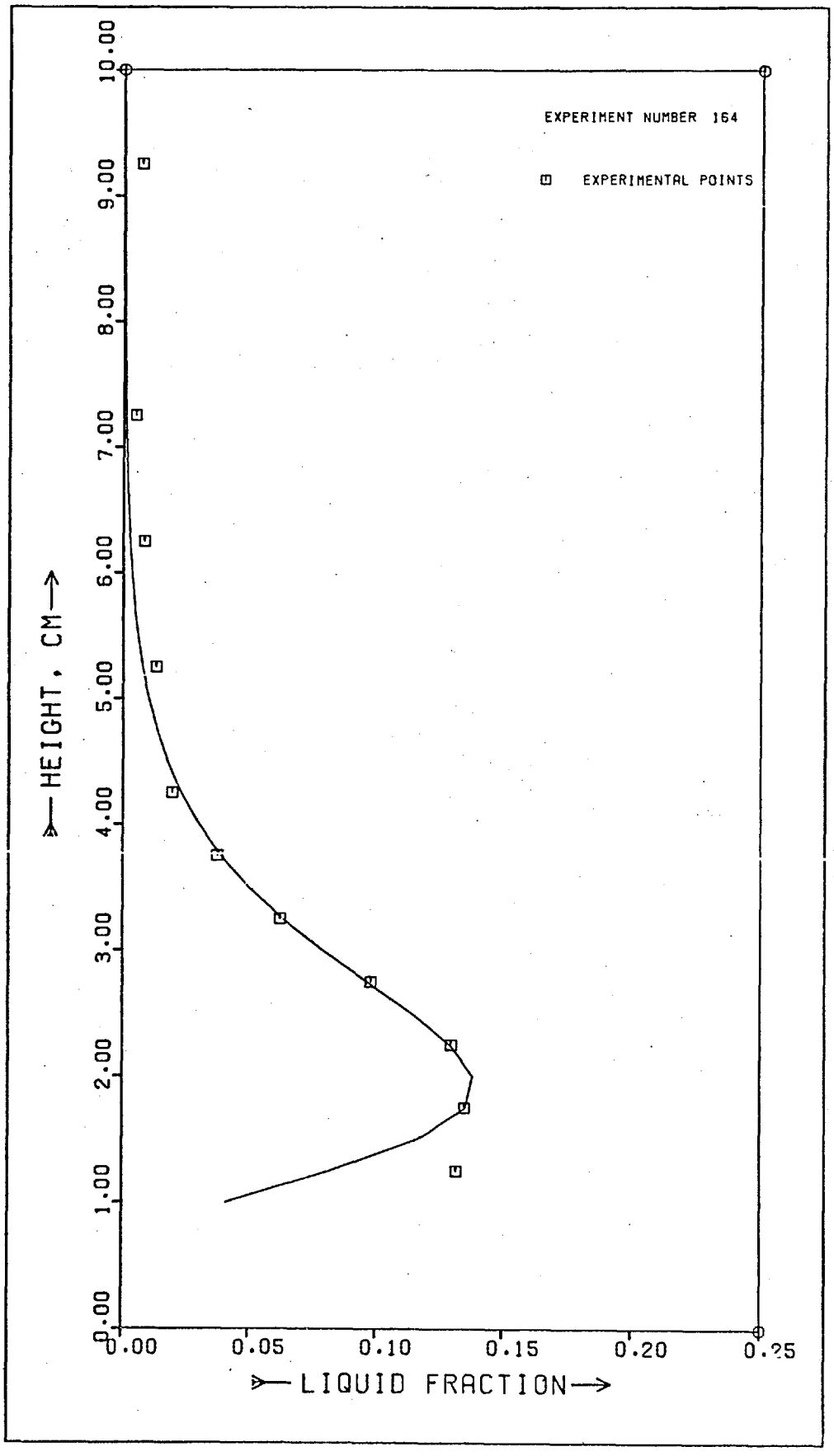

Fig.III.53.- Dispersion density profile and fitting curve.

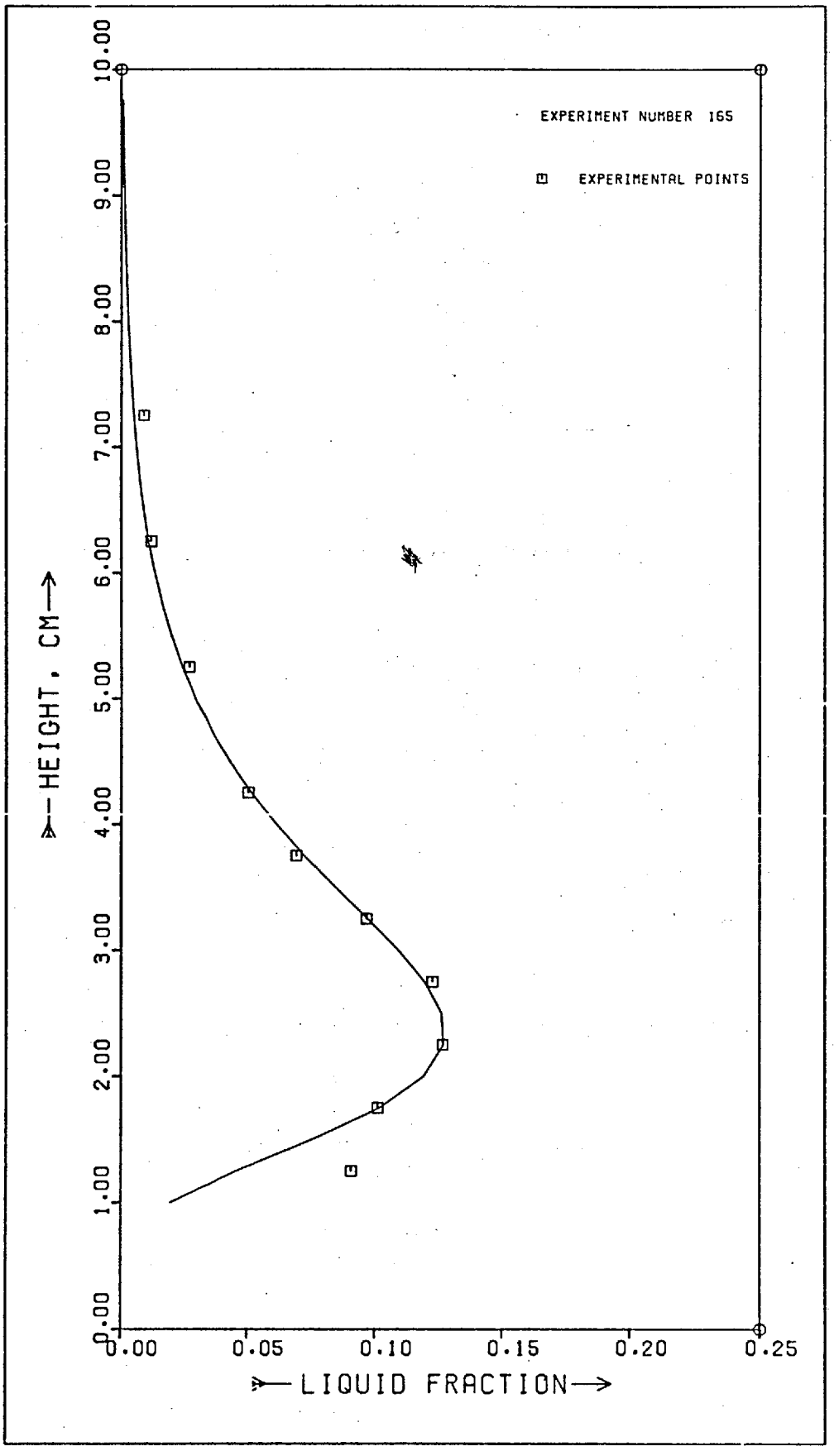

Fig.III.54.- Dispersion density profile and fitting curve.

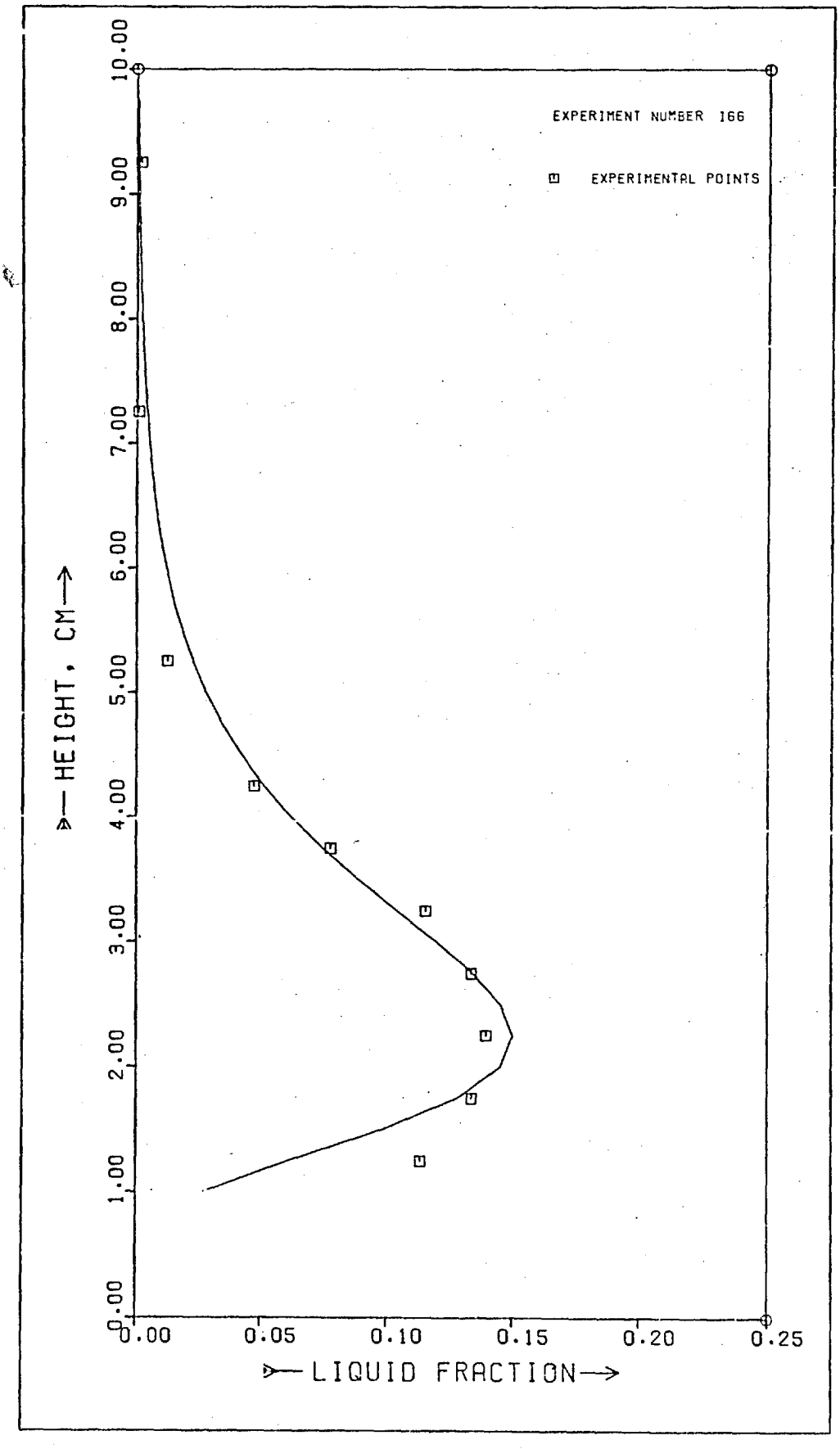

Fig.III.55.- Disporsion density profile and fitting curve.

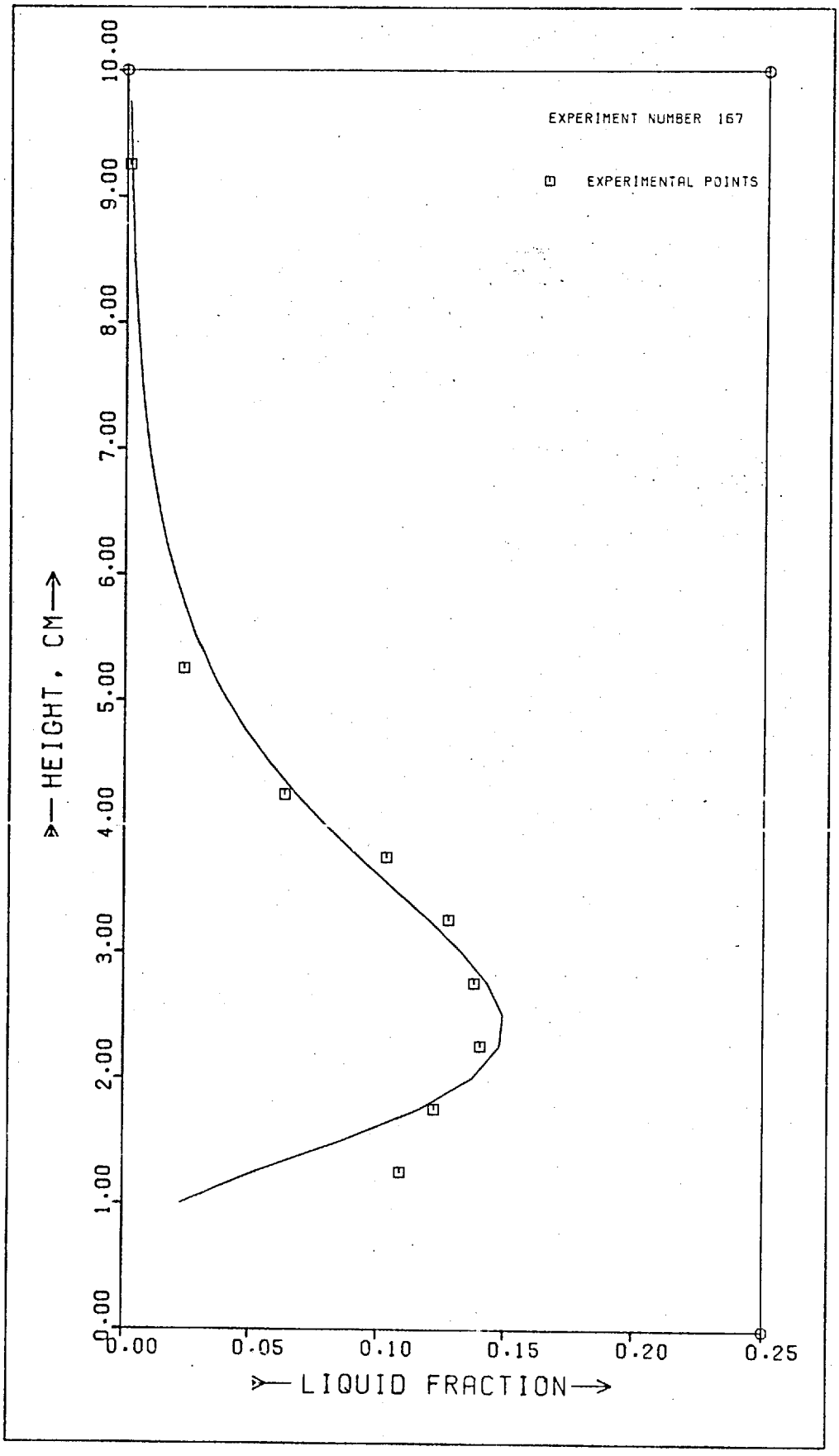

Fig.III.56.- Dispersion density profile and fitting curve.

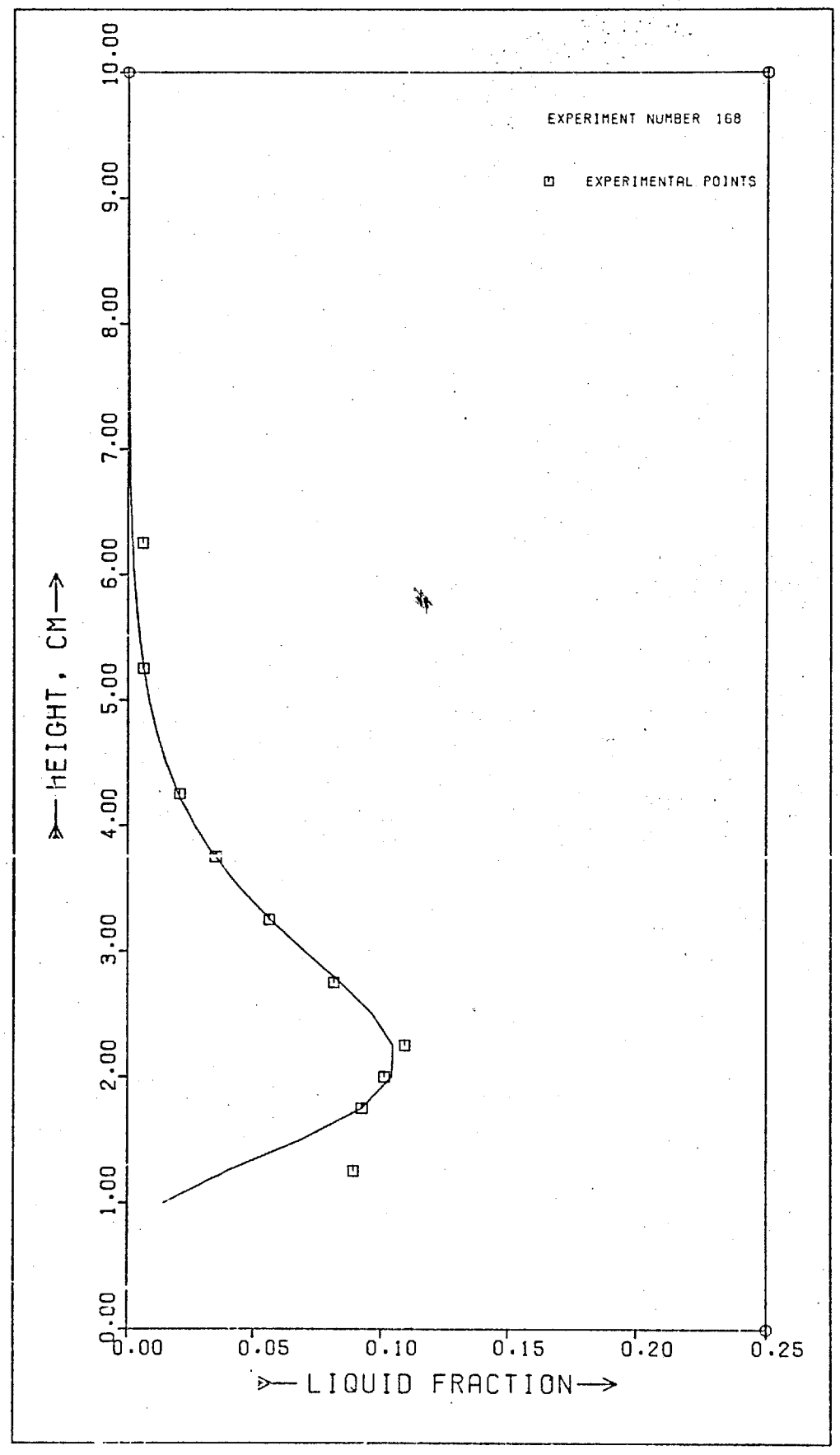

Fig.III.57.- Dispersion density profile and fitting curve.

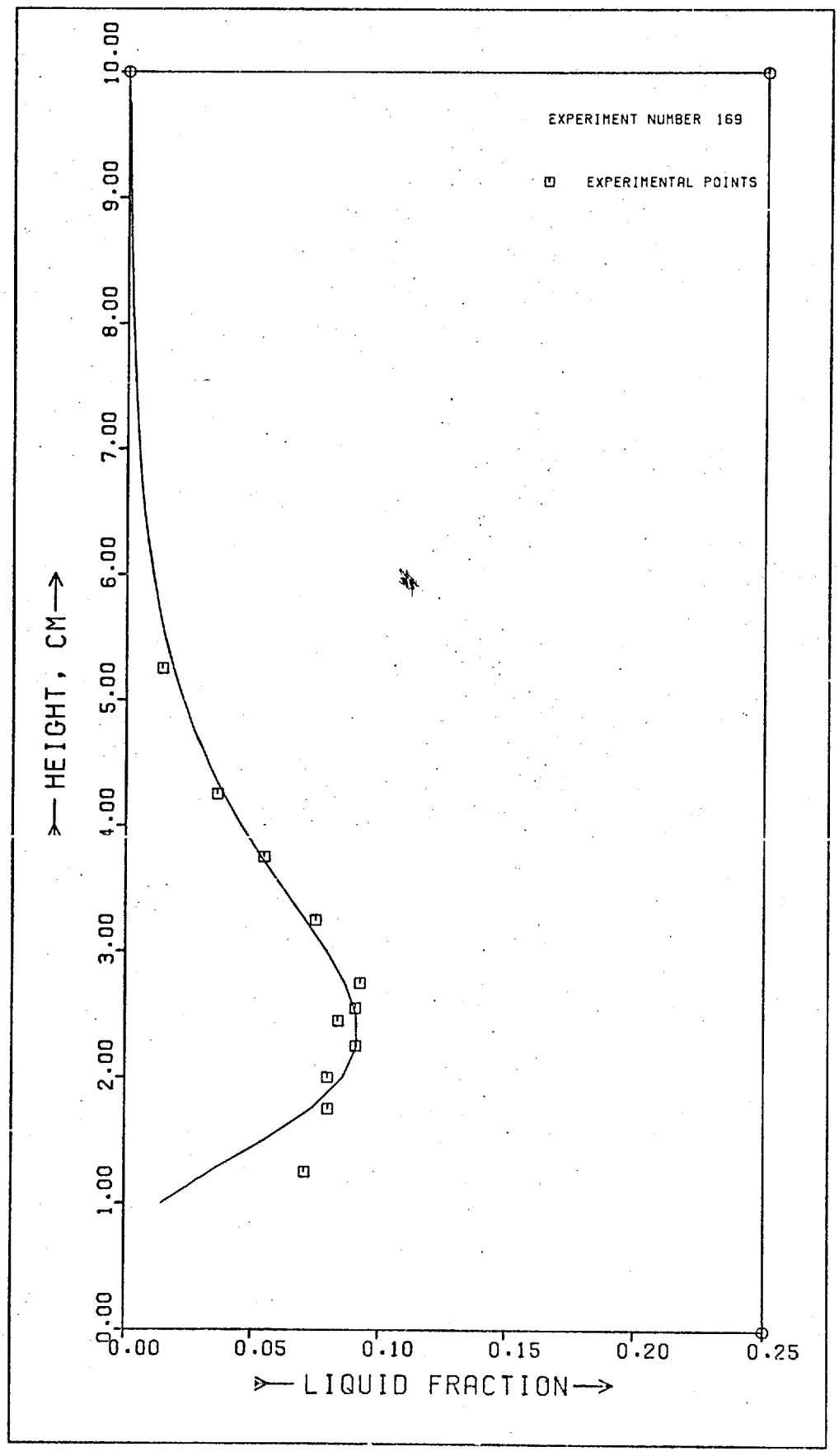

Fig.III.58.- Dispersion density profile and fitting curve.

APPENDIX IV

SURFACE AREA DATA AND DERIVED RESULTS

Table IV.1.- Surface area per unit volume data for system aqueous methanol / air (experimental conditions in Table III.2.

Table IV.2.- Values of parameter A (defined by equation 4.109) calculated from simultaneous measurements of dispersion density and surface area of drops.

Nomenclature

A	parameter defined by $v_p = A d_p^{-0.93}$ where v_p is initial projection of drops of size d_p
LEVEL	level reading (cm). Plate floor at reading of 58.50
PATH LENGTH	optical path length
READING	fraction of light transmitted through the dispersion

TABLE IV.1

SPECIFIC SURFACE AREA DATA

SYSTEM AQUEOUS METHANOL / AIR

EXP.118 DATA POINTS (LEVEL,READING), PATH LENGTH= 2.83 CM

62.50 .500 63.00 .630 63.50 .710 64.00 .750 66.00 .820 68.00 .860 70.00 .890

EXP.124 DATA POINTS (LEVEL,READING) PATH LENGTH= 2.83

62.00 .710 62.50 .780 63.00 .840 63.50 .875 64.00 .890 65.00 .910 66.00 .925
68.00 .940 70.00 .960

EXP.125 DATA POINTS (LEVEL,READING) PATH LENGTH= 2.83

61.50 .240 62.00 .435 62.50 .570 63.00 .660 63.50 .740 64.00 .760 65.00 .840
66.00 .870 68.00 .910 70.00 .960

EXP.126 DATA POINTS (LEVEL,READING) PATH LENGTH= 2.83

62.00 .500 62.50 .670 63.00 .790 63.50 .850 64.00 .860 64.50 .890 65.00 .910
66.00 .930 68.00 .940 70.00 .960

EXP.127 DATA POINTS (LEVEL,READING) PATH LENGTH= 2.83

62.00 .200 62.50 .520 63.00 .660 63.50 .780 64.00 .835 64.50 .850 65.00 .885
66.00 .900 68.00 .930 70.00 .960

EXP.128 DATA POINTS (LEVEL,READING) PATH LENGTH= 2.83

62.50 .420 63.00 .550 63.50 .650 64.00 .710 64.50 .750 65.00 .780 66.00 .820
68.00 .855 70.00 .900

EXP.129 DATA POINTS (LEVEL,READING) PATH LENGTH= 2.83

63.50 .730 64.00 .750 64.50 .800 65.00 .830 66.00 .865 68.00 .885 70.00 .920

TABLE IV.2

VALUES OF PARAMETER A

Run:	118	124	125	126	127	128	129
A:	0.00272	0.00184	0.00271	0.00353	0.00306	0.00344	0.00453

APPENDIX V

PROGRAM EXPPROF

This program fits dispersion density and surface area profiles, plotting graphic in microfilm.

```
JOB(UMFCC02,J1)                                                          _0001
PASSWOR(        )                                                        _0002
MNF(B=BIN,T)                                                             _0003
MTCFOR(L=BIN)                                                            _0004
REPLACE(BIN)                                                             _0005
-                                                                        _0006
      PROGRAM EXPPROF(INPUT,OUTPUT,TAPE5=INPUT,TAPE6=OUTPUT,TAPE62)      _0007
      EXTERNAL CALCFG,CALCFH                                             _0008
      DIMENSION T(2,46),Y(2,46),ICON(2)                                  _0009
      DIMENSION E(6),G(6),X(6),W(54)                                     _0010
      COMMON ZZ(46),CR(46),Z(46),RD(46),FL(46),A(46),NA,NB,S,ZZM,FLM,AM  _0011
     1 ,ZM,P(46),R(46),NX                                                _0012
COMMENT  PROGRAM NOT WORKING FOR NA AND NB BOTH NOT EQUAL TO ZERO        _0013
      READ(5,110) NX                                                     _0014
  110 FORMAT(A3)                                                         _0015
      DECODE(3,120,NX)NE                                                 _0016
  120 FORMAT(I3)                                                         _0017
      WRITE(6,130) NE                                                    _0018
  130 FORMAT(20H EXPERIMENT NUMBER  ,I3)                                 _0019
      CALL PROFILS                                                       _0020
      N=3                                                                _0021
      X(1)=0.073                                                         _0022
      X(2)=2.                                                            _0023
      X(3)=0.4                                                           _0024
      S=X(3)                                                             _0025
      IPRINT=1                                                           _0026
      DO 10 I=1,N                                                        _0027
      E(I)=0.001*X(I)                                                    _0028
   10 CONTINUE                                                           _0029
      ESCALE=1000.                                                       _0030
      FMIN=0.                                                            _0031
      MAXIT=80                                                           _0032
      MXITFG=20                                                          _0033
      N3N=N*(N+3)                                                        _0034
      K=2                                                                _0035
      IF(NA.EQ.0) GO TO 1                                                _0036
      CALL VA01A(X,E,G,N,F,FMIN,ESCALE,IPRINT,MAXIT,MXITFG,CALCFG,W,N3N) _0037
      FLM=X(1)                                                           _0038
      ZZM=X(2)                                                           _0039
      S=X(3)                                                             _0040
      ST=S*EXP(0.5*(S**2) )                                              _0041
      WRITE(6,100) (ZZ(I),CR(I),FL(I),P(I),I=1,NA)                       _0042
  100 FORMAT(8F8.4)                                                      _0043
      HDROP=2.5066*FLM*ZZM*ST                                            _0044
      WRITE(6,400) HDROP,X(1),X(2),S                                     _0045
  400 FORMAT(18H HOLD-UP OF DROPS= ,F8.4,6H X(1)= ,F12.6,6H X(2)= ,E12.6 _0046
     1    , 3H S= ,E12.6)                                               _0047
      ICON(1)=NA                                                         _0048
      ICON(2)=NA                                                         _0049
      DO 20 I=1,NA                                                       _0050
      TZ=ZZ(I)                                                           _0051
      Y(1,I)=TZ                                                          _0052
      Y(2,I)=TZ                                                          _0053
      TF=FL(I)                                                           _0054
      TP=P(I)                                                            _0055
      T(1,I)=TF                                                          _0056
      T(2,I)=TP                                                          _0057
   20 CONTINUE                                                           _0058
      IPRINT=0                                                           _0059
      CALL GRAPH2 (T,Y,K,ICON,NA,IPRINT)                                 _0060
    1 CONTINUE                                                           _0061
      ST=S*EXP(0.5*(S**2))                                               _0062
      ITEST=2                                                            _0063
      IF(NA.EQ.0) READ(5,200)FLM,ZZM,S                                   _0064
```

```
  200 FORMAT(3F7.4)                                                     _0065
      IF(NB.EQ.0) GO TO 2                                               _0066
      AEXP=2.355E-3                                                     _0067
      ABSACC=1.E-7                                                      _0068
      RELACC=1.E-4                                                      _0069
      ASTEP=0.2*AEXP                                                    _0070
      N=2                                                               _0071
   80 B=-0.93                                                           _0072
      X(2)=ZZM*EXP(-0.5*S**2/B)                                         _0073
      X(1)=6.*FLM*ZZM/X(2)*(0.196*ZZM/AEXP**2)**(-0.5/B)*               _0074
     1     EXP(-0.25*(S/B)**2*(2*B-0.5))                                _0075
      CALL CALCFH(X,G,N,F)                                              _0076
      IF(ITEST.EQ.3) GO TO 90                                           _0077
   40 CALL VD01A(ITEST,AEXP,F,MAXIT,ABSACC,RELACC,ASTEP)                _0078
      GO TO(90,60,60,60),ITEST                                          _0079
   60 WRITE(6,70) ITEST,AEXP                                            _0080
   70 FORMAT(7H ITEST=,I2,4H A= ,F12.6)                                 _0081
      ITEST=3                                                           _0082
      GO TO 80                                                          _0083
   90 CONTINUE                                                          _0084
      AM=X(1)                                                           _0085
      ZM=X(2)                                                           _0086
      WRITE(6,100) (Z(I),RD(I),A(I),R(I),I=1,NB)                        _0087
      TAREA=2.5066*AM*ZM*ST                                             _0088
      WRITE(6,300) TAREA                                                _0089
  300 FORMAT(21H TOTAL AREA OF DROPS= ,F7.4,5H CM-1 )                   _0090
      ICON(1)=NB                                                        _0091
      ICON(2)=NB                                                        _0092
      DO 30 I=1,NB                                                      _0093
      TZ=Z(I)                                                           _0094
      Y(1,I)=TZ                                                         _0095
      Y(2,I)=TZ                                                         _0096
      TF=A(I)                                                           _0097
      TP=R(I)                                                           _0098
      T(1,I)=TF                                                         _0099
      T(2,I)=TP                                                         _0100
   30 CONTINUE                                                          _0101
      IPRINT=0                                                          _0102
      CALL GRAPL2 (T,Y,K,ICON,NB,IPRINT)                                _0103
    2 CONTINUE                                                          _0104
      IF(NA.EQ.0) STOP                                                  _0105
      CALL CURVES                                                       _0106
      STOP                                                              _0107
      END                                                               _0108
C                                                                       _0109
      SUBROUTINE PROFILS                                                _0110
      COMMON ZZ(46),CR(46),Z(46),RD(46),FL(46),A(46),NA,NB,S,ZZM,FLM,AM  _0111
     1 ,ZM,P(46),R(46),NX                                               _0112
      READ(5,100) CR0,NA,NB                                             _0113
  100 FORMAT(F7.2,2I3)                                                  _0114
      IF(NA.EQ.0) GO TO 1                                               _0115
      READ(5,200)(ZZ(I),CR(I),I=1,NA)                                   _0116
  200 FORMAT((1X,6(F6.2,F7.2)))                                         _0117
    1 CONTINUE                                                          _0118
      IF(NB.EQ.0) GO TO 2                                               _0119
      READ(5,300)(Z(I),RD(I),I=1,NB)                                    _0120
  300 FORMAT((1X,6(F6.2,F6.3)))                                         _0121
    2 CONTINUE                                                          _0122
      IF(NA.EQ.0) GO TO 10                                              _0123
      DO 10 I=1,NA                                                      _0124
      ZZ(I)=ZZ(I)-66.75                                                 _0125
      FL(I)=0.6091*ALOG(CR0/CR(I))                                      _0126
      IF(ZZ(I).GT.10.0) ZZ(I)=10.                                       _0127
      IF(ZZ(I).LE.0.) ZZ(I)=1.E-20                                      _0128
      IF(FL(I).GT.0.25) FL(I)=0.25                                      _0129
   10 CONTINUE                                                          _0130
      IF(NB.EQ.0) GO TO 20                                              _0131
      DO 20 I=1,NB                                                      _0132
      Z(I)=Z(I)-58.50                                                   _0133
      A(I)=-4./2.83*ALOG(RD(I))                                         _0134
   20 CONTINUE                                                          _0135
      RETURN                                                            _0136
      END                                                               _0137
C                                                                       _0138
      SUBROUTINE CURVES                                                 _0139
      DIMENSION NUM(2)                                                  _0140
      COMMON ZZ(46),CR(46),Z(46),RD(46),FL(46),A(46),NA,NB,S,ZZM,FLM,AM  _0141
     1 ,ZM,P(46),R(46),NX                                               _0142
      CALL START(2)                                                     _0143
      I=NA+1                                                            _0144
      J=I+1                                                             _0145
      K=J+1                                                             _0146
      FL(I)=0.                                                          _0147
      ZZ(I)=10.                                                         _0148
```

```
      FL(J)=0.25                                                        _0149
      ZZ(J)=10.                                                         _0150
      FL(K)=0.25                                                        _0151
      ZZ(K)=0.                                                          _0152
      NUM(1)=NA                                                         _0153
      NUM(2)=3                                                          _0154
      CALL SYMBOL(4.7,12.5,0.07,17HEXPERIMENT NUMBER,0.,17)             _0155
      CALL SYMBOL(6.0,12.5,0.07,NX,0.,3)                                _0156
      CALL SYMBOL(4.7,12.035,0.07,0.0,-1)                               _0157
      CALL SYMBOL(5.0,12.,0.07,19HEXPERIMENTAL POINTS,0.,19)            _0158
      CALL INTENSE(20)                                                  _0159
      CALL PLOT(2.,3.,-3)                                               _0160
      CALL GRAF(FL,ZZ,NUM,2.,-1,15HLIQUID FRACTION,15.,10HHEIGHT, CM,10.,5.  _0161
     1 ,10.)                                                            _0162
      CALL PLOT(-6.4,0.,-3)                                             _0163
      NUM(1)=36                                                         _0164
      NUM(2)=3                                                          _0165
      DO 10 I=1,36                                                      _0166
      AX=I                                                              _0167
      ZZ(I)=0.75+0.25*AX                                                _0168
      AI=ZZ(I)/ZZM                                                      _0169
      BI=ALOG(AI)/S                                                     _0170
      CI=EXP(-0.5*BI**2)                                                _0171
      P(I)=FLM*CI                                                       _0172
   10 CONTINUE                                                          _0173
      ZZ(37)=10.                                                        _0174
      P(37)=0.0                                                         _0175
      ZZ(38)=10.                                                        _0176
      P(38)=0.25                                                        _0177
      ZZ(39)=0.                                                         _0178
      P(39)=0.25                                                        _0179
      CALL GRAF(P,ZZ,NUM,2.0,15HLIQUID FRACTION,15.,10HHEIGHT, CM,10.,5.  _0180
     2 ,10.)                                                            _0181
      CALL ENPLOT                                                       _0182
      RETURN                                                            _0183
      END                                                               _0184
                                                                        _0185
      SUBROUTINE VD01A (ITEST,X,F,MAXFUN,ABSACC,RELACC,XSTEP)           _0186
      ABSF(ABC123)=ABS(ABC123)                                          _0187
      GO TO (1,2,2),ITEST                                               _0188
    2 IS=6-ITEST                                                        _0189
      ITEST=1                                                           _0190
      IINC=1                                                            _0191
      XINC=XSTEP+XSTEP                                                  _0192
      MC=IS-3                                                           _0193
      IF (MC) 4,4,15                                                    _0194
    3 MC=MC+1                                                           _0195
      IF (MAXFUN-MC) 12,15,15                                           _0196
   12 ITEST=4                                                           _0197
   43 X=DB                                                              _0198
      F=FB                                                              _0199
      IF (FB-FC) 15,15,44                                               _0200
   44 X=DC                                                              _0201
      F=FC                                                              _0202
   15 RETURN                                                            _0203
    1 GO TO (5,6,7,8),IS                                                _0204
    8 IS=3                                                              _0205
    4 DC=X                                                              _0206
      FC=F                                                              _0207
      X=X+XSTEP                                                         _0208
      GO TO 3                                                           _0209
    7 IF (FC-F) 9,10,11                                                 _0210
   10 X=X+XINC                                                          _0211
      XINC=XINC+XINC                                                    _0212
      GO TO 3                                                           _0213
    9 DB=X                                                              _0214
      FB=F                                                              _0215
      XINC=-XINC                                                        _0216
      GO TO 13                                                          _0217
   11 DB=DC                                                             _0218
      FB=FC                                                             _0219
      DC=X                                                              _0220
      FC=F                                                              _0221
   13 X=DC+DC-DB                                                        _0222
      IS=2                                                              _0223
      GO TO 3                                                           _0224
    6 DA=DB                                                             _0225
      DB=DC                                                             _0226
      FA=FB                                                             _0227
      FB=FC                                                             _0228
   32 DC=X                                                              _0229
      FC=F                                                              _0230
      GO TO 14                                                          _0231
    5 IF (FB-FC) 16,17,17                                               _0232
```

```
   17 IF (F-FB) 18,32,32                                                _0233
   18 FA=FB                                                             _0234
      DA=DB                                                             _0235
   19 FB=F                                                              _0236
      DB=X                                                              _0237
      GO TO 14                                                          _0238
   16 IF (FA-FC) 21,21,20                                               _0239
   20 XINC=FA                                                           _0240
      FA=FC                                                             _0241
      FC=XINC                                                           _0242
      XINC=DA                                                           _0243
      DA=DC                                                             _0244
      DC=XINC                                                           _0245
   21 XINC=DC                                                           _0246
      IF ((D-DB)*(D-DC)) 32,22,22                                       _0247
   22 IF (F-FA) 23,24,24                                                _0248
   23 FC=FB                                                             _0249
      DC=DB                                                             _0250
      GO TO 19                                                          _0251
   24 FA=F                                                              _0252
      DA=X                                                              _0253
   14 IF (FB-FC) 25,25,29                                               _0254
   25 IINC=2                                                            _0255
      XINC=DC                                                           _0256
      IF (FB-FC) 29,45,29                                               _0257
   29 D=(FA-FB)/(DA-DC)-(FA-FC)/(DA-DC)                                 _0258
      IF (D*(DB-DC)) 33,37,37                                           _0259
   37 D=0.5*(DB+DC-(FB-FC)/D)                                           _0260
      IF (ABSF(D-X)-ABSF(ABSACC)) 34,34,35                              _0261
   35 IF (ABSF(D-X)-ABSF(D*RELACC)) 34,34,36                            _0262
   34 ITEST=2                                                           _0263
      GO TO 43                                                          _0264
   36 IS=1                                                              _0265
      X=D                                                               _0266
      IF ((DA-DC)*(DC-D)) 3,26,38                                       _0267
   38 IS=2                                                              _0268
      GO TO (39,40),IINC                                                _0269
   39 IF (ABSF(XINC)-ABSF(DC-D)) 41,3,3                                 _0270
   33 IS=2                                                              _0271
      GO TO (41,42),IINC                                                _0272
   41 X=DC                                                              _0273
      GO TO 10                                                          _0274
   40 IF (ABSF(XINC-X)-ABSF(X-DC)) 42,42,3                              _0275
   42 X=0.5*(XINC+DC)                                                   _0276
      IF ((XINC-X)*(X-DC)) 26,26,3                                      _0277
   45 X=0.5*(DB+DC)                                                     _0278
      IF ((DB-X)*(X-DC)) 26,26,3                                        _0279
   26 ITEST=3                                                           _0280
      GO TO 43                                                          _0281
      END                                                               _0282
-                                                                       _0283
      SUBROUTINE GRAPH2(X,Y,MFIT,ICON,MMAX,IPRINT)                      _0284
C                                                                       _0285
C                                                                       _0286
C     1/ PURPOSE.                                                       _0287
C                                                                       _0288
C     THE SUBROUTINE GRAPH2 IS A MODIFICATION OF SUBROUTINE GRAPH. IT   _0289
C     PLOTS UP TO 9 GRAPHS ON THE SAME SET OF AXES USING THE PRINTER.   _0290
C     THE USER MUST CALCULATE EACH Y(I,J) AS A FUNCTION OF THE          _0291
C     CORRESPONDING X(I,J).                                             _0292
C                                                                       _0293
C                                                                       _0294
C     2/ ARGUMENTS                                                      _0295
C                                                                       _0296
C     SUBROUTINE GRAPH2(X,Y,MFIT,ICON,MMAX,IPRINT)                      _0297
C                                                                       _0298
C     X       A TWO-DIMENSIONAL ARRAY DIMENSIONED X(MFIT,MMAX)          _0299
C             X(I,J) CONTAINS THE JTH X -VALUE ON THE ITH CURVE.        _0300
C     Y       A TWO-DIMENSIONAL ARRAY DIMENSIONED Y(MFIT,MMAX)          _0301
C             Y(I,J) CONTAINS THE JTH Y-VALUE ON THE ITH CURVE.         _0302
C     MFIT    IS THE NUMBER OF LINES TO BE DRAWN ON THE SAME SYSTEM     _0303
C             OF AXES.                                                  _0304
C     ICON    ONE DIMENSIONAL ARRAY DIMENSIONED AT LEAST MFIT.          _0305
C             ICON(1)  CONTAINS THE NUMBER OF POINTS ON THE FIRST LINE. _0306
C             ICON(2)  CONTAINS THE NUMBER OF POINTS ON THE SECOND LINE._0307
C             ICON(3)  ETC.                                             _0308
C     MMAX    GREATER THAN OR EQUAL TO MAX VALUE OF ICON(1)...ICON(MFIT)_0309
C                                                                       _0310
C        IPRINT  SET ON ENTRY                                           _0311
C            = 0 - INDICATES GRAPH ONLY IS TO BE PRINTED                _0312
C            = 1 - INDICATES GRAPH AND TABLE OF VALUES ARE TO BE PRINTED_0313
C     **WARNING**  IPRINT = 1 MAY PRODUCE EXCESSIVE OUTPUT              _0314
C                  TABLE OF VALUES ARE PRINTED ONE PER LINE           _0315
C                                                                       _0316
```

```
C     THE ITH CURVE IS PLOTTED WITH THE SYMBOL I.  WHERE TWO POINTS
C     COINCIDE THE SYMBOL  *  IS USED.
C
      DIMENSION X(MFIT,MMAX), Y(MFIT,MMAX), ICON(MFIT), LINE(111),
     1  ILIN(9), VAL(6)
      DATA IBLANK, IDASH, ICHAR, ISTAR/1H ,1H-,1HI,1H*/,
     1  ILIN/1H1,1H2,1H3,1H4,1H5,1H6,1H7,1H8,1H9/
C
C       CALCULATE MAXIMUM AND MINIMUM VALUES FOR X AND Y
C
      XMAX=X(1,1)
      XMIN=X(1,1)
      YMAX=Y(1,1)
      YMIN=Y(1,1)
      DO 10 M=1,MFIT
      ICM=ICON(M)
      DO 20 N=1,ICM
      IF(X(M,N).GT.XMAX)GO TO 21
      IF(X(M,N).LT.XMIN)XMIN=X(M,N)
   23 IF(Y(M,N).GT.YMAX)GO TO 22
      IF(Y(M,N).LT.YMIN)YMIN=Y(M,N)
      GO TO 20
   21 XMAX=X(M,N)
      GO TO 23
   22 YMAX=Y(M,N)
   20 CONTINUE
   10 CONTINUE
      XL=(XMAX-XMIN)/110.
      YL=(YMAX-YMIN)/50.
C
      DO 50 J=1,51
C       INITIALISE CURRENT LINE OF GRAPH TO BLANKS
      DO 40 K=1,111
      LINE(K)=IBLANK
   40 CONTINUE
C       PICK OUT Y VALUES TO BE PRINTED
      DO 60 M=1,MFIT
      ICM=ICON(M)
      DO 70 N=1,ICM
      LN=(Y(M,N)-YMIN)/YL+1.5
      IF(LN+1.NE.J)GO TO 70
      K=(X(M,N)-XMIN)/XL+1.5
      IF(LINE(K).NE.IBLANK)GO TO 81
      LINE(K)=ILIN(M)
      GO TO 70
   81 LINE(K)=ISTAR
   70 CONTINUE
   60 CONTINUE
C       PRINT CURRENT LINE OF GRAPH
      IF(MOD(J,10).NE.1)GO TO 100
      VALY=YMIN+FLOAT(51-J)*YL
      WRITE(6,1000)VALY,LINE
 1000 FORMAT(1X,E11.4,2H-I,111A1)
      GO TO 50
  100 WRITE(6,1010)LINE
 1010 FORMAT(13X,1HI,111A1)
   50 CONTINUE
C
C       PRINT X-AXIS
C
      DO 160 K=1,111
      LINE(K)=IDASH
  160 CONTINUE
      DO 170 K=1,111,20
      LINE(K)=ICHAR
  170 CONTINUE
      WRITE(6,1020)LINE
 1020 FORMAT(13X,1H-,111A1)
      DO 180 K=1,6
      VAL(K)=XMIN+XL*20.*FLOAT(K-1)
  180 CONTINUE
      WRITE(6,1030)VAL
 1030 FORMAT(3X,6(E20.4)//)
C
C       PRINT TABLE OF VALUES
C
      IF(IPRINT.EQ.0) RETURN
      DO 190 M=1,MFIT
      WRITE(6,1040)M
 1040 FORMAT(//10X,5HGRAPH,I3,10X,8HX VALUES,10X,8HY VALUES)
      ICM=ICON(M)
      WRITE(6,1050)(X(M,N),Y(M,N),N=1,ICM)
 1050 FORMAT(27X,E11.4,7X,E11.4)
  190 CONTINUE
```

```
      RETURN                                                            _0401
      END                                                               _0402
                                                                        _0403
      SUBROUTINE VA01A(X,F,G,U,E,FMIN,ESCALF,IPRINT,MAXIT,MXITFG,       _0404
     1                 CALCFG,W,N3N)                                    _0405
      REAL X(N),E(N),G(N)                                               _0406
      REAL W(N3N)                                                       _0407
      ABSF(ABC123)=ABS(ABC123)                                          _0408
      SQRTF(ABC123)=SQRT(ABC123)                                        _0409
      IF(N3N-N*(N+3)) 8000,8002,8002                                    _0410
 8000 WRITE(6,8001)                                                     _0411
 8001 FORMAT(26H DIMENSION OF W TOO SMALL )                             _0412
      STOP                                                              _0413
 8002 CONTINUE                                                          _0414
      NN=N                                                              _0415
      K=0                                                               _0416
      IMAX=0                                                            _0417
      DO 2 I=1,NN                                                       _0418
      DO 3 J=1,NN                                                       _0419
      K=K+1                                                             _0420
      W(K)=0.                                                           _0421
      IF (I-J) 3,4,3                                                    _0422
    4 W(K)=1.                                                           _0423
    3 CONTINUE                                                          _0424
    2 CONTINUE                                                          _0425
      N1=K                                                              _0426
      N2=NN+K                                                           _0427
      N3=NN+N2                                                          _0428
      NCOUNT=NN                                                         _0429
      ICOUNT=0                                                          _0430
      CALL CALCFG (X,F,N,FX)                                            _0431
    1 IF (IMAX-MAXIT) 58,59,58                                          _0432
   58 FMAX=0.                                                           _0433
      IXITFG=0                                                          _0434
      IMAX=IMAX+1                                                       _0435
      K=0                                                               _0436
      DO 5 I=1,NN                                                       _0437
      K1=N1+I                                                           _0438
      K2=N2+I                                                           _0439
      SUM=0.                                                            _0440
      DO 6 J=1,NN                                                       _0441
      K=K+1                                                             _0442
      SUM=W(K)*G(J)+SUM                                                 _0443
    6 CONTINUE                                                          _0444
      W(K2)=G(I)                                                        _0445
      A=ABSF(SUM/E(I))                                                  _0446
      W(K1)=-SUM                                                        _0447
      IF (FMAX-A) 7,5,5                                                 _0448
    7 FMAX=A                                                            _0449
    5 CONTINUE                                                          _0450
      FA=FX                                                             _0451
      SCALF=ESCALE/FMAX                                                 _0452
      FCOMP=FA+ABSF(0.000001*FA)                                        _0453
      IS=1                                                              _0454
    8 GC=0.                                                             _0455
      DO 9 I=1,NN                                                       _0456
      K1=N1+I                                                           _0457
      GC=G(I)*W(K1)+GC                                                  _0458
    9 CONTINUE                                                          _0459
      GO TO (10,11,12),IS                                               _0460
   10 IF (GC) 14,14,13                                                  _0461
   13 CONTINUE                                                          _0462
      WRITE(6,15)                                                       _0463
   15 FORMAT (5X,30HERROR DUE TO ROUNDING IN VA01A/1H1)                 _0464
      GO TO 16                                                          _0465
   14 Y=1.                                                              _0466
      GA=GC                                                             _0467
      IF (SCALE-Y) 17,18,18                                             _0468
   17 Y=SCALE                                                           _0469
   18 IS=2                                                              _0470
      YS=Y                                                              _0471
   19 DO 20 I=1,NN                                                      _0472
      K1=N1+I                                                           _0473
      X(I)=X(I)+YS*W(K1)                                                _0474
   20 CONTINUE                                                          _0475
      CALL CALCFG (X,G,N,FX)                                            _0476
      IXITFG=IXITFG+1                                                   _0477
      IF(IXITFG.LT.MXITFG) GO TO 8004                                   _0478
      WRITE(6,8003) IXITFG                                              _0479
 8003 FORMAT(1HO,I5,45H  FUNCTION AND DERIVATIVES FOR THIS ITERATION   ) _0480
      RETURN                                                            _0481
 8004 CONTINUE                                                          _0482
      GO TO 8                                                           _0483
   11 FMAX=ABSF(1000000.*GA*Y)                                          _0484
```

```
      FB=FX                                                             _0485
      GB=GC                                                             _0486
      IF (FMAX-ABSF(FA)) 22,24,24                                       _0487
   22 IF (FMAX-ABSF(FB)) 23,24,24                                       _0488
   23 YP=Y*GA/(GA-GB)                                                   _0489
      GO TO 25                                                          _0490
   24 SUM=3.*(FA-FB)+Y*(GA+GB)                                          _0491
      FMAX=SUM*SUM-Y*Y*GA*GB                                            _0492
      IF (FMAX) 27,27,26                                                _0493
   26 YP=Y*Y*GA/(Y*GA+SUM-SQRTF(FMAX))                                  _0494
   25 IF (YP) 27,27,28                                                  _0495
   28 IF ( SCALE-YP) 27,40,40                                           _0496
   40 IF (NCOUNT) 41,41,29                                              _0497
   41 IF (SCALE-ESCALE) 29,29,42                                        _0498
   42 IF (SCALE-YP*ESCALE) 29,29,16                                     _0499
   16 F=FX                                                              _0500
      RETURN                                                            _0501
   27 YP=SCALE                                                          _0502
   29 IF (YP-Y) 31,30,31                                                _0503
   31 IS=3                                                              _0504
      DO 32 I=1,NN                                                      _0505
      K3=N3+I                                                           _0506
      W(K3)=G(I)                                                        _0507
   32 CONTINUE                                                          _0508
      YS=YP-Y                                                           _0509
      GO TO 19                                                          _0510
   12 IF (FCOMP-FX) 33,33,34                                            _0511
   34 IF (FB-FX) 33,33,30                                               _0512
   33 IF (FCOMP-FB) 35,36,36                                            _0513
   35 Y=YP                                                              _0514
      GO TO 11                                                          _0515
   36 DO 21 I=1,NN                                                      _0516
      K1=N1+I                                                           _0517
      K3=N3+I                                                           _0518
      X(I)=X(I)-YS*W(K1)                                                _0519
      G(I)=W(K3)                                                        _0520
   21 CONTINUE                                                          _0521
      YP=Y                                                              _0522
      FX=FB                                                             _0523
      GC=GB                                                             _0524
   30 IF (FX-FMIN) 37,37,38                                             _0525
   37 WRITE(6,39)                                                       _0526
   39 FORMAT (5X,35HFUNCTION VALUE LESS THAN FMIN FOUND/1H1)            _0527
      GO TO 16                                                          _0528
   38 IF (IPRINT) 44,44,43                                              _0529
   43 ICOUNT=ICOUNT+1                                                   _0530
      IF (IPRINT-ICOUNT) 44,45,44                                       _0531
   45 WRITE(6,46) FX,(X(I),I=1,NN)                                      _0532
   46 FORMAT (//E14.6/(8E14.6/))                                        _0533
      ICOUNT=0                                                          _0534
   44 A=1./(GC-GA)                                                      _0535
      FMAX=-A*GA                                                        _0536
      IF (A) 1,1,48                                                     _0537
   48 IF (2.*SCALE-YP*FMAX) 47,47,49                                    _0538
   49 DO 50 I=1,NN                                                      _0539
      K2=N2+I                                                           _0540
      W(K2)=G(I)-W(K2)                                                  _0541
   50 CONTINUE                                                          _0542
      K=0                                                               _0543
      B=0.                                                              _0544
      DO 51 I=1,NN                                                      _0545
      K3=N3+I                                                           _0546
      SUM=0.                                                            _0547
      DO 52 J=1,NN                                                      _0548
      K2=N2+J                                                           _0549
      K=K+1                                                             _0550
      SUM=W(K)*W(K2)+SUM                                                _0551
   52 CONTINUE                                                          _0552
      K2=N2+I                                                           _0553
      W(K3)=SUM                                                         _0554
      B=W(K2)*SUM+B                                                     _0555
   51 CONTINUE                                                          _0556
      A=YP*A                                                            _0557
      B=-1./B                                                           _0558
      NCOUNT=NCOUNT-1                                                   _0559
   53 K=0                                                               _0560
      DO 54 I=1,NN                                                      _0561
      K1=N1+I                                                           _0562
      K3=N3+I                                                           _0563
      A1=A*W(K1)                                                        _0564
      B1=B*W(K3)                                                        _0565
      DO 55 J=1,NN                                                      _0566
      K1=N1+J                                                           _0567
      K3=N3+J                                                           _0568
```

```
      K=K+1                                                              _0569
      W(K)=A1*W(K1)+B1*W(K3)+W(K)                                        _0570
   55 CONTINUE                                                           _0571
   54 CONTINUE                                                           _0572
      GO TO 1                                                            _0573
   47 IF (YP-SCALE) 1,56,56                                              _0574
   56 IF (SCALE-0.8) 1,1,57                                              _0575
   57 A=(YP-2.*SCALE*YP)/(SCALE*GA)                                      _0576
      B=0.                                                               _0577
      GO TO 53                                                           _0578
   59 WRITE(6,60) IMAX                                                   _0579
   60 FORMAT (I10,21H ITERATIONS COMPLETED/1H1)                          _0580
      GO TO 16                                                           _0581
      END                                                                _0582
                                                                         _0583
      SUBROUTINE CALCFG(X,G,N,F)                                         _0584
      DIMENSION E(6),G(6),X(6),W(54)                                     _0585
      COMMON ZZ(46),CR(46),Z(46),RD(46),FL(46),A(46),NA,NB,S,ZZM,FLM,AM  _0586
     1 ,ZM,P(46),R(46),NX                                                _0587
      F=0.                                                               _0588
      S=X(3)                                                             _0589
      DO 10 I=1,N                                                        _0590
      G(I)=0.                                                            _0591
   10 CONTINUE                                                           _0592
      DO 20 I=1,NA                                                       _0593
      AI=ZZ(I)/X(2)                                                      _0594
      BI=ALOG(AI)/S                                                      _0595
      CI=EXP(-0.5*BI**2)                                                 _0596
      PI=X(1)*CI                                                         _0597
      P(I)=PI                                                            _0598
      IF(ZZ(I).LT.1.5) GO TO 20                                          _0599
      ERI=PI-FL(I)                                                       _0600
      GI=2.*ERI*CI                                                       _0601
      HI=GI*BI*X(1)/S                                                    _0602
      G(1)=G(1)+GI                                                       _0603
      G(2)=G(2)+HI/X(2)                                                  _0604
      G(3)=G(3)+HI*BI                                                    _0605
      F=F+ERI**2                                                         _0606
   20 CONTINUE                                                           _0607
      RETURN                                                             _0608
      END                                                                _0609
                                                                         _0610
      SUBROUTINE CALCFH(X,G,N,F)                                         _0611
      DIMENSION E(6),G(6),X(6),W(54)                                     _0612
      COMMON ZZ(46),CR(46),Z(46),RD(46),FL(46),A(46),NA,NB,S,ZZM,FLM,AM  _0613
     1 ,ZM,P(46),R(46),NX                                                _0614
      F=0.                                                               _0615
      DO 10 I=1,N                                                        _0616
      G(I)=0.                                                            _0617
   10 CONTINUE                                                           _0618
      DO 20 I=1,NB                                                       _0619
      AI=Z(I)/X(2)                                                       _0620
      BI=ALOG(AI)/S                                                      _0621
      CI=EXP(-0.5*BI**2)                                                 _0622
      PI=X(1)*CI                                                         _0623
      R(I)=PI                                                            _0624
      IF( Z(I).LT.1.5) GO TO 20                                          _0625
      ERI=PI-A(I)                                                        _0626
      GI=2.*ERI*CI                                                       _0627
      HI=GI*BI*X(1)/S                                                    _0628
      G(1)=G(1)+GI                                                       _0629
      G(2)=G(2)+HI/X(2)                                                  _0630
      F=F+ERI**2                                                         _0631
   20 CONTINUE                                                           _0632
      RETURN                                                             _0633
      END                                                                _0634
                                                                         _0635
```